Polymeric Scaffolds as Building Blocks for Nanomaterials with Biomedical Applications

by

Daniel Nicolae Crisan

A thesis submitted to the University of Birmingham for the degree of

DOCTOR OF PHILOSOPHY

School of Chemistry

College of Engineering and Physical Sciences

University of Birmingham

September 2017

Abstract of the Thesis

Polymeric Scaffolds as Building Blocks for Nanomaterials

with Biomedical Applications

Daniel N. Crisan

Functional polymers are emerging as strong candidates for a variety of biomedical applications, but progress in this field is slow due to the difficulties associated with the synthesis of libraries of polymers. Polymeric scaffolds facilitate the rapid synthesis of such functional polymers by employing Click chemistries as a tool for post-polymerisation modification. Acrylic and acetylene based polyhydrazides have been explored as potential scaffolds for the in situ screening of functionalised polymers for biomedical applications. Poly(acryloyl hydrazide) was prepared from commercially available starting materials using RAFT polymerisation in a three step synthesis, and its post-polymerisation modification using a variety of hydrophilic and hydrophobic aldehydes was investigated. Biocompatible solvents and reaction conditions were determined such that the post-polymerisation modification could be achieved with good yields or better. The applicability of the scaffold was shown during the in situ screening of functional polymers for siRNA delivery, which required no isolation or purification of candidate polymers. Poly(4-ethynylbenzohydrazide) was synthesised using Rh catalysed polymerisation conditions, towards achieving a helical polymer scaffold. Despite the lack of solubility in aqueous solvents, the stability and post-polymerisation modification was analysed in a variety of conditions, opening the possibility of synthesising biodegradable mimics to naturally occurring helical moieties (e.g. anti-microbial peptides).

Acknowledgements

There comes that time in the life of every PhD student, when he can afford a moment to reflect, not on his work, but upon those people who have had such an important impact and influence in his life over the years that have passed.

Firstly, to my supervisor, Dr Francisco (Paco) Fernandez-Trillo without whom this wouldn't have been possible, who has mentored me and challenged me to become the best that I could be, I say to you a massive and sincere "Thank You!".

I would like to express my gratitude towards the University of Birmingham, the School of Chemistry and the excellent staff, both academic and technical, for the outstanding training and teaching bestowed upon me over the past 7 years.

Special mentions go to Dr Chi Tsang, Dr Cecile Le Duff, Dr Allen Bowden, Dr Neil Spencer and Dr Jonathon Snelling for their support in helping me analyse and characterise my compounds. To Ben Martyn at Warwick University for his help with SEC/GPC analysis when we were still starting up our laboratory.

To Dr Ignacio "Nacho" Insua, we began our PhDs at the same time, we set up and managed the lab together, and we have been through some memorable times. I thank you for your friendship, advice and putting a beer in my hand when needed.

To the people in the BioMedNanoLab, Emma Lilley, Oliver Creese, Andy Wilkinson, Arka Chakraborty, Julia Lipecki and Jose (Zelu) Brioso Jimenez whom I have had the privilege to train, teach and supervise over the years. You have helped me develop into a patient mentor and I hope that I have managed to pass on as much knowledge and experience as I could.

It would have been a different experience without the other colleagues in the group, the many friends in the office, Xavi Hueso and Adam Kolodziej with whom I've shared great scientific and non-scientific conversations and many happy hours at the staff house. I thank you all!

I am particularly indebted to Mr. John Evans for his generous financial contribution that funded my scholarship and my research. I hope this work can evolve into something truly impactful.

I would also like to thank our collaborators at the University of Santiago de Compostela, Juan Priegue and Dr. Javier Montenegro. It has been an immense pleasure to work with you, and you have been great hosts during my visit there. Of course, special gratitude to the Royal Society of Chemistry for making it possible through the Researcher Mobility Grant.

To Nohora J. Rueda, I will cherish the late evenings exchanging expertise on chemistry and microbiology during our collaboration, discussing culture, reggaeton and Game of Thrones and showing you snow for the very first time. I am grateful to Dr. Alvaro Mauricio Florez and The University of Santander for making my visit to Colombia such an insightful experience.

Importantly, to my fiancee Georgiana, who has been there wholeheartedly during the best times of my PhD, but especially during the difficult moments. You are my person.

Finally, I would like to thank my parents Mirela and Adrian, and my brother Lucian for their wise counsel, sympathetic ear, for always believing in me and urging me to keep going strong. Also, to my Alsatian, Lady and my three cats, Mitzi, Garfield and now Floki, over the past four years you have made the holidays home relaxing and fun.

Disclaimer

The information, analysis and opinions expressed in this thesis are solely of the author of the thesis. All the experimental work presented, is the work of the author unless specified otherwise. Data from experimental work carried out by other people and included in this thesis was independently analysed and presented by the author of this thesis will full permission from the parties involved. The following set of experiments were carried out by other people independently or with the support and guidance of the author of this thesis.

Ben Martyn, independently, carried out the SEC/GPC analysis of the polymerisation kinetics of *tert*-butyl 2-acryloylhydrazine-1-carboxylate. The polymerisation reactions were set up by the author and analysis of the SEC/GPC data was carried out by the author.

Julia Lipecki, under the guidance of the author, carried out polymerisation reactions involving acryloyl hydrazide synthesised by the author, and cyanomethyl methyl(pyridin-4-yl)carbamodithioate as the chain transfer agent.

Andrew Wilkinson followed by Arka Chakraborty with the support and guidance of the author, carried out the synthesis and polymerisation of 1-(*tert*-butyl) 2-(prop-2-yn-1-yl) hydrazine-1,2-dicarboxylate. Arka Chakraborty carried out the functionalisation studies of poly(prop-2-yn-1-yl hydrazine carboxylate) acetate with aldehydes. The experiments were planned and analysed under the guidance of the author.

Collaborative published work is presented with license from the publishing company, more specifically John Wiley and Sons.

Table of Contents

List of Symbols and Abbreviations

AcOH	Acetic Acid
ACVA	4,4′-Azobis(4-cyanovaleric acid)
AMP	Anti-microbial peptide
aq.	aqueous
ATRP	Atom-transfer radical-polymerisation
BAP	Borane-Pyridine
Boc	*tert*-Butyloxycarbonyl
CTA	Chain Transfer Agent
Đ	Dispersity
Da	Dalton
DCM	Dichloromethane
DIPEA	*N*,*N*-Diisopropylethylamine
DMF	Dimethylformamide
DMSO	Dimethyl sulfoxide
DNA	Deoxyribonucleic acid
DP	Degree of polymerisation
DPBS	Dulbecco's phosphate-buffered saline
DTNB	5,5'-dithiobis-(2-nitrobenzoic acid
EDC	1-Ethyl-3-(3-dimethylaminopropyl)carbodiimide
EDA	1,2-ethylenediamine
EMA	European Medicines Agency
equiv.	Molar equivalence
Et_2O	Diethyl ether
Et_3N	Triethylamine
EtOAc	Ethyl acetate
EtOH	Ethanol
EYPC	Egg yolk phosphatidylcholine
FDA	Food and Drug Administration

FITC	Fluorescein isothiocyanate
FT-IR	Fourier transform infrared spectroscopy
GFP	Green fluorescent protein
h	Hour
HIV	Human immunodeficiency virus
M	Molar
mAU	Milli-Absorbance (Arbitrary) Unit
MeOH	Methanol
mg	Milligram
MHz	Megahertz
min	Minute
mL	Millilitre
mM	Millimolar
M_n	Number average molecular weight
mol	Moles
M_w	Weight average molecular weight
$NaBH(AcO)_3$	Sodium triacetoxyborohydride
nbd	Norbornadiene
NHS	*N*-hydroxysuccinimide
NMR	Nuclear magnetic resonance
PEG	Poly(ethylene glycol)
PMMA	Poly(methyl methacrylate)
ppm	Parts per million
r.t.	Room temperature
RAFT	Reversible addition-fragmentation chain transfer
RI	Refractive Index
RISC	RNA-induced silencing complex
ROMP	Ring opening metathesis polymerisation
sat.	Saturated
SEC/GPC	Size Exclusion Chromatography/Gel Permeation Chromatography
siRNA	Small interfering ribonucleic acid

soln.	Solution
t	Time
TEA	Triethylamine
TFA	Trifluoroacetic acid
THF	Tetrahydrofuran
TMS	Trimethylsilyl
TOF ES	Time-of-flight electrospray ionisation mass spectrometry
TsOH	*p*-Toluenesulfonic acid
UV-Vis	Ultraviolet-visible
λem	Emission wavelength
λex	Excitation wavelength
μL	Microlitre
μm	Micrometre
μRIU	Micro-Refractive Index Unit

List of Figures, Schemes and Tables

Introduction

Introduction

The beginning of the 21st century poses a diversity of challenges but also many opportunities from a healthcare and biomedical point of view. Infections with antimicrobial-resistant bacteria are predicted to be the main cause of death by 2050.[1] Furthermore, these are also expected to complicate treatments for currently manageable diseases like HIV, Tuberculosis and Malaria. As longevity is increasing worldwide, so are the rates of cancer incidence and new types of cancer. Moreover, the threat of existent and new viruses is omnipresent, which in a globalised world makes an epidemic scenario a matter of when rather than if. These human cost is predicted to be accompanied by considerable economic costs, which could cost up to $100 trillion just due to antimicrobial resistance.

All is not bleak however, as research and progress into such fields as gene therapy,[2-4] siRNA delivery,[5-9] novel antibiotics based on mimics of antimicrobial peptides (AMPs),[10-18] antimicrobial surfaces and anti-adhesion coatings,[19-23] is advancing rapidly with promising and exciting results. Among these fields, materials based around functionalised polymers are emerging as possible solutions.[4,16,20]

Polymers are macromolecules that can be synthesised in a variety of sizes and shapes. Their physical and chemical properties can be adjusted to suit multiple applications, can be used to produce mimics of naturally occurring biomolecules in a cheap and facile way, and can be combined in such ways to obtain powerful synergistic effects, especially in biomedical applications. Historically, the use of polymers in biomedical applications has been limited, mainly due to the drawbacks of "traditional" (e.g. uncontrolled free radical, condensation etc.) polymerisations, which do not readily support the high-throughput synthesis required for libraries of compounds that need to be tested. Although these techniques are industrially mainstream, their limitation towards wide-spread use for exploring functional polymers for biological applications, originates from several synthesis related drawbacks.[24-26]

Firstly and most importantly, these techniques can be highly substrate specific and they can be difficult to carry out with monomers that contain multiple functional groups. This is a key requirement for synthesising libraries of functionalised polymers. Furthermore, experimental conditions are often not interchangeable between different monomers and optimisation for each new reaction would normally be required. This is an expensive and time consuming process. Secondly, uncontrolled polymerisations exhibit poor control over the key features required for the preparation of materials with well-defined molecular weights, dispersities (ratio between weight-average and number-average molar mass) and structures. To evaluate the structure-activity of a library of functionalised polymers,[27,28] it is desired that the sizes of the members are within the same range of each other, in order to observe trends related to their functionality not molecular weight. Furthermore, a narrow dispersity is more desirable in order to determine if an active polymer (e.g. a polymeric antimicrobial) is active over a wide range of sizes or only within a narrow molecular weight range. This should also facilitate approval from regulatory agencies (i.e. EMA, FDA) if a product were to be marketed, as their stringent regulations usually require a thorough knowledge of the structure of the active molecule. Finally, the synthesis of hundreds, if not thousands, of functional polymers would generally be considered highly time consuming and economically prohibitive.

Two scientific breakthroughs at the end of the 1990's lead to a "revolution" in thinking about the use functional polymers for biomedical applications. These breakthroughs were the advances in controlled polymerisation techniques[29-32] and the development of "click chemistry" reactions.[33,34]

Controlled polymerisation techniques such as Ring-Opening Metathesis (ROMP),[35-40] Atom-Transfer Radical (ATRP)[41-46] and Reversible Addition-Fragmentation Chain-Transfer (RAFT)[47-53] (**Fig. I.1**) have paved the way towards the synthesis of polymers incorporating a range of functionalities. They are normally distinguished by their high tolerance of many functional groups, ability to polymerise cheap monomers, using inexpensive catalysts, to produce valuable products or intermediates, and ability to produce well-defined polymers, of different architectures (i.e. linear, block co-polymers, polymer brushes or combs, star) with narrow dispersities and molecular weights that can be controlled by adjusting the ratio between monomer and catalyst or by quenching the reactions at different times. Furthermore, reaction conditions are generally quite compatible across substrates with similar chemical properties. Although these features solve some of the fundamental drawbacks of "traditional" polymerisation techniques and allow the synthesis of complex and well-defined polymeric molecules, one key drawback remains unaddressed. The synthesis and characterisation of libraries of hundreds of such complex polymers remains time-consuming, which is detrimental to the identification of targets with useful biological properties. However, by providing the tools to incorporate a variety of functional groups as side-chains of these polymers, the solution to rapidly produce large numbers of functional polymers was achieved in the form of polymer scaffolds. Polymer scaffolds are functional polymers that use

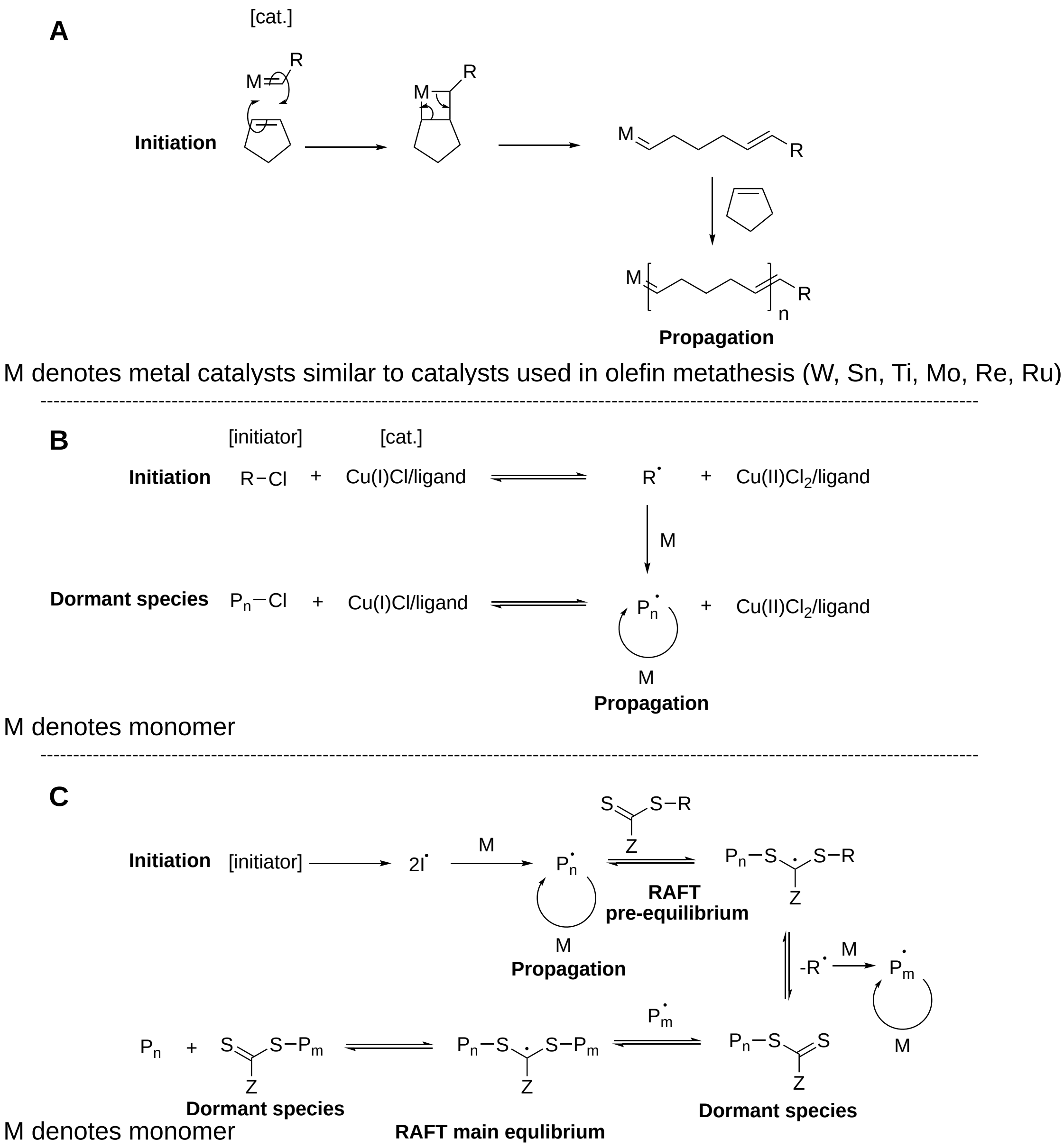

Figure I.1: Schematic diagrams showing controlled polymerisation processes: ROMP (**A**), ATRP (**B**) and RAFT (**C**).

auxiliary functional groups (**Fig. I.2**) for modification post-polymerisation, to quickly synthesise many new functional polymers without having to synthesise and polymerise the "equivalent" monomers. This is achieved by reacting the side-chain's functional group with small, multi-functional molecules (usually orthogonal to each other). Importantly, this allows the incorporation of functional groups that are still poorly tolerated, even by controlled polymerisation techniques. Furthermore, by reacting the scaffold with multiple decorating molecules, at the same time or sequentially, polymers with multiple functional groups can be synthesised. These are particularly useful in biological applications such as, but not restricted to, siRNA delivery (see **Chapter 3**) or mimics of antimicrobial peptides that normally require a mixture of cationic and hydrophobic residues. Aside from these evident advantages, another key aspect is that all polymers in these libraries will have stemmed from the same parent scaffold. As such, the size of the polymer (degree of polymerisation, DP) and the dispersity (Đ) will remain constant throughout. Any significant differences in biological activity between members of the library will have resulted from structural differences only (and the physicochemical properties imparted as a consequence) but not from size. Indeed, not at all surprisingly, functional polymers with different

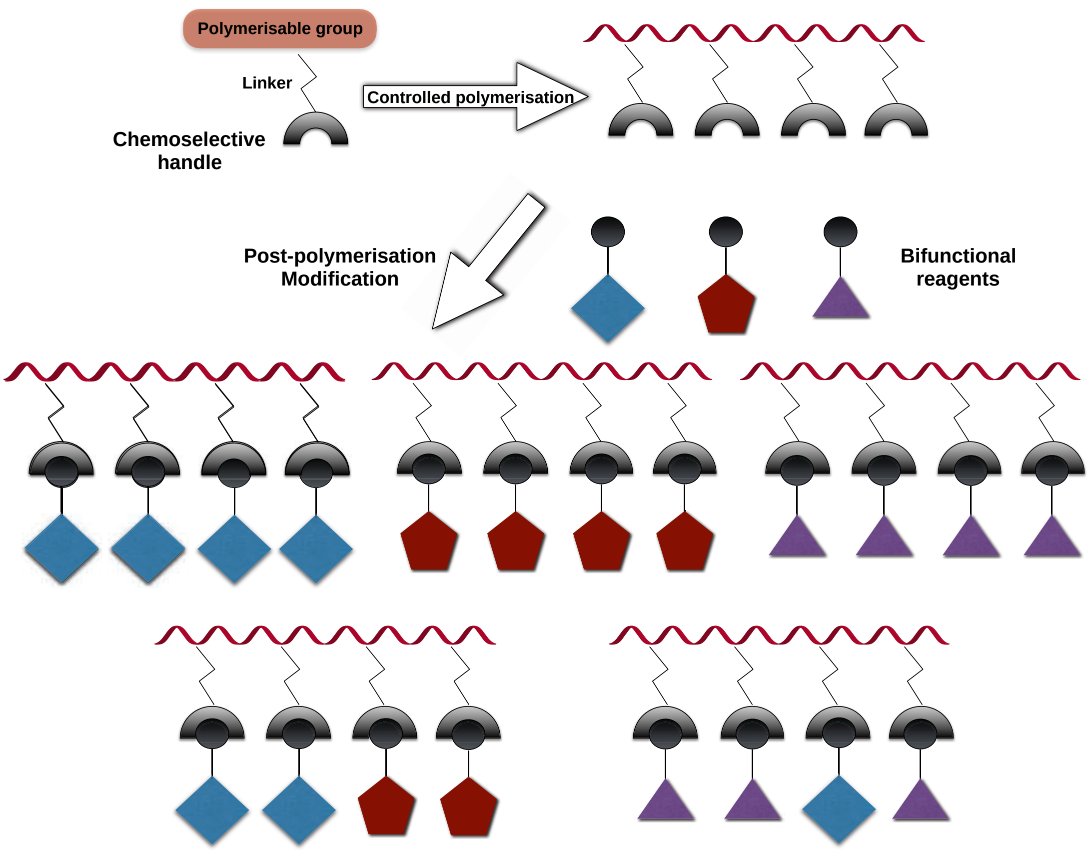

Figure I.2: Schematic representation of the synthesis of a polymer scaffold and post-polymerisation modification to synthesise libraries of functional polymers.

DPs has been reported to show different biological activity.[27,54,55] In addition to providing a faster synthetic pathway to libraries of functional polymers, polymer scaffolds also simplify and reduce the number of characterisation steps required (i.e. SEC/GPC, on the polymer scaffold is sufficient to determine DP and Đ for the whole population, or ^{1}H NMR spectroscopy and mass spectrometry for determination of DP), saving time and resources. Very often, these characterisation steps will not work efficiently for particular polymers (e.g. sample may not fly in mass spectrometry, special columns and solvent conditions may be required for SEC/GPC, etc.). As such, the one key element of characterisation for functional polymers, synthesised via polymer scaffolds, is the determination of percentage loading (i.e. how many of the scaffold's side-chains have reacted with the "decorating" functional small molecules). One of the shortfalls of functional polymers derived from scaffolds versus direct polymerisation of functional monomers is that in the latter, it is known as a certainty that all side-chains contain the target functional group, whilst in the former, it has to be determined and it is highly dependent on the efficiency of the chemistry used to decorate the scaffold's side-chains.

As a consequence of the aforementioned, a key necessity of polymer scaffolds is to use very efficient chemistries such as "click chemistry" reactions (but not restricted to) in the post-polymerisation modifications. Click chemistry[33,56] represents a whole class of reactions defined by the linking of small units thorough the formation of heteroatom links (C−X−C) and which abide to a set of criteria. Among the criteria, click chemistry reactions have to be modular (i.e. bringing different "building blocks" together) and wide in scope (i.e. applicable to diversity of substrates containing the same functional group), they must be high yielding, and ideally generate zero or inoffensive byproducts that can be removed by non-chromatographic purification techniques (i.e. by recrystallisation, distillation, liquid-liquid extraction). Furthermore, the reactions should be carried out under simple conditions (i.e. insensitive to oxygen and water, ideally in the absence of solvents, in water or solvents that are easily removed). Click chemistry reactions are considered “spring-loaded”, or highly selective towards a single product. This is due to a high thermodynamic driving force, which also leads to processes that reach completion quickly. Often, reactions proceed faster in hot water[33] (compared to organic media) even if one or more of the

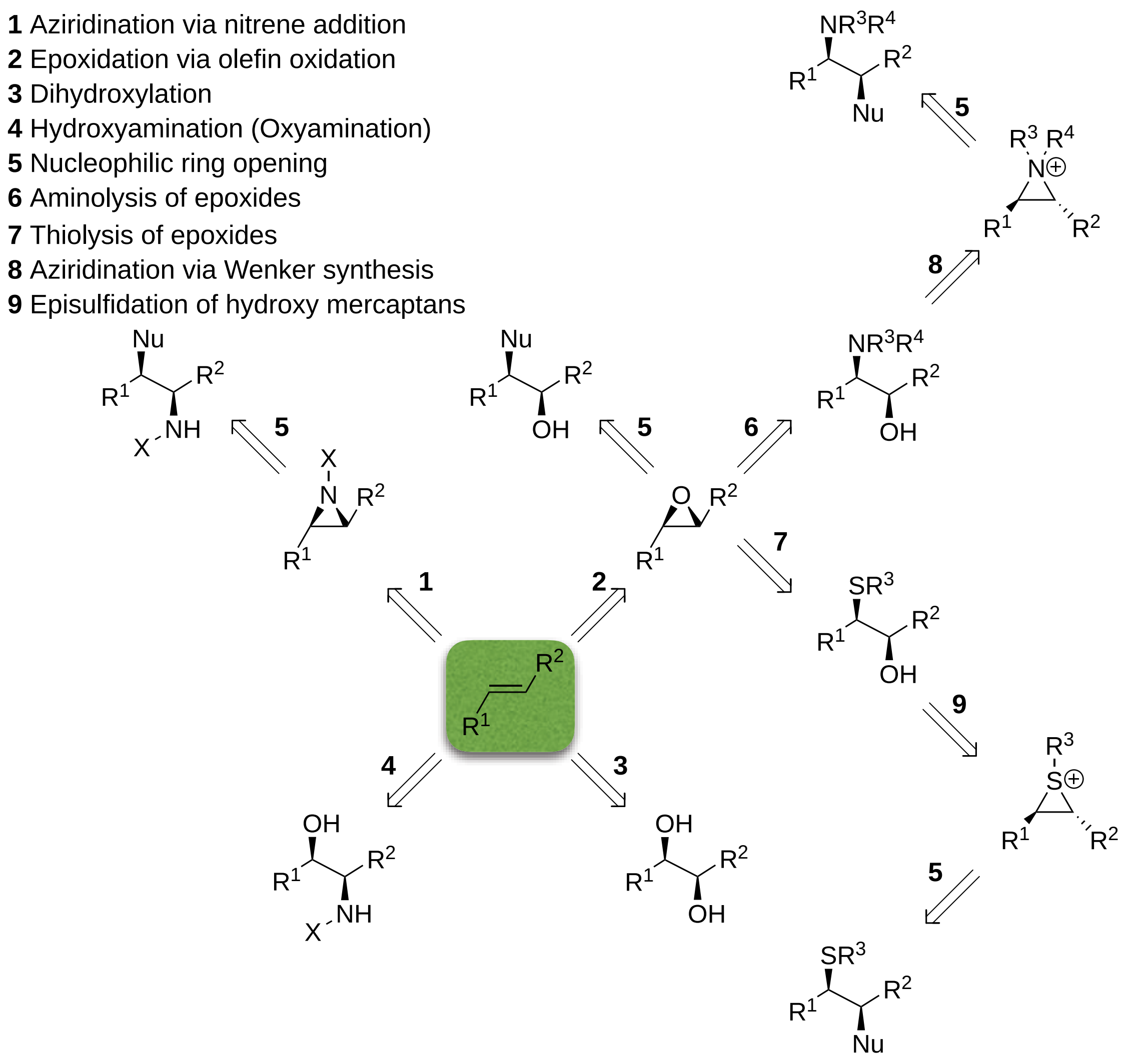

Figure I.3: Representative “click chemistry” reactions involving several transformations of olefin bonds.

reactants are or appear insoluble in the medium. This is believed to be due to the organic molecules having more free energy when poorly solvated, imparting increased reactivity and resulting in a higher rate constant, which compensates for the low concentration of the reactants in solution.

Common examples of chemical transformations that broadly fall under the classification of “click chemistry” include additions to C=C bonds / olefin oxidation to form ring strained epoxides or aziridines, dihydroxylation and oxyamination (**Fig. I.3**). The ring strained epoxides and aziridines can then be easily opened with a range of nucleophiles to form libraries of 1,2-difunctionalised compounds. A wide variety of thiol chemistry can also be considered as click chemistry such as thiol-ene/yne addition, disulfide formation, alkyl halide substitution, reaction with isocyanates to form thiocarbamates and thiol-Michael addition (**Fig. I.4**). Carbonyl chemistry of the non-aldol type is frequently used as click chemistry in reactions such as isocyanate reactions with amines or thiols to form ureas or thiocarbamates, reactions of

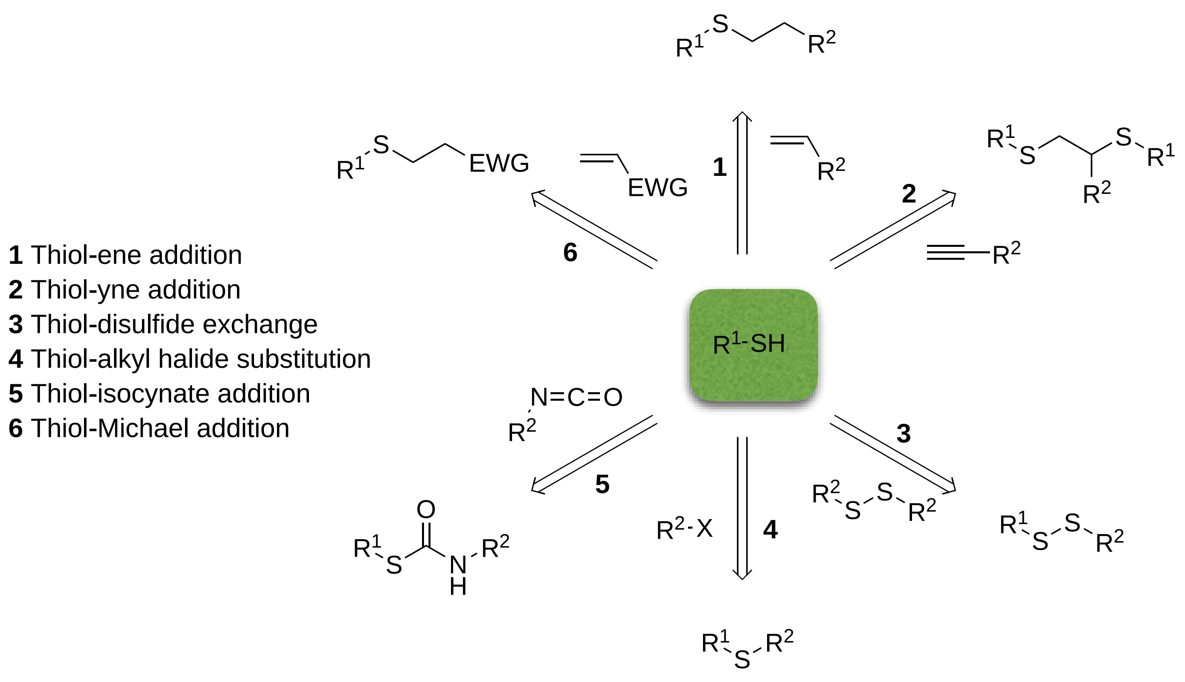

Figure I.4: Representative “click chemistry” reactions involving several transformations using thiol derivatives.

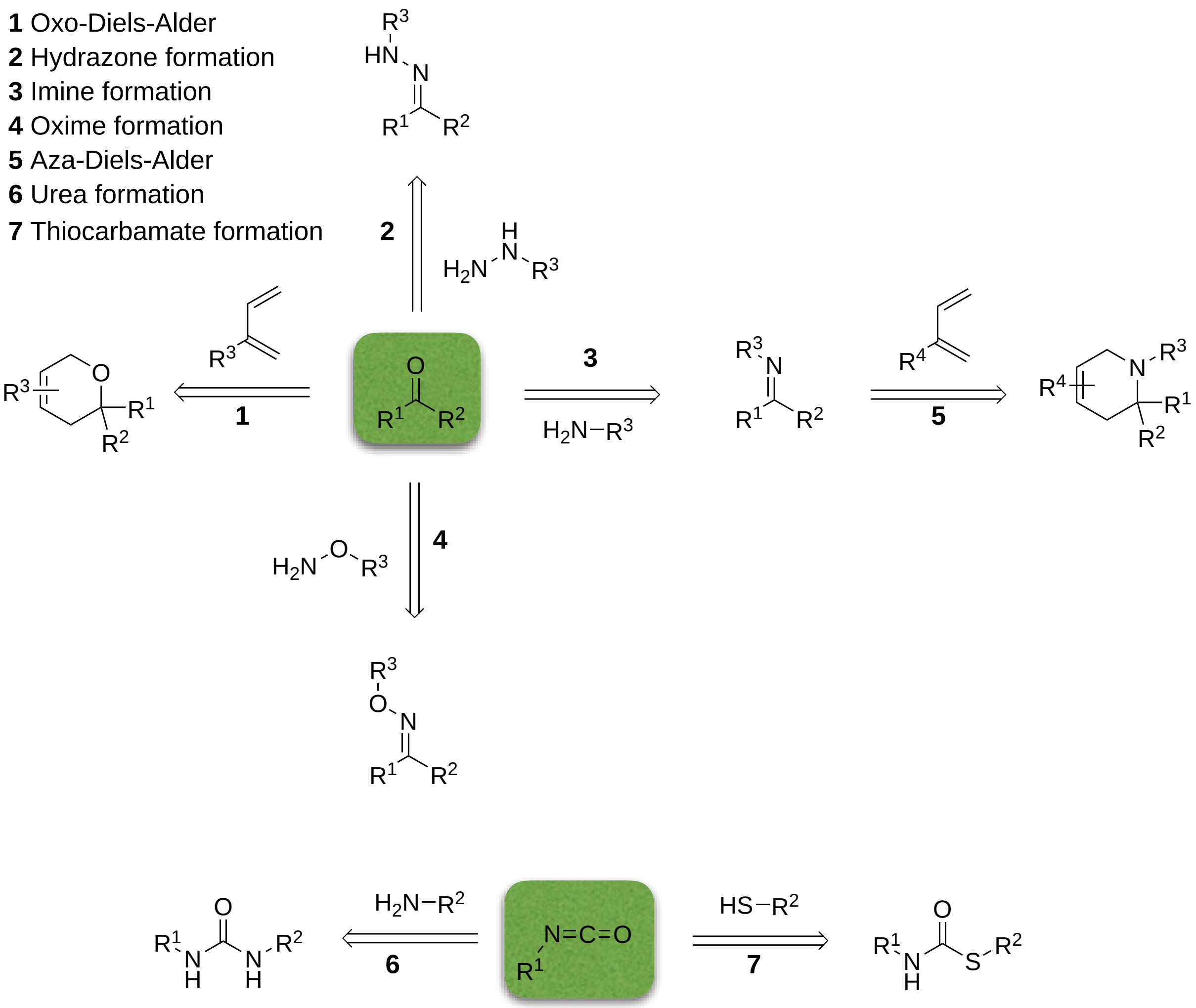

Figure I.5: Representative "click chemistry" reactions involving carbonyl chemistry of the non-aldol type.

aldehydes or ketones with amines, hydrazines, hydroxylamines to form imines, hydrazones and oximes respectively, or aldehydes / imines reactions with dienes in hetero-Diels-Alder reactions (oxo-Diels-Alder and aza-Diels-Alder respectively) to form heterocyclic compounds (**Fig. I.5**). Lastly, "the cream of the crop" of "click chemistry" as referred to by Barry Sharpless[33] is the Copper (I) catalysed Azide-Alkyne Huisgen cycloaddition (CuAAC).

In the context of polymer scaffolds,[57-63] many of these click chemistry reactions as well as other highly efficient chemistries (e.g. reaction with activated esters, anhydrides) have been used successfully for the synthesis of functional polymers each with their own advantages and disadvantages. These scaffolds were analysed from the point of view of suitability towards synthesis of functional polymers for biological applications. It is the author's belief that the best system for high-throughput screening should ideally involve a one-pot, or *in–situ* approach between post-polymerisation modification and biological testing. For this to be possible, functionalisation reactions would need to be carried out in water or biocompatible solvents (i.e. DMSO) and require no purification steps. The scaffold should be soluble and stable under aqueous conditions. The reaction should ideally proceed with no by-products at all, or water as a by-product. Other non-toxic molecules as by-products would not be to far from ideal, but would require additional control studies (i.e. does the by-product play a role in any biological effect observed for the functional polymer?). Finally, the reagents should be non-toxic or react in a 1:1 stoichiometry with the scaffold (i.e. full consumption so no free reagents in biological testing to account for); any catalysts used in the reaction should similarly be bio-compatible. As such, metal catalysed reactions would not be considered ideal for high-throughput screening due to their usual cell toxicities.

1) Scaffolds containing epoxide side-chains

Although there are many tools available in the olefin oxidation click chemistry arsenal, their use in polymer scaffolds is mostly represented by epoxide chemistry. Poly(glycidyl methacrylate)[64-67] (poly(GMA)) and poly(epoxystyrene)[68] are the best examples (**Fig. I.6**) in this category. These polymers were synthesised using a variety of techniques including free radical, ATRP and RAFT polymerisation.

Figure I.6: Representative examples of polymer scaffolds containing epoxide functional groups.

Poly(GMA) was used as a reactive coating for silica nanoparticles[64] in order to attach fluorescent tags and ATRP initiators for grafting polymer layers such as oligo(ethylene glycol) methyl ether methacrylate. Another exemplification of the use of poly(GMA) as a scaffold is in brushes on silicon wafers[65] and their subsequent chemical modification. In these examples, the modification of the oxirane group was carried out in solvents such as methyl ethyl ketone and ethanol and also exposed during the polymer synthesis and purification to solvents such as methanol, diethyl ether, DCM and even water without affecting the functional group. The modifications were carried out successfully with compounds containing carboxylic acid or amine functional groups. Amines, however, were found to react with multiple oxirane side-chains resulting in cross linking. Despite stability and reactivity in a diversity of solvents, there has been very little investigation into the functionalisation of such scaffolds in water or with a diversity of different substrates to produce libraries of functional polymers. The chemistry is elegant in that it produces no by−products so requires no post-functionalisation purification, but there is currently no information if complete functionalisation can be achieved and if the reaction is stoichiometric. A further negative aspect of the reaction is the reactivity of an amine functional group with multiple oxirane groups. This can lead to intra- and inter-molecular cross linking, which deviates from the idea of functionalised chains and leads into the territory of single chain nanoparticles and extensive cross linked systems.

2) Scaffolds containing alkene side-chains

There are many diverse examples of polymeric systems containing reactive alkenes[69-78] as part of their side-chains or backbone (**Fig. I.7**). Most often, these scaffolds have been used to form functional polymers by photo or thermal thiol-ene click chemistry additions. Homo- and co-polymers were synthesised mainly via different (anionic, cationic, metal-catalysed, enzymatic) ring-opening polymerisation techniques, but there are also examples of RAFT polymerisation[77] despite the risk of cross-linking dienes. Efficient functionalisation has been reported in most cases, including reported cases of close to 100% conversion regardless of the alkene content in the polymer. Thiols containing other different functional groups have been successfully reacted, including amino, hydroxyl, carboxyl group as well as short amino acid sequences. One potential issue with these systems is the potential for cross-linking and cyclisation between the thiol and alkene groups when exposed to the conditions required for radical thiol-ene addition. Studies have been carried out to determine reaction conditions which suppress this cross-linking, however these generally involve using a large excess of the thiol reactant. Full thiol consumption without side-reactions has also been shown when sub-stoichiometric amounts of thiols were used, with a view to use the remaining alkenes for further functionalisation. Reported functionalisation conditions are varied both in temperature (-35 ℃ up to 90 ℃) and time (0.5 h up to 24 h). However, because of the poor solubility of the scaffolds in water, most reported functionalisations were in solvents

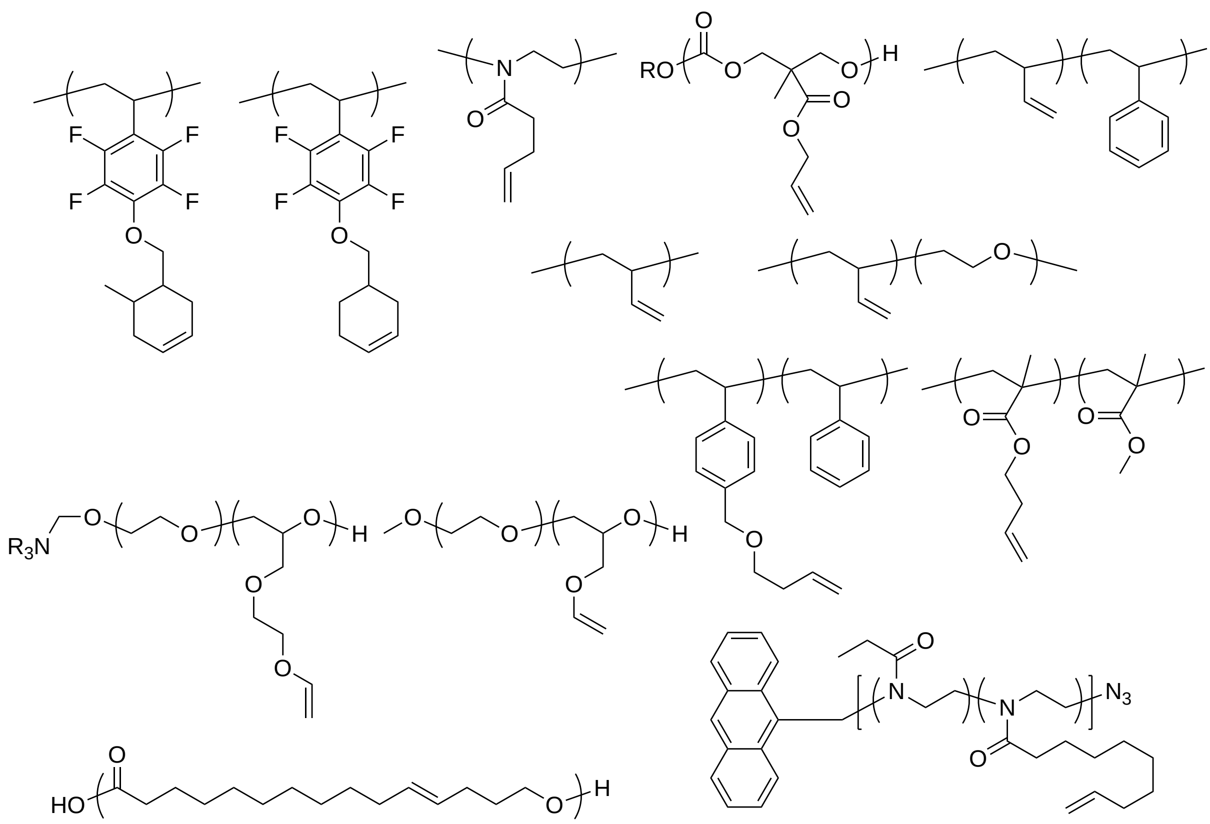

Figure I.7: Representative examples of polymer scaffolds containing alkene functional groups.

(usually dry and under an argon or N_2 atmosphere) such as DMF, THF, chlorinated solvents, dioxane, or toluene.

Overall, the efficiency of this chemistry, lack of by-products and achievement of full conversion with a variety of thiols containing other diverse functional groups make this a powerful tool towards the synthesis of functional polymer. However, the solvent requirements and the apparent need for excess thiol reagents impose the need for a post-functionalisation purification step, which is a major disadvantage when considering high−throughput screening.

3) Scaffolds containing disulfide side-chains

An alternative reactive scaffold for thiols instead of addition to alkene bonds, is the use of disulfide exchange bonding. A key difference between these two chemistries is the reversible nature of the disulfide under redox conditions. This makes this bonding particularly useful for drug release or dynamic systems. Significant examples (**Fig. I.8**) of scaffolds using this chemistry include polymers and co-polymers synthesised via free radical and RAFT polymerisation. In these examples,[79-83] the thiol exchange group is represented by a pyridyldisulfide group. The advantages of this group is that the exchange results in 2−pyridinethione as a by-product, which is both inert and it also has a characteristic UV-Vis absorption that has been successfully used to determine the percentage functionalisation. Co-polymers and ter-polymers containing up to 10% mole of the pyridyldisulfide were functionalised either in DMF or in aqueous buffers. Up to 100% functionalisation has achieved both with small molecules and large peptides, albeit in some instances

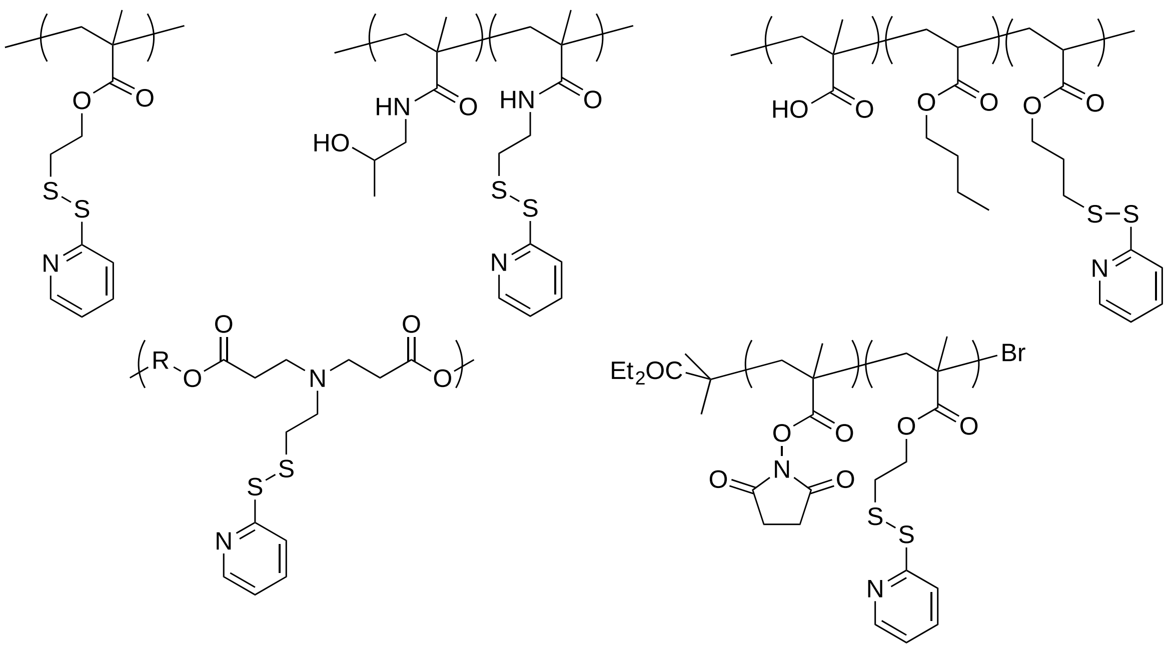

Figure I.8: Representative examples of polymer scaffolds containing disulfide groups for thiol exchange.

excess reagent was used and post-functionalisation purification was carried out as a consequence. One complication of carrying out the functionalisation in water is the hydrolysis of the disulfide bonds, the rate of which increases with increased pH, however water soluble polymers have been shown to be stable in solution for long term at -20 ℃. The extent of functionalisation in aqueous conditions is also highly dependent on the pH with rates of reaction decreasing with decreasing pH (from pH 8 to 3). Functionalisation of water-insoluble homo-polymers in DMF or DMSO have shown that these scaffolds are wide in scope, and suitable towards a diversity of thiols. Generally, when up to 60% of the side-chains are targeted with stoichiometric amounts of thiols, a linear relationship is observed, however beyond that its has been reported that up to two-fold excess reagent is required for full conversion. Generally, values around 90% conversion are reported for a variety of thiols but with clearly significant variations in the rate of reactions (30 min to 14 h) due to increased steric hindrance (i.e. small molecules will react much faster than larger bulkier thiols). Another interesting example of a scaffold, involves the ATRP co-polymerisation of methacrylate monomers containing *N*-hydroxysuccinimide (NHS) and pyridyldisulfide reactive handles. The NHS ester is an active easter, reactive towards amines and orthogonal to the thiol-disulfide exchange chemistry. This co-polymer is a prime example of scaffolds using orthogonal chemistries reactive towards amines and thiols. As a whole, scaffolds using disulfides as the reactive handle have been shown to be wide in scope with high efficiency of functionalisation with a large variety of thiols. Although polymers tend to be water-insoluble, derived products can become soluble depending on the nature of the thiols attached. Co- and ter-polymers have been shown to be stable water soluble scaffolds that can be functionalised under aqueous conditions. A negative aspect is the necessity to use excess reagents to achieve maximum conversion possible (~90%), so post-functionalisation purifications may be required.

4) Scaffolds containing isocyanates side-chains

Isocyanates can be considered as one of the best tools for click chemistry reactions. They are reactive towards a large variety of nucleophiles particularly amines, thiols and alcohols. Polymer scaffolds, in solution or as polymer brushes, with isocyanate side-chains[84-86] (**Fig. I.9**) have been synthesised via radical or RAFT polymerisation, and their functionalisation with nucleophiles has been carefully investigated. It has been found that the reaction with equimolar amounts of primary and secondary amines proceeds quantitatively and rapidly, a feature observed also for thiols but in the presence of a base catalyst. The reaction with alcohols has been shown to be slower and requires dibutyltin dilaureate as a catalyst, however, quantitative functionalisation was reported.[84] Because of the different alcohol/thiol catalyst conditions, selectivity can be tuned with regards to bifunctional reagents. Aminoalcohols will react selectively via the amine functional group due to its increased nucleophilicity. Selectivity in mercaptoalcohols can adjusted by increasing the amount of dibutyltin dilaureate to favour the reaction via the alcohol group. Under base catalysed conditions the reaction proceeds rapidly via the thiol group. Key advantages of using isocyanates as reactive handles is the lack of byproducts formed and quantitative functionalisation with equimolar amounts of reagents. This means that post-functionalisation purification is required only for removal of the dibutyltin dilaureate catalyst when functionalisation with alcohol is desired, or the

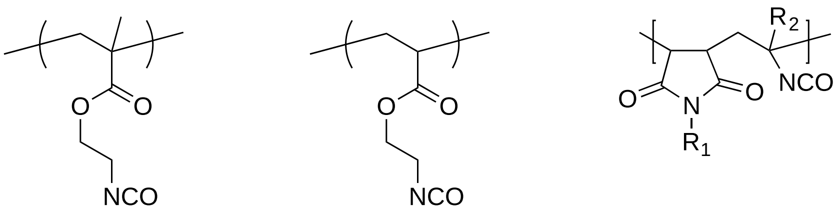

Figure I.9: Representative examples of polymer scaffolds containing isocyanate functional groups.

base catalyst when functionalisation via thiols is carried out (although this should be synthetically much easier, or not required at all). The main negative aspects of isocyanates scaffolds in the context of high-throughput testing for biomedical applications is the inability to carry out the functionalisation in water. Water itself reacts with isocyanates to release carbon dioxide and form a primary amine. Reported functionalisations have been carried out in chloroform, DMF or THF, which are not biocompatible and need to be removed, however, perhaps functionalisations in DMSO would be a suitable solution in the future to allow in-situ functionalisation and biological testing without purification and solvent removal.

5) Scaffolds containing alkynes or azide side-chains

The copper(I) catalysed azide-alkyne cycloaddition to produce a 1,2,3-triazole has been widely incorporated into many polymer scaffolds (**Fig. I.10**), ranging from methacrylates via ATRP[87,88] or RAFT polymerisation,[89,90] to polycarbonates,[91,92] glycopolymers,[93,94] polymer brushes[88] and modified cyclodextrins.[95] This modular reaction has been shown to be generally quantitative, and can be carried out in a variety of solvents (e.g. THF, DMF, DMSO) including aqueous conditions, which is a key advantage. There are however several drawbacks that disqualify these systems according to the parameters desired for an optimum system. First, and most importantly, the azide-alkyne reaction is catalysed by copper(I) catalysts. Copper ions are known for their cytotoxicity[96] and as such would require thorough removal from the system before the polymers can be tested. Furthermore, although many examples have shown the reaction to be wide in scope and quantitative, usually the reactions have been carried out with excess reagent (1.1 - 2.0 equiv.), which enforces the requirement for post-functionalisation purification.

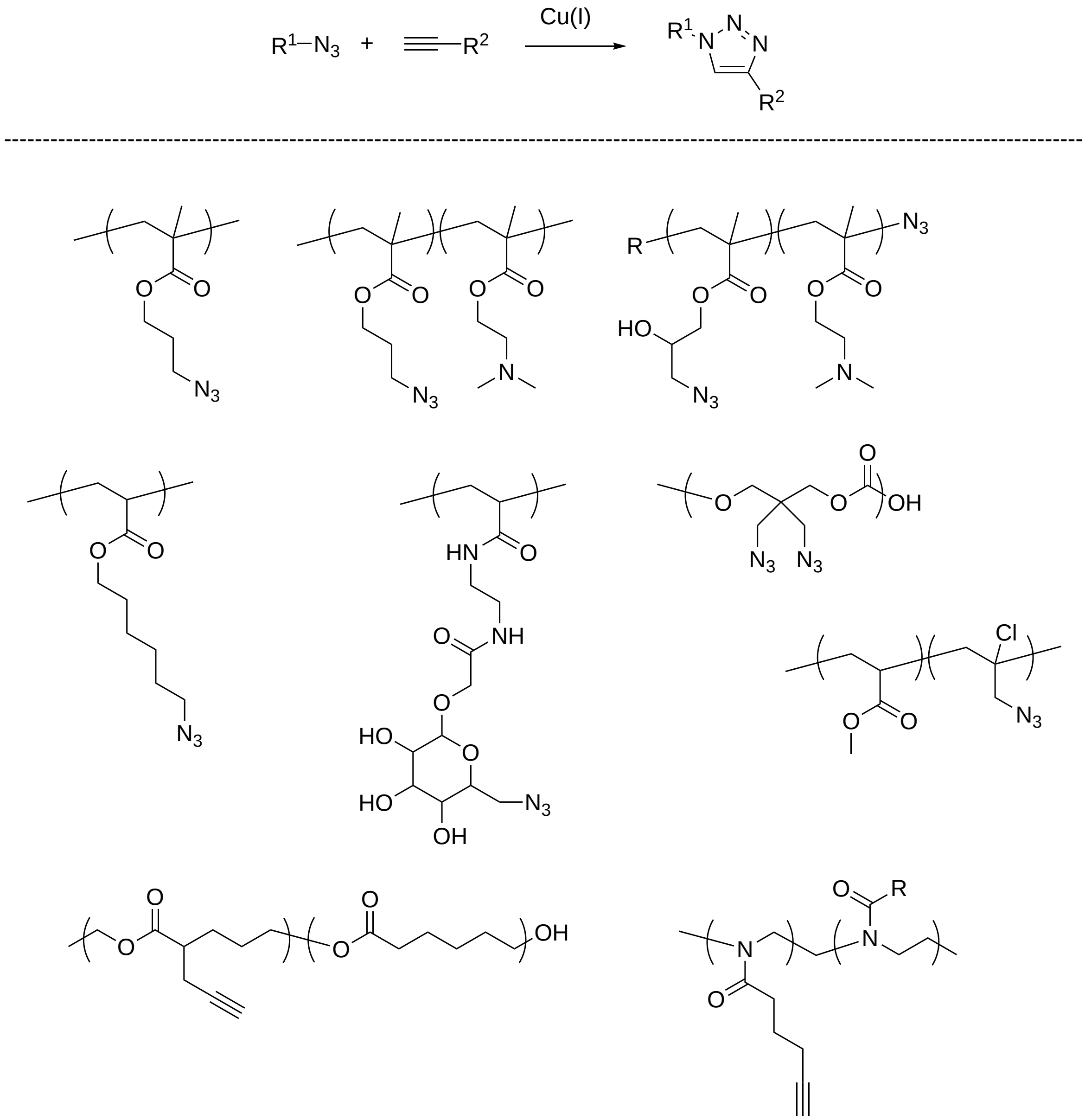

Figure I.10: Copper(I) catalysed azide-alkyne cycloaddition (top). Representative examples of polymer scaffolds containing azide or alkyne functional groups (bottom).

6) Scaffolds containing activated ester side-chains

Polymers containing activated ester side-chains have featured prominently in the research on polymeric scaffolds. This is in part due to the high control and efficiency in polymerising monomers containing activated ester side-chains such as (but not limited to) NHS,[97-100] fluorophenyl[101-106] and nitrophenyl-groups[107,108] (**Fig. I. 11**). The reactivity of activated esters scaffolds such as acrylates and methacrylates obtained via ATRP or RAFT polymerisation, or norborenes from ROMP, with amines has been throughly investigated. It has been shown that both the steric bulk and the reactivity of the amine group play an important role in the percentage conversion. Primary amines, such as *tert*-butyl amine, benzyl amine and cyclohexylamine were shown to react quantitatively with a tetrafluorophenyl methacrylate scaffold (2 equiv. amine), however aromatic amines were shown to be completely unreactive. The reactivity of pentaflurophenyl methacrylate with a library of nine water soluble amines with different steric bulk was investigated by Gibson *et al*.[106] to show conversions between 60-80% when 2 equiv. amine was used. Complete conversion has been reported by Hu *et al*.[99] in the reaction between poly(*N*-acryloxysuccinimide) and 0.2 equiv. galactosamine followed by 1.6 equiv. ethanolamine. Similarly pegylated poly(*N*-acryloxysuccinimide) copolymers were fully functionalised with mixtures of amines towards forming complexes with plasmid DNA and functional polymers. The functionalisation reactions were commonly carried out in dry solvents (e.g. THF, DMF or DMSO) under an inert atmosphere at 50 ℃. These conditions are required to minimise ester hydrolysis. Under open air, ~3% hydrolysis was observed in DMSO at 50 ℃ for poly(*N*-acryloxysuccinimide), while complete hydrolysis was reported for poly(*p*-nitrophenyl methacrylate) under reflux for 24 hours with 4 equiv. hydroxide.

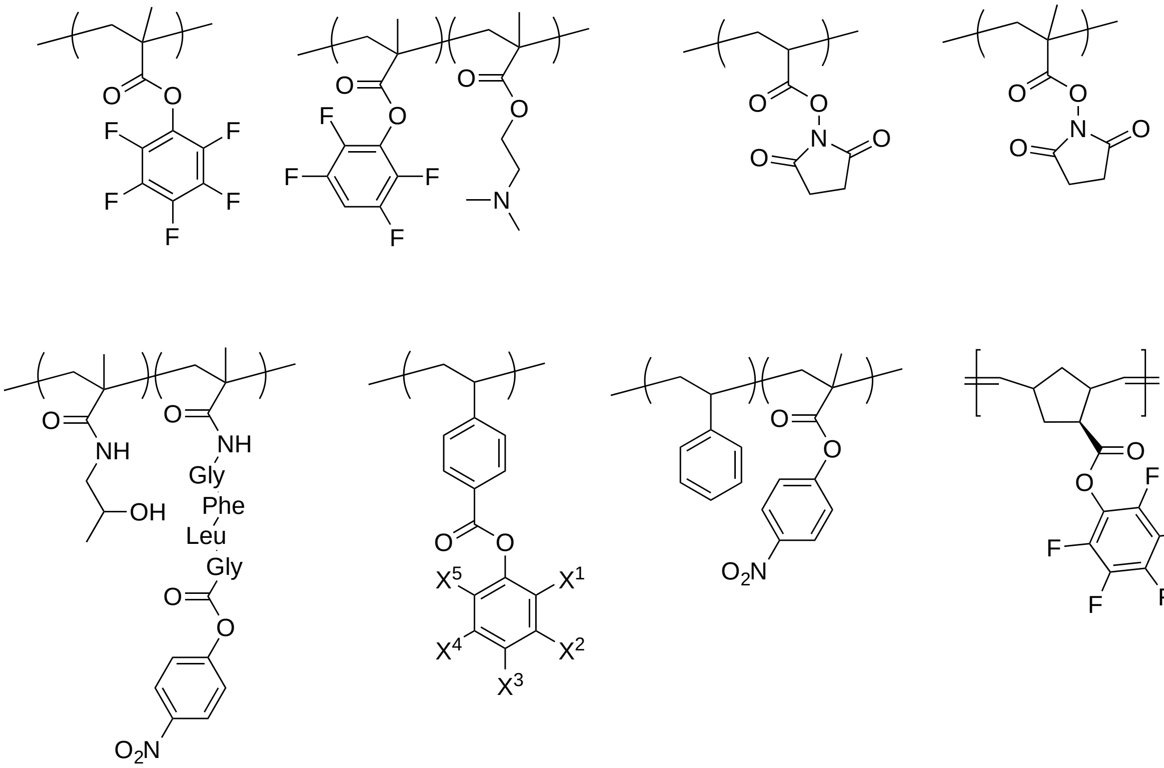

Figure I.11: Representative examples of polymer scaffolds containing an active ester side-chain.

The rate of hydrolysis was shown to increase with increased pH (7.4 to 8.5) but overall aminolysis is normally faster than hydrolysis at the reported pH range. With regards to post-functionalisation purification, the requirement of excess amine and the release of alcohols as by-products, as well as the use of non-aqueous solvents, suggests that purification would be required before the biological testing could be carried out.

7) Scaffolds containing aldehyde or ketone side-chains

Aldehydes and ketones can readily react with amines, hydrazines and hydroxylamines to form imines, hydrazones and oximes.[109] These are reversible and pH dependent reactions, which make them ideal for dynamic systems and delivery applications. Imines are labile under aqueous conditions but hydrazones and oximes are hydrolytically stable between pH 5-7 and pH 2-7 with rapid decomposition occurring above pH 9.[110,111] Polymers containing aldehyde or ketone side-chains (**Fig. I.12**) have been synthesised via RAFT, ATRP or ROMP and their functionalisation properties have been investigated.[107,112-123] Functionalisation of benzylaldehydes with hydroxylamines and hydrazides has been shown to be quantitative in THF at 25 ℃ with an excess of reagent. Fulton *et al.*[113] showed the dynamic character of the system by reacting a benzaldehyde scaffold with short, medium and long alkyl chain hydrazides and showing that a mixture of two functional polymers re-equilibrates into a single polymer species by interchanging hydrazone bonds between the scaffolds. Co- and ter- polymer scaffolds containing aliphatic aldehyde/ketone side-chains and other chemo-selective handles such as azide and maleimides have been successfully developed[115,123] for orthogonal multi-functionalisation. Quantitative yields have been observed in the reaction between these scaffolds and different hydrazides in DMF or THF, at different temperatures but again with excess reagents. Poly(methyl vinyl ketone) has been functionalised with oligosaccharides under aqueous conditions.[116] Although long reactions times (96 hours), relatively high temperatures (95 ℃) and 2-3 equiv. modified oligosaccharides were used, quantitative functionalisation was achieved. The reaction between aldehyde/ketones and amines, hydrazines, hydrazides or hydroxylamines produces water as a by-product, which is a great advantage in terms of requirement for post-functionalisation purification. However, most scaffolds explored are not soluble in water. Very few commercially available hydrazides or hydroxylamines with multiple functional groups exist, limiting the rapid screening of large libraries of functional

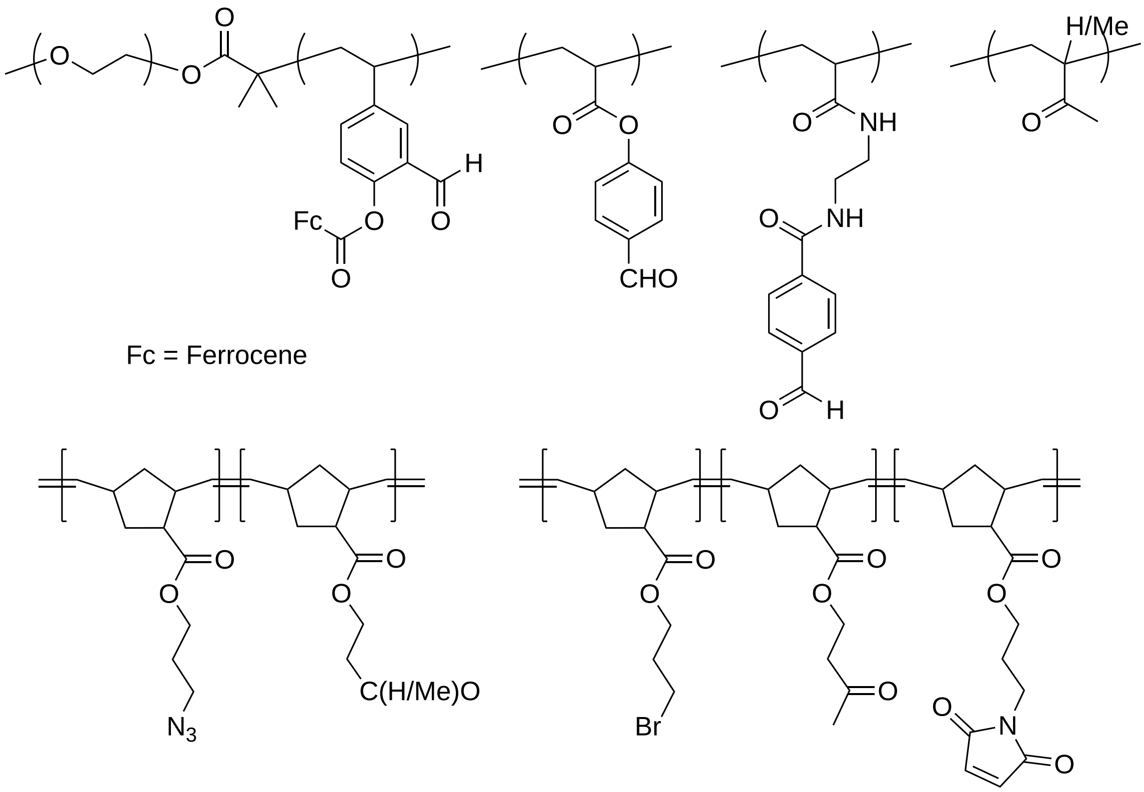

Figure I.12: Representative examples of polymer scaffolds containing aldehyde or ketone functional groups.

polymers. Whilst amines can be widely used, the labile nature of imines under aqueous conditions suggests they are not ideal for biological applications.

8) Scaffolds containing hydrazide or hydroxylamine side-chains

The advantages of the previously described system (i.e. quantitative yields, water by-product, reactivity in water and pH dependent stability under aqueous conditions) can be maintained and the disadvantages of aldehyde/ketone containing polymeric scaffolds (i.e. scaffold insolubility in water, a general lack of commercially available hydrazide, hydrazine or hydroxylamine building blocks to use for functionalisation) can be solved by reversing the chemo-selective handle such that a polyhydrazide or a polyhydroxylamine scaffold is used instead. The water solubility of these systems is expected to be greatly enhanced (dependent to a degree on the backbone involved) due to the favourable H-bonding interactions possible when side-chains rich in N and O atoms are present. Furthermore, aldehyde/ketone building blocks are widely commercially available and a key aspect is that usually, aldehyde and ketones are less toxic and easier to handle compared to their amine equivalents that would be used with many of the aforementioned scaffolds. Scaffolds containing hydroxylamine (**Fig. I.13**) side-chains have been synthesised via RAFT in the form of poly(*O*-(4-vinylbenzyl)-hydroxylamine)[124] via a protected phthalamide precursor. Functionalisation studies were carried out with a few aldehydes and ketones in THF. Near-quantitative conversions have been observed with 1 equiv. reagent, while with 0.5 equiv. conversions of 98% are reported. Importantly, conversions were not improved upon using an excess of reagent (2 equiv.) suggesting a limitation based on steric hindrance. Reactions were carried out at 60 ℃ with maximum conversion obtained in a 3-5 hour timeframe, but the same conversion could be achieved at room temperature albeit after 24 hours. The incorporation of hydrazide side-chains into polymers towards libraries of functionalised polymers had been relatively little explored. Bertozzi's group synthesised poly(acryloyl hydrazide) via the RAFT polymerisation of acetoxime acrylate followed by reaction with excess hydrazine.[125] The scaffold was successfully functionalised with eighteen saccharides of different complexities to form glycopolymers for microarray applications. The coupling reaction was carried out in an acetate buffer at 50 ℃ with 1.1 equiv. of glycan, with most yields good and above after 24 hours. Improved yields were reported only in a minority of cases when 2.0 equiv. of glycan was used. The stability of the glycopolymers to hydrolysis was evaluated at pH values above 7. More recently poly(acryloyl hydrazide) was synthesised from poly(methyl acrylate)[126] and its applicability towards

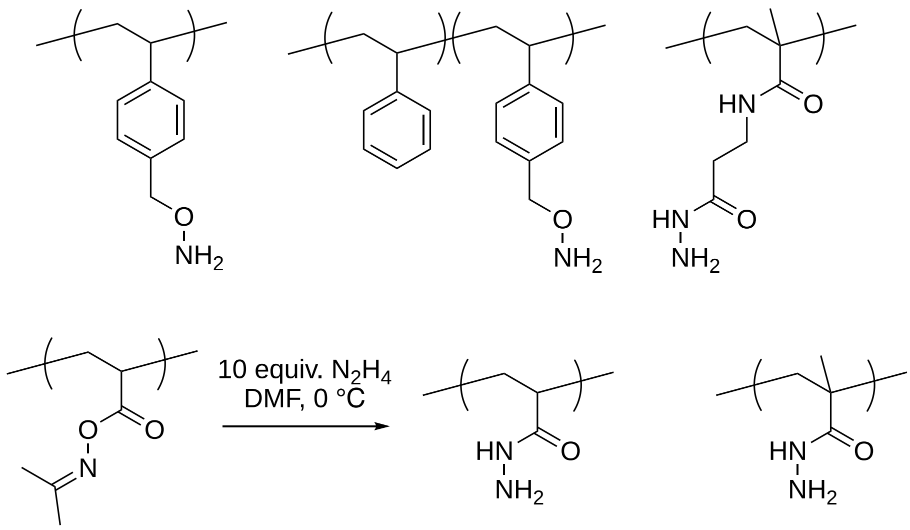

Figure I.13: Representative examples of polymer scaffolds containing *O*–hydroxylamine or hydrazide side-chains.

a wide-range of applications was shown using different hydrazide click-chemistries. The reaction between an aldehyde containing dye and the scaffold at a ratio of 1:75 (CHO:CONH-NH_2) was probed, which showed reaction completion in under 10 minutes in aqueous conditions. Experiments with 2-hydroxy-1-napthaldehyde (0.5 equiv.) showed complete conversion after overnight reflux in a mixture of MeOH:H_2O (1:15). The reversibility of the reaction was investigated at pH 5.0 at 37 ℃ and revealed 75% release of the aldehyde over an 11 days period. This evidences both that the functional polymer is stable to hydrolysis in a pH dependent manner, enough for immediate use, testing and analysis, but also labile enough for drug-release or dynamic applications. In the past few months, the direct synthesis via RAFT polymerisation of poly(methacryloyl hydrazide) and poly(2-methacrylamidoethyl carbohydrazide) in aqueous conditions has been achieved with good control.[127] This has been the first reported synthesis of polyhydrazides that didn't require protecting groups, as in the past it was observed that the hydrazide side-chains attack and destroy the CTA. As shown by Bertozzi *et al.*[125] that poly(acryloyl hydrazide) can be functionalised with a diversity of saccharides with different conjugation efficiencies, however studies into the functionalisation of such systems with a wide array of aldehydes have not been identified.

Objectives

Considering the properties that are believed to be desirable by the author, for a scaffold that can be wide in scope and can be employed rapidly and easily towards functional polymers for biomedical applications, polymers incorporating hydroxylamine or hydrazide side-chains can be argued to be the candidates with most potential. Firstly, the available evidence shows that these scaffolds can be both soluble and inert in water. Secondly the reaction between these functional groups and aldehyde or ketones produces water as a by-product. Thirdly, functionalisation studies have shown that the coupling reaction is overall high yielding or near-quantitative when equimolar amounts of reagents are used. There is no requirement for complex catalyst aside from the addition of an acid catalyst that could be easily neutralised. These properties suggest that these scaffolds could be functionalised and tested for biomedical application without the need for any post-functionalisation purification. However, due to the non-quantitative nature of the reaction, additional control studies may be warranted to amount for the effects of free reagents in solution (i.e. unconsumed aldehyde/ketone). Considering the reversible and dynamic character of the hydrazone and oxime bonds, such control studies would also acknowledge the effects of released molecules *in situ*.

Although, the discussion was condensed on the non-aldol carbonyl click-chemistry it is worth mentioning that hydrazides and hydroxylamines can be used in the other click-chemistry type reactions where amines are used as chemical modulators (e.g. reaction with epoxides, isocyanates, active esters) to form non-reversible covalent bonds. This could be potentially useful, if a permanent chemical modification (e.g. attaching a dye or a receptor) is required, while still being able to synthesise subsequent combinatorial libraries.

The main differences between hydrazines, hydroxylamines and hydrazides are their basicity and the stability to hydrolysis of the resulting hydrazones and oximes. The basicity decreases in order, from hydrazines to hydroxylamines to hydrazides with some reported pKa values for protonated hydrazines (~ pKa 8), hydroxylamines (~pKa 6) and hydrazides (~ pKa 3.5).[128-130] This would suggest that at neutral pH a hydrazine scaffold will be strongly protonated, a hydroxylamine scaffold would be less than 50% protonated while a hydrazide scaffold would be only weekly protonated. It is well established that cationic polymers are generally more cytotoxic than neutral polymers,[15,131-133] and it is believed in the context of biological applications (e.g. mimics of antimicrobial peptides) that a non-cytotoxic scaffold is preferred. As such, polyhydrazides are potentially the better candidates out of the three categories with regards to decreased cytotoxicity. In terms of stability to hydrolysis, oximes are more stable over a larger pH range (pH 2-7) compared to the smaller range (pH 5-7) for hydrazones, but both are labile at basic pH (> pH 9). The smaller pH stability range in hydrazones would suggest that scaffolds based on this type of bonding would have a more dynamic character, and would open the avenue for template driven combinatorial libraries, as well as applications of targeted delivery (e.g. drugs, siRNA) based on pH differences (e.g. acidic pH in tumour cells). Given the properties described above, it is the author’s belief that polymeric scaffolds containing hydrazide side-chains for post-polymerisation functionalisation with aldehydes offer great promise for the discovery of functional polymers for biological applications.

In this research the aims were to synthesise a set of polyhydrazide scaffolds, investigate the functionalisation of these polymers with aldehydes and evaluate the performance of libraries of functional polymers as carriers for siRNA delivery.

The initial target was to develop a direct synthetic route of poly(acryloyl hydrazide) via RAFT polymerisation (see **Chapter 1**), ideally in aqueous conditions, taking advantage of the good track of the polymerisation of polyacrylamides using RAFT. Although poly(acryloyl hydrazide) had been synthesised previously by Bertozzi *et al.*[125] the reported route involved the use of an oxime monomer, transformed post–polymerisation into a hydrazide using rather harsh conditions in both steps (i.e. dioxane, hydrazine).

Following on, the metal catalysed polymerisations of alkynes[134] was pursued to synthesise poly(acetylene hydrazide) and poly(phenylacetylene hydrazide) (see **Chapter 2**) to exploit their intrinsic helicity. Helical scaffolds would be of particular value for two reasons. Firstly, the functionalisation of such structures is predicted to be more efficient on entropic grounds compared to linear polymer scaffolds, which need to surrender considerable degrees of freedom during binding. Polyacetylene backbones have inherently less conformational freedom and should exhibit better template binding. Secondly, many naturally occurring biologically interesting motifs (e.g. antimicrobial peptides) exhibit helical conformations with segregated hydrophobic and hydrophilic faces.[135] Libraries of synthetic mimics of such molecules via functional polymers could be accessed rapidly starting from a helical scaffold.

Finally, having analysed the functionalisation of these different scaffolds, the author pursued to prove the usefulness of poly(acryloyl hydrazide) to synthesise and identify non-toxic amphiphilic polymers that can bind siRNA, transport the cargo across membranes and release the cargo inside cells (see **Chapter 3**).

References

1. J. O'Neill, The Review on Antimicrobial Resistance. 2014.
2. R. C. Mulligan, *Science*, 1993, **260**, 926–932.
3. Y. Ramgopal, D. Mondal, S. S. Venkatraman, W. T. Godbey and G. Y. Yuen, *J. Biomed. Mater. Res. Part B Appl. Biomater.*, 2009, **89**, 439–447.
4. P. M. Klein and E. Wagner, *Antioxid. Redox Signal.*, 2014, **21**, 804–817.
5. M. B. Dreifke, A. A. Jayasuriya and A. C. Jayasuriya, *Mater. Sci. Eng. C*, 2015, **48**, 651–662.
6. J.-P. Behr, *Acc. Chem. Res.*, 2012, **45**, 980–984.
7. H. Shen, T. Sun and M. Ferrari, *Cancer Gene Ther.*, 2012, **19**, 367–373.
8. S. Monteagudo, F. C. Pérez-Martínez, M. D. Pérez-Carrión, J. Guerra, S. Merino, M. P. Sánchez-Verdú and V. Ceña, *Nanomedicine*, 2012, **7**, 493–506.
9. J. C. Burnett and J. J. Rossi, *Chem. Biol.*, 2012, **19**, 60–71.
10. E.-R. Kenawy, S. D. Worley and R. Broughton, *Biomacromolecules*, 2007, **8**, 1359–1384.
11. K. A. Brogden, *Nature Rev. Microbiol.*, 2005, **3**, 238–250.
12. K. Kuroda and W. F. DeGrado, *J. Am. Chem. Soc.*, 2005, **127**, 4128–4129.
13. L. Arnt, J. R. Rennie, S. Linser, R. Willumeit and G. N. Tew, *J. Phys. Chem. B*, 2006, **110**, 3527–3532.
14. K. Nusslein, *Microbiology*, 2006, **152**, 1913–1918.
15. K. Fukushima, S. Liu, H. Wu, A. C. Engler, D. J. Coady, H. Maune, J. Pitera, A. Nelson, N. Wiradharma, S. Venkataraman, Y. Huang, W. Fan, J. Y. Ying, Y. Y. Yang and J. L. Hedrick, *Nat. Commun.*, 2013, **4**, 1–9.
16. G. N. Tew, D. Liu, B. Chen, R. J. Doerksen, J. Kaplan, P. J. Carroll, M. L. Klein and W. F. DeGrado, *Proc. Natl. Acad. Sci. U.S.A.*, 2002, **99**, 5110–5114.
17. R. Tejero, D. López, F. López-Fabal, J. L. Gómez-Garcés and M. Fernández-García, *Polym. Chem.*, 2015, **6**, 3449–3459.
18. A. C. Engler, J. P. K. Tan, Z. Y. Ong, D. J. Coady, V. W. L. Ng, Y. Y. Yang and J. L. Hedrick, *Biomacromolecules*, 2013, **14**, 4331–4339.
19. A. M. Krachler and K. Orth, *Virulence*, 2014, **4**, 284–294.
20. M. W. Jones, L. Otten, S. J. Richards, R. Lowery, D. J. Phillips, D. M. Haddleton and M. I. Gibson, *Chem. Sci.*, 2014, **5**, 1611–1616.
21. M. Hartmann, H. Papavlassopoulos, V. Chandrasekaran, C. Grabosch, F. Beiroth, T. K. Lindhorst and C. Röhl, *FEBS Lett.*, 2012, **586**, 1459–1465.
22. P. Klemm, R. M. Vejborg and V. Hancock, *Appl. Microbiol. Biotechnol.*, 2010, **88**, 451–459.
23. N. Sharon, *Biochim. Biophys. Acta,* 2006, **1760**, 527–537.
24. K. Matyjaszewski and J. Spanswick, *Mater. Today*, 2005, **8**, 26–33.
25. C. J. Hawker, *Acc. Chem. Res.*, 1997, **30**, 373–382.

26. V. Mishra and R. Kumar, *J. Sci. Res.*, 2012, **56**, 141–176.
27. M. F. Ilker, K. Nüsslein, G. N. Tew and E. B. Coughlin, *J. Am. Chem. Soc.*, 2004, **126**, 15870–15875.
28. D. Liu, S. Choi, B. Chen, R. J. Doerksen, D. J. Clements, J. D. Winkler, M. L. Klein and W. F. DeGrado, *Angew. Chem. Int. Ed.*, 2004, **43**, 1158–1162.
29. A. H. E. Müller and K. Matyjaszewski, *Controlled and Living Polymerizations: From Mechanisms to Applications, Wiley-VCH*, 2010.
30. L. E. N. Allan, M. R. Perry and M. P. Shaver, *Prog. Polym. Sci.*, 2012, **37**, 127–156.
31. N. V. Tsarevsky and K. Matyjaszewski, *Fundamentals of Controlled/Living Radical Polymerization, Chapter 8, RSC*, 2013, 287–357.
32. K. Matyjaszewski, *Controlled Radical Polymerization, Chapter 1, Am. Chem. Soc.*, 2009, **685**, 2–30.
33. H. C. Kolb, M. G. Finn and K. B. Sharpless, *Angew. Chem. Int. Ed.*, 2001, **40**, 2004-2021
34. R. K. Iha, K. L. Wooley, A. M. Nystro m, D. J. Burke, M. J. Kade and C. J. Hawker, *Chem. Rev.*, 2009, **109**, 5620–5686.
35. C. W. Bielawski and R. H. Grubbs, *Prog. Polym. Sci.*, 2007, **32**, 1–29.
36. H. Clavier, K. Grela, A. Kirschning, M. Mauduit and S. P. Nolan, *Angew. Chem. Int. Ed.*, 2007, **46**, 6786–6801.
37. S. R. S. Ting, G. Chen and M. H. Stenzel, *Polym. Chem.*, 2010, **1**, 1392–21.
38. S. Sutthasupa, M. Shiotsuki and F. Sanda, *Polym. J.*, 2010, **42**, 905–915.
39. D. Le, G. Morandi, S. Legoupy, S. Pascual, V. Montembault and L. Fontaine, *Eur. Polym J*, 2013, **49**, 972–983.
40. O. Nuyken and S. Pask, *Polymers*, 2013, **5**, 361–403.
41. C. Boyer, N. A. Corrigan, K. Jung, D. Nguyen, T.-K. Nguyen, N. N. M. Adnan, S. Oliver, S. Shanmugam and J. Yeow, *Chem. Rev.*, 2016, **116**, 1803–1949.
42. C. M. Hui, J. Pietrasik, M. Schmitt, C. Mahoney, J. Choi, M. R. Bockstaller and K. Matyjaszewski, *Chem. Mater.*, 2014, **26**, 745–762.
43. V. Coessens, T. Pintauer and K. Matyjaszewski, *Prog. Polym. Sci*, 2001, **26**, 337–377.
44. J. L. Hedrick, M. Trolls s, C. J. Hawker, B. Atthoff, H. Claesson, A. Heise, R. D. Miller, *Macromolecules*, 1998, **31**, 8691–8705.
45. T. E. Patten and K. Matyjaszewski, *Adv. Mater.*, 1998, **10**, 901–915.
46. W. A. Braunecker and K. Matyjaszewski, *Prog. Polym. Sci*, 2007, **32**, 93–146.
47. D. J. Keddie, *Chem. Soc. Rev.*, 2014, **43**, 496–505.
48. H. Willcock and R. K. O'Reilly, *Polym. Chem.*, 2010, **1**, 149–157.
49. A. B. Lowe and C. L. McCormick, *Prog. Polym. Sci.*, 2007, **32**, 283-351.
50. S. Perrier and P. Takolpuckdee, *J. Polym. Sci. A Polym. Chem.*, 2005, **43**, 5347–5393.

51. G. Moad, E. Rizzardo and S. H. Thang, *Aust. J. Chem.*, 2012, **65**, 985–1076.
52. C. L. McCormick and A. B. Lowe, *Acc. Chem. Res.*, 2004, **37**, 312–325.
53. A. Goto and T. Fukuda, *Prog. Polym. Sci*,, 2004, **29**, 329–385.
54. L. Arnt, K. N sslein and G. N. Tew, *J. Polym. Sci. A Polym. Chem.*, 2004, **42**, 3860–3864.
55. K. Lienkamp and G. N. Tew, *Chem. Eur. J.*, 2009, **15**, 11784–11800.
56. H. C. Kolb and K. B. Sharpless, *Drug Discov. Today*, 2003, **8**, 1128–1137.
57. M. A. Gauthier, M. I. Gibson and H.-A. Klok, *Angew. Chem. Int. Ed.*, 2008, **48**, 48–58.
58. K. A. Günay, P. Theato and H.-A. Klok, *Functional Polymers by Post-Polymerization Modification: History of Post-Polymerisation Modification, Chapter 1, Wiley-VCH*, 2013, 1–44.
59. J. M. J. Frechet, G. D. Darling, S. Itsuno, P.-Z. Lu, M. V. de Meftahi and W. A. Rolls Jr, *Pure Appl. Chem.*, 1987, **60**, 353–364.
60. E. Elacqua, D. S. Lye and M. Weck, *Acc. Chem. Res.*, 2014, **47**, 2405–2416.
61. M. S. Shoichet, *Macromolecules*, 2010, **43**, 581–591.
62. P. Theato and H.-A. Klok, *Functional Polymers by Post-Polymerization Modification, Wiley-VCH,* 2013.
63. J. Romulus, J. T. Henssler and M. Weck, *Macromolecules*, 2014, **47**, 5437–5449.
64. V. Tsyalkovsky, V. Klep, K. Ramaratnam, R. Lupitskyy, S. Minko and I. Luzinov, *Chem. Mater.*, 2008, **20**, 317–325.
65. S. Edmondson and W. T. S. Huck, *J. Mater. Chem.*, 2004, **14**, 730–734.
66. M. M. Nasef, P. Sithambaranathan, A. Ahmad and E. Abouzari-lotf, *Radiat. Phys. and Chem.*, 2017, **134**, 56–61.
67. N. Ezaki, Y. Watanabe and H. Mori, *J. Appl. Polym. Sci.*, 2017, **134**.
68. R. G. Jones, S. Yoon and Y. Nagasaki, *Polymer*, 1999, **40**, 2411–2418.
69. J. Justynska, Z. Hordyjewicz and H. Schlaad, *Polymer*, 2005, **46**, 12057–12064.
70. A. Gress, A. Antje Völkel and H. Schlaad, *Macromolecules*, 2007, **40**, 7928–7933.
71. L. M. Campos, K. L. Killops, R. Sakai, J. M. J. Paulusse, D. Damiron, E. Drockenmuller, B. W. Messmore and C. J. Hawker, *Macromolecules*, 2008, **41**, 7063–7070.
72. N. ten Brummelhuis, C. Diehl and H. Schlaad, *Macromolecules*, 2008, **41**, 9946–9947.
73. S. Tempelaar, L. Mespouille, P. Dubois and A. P. Dove, *Macromolecules*, 2011, **44**, 2084–2091.
74. B. Obermeier and H. Frey, *Bioconjugate Chem.*, 2011, **22**, 436–444.
75. C. Mangold, C. Dingels, B. Obermeier, H. Frey and F. Wurm, *Macromolecules*, 2011, **44**, 6326–6334.

76. K. Kempe, R. Hoogenboom, M. Jaeger and U. S. Schubert, *Macromolecules*, 2011, **44**, 6424–6432.
77. J. Ma, C. Cheng and K. L. Wooley, *Macromolecules*, 2009, **42**, 1565–1573.
78. Z. Ates, P. D. Thornton and A. Heise, *Polym. Chem.*, 2011, **2**, 309–312.
79. V. Bulmus, *J. Control. Release*, 2003, **93**, 105–120.
80. Laixin Wang, A. Jakob Kristensen and D. E. Ruffner, *Bioconjugate Chem.*, 1998, **9**, 749–757.
81. G. T. Zugates, D. G. Anderson, S. R. Little, I. E. B. Lawhorn and R. Langer, *J. Am. Chem. Soc.*, 2006, **128**, 12726–12734.
82. S. Ghosh, S. Basu and S. Thayumanavan, *Macromolecules*, 2006, **39**, 5595–5597.
83. L. Wong, C. Boyer, Z. Jia, H. M. Zareie, T. P. Davis and V. Bulmus, *Biomacromolecules*, 2008, **9**, 1934–1944.
84. J. D. Flores, J. Shin, C. E. Hoyle and C. L. McCormick, *Polym. Chem.*, 2010, **1**, 213–220.
85. R. M. Hensarling, S. B. Rahane, A. P. LeBlanc, B. J. Sparks, E. M. White, J. Locklin and D. L. Patton, *Polym. Chem.*, 2011, **2**, 88–90.
86. M. Dörr, R. Zentel, R. Dietrich, K. Meerholz, C. Bräuchle, J. Wichern, S. Zippel and P. Boldt, *Macromolecules*, 1998, **31**, 1454–1465.
87. Brent S Sumerlin, Nicolay V Tsarevsky, Guillaume Louche, A. Robert Y Lee and K. Matyjaszewski, *Macromolecules*, 2005, **38**, 7540–7545.
88. Nicolay V Tsarevsky, A. Sidi A Bencherif and K. Matyjaszewski, *Macromolecules*, 2007, **40**, 796–803.
89. Y. Li, J. Yang and B. C. Benicewicz, *J. Polym. Sci. A Polym. Chem.*, 2007, **45**, 4300–4308.
90. G. Li, H. Wang, H. Zheng and R. Bai, *J. Polym. Sci. A Polym. Chem.*, 2010, **48**, 1348–1356.
91. X. Zhang, Z. Zhong and R. Zhuo, *Macromolecules*, 2011, **44**, 1755–1759.
92. J. Xu, F. Prifti and J. Song, *Macromolecules*, 2011, **44**, 2660–2667.
93. O. Abdelkader, S. Moebs Sanchez, Y. Queneau, J. Bernard and E. Fleury, *J. Polym. Sci. A Polym. Chem.*, 2011, **49**, 1309–1318.
94. X. Zhang, X. Lian, L. Liu, J. Zhang and H. Zhao, *Macromolecules*, 2008, **41**, 7863–7869.
95. O. Jazkewitsch, A. Mondrzyk, R. Staffel and H. Ritter, *Macromolecules*, 2011, **44**, 1365–1371.
96. G. Nordberg, B. Sandström, G. Becking and R. A. Goyer, *J. Trace Elem. Exp. Med.*, 2001, **14**, 261–273.
97. P. Ferruti, A. Bettelli and A. Feré, *Polymer*, 1972, **13**, 462–464.
98. E. Pedone, X. Li, N. Koseva, O. Alpar and S. Brocchini, *J. Mater. Chem.*, 2003, **13**, 2825–2837.

99. Z. Hu, Y. Liu, C. Hong and C. Pan, *J. Appl. Polym. Sci.*, 2005, **98**, 189–194.
100. H. Murata, O. Prucker and J. Rühe, *Macromolecules*, 2007, **40**, 5497–5503.
101. M. Eberhardt, R. Mruk, R. Zentel and P. Theato, *Eur. Polym. J.*, 2005, **41**, 1569–1575.
102. N. Vogel and P. Theato, *Macromol. Symp.*, 2007, **249-250**, 383–391.
103. K. Nilles and P. Theato, *Eur. Polym. J.*, 2007, **43**, 2901–2912.
104. K. Nilles and P. Theato, *J. Polym. Sci. A Polym. Chem.*, 2010, **48**, 3683–3692.
105. X. S. Li, L. H. Gan and Y. Y. Gan, *Polymer*, 2008, **49**, 1879–1884.
106. M. I. Gibson, E. Fröhlich and H.-A. Klok, *J. Polym. Sci. A Polym. Chem.*, 2009, **47**, 4332–4345.
107. J. Hwang, R. C. Li and H. D. Maynard, *J. Control. Release*, 2007, **122**, 279–286.
108. Y. Liu, L. Wang and C. Pan, *Macromolecules*, 1999, **32**, 8301–8305.
109. J. P. Adams, *J. Chem. Soc., Perkin Trans. 1*, 2000, 125–139.
110. J. Shao and J. P. Tam, *J. Am. Chem. Soc.*, 1995.
111. K. Rose, *J. Am. Chem. Soc.*, 1994, **116**, 30–33.
112. S. Mukherjee, A. P. Bapat, M. R. Hill and B. S. Sumerlin, *Polym. Chem.*, 2014.
113. D. A. Fulton, *Org. Lett.*, 2008, **10**, 3291–3294.
114. R. M. Arnold, D. L. Patton, V. V. Popik and J. Locklin, *Acc. Chem. Res.*, 2014, **47**, 2999–3008.
115. S. K. Yang and M. Weck, *Soft Matter*, 2009, **5**, 582–585.
116. D. Rabuka, R. Parthasarathy, G. S. Lee, X. Chen, J. T. Groves and C. R. Bertozzi, *J. Am. Chem. Soc.*, 2007, **129**, 5462–5471.
117. Z.-P. Xiao, Z.-H. Cai, H. Liang and J. Lu, *J. Mater. Chem.*, 2010, **20**, 8375–8381.
118. R. C. Li, R. M. Broyer and H. D. Maynard, *J. Polym. Sci. A Polym. Chem.*, 2006, **44**, 5004–5013.
119. N. Boehnke, C. Cam, E. Bat, T. Segura and H. D. Maynard, *Biomacromolecules*, 2015, **16**, 2101–2108.
120. G. N. Grover, R. L. Braden and K. L. Christman, *Adv. Mater.*, 2013, **25**, 2937–2942.
121. C. S. Mahon and D. A. Fulton, *Nat. Chem.*, 2014, **6**, 665–672.
122. C. S. Mahon, M. A. Fascione, C. Sakonsinsiri, T. E. McAllister, W. Bruce Turnbull and D. A. Fulton, *Org. Biomol. Chem.*, 2015, **13**, 2756–2761.
123. A. Si Kyung YangMarcus Weck, *Macromolecules*, 2007, **41**, 346–351.
124. M. R. Hill, S. Mukherjee, P. J. Costanzo and B. S. Sumerlin, *Polym. Chem.*, 2012, **3**, 1758–1762.
125. K. Godula and C. R. Bertozzi, *J. Am. Chem. Soc.*, 2010, **132**, 9963–9965.
126. A. Kumar, R. R. Ujjwal, A. Mittal, A. Bansal and U. Ojha, *ACS Appl. Mater. Interfaces*, 2014, **6**, 1855–1865.

127. E. A. Hoff, B. A. Abel, C. A. Tretbar, C. L. McCormick and D. L. Patton, *Polym. Chem.*, 2017, **128**, 15602–5.
128. J. Mollin, F. Kasparek and J. Lasovsky, *Chem. Zvesti*, 1975, **29**, 39–43.
129. C. R. Lindegren and C. Niemann, *J. Am. Chem. Soc.*, 1949, **71**, 1504–1504.
130. J. Collins, Z. Xiao, M. Müllner and L. A. Connal, *Polym. Chem.*, 2016, **7**, 3812–3826.
131. A. Strassburg, F. Kracke, J. Wenners, A. Jemeljanova, J. Kuepper, H. Petersen and J. C. Tiller, *Macromol. Biosci.*, 2015, **15**, 1710–1723.
132. S. Buffet-Bataillon, P. Tattevin, M. Bonnaure-Mallet and A. Jolivet-Gougeon, *Int. J. Antimicrob. Agents*, 2012, **39**, 381–389.
133. M. Zasloff, *Nature,* 2002, **415**, 389–395.
134. F. Sanda, M. Shiotsuki and T. Masuda, *Polymer Science: A Comprehensive Reference Volume 3, 3.27 Alkyne Polymerization*, *Elsevier B.V.*, 2012, 875–954.
135. F. Sgolastra, B. M. deRonde, J. M. Sarapas, A. Som and G. N. Tew, *Acc. Chem. Res.*, 2013, **46**, 2977-2987.

Chapter 1

Acrylic Polymer Scaffolds via RAFT Polymerisation

Extracts from this chapter can be found in the following article:

D. N. Crisan, O. Creese, R. Ball, J. L. Brioso, B. Martyn, J. Montenegro and F. Fernández-Trillo, *Polym. Chem.*, 2017, **8**, 4576–4584

1.1 Background

The reversible addition-fragmentation chain transfer (RAFT) process is a powerful tool in modern living/free radical polymerisation. Its wide versatility with regards to substrates, solvents and reaction conditions, has caused increased interest from both the academic and industrial sectors since the initial report in 1998[1]. The process relies on the use of transfer agents to control the rate of polymerisation reactions, polymer chain lengths and polydispersity. These unsaturated compounds with general structure **1.1** act through a two-step addition-fragmentation mechanism shown below (**Scheme 1.1**). One of the essential components in these molecules is a C=X reactive double bond where X is most often a methylene group or a sulfur group. The Z group is chosen so that it can provide the optimum balance between reactivity with monomer and stability of the resulting intermediate. The R group must be a suitable good free radical leaving group but also a good initiating radical. An efficient RAFT process requires that the product of the chain transfer process to act as a chain transfer agent with activity similar to, or greater than, the initial transfer agent. As a consequence, group A is most commonly also a methylene or sulfur group and generally the same as X.

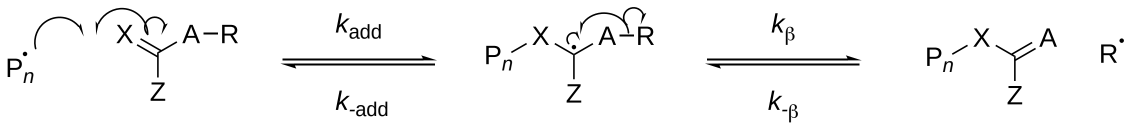

1.1

Scheme 1.1: Addition-Fragmentation mechanism.

Kinetic RAFT polymerisation

RAFT polymerisations generally follow first-order kinetics, and as a consequence, the rate of polymerisation is proportional to the concentration of monomer in the reaction. From the integrated first order rate law:

$$\ln[\mathrm{M}] = -\mathrm{kt} + [\mathrm{M_0}] \text{ or}$$

$$\ln([\mathrm{M}]/[\mathrm{M_0}]) = -\mathrm{kt} \text{ or}$$

$$\ln([\mathrm{M_0}]/[\mathrm{M}]) = \mathrm{kt}$$

where [M] is the concentration of monomer at time t. Since [M] is inversely proportional to the percentage conversion, and in a controlled polymerisation, the molecular weight of polymer chains in the reaction increases proportionally to the consumption of monomer, it is expected that the molecular weight (M_w) follows a linear relationship with percentage conversion. Furthermore, controlled polymerisations like RAFT are characterised by low dispersity indexes throughout the reaction.

As observed in **Scheme 1.1**, radicals are neither formed nor destroyed as a consequence of the RAFT equilibria.[2] The RAFT agent can behave as an ideal transfer agent once a steady state is established, thus, its presence in the polymerisation medium does not affect the rate of reaction. As long as the fragmentation of the RAFT adduct radical and subsequent re-initiation are rapid and not rate determining, the RAFT mechanism does not induce any inherent rate retardation. In the initiation step of the reaction, short chains are generated, which progressively increase in size as part of the subsequent RAFT equilibration, reinitiation and chain equilibration steps (**Scheme 1.2**). The rate coefficients of the above steps are very often dependent on the chain length, particularly the termination and propagation steps. Because of this dependence, rate of polymerisations under RAFT agent control are often very different than those under normal radical polymerisation conditions.

Apart from the above-mentioned factors, addition of a RAFT agent to a polymerisation reaction can significantly influence its reaction kinetics, through either of two phenomena:

- an inhibition period at the beginning of the reaction where little or no polymerisation is observed.
- rate retardation, in which addition of the RAFT agent significantly decreases the rate of polymerisation compared to its analogous radical reaction for the duration of the entire process.

Inhibition phenomena are generally associated with the pre-equilibrium (initialisation) stage in which the original RAFT compound is converted to the polymeric RAFT agent. Other inhibition phenomena can be attributed to impurities in the RAFT agent or by-products of the polymerisation reaction. The effects of the former can be minimised or eliminated by an appropriate choice of stabilising group Z and leaving group R. Rate retardation and inhibition effects are most prone in RAFT agents carrying Z groups that most effectively stabilise the adduct radicals. Agents where the group is a phenyl or other aromatics are known to show strong inhibitory effects. To completely avoid inhibition phenomena associated with the pre-equilibrium and initialisation stages, a macromolecular or polymeric RAFT agent can be employed. Alternatively, agents such as trithiocarbonates which have a more reactive C=S double bond can be used.

Another important observation in RAFT-mediated polymerisations is called hybrid behaviour. This manifests as a rapid increase in molecular weight and a broad initial polydispersity that narrows with increasing conversion, but it also displays significant rate retardation as the molecular weight approaches the calculated molecular weight based on full conversion. This behaviour is generally observed with macromonomer RAFT polymerisation and in the case of less active thiocarbonylthio compounds. The experimental observations and approximate trends can generally be summarised as follows:

i. The RAFT process should not induce any rate retardation/inhibition effects if the RAFT adduct radicals are fast to fragment.

ii. The more reactive the propagating radical (the less reactive the monomer), the higher the equilibrium constants in both the pre- and main equilibrium.

iii. An increasing stability of the RAFT adduct radical and inability of the leaving group to reinitiate polymerisation increases the chances of inhibition/rate retardation occurrences for a given monomer.

iv. Less reactive propagating radicals (derived from more reactive monomers) require RAFT agents with increased C=S double bond reactivity to minimise possibility of hybrid behaviour.

The Mechanism of the RAFT process

Mechanistically, the RAFT polymerisation (**Scheme 1.2**) is initiated (Step I) in the same manner as traditional radical addition polymerisations. The short polymeric chains formed are then transferred onto the RAFT agent that releases a new radical initiator (Step II). In this re-initiation step (Step III), new short polymeric chains are formed. An equilibrium (Step IV) is established wherein the “radical” is “passed” between polymeric chains via the RAFT agent. The chain holding the radical can react and grow with monomer still present in solution in the same fashion as radical addition polymerisation. In the termination step (Step V) two radical containing chains

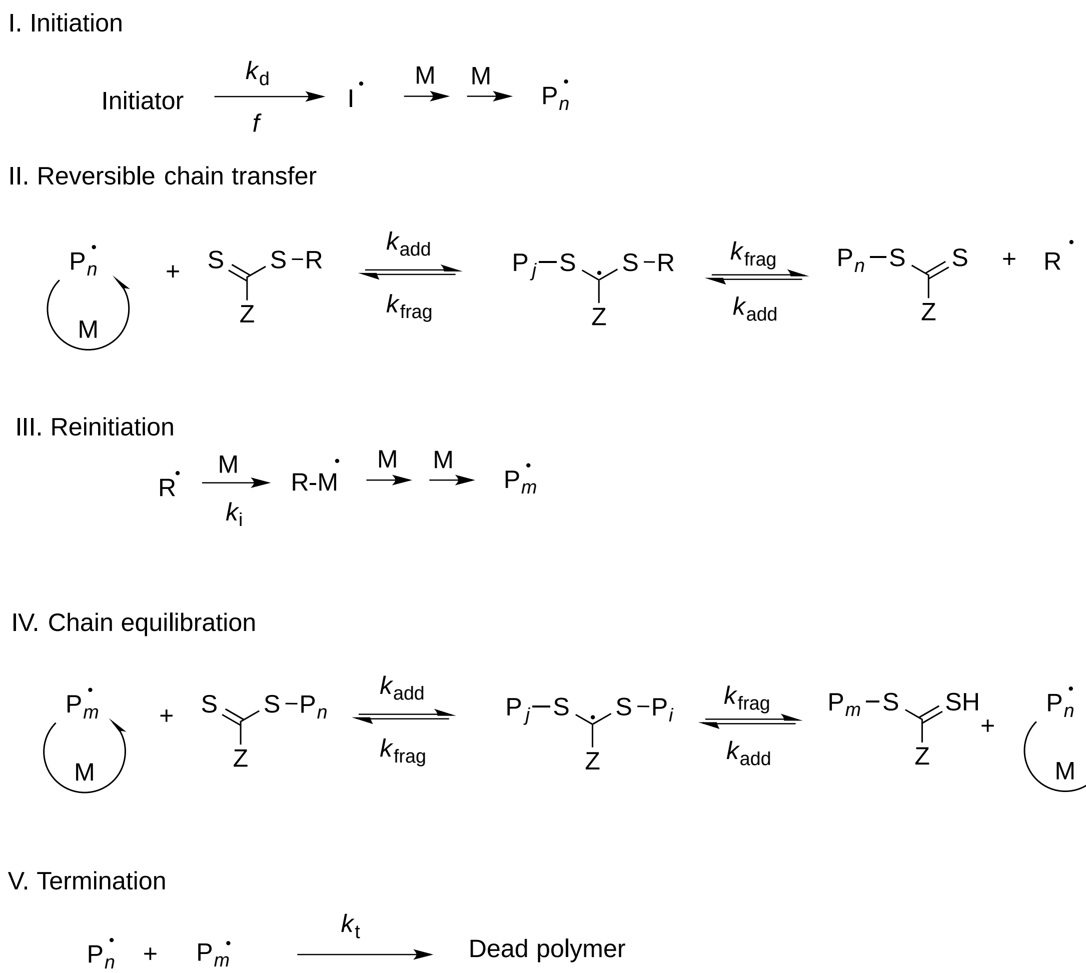

Scheme 1.2: The mechanism of RAFT polymerisations. Reaction control is highly dependent on the equilibrium constants associated with the two equilibria.

react, resulting in a dead polymer, which cannot be reinitiated. Indeed, during RAFT polymerisation, termination through the formation of dead polymers is undesirable as it leads to increased dispersity.

RAFT agents and their substrate compatibilities

The effectiveness of a RAFT agent depends strongly on the monomer polymerised and on the properties of the free radical leaving group R and the group Z[3,4], which is tuned to activate or deactivate the thiocarbonyl double bond and to modify the stability of the intermediate radicals. RAFT agents (**Fig. 1.1**) can be classified with respect to the Z group into dithioesters, trithiocarbonates, xanthates, dithiocarbamates and other highly specific moieties.

Dithioesters that display an aromatic Z group are amongst the most active RAFT agents. In the presence of a suitable R group they form the class of agents most suited for (meth)acrylic (MMA, MA) and styrenic (S) monomers. A downside in their use is that when used in high-concentrations to afford low-molecular weight

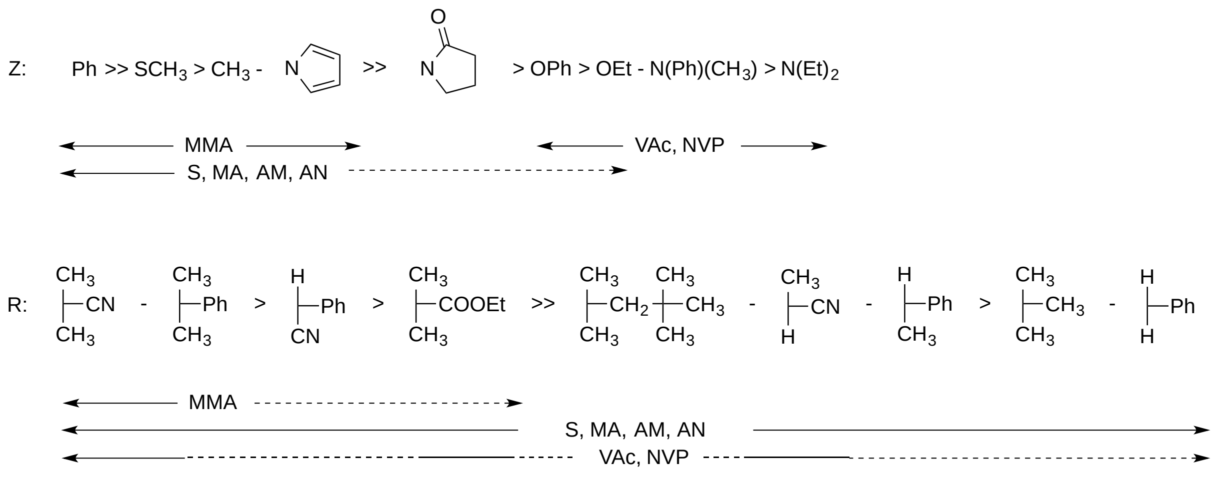

Figure 1.1[2]**:** Guidelines for the selection of RAFT agents for a variety of monomers. From left to right: for Z, addition rates decrease and fragmentation rates increase; for R, fragmentation rates decrease. Dashed lines indicate partial control during polymerisation (i.e. control over molecular weight but poor polydispersity).

polymers, polymerisations suffer from rate-retardation. Additionally, they are susceptible to hydrolysis and decomposition in the presence of Lewis acids. RAFT agents based around trithiocarbonates, despite being less active than dithioesters, provide good control in the polymerisation of (meth)acrylic (MMA, MA) and styrenic (S) monomers whilst being less prone to degradation. Dithiocarbamates and xanthates are useful RAFT agents in polymerisations where the propagating radical is a poor homolytic leaving group. Monomers related to vinyl acetate (VAc) or *N*–vinylpyrrolidone (NVP) are suitable species that can be polymerised by the less active transfer agents.

Solvent Selection

RAFT polymerisation remains in effect a radical polymerisation. As a consequence, it remains highly versatile in terms of reaction media. A large variety of solvents are tolerated including protic solvents such as alcohols and water. Furthermore, RAFT polymerisation can be also be carried out in unconventional media such as ionic liquids[5]. Ultimately, the choice of solvent has to be made with regards to the requirements of the chain transfer agent used and the monomer polymerised. It also needs to be remembered that the more active dithioesters chain transfer agents are susceptible to hydrolysis.

1.2 Objectives

The primary objective was to synthesise a simple acrylic polymer with a hydrazide side chain as the anchor for aldehydes. The target of choice was poly(acryloyl hydrazide) **P1** (**Scheme 1.3**).

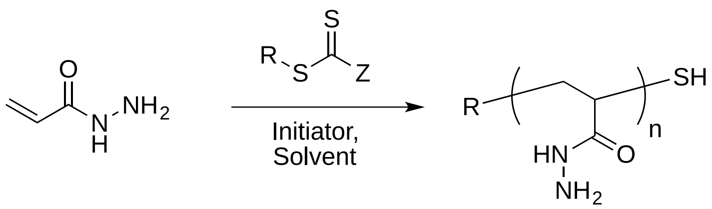

1.2 **P1**

Scheme 1.3: Primary objective. The synthesis of poly(acryloyl hydrazide) **P1** from acryloylhydrazide **1.2** via RAFT polymerisation.

Initially, the development of a robust, efficient and clean synthesis to obtain monomer **1.2** was targeted. It was considered best, those synthetic pathways that rely on the use of safer chemicals and facile purification methods. By facile, it was generally meant purification techniques such as phase-separation, recrystallization and trituration while generally avoiding techniques such as chromatography. Once the initial step was achieved the synthesis and characterisation of poly(acryloyl hydrazide)s **P1** of different molecular weights was attempted.

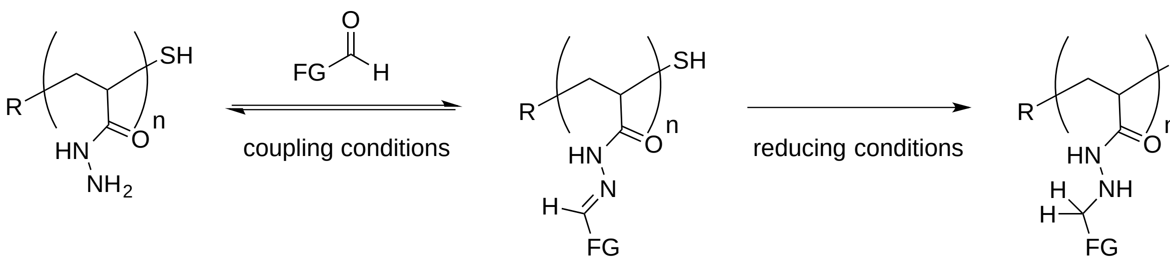

P1

Scheme 1.4: Second objective. To investigate the coupling of **P1** with aldehydes to afford functional polymers, and as a minor subsequent aim, investigate reducing conditions to immobilise the aldehyde.

Secondly, it was aimed to test the polymer's reactivity through its hydrazide side-chains with several aldehydes to determine hydrazone formation, binding efficiency, reaction conditions and polymer size effects on the chemistry investigated. The investigation into different chemistries suitable for the reduction of hydrazones to hydrazines (**Scheme 1.4**) to permanently immobilise aldehydes to the polymer scaffold was also planned. The final objective was to develop suitable pathways to attach fluorescent dyes using the polymer's end group towards fluorescent polyhydrazide scaffolds (**Scheme 1.5**).

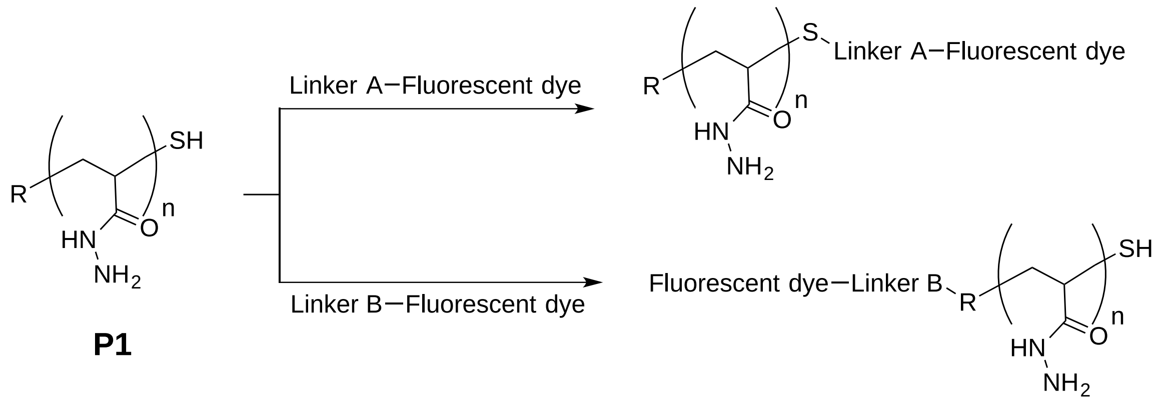

Scheme 1.5: Final objective. To investigate suitable pathways to functionalise **P1** with fluorescent dyes through its end groups.

1.3 Results and Discussion

Synthesis of poly(acryloyl hydrazide) P1

To synthesise acryloylhydrazide **1.2** reactions involving the formation of similar molecules were looked into, especially the formation of amides. The most frequent approaches[6-8] involve the reaction of an amine with an acid chloride or with an activated carboxylic acid. The immediate equivalent would have been to react acryloyl chloride directly with hydrazine, but in retrospect to the synthetic guidelines detailed in the objectives, hydrazine had two main shortfalls. Firstly, the safety hazards associated with hydrazine make it unattractive to use, but also, its ability to react at both ends meant that di-substitution side reactions were possible, resulting in the requirement for more complex purification methods such as chromatography. As a consequence, a Boc-protected hydrazine in the form of *tert*-butyl carbazate was chosen. The reaction (**Scheme 1.6**), which produced the target *tert*-butyl 2-acryloylhydrazine-1-carboxylate **1.3**, was carried out in a THF/$NaOH_{(aq)}$ emulsion to neutralise the HCl produced as the reaction by-product.

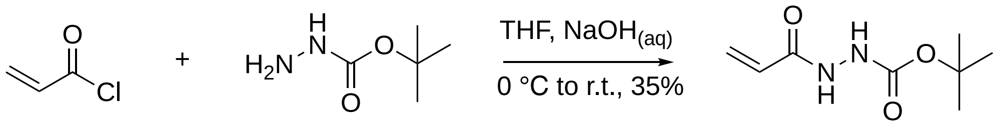

1.3

Scheme 1.6: Reaction scheme showing the initial synthesis of the target precursor *tert*-butyl-2-propiolohydrazine-1-carboxylate (**1.3**).

Although the reaction was efficient in the sense that the product could be obtained using facile work-up procedures, the relatively poor overall yield (<35%) correlated to long reaction times (>4 hours) made it unattractive for larger scale synthesis. Additionally, during attempts to scale-up the reaction, new unidentified side-products were observed. The target compound could not be purified by simple separation techniques. Consequently, an alternative conjugation pathway[9] was explored and adapted so that *tert*-butyl carbazate was reacted with acrylic acid activated using 1−ethyl−3−(3−dimethylaminopropyl)carbodiimide (EDC) (**Scheme 1.7**).

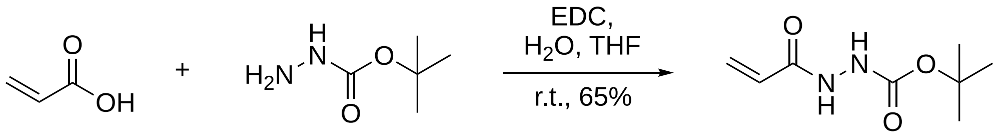

1.3

Scheme 1.7: Optimised synthetic route to *tert*-butyl-2-acryloylhydrazine-1-carboxylate (**1.3**).

Modifications from the original reported conditions[9] were made to accommodate the product's poor solubility in water. As a consequence, THF was added as a co-solvent in a 1:2 mixture with water. An unknown minor side-product seems to be produced in this reaction, which required the introduction of a recrystallization step after work-up. With an average percentage yield of ~65% after two recrystallization cycles, this method was deemed suitable, especially since it could be performed on larger scales (i.e. 8 g starting material).

Characterisation data obtained via ^{1}H and PENDANT ^{13}C NMR spectroscopies for the isolated product (**Fig. 1.2**) showed proton environments consistent with two amide, two alkene (no distinguishable difference in chemical shift between the cis/ trans protons was observed) and one alkyl proton environment, as well as carbon environments consistent with two 4° carbonyls, a 2° alkene and a 3° alkene, a 4° alkyl and a 1° alkyl carbon environment. This was in agreement with the expected results and the results in the literature.[41] Mass spectra obtained were difficult to elucidate as they showed a high degree of fragmentation and recombination to afford ions with molecular weight higher. Although the molecular ion peak $[M+Na]^+$ is observed (m/z = 209.085), the highest intensity peaks are attributed to dimers,

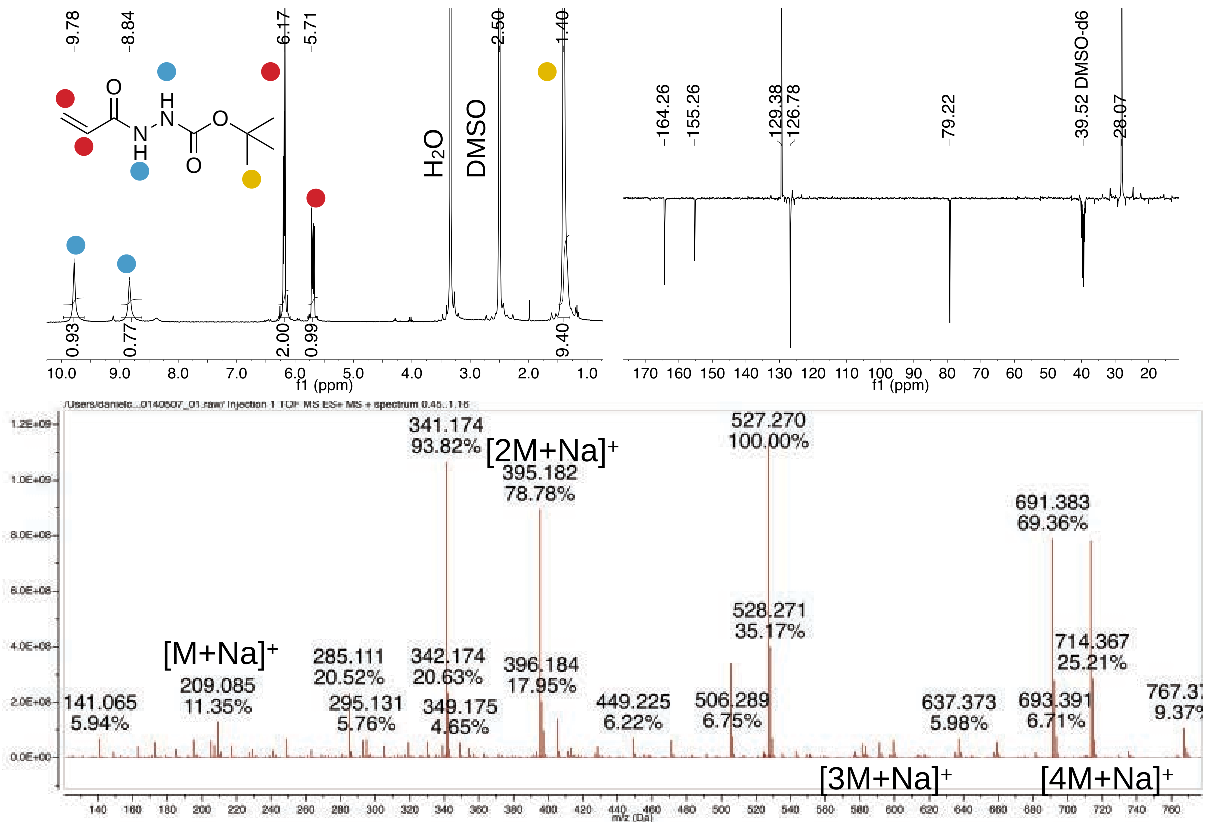

Figure 1.2: (Top) ^{1}H and PENDANT ^{13}C NMR spectra of hydrazide **1.3** in DMSO-*d6*. (Bottom) TOF MF ES+ spectrum of hydrazide **1.3** showing the molecular ion peak plus sodium at m/z=209.085.

trimers and tetramers and fragmentation products of these higher molecular species. It is believed that these substrates could be relatively reactive in the gas phase and as a consequence, they are prone to form higher molecular weight ions via repeated fragmentations and recombinations. Tandem mass spectrometry was carried out in which the molecular ion peak was selected for the second stage of mass spectrometry. This showed the same pattern of peaks where the higher molecular weight peaks had a higher intensity compared to the molecular ion peak.

Deprotection of hydrazide **1.3** (**Scheme 1.8**) was performed using 1M $HCl_{(aq)}$ and relatively long reaction times (48 hours) to afford the hydrazide hydrochloride **1.4**. To avoid suspected nucleophilic addition and self-polymerisation products, reaction temperatures had to be kept at room temperatures or below, especially when the excess HCl was removed under reduced pressure. The product was isolated in quantitative yields by freeze-drying the remaining water. The ^{1}H NMR spectrum (**Fig. 1.3**) confirmed that the deprotection was successful due to the absence of the $(CH_3)_3$ peak at 1.40 ppm. Alternative deprotection strategies were attempted including treatment with TFA, but the compound was never isolated pure due to difficulties in removing residual TFA and formation of impurities at that stage.

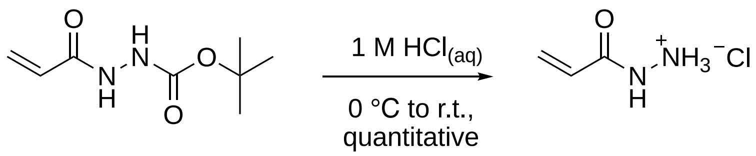

1.3 **1.4**

Scheme 1.8: Deprotection of intermediate **1.3** to afford the target monomer as the acryloylhydrazide hydrochloride **1.4**.

In order to polymerise the acryloylhydrazide monomer **1.4**, under aqueous buffer conditions, a suitable water soluble RAFT had to be chosen. Trithiocarbonate **CTA1** was opted for, as there is a good track record[8,10,11] of polymerisation of acrylamides and methacrylamides with this family of agents and there was previous experience in the laboratory with this molecule. This bright yellow compound was synthesised directly on a large scale (3 g, 47 mmol EtSH) according to the following reaction[12] (**Scheme 1.9**):

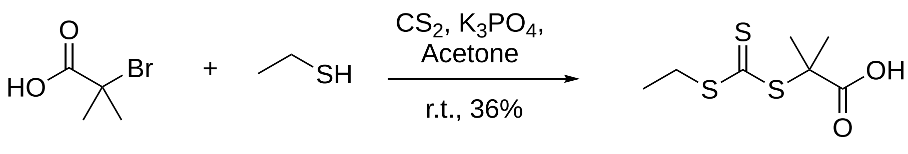

CTA1

Scheme 1.9: Synthesis of trithiocarbonate **CTA1**, the chosen RAFT agent for the polymerisation of the alkene monomer.

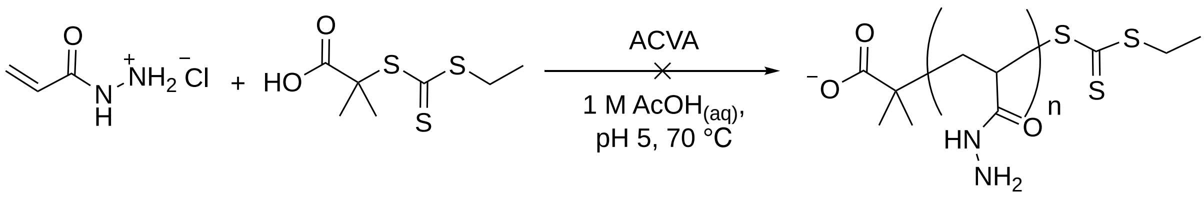

1.4 **CTA1** **P1**

Scheme 1.10: Proposed polymerisation conditions of the deprotected monomer **1.4** in aqueous conditions.

Having designed a synthetic route to the target monomer and a suitable RAFT agent, the investigation of the polymerisation under aqueous buffer conditions was carried out. Reactions were carried out in 1 M AcOH buffer at pH 5 to ensure that the RAFT agent was deprotonated to enhance its solubility (**Scheme 1.10**). At pH 5 the hydrazide functionality should also be partially protonated[13,14] thus decreasing its nucleophilicity with respect to the carbonothioyl group. This was considered important to avoid destruction of the RAFT agent.

Despite observing almost complete monomer consumption by ^{1}H NMR spectroscopy within four hours, the expected broad proton signals for the polymer in the alkyl region (1.8 - 1.2 ppm) were not observed (**Fig. 1.3**). Instead two broad peaks at 2.86 and 2.21 ppm were observed. This is akin to R_2N-C*H* environments

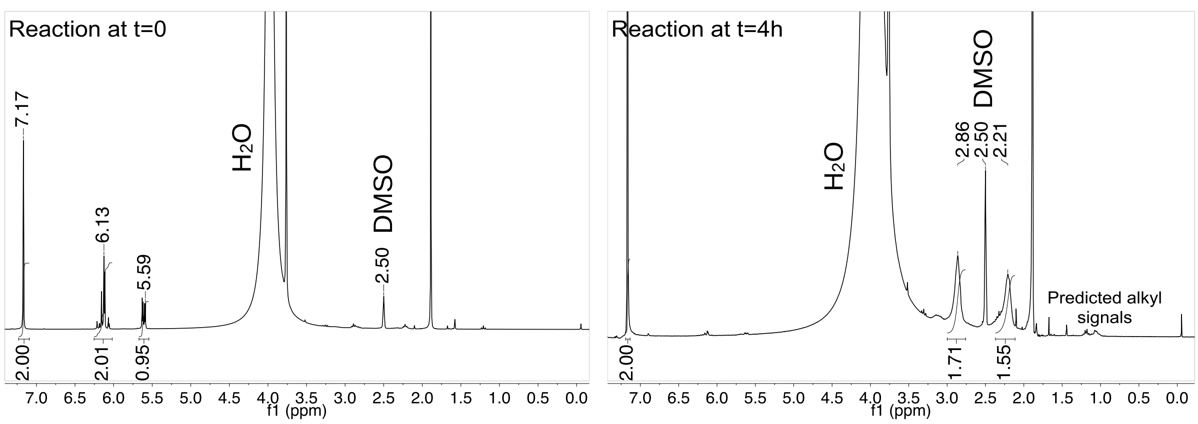

Figure 1.3: ^{1}H NMR spectra of the polymerisation reaction of monomer **1.4** in the presence of RAFT agent **CTA1** at the beginning (left) and end of the reaction (right). The attempts to form **P1** failed using this strategy.

suggesting formation of polyethylenimine type bonds through nucleophilic conjugate addition. Furthermore, after purification by dialysis and lyophilisation to remove the water, only a very small amount of a mixture of grey and white precipitate was isolated. Based on the visual observation that the initial yellow solution turned murky within an hour of starting the reaction, it was hypothesised that RAFT agent degradation was occurring.[15] Radical polymerisation reactions in the absence of a chain transfer agent or in the presence of a non-degradable chain transfer agent were carried out. The latter showed very poor monomer consumption while the former despite exhibiting over 60% consumption after eighteen hours, did not display the expected polymer characteristics. The trace amount of sample isolated after dialysis proved to be similar to the product isolated from the RAFT polymerisation.

Research conducted by Julia Lipecki under the guidance of the author of this thesis, investigated the polymerisation of the deprotected monomer by using a different RAFT agent. Dithiocarbamate **CTA2** has been shown by Keddie *et al.*[16] to be a pH switchable CTA in the sense that in the presence of two distinct monomers, each can be selectively polymerised by changing the pH of the aqueous solution. Furthermore, the agent was shown to be very robust under strong acidic conditions. Different ratios of monomer, CTA and *p*-toluenesulfonic acid were experimented with

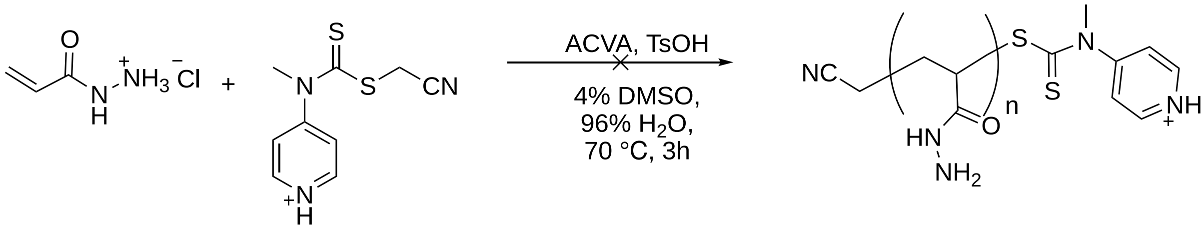

1.4 **CTA2** **P1**

Scheme 1.11: Alternative conditions attempted for the polymerisation of the deprotected monomer **1.4** in aqueous conditions using a dithiocarbamate CTA.

(**Scheme 1.11**), starting from the original reported conditions[16] (100/1/1/) going as far as 100/1/200 to ensure full protonation of the hydrazide monomer. In those experiments, similar polymerisation products as those under trithiocarbamate **CTA1** were observed. Reactions between monomer **1.4** and RAFT agent **CTA2** under acidic conditions in the absence of a radical initiator confirmed that reactions between the hydrazide and thiocarbonyl groups are occurring and are competing with the polymerisation process. Recent work[38] on the polymerisation of a couple of methacryl hydrazides, investigated and confirmed the observed nucleophilic attack by the hydrazide on the CTA. This was successfully prevented at pH 0 when a hydrazide monomer with a acyl side-chain was used.

Having analysed that the deprotection step was cumbersome and the polymerisation of the deprotected monomer required further investigation, it was decided to attempt the polymerisation of the protected hydrazide monomer **1.3** in organic solvents with a view to remove the Boc protecting group post-polymerisation. In choosing an appropriate organic solvent for the reaction, three conditions had to be satisfied. The first condition was that all three reagents (i.e. the protected monomer, the RAFT agent and the radical initiator) had to be soluble. The second was that solvent had to dissolve the monomer at a concentration of at least 0.9 M or above for good reaction times and conversion. The last condition was that the solvent's boiling point had to be above that of the reaction temperature required for the efficient thermal decomposition of the radical initiator (70 ℃). Polar solvents like THF and MeOH showed good potential in terms of solubility, but their low boiling point and volatility upon degassing with argon gas meant they were unreliable to maintain the same constant concentration during the reaction. Ethyl acetate satisfied

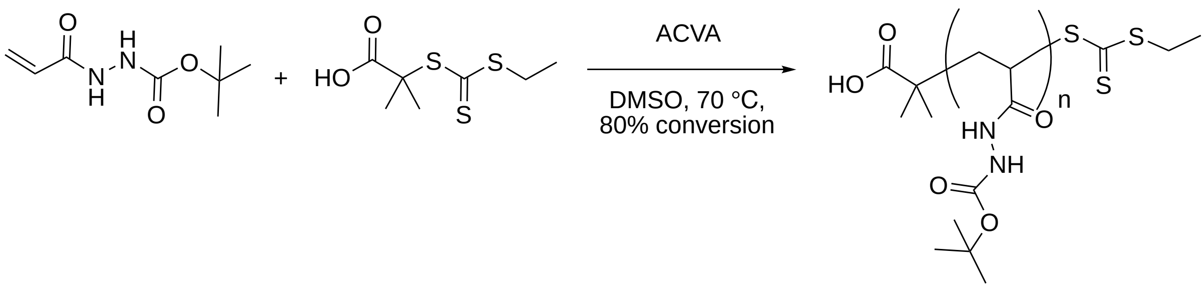

1.3 **CTA1** Boc-**P1**

Scheme 1.12: RAFT Polymerisation conditions of the Boc-protected acryloyl hydrazide monomer **1.3** to afford Boc-**P1**.

the above conditions but it was found that upon cooling down, from 70 ℃, immediate precipitation of Boc-**P1** was occurring. This made it difficult to investigate the kinetics of the reaction as the polymer precipitated in the syringe during aliquot sampling. Ultimately, DMSO was chosen (**Scheme 1.12**) as it not only satisfied all the conditions better than other common organic solvents, but its solubility in water, meant that it could be easily removed during dialysis.

To test the reaction conditions, a series of kinetic experiments were carried out to evaluate the optimum reaction time for different molecular weights. Monomer conversion was monitored by ^{1}H NMR spectroscopy at different time intervals (**Fig. 1.4**) and the aliquots were further analysed by SEC/GPC. Syringic acid was added to ^{1}H NMR spectroscopy samples as an internal standard, and the integration of the aromatic proton signal at 7.20 ppm was compared against the vinyl proton signals from the monomers (6.18 and 5.68 ppm). Two sets of kinetic experiments were carried out to verify the observed findings. According to literature,[2] polymerisations under the influence of a RAFT agent should follow first order kinetics. In both cases a deviation from this expected relationship was observed (**Fig. 1.5**). The plateauing feature observed, after reacting for five hours, is consistent with hybrid behaviour of RAFT agents, in which significant rate retardation is observed as the polymerisation approaches higher monomer consumption. Nonetheless, optimisation of the process was carried out to achieve monomer conversions between 80-90% and polymers with degrees of polymerisation (DPs) ranging from DP 43-127 and dispersities (Đ) ranging between 1.38-1.52.

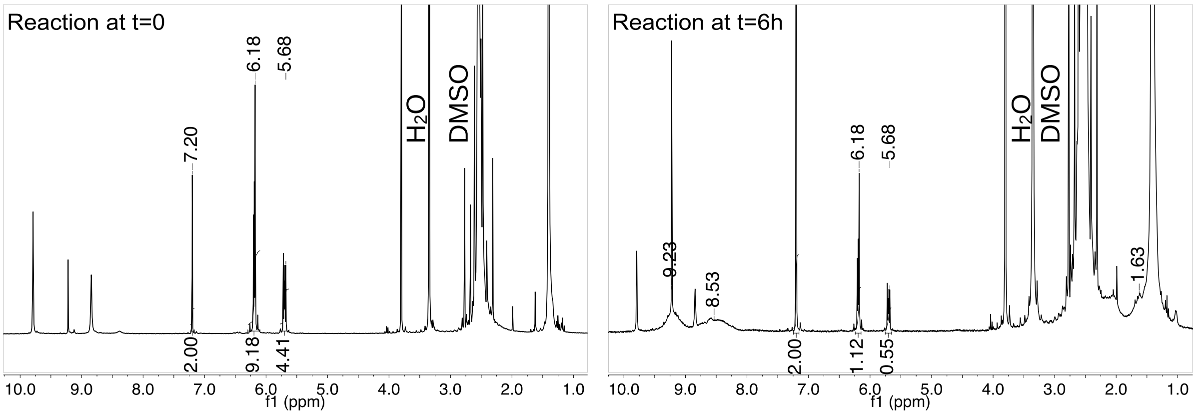

Figure 1.4: ^{1}H NMR spectra of representative aliquots from a polymerisation reaction of monomer **1.3** with **CTA1** in DMSO-*d6* at 70 ℃. The NMR samples were spiked with syringic acid as an internal standard. The integration of the monomer's vinyl peaks (6.18 and 5.68 ppm) was compared against the integration of the aromatic peaks of syringic acid (7.20 ppm) to obtain the percentage conversion.

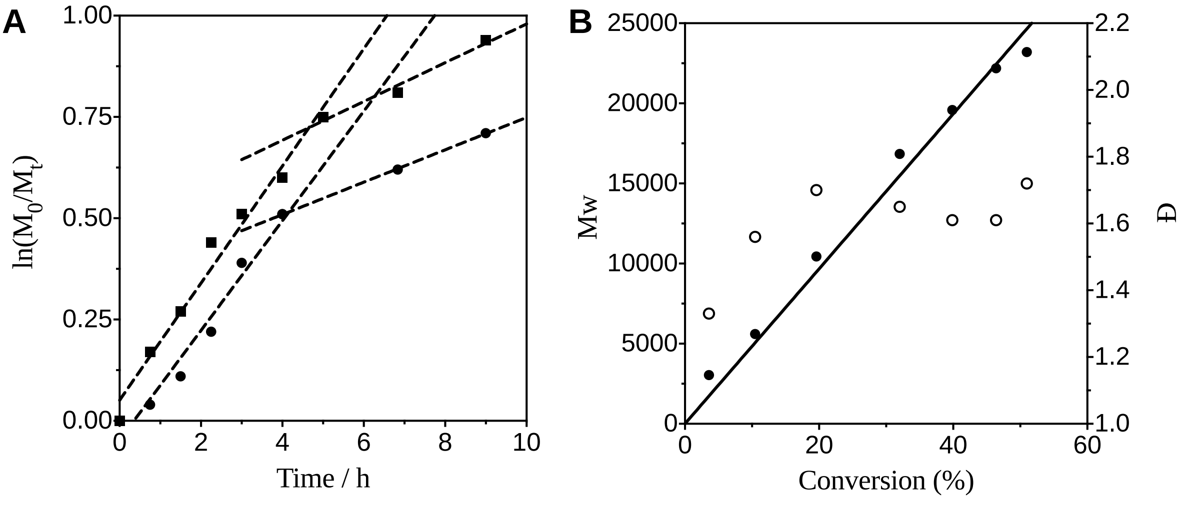

Figure 1.5: A) Representative linear plot of $\ln[M]_0/[M]_t$ vs. time. Conditions: squares [M]=0.9 M, [M]/[CTA]/[ACVA]=100/1/0.2; circles [M]=0.9 M, [M]/[CTA]/[ACVA]=100/1/0.11.
B) Representative plot of measured M_w vs. conversion (solid) and Đ vs. conversion (hollow). M_w were obtained using SEC/GPC carried out by the Gibson Laboratory (Prof. Matt Gibson) at the University of Warwick.

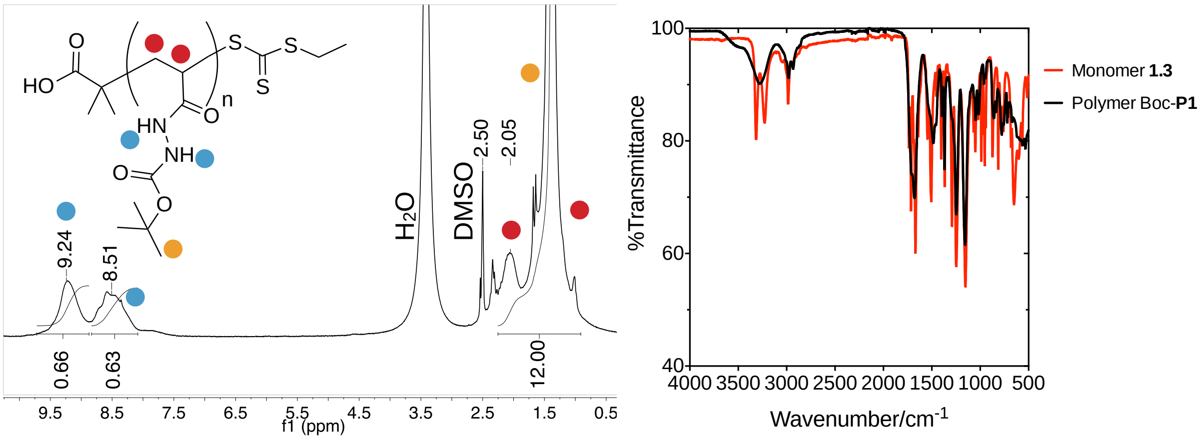

Figure 1.6: ^{1}H NMR spectrum of a representative sample of polymer Boc-**P1** in DMSO-*d*6 (left). FT-IR spectra of monomer **1.3** and polymer Boc-**P1** showing the changes from sharp to broadened peaks (right).

To extract and purify polymer Boc-protected poly(acryloyl hydrazide) Boc-**P1**, the unreacted monomer was removed alongside the DMSO solvent and other by-products by dialysis. The polymer was isolated as a white powder after lyophilisation. Boc-**P1** was characterised by ^{1}H NMR, IR, and UV-Vis spectroscopies for structural determination and SEC/GPC for molecular weight determination.

The ^{1}H NMR spectrum (**Fig. 1.6**) showed broad amide peaks at 9.24 and 8.51 ppm instead of the previously sharp peaks at 9.74 and 8.84 ppm for the monomer. The differences in chemical shift could be attributed to the changes in electronic effects in going from the alkene to the alkyl-polymer backbone. Broadness was expected as a consequence of tacticity. New broad peaks were also observed in the alkyl region between 2.20 and 0.90 ppm where the alkyl backbone was expected, however some broad peaks were obstructed by a broadened (CH_3)$_3$ from the Boc group. The FT-IR spectrum (**Fig. 1.6**) showed significant broadening in most peaks, but most relevantly in the amide N-H stretches at 3250 cm^{-1}, the C-H stretches at 2920 cm^{-1} and the C=O stretches that coalesced into a single broad peak at 1670 cm^{-1}.

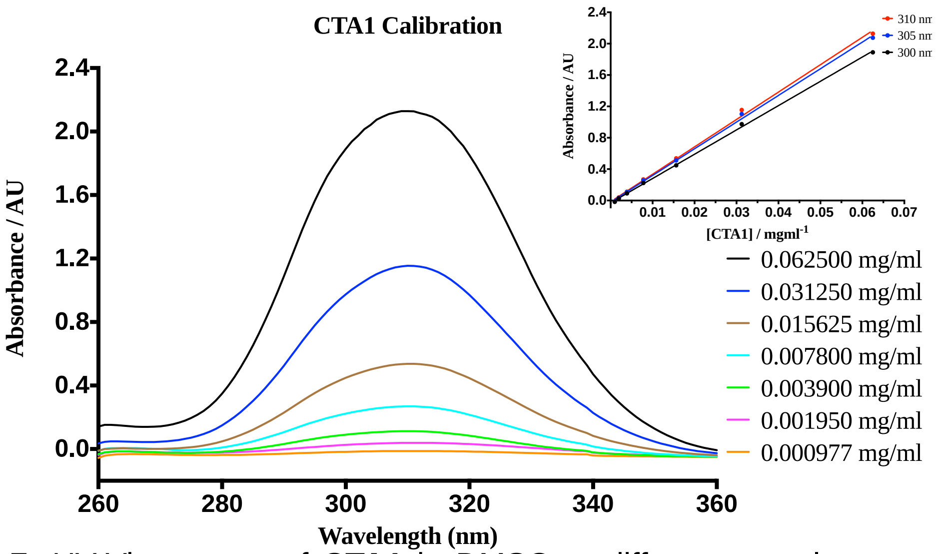

Figure 1.7: UV-Vis spectra of **CTA1** in DMSO at different sample concentrations (main). Calibration curves plotted at λ_{300} (max. for Boc-**P1**), λ_{305} and λ_{310} (max for **CTA1**) (inset).

UV-Vis spectroscopy was used to investigate the presence of the trithiocarbonyl group from the CTA, which should be incorporated at the end of the polymer chains. **CTA1** has a characteristic strong absorbance with λ_{max} at 310 nm (**Fig. 1.7**) and its presence in the polymer would be predicted by a similar absorbance peak. Indeed, it was observed that Boc-**P1** showed a peak with a blueshift in the λ_{max} (**Fig 1.8**). By measuring the absorbance of known concentrations of **CTA1** a calibration curve was plotted (**Fig. 1.7**) that was used to extrapolate the percentage weight contribution of the trithiocarbonyl group to the mass of a weighed sample of Boc-**P1**. Using this technique the molar ratio of monomers to trithiocarbonyl group was caluculated, which would give an approximate value of DP. This assumed that all polymer chains are terminated with the carbonothioyl group, which is not necessarily true. It was hoped to observe DP values close to [M]:[CTA1] x percentage monomer conversion (*c*). Overall the values obtained (DP_{UV}) (**Table 1.1**) this way were lower than those predicted according to the percentage conversion (DP_{th}). This suggested that there was more **CTA1** incorporated than there

Polymer	[M]/[CTA]	c^a	DP_{th}^b	DP_{UV}^c	Mn^d	$Đ^d$
Boc-**P1**$_{40}$	50	86%	43	16	9810	1.38
Boc-**P1**$_{80}$	99	79%	78	40	20306	1.52
Boc-**P1**$_{130}$	151	84%	127	93	31552	1.51
Boc-**P1**$_{170}$	195	87%	170	110	44826	1.95

Table 1.1: Boc-protected poly(acryloyl hydrazide)s (Boc-**P1**$_x$) described in this research. [a]calculated from 1H NMR peak integration of alkene signals versus a known standard. [b][M]/[CTA] x *c*. [c]calculated by calibration to CTA content. [d]calculated by SEC/GPC.

should have been. However we need to consider that the difference in λ_{max} between **CTA1** and Boc-**P1** could lead to a degree of error when extrapolating from the calibration curve. Furthermore, there is no indication to differences in the extinction coefficient of the **CTA1** compared to Boc-**P1** containing the same trithio end group. As expected, polymer batches synthesised with a higher [M]:[CTA] ratio, so as to produce polymers with larger DPs, showed a weaker absorbance at 300 nm (**Fig. 1.8**). Overall, this was an interesting attempt to calculate DPs by UV-Vis spectroscopy at a time when SEC/GPC was not available to the laboratory, and it was useful in showing that batches of polymer with different DPs could be produced.

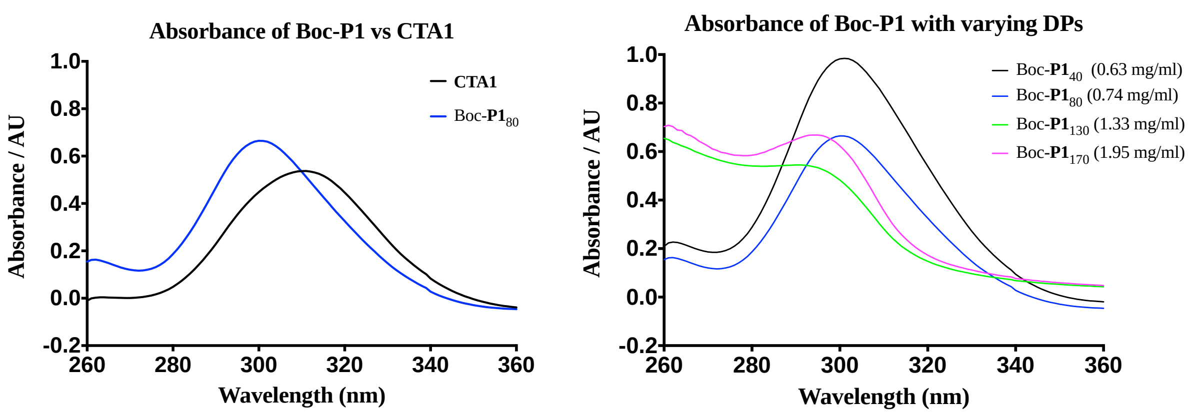

Figure 1.8: UV-Vis spectra of Boc-**P1**$_{80}$ (DP 80) and **CTA1** in DMSO showing the difference in λ_{max} (left). UV-Vis spectra of Boc-**P1** with varying DPs (40, 80, 130, 170) at different concentrations, showing a decrease in incorporated trithiocarbonyl groups at the end of the polymer chains (right).

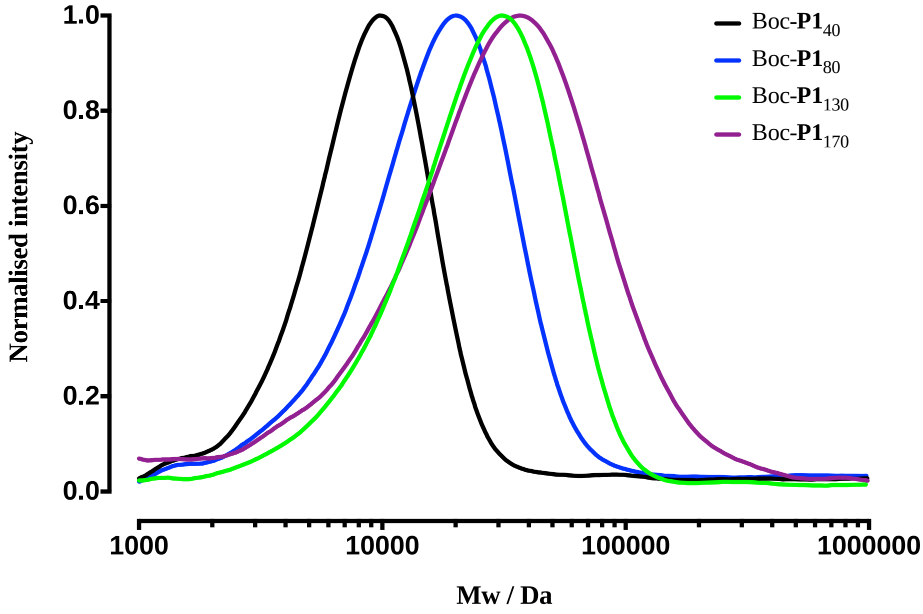

Figure 1.9: SEC/GPC chromatograms of Boc-**P1**$_{X}$. Eluent: DMF (0.05M LiBr) at 60^{o}C; Flow: 1.0 mL min^{-1}; Columns: Polymer Labs PolarGel guard column (50 x 7.5 mm, 5 μm), 2 x PLGel PL1110-6540 columns (300 x 7.5 mm, 5 μm). Molecular weights were calculated based on a standard calibration method using PMMA.

Initially, the characterisation of Boc-protected poly(acryloyl hydrazide) Boc-**P1** by SEC/GPC using two PLGel columns and THF or acetone as eluents was attempted. Despite being soluble, no polymer peaks were visibly separated from the solvent front in either of the two solvents. Using DMF as an eluent resolved the separation problems but the observed Đ were suspiciously high (3.49-5.92). Indeed, addition of 0.05M LiBr to DMF lead to significant improvements to Đ values (**Table 1.1**) as the salt suppresses sample-stationery phase interactions.[39] SEC/GPC confirmed that the synthesis of polymers up to DP 130 with a fair degree of control over size and Đ (up to 1.52) (**Fig. 1.9**) was achieved. Polymers with around DP 170 were also synthesised but the Đ values were higher (1.95).

Having accomplished this relatively rapid, reproducible and scalable route from starting materials to the protected polymer, possible deprotection and

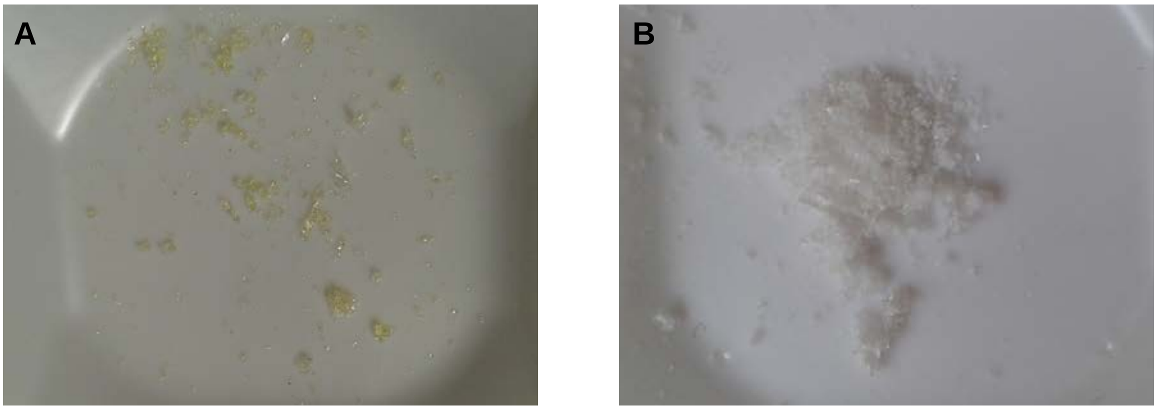

Figure 1.10: Photographs showing: **A)** Sample of Boc-**P1** deprotected and lyophilised without basic treatment. **B)** Sample of Boc-**P1** deprotected, treated with a sat. soln. $NaHCO_3$, dialysed and lyophilised.

purification strategies were explored. A sample of polymer was dissolved in trifluoroacetic acid (TFA, 1 ml to 100 mg polymer) and immediate gas evolution related to the emission of CO_2 was observed as part of the Boc group removal. After precipitation in Et_2O, the sample was dissolved in water, and two purification strategies were tested. One strategy involved direct lyophilisation to afford yellow coloured crystals (**Fig 1.10**), while in the second strategy, the sample was first treated with a saturated solution of $NaHCO_3$ and dialysed against water. This was done to deprotonate the hydrazide TFA salt resulted as part of the deprotection reaction, and immediate bubbling consistent with the break down of carbonic acid was observed. After lyophilisation a white powder was isolated (**Fig. 1.10**), posing questions regarding the structural differences leading to different colours between the two samples.

Ultraviolet-visible spectrometry showed that the sample that was treated with sat. soln. $NaHCO_3$ had lost its absorbance at 300 nm caused by the presence of the RAFT group (**Fig. 1.11**). Furthermore, the same sample gave a rapid coloured response when exposed to Ellman’s Reagent (DTNB, 5,5’-dithiobis-(2-nitrobenzoic

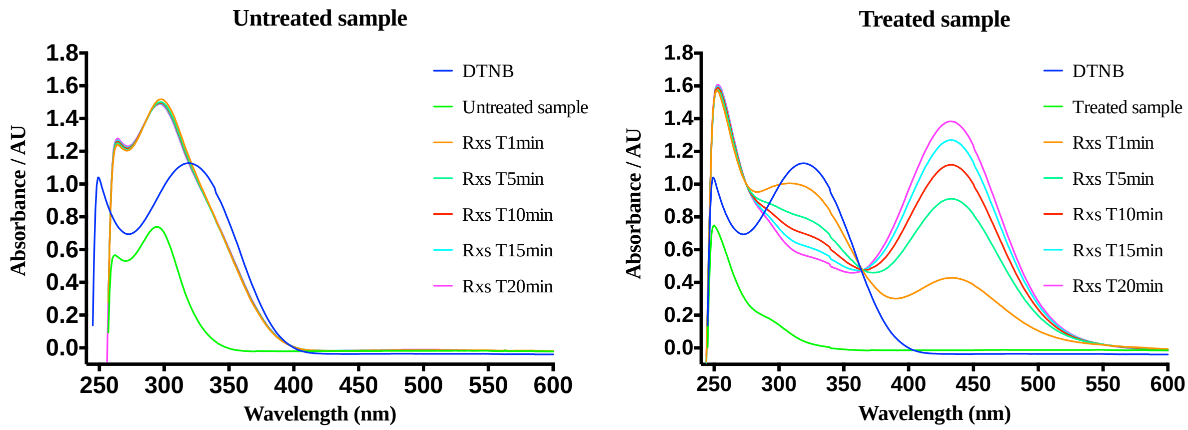

Figure 1.11: UV-Vis spectra showing of the absorbance of deprotected Boc-**P1** isolated via two different methods and its reaction with DTNB. **P1** that was not treated with $NaHCO_3$ still shows the characteristic peak at λ_{300} nm due to the trithiocarbonyl group (left). **P1** treated with $NaHCO_3$ no longer displays a peak at λ_{300} nm and the newly formed thiol is evidenced by its reaction with DTNB (right).

acid), a common test for thiols) with a characteristic absorbance peak at λ_{435} nm. The non-dialysed sample still had its absorbance at 300 nm and tested negative in the presence of DTNB as evidenced by the absence of a peak at λ_{435} nm.

Since RAFT groups are unstable in basic media or in the presence of primary or secondary amines it is believed that the hydrazide side-chains could react with the trithiocarbonyl group as a side-reaction during their functionalisation with aldehydes. By combining the deprotection step with a $NaHCO_3$ neutralisation step a cascade reaction (**Scheme 1.13**) was developed that would result in the target polymer scaffold **P1**.

Poly(acryloyl hydrazide) **P1** was isolated as a white powder after purification via dialysis against water and lyophilisation, and characterised via ^{1}H and ^{13}C NMR spectroscopy and SEC/GPC. UV-Vis spectroscopy was used to confirm to transformation of the trithiocarbonyl group into a thiol. **P1** was insoluble in all organic solvents, however dissolution could be achieved by first dissolving the sample in aqueous solvents and adding a miscible organic solvent. Solubility could be achieved

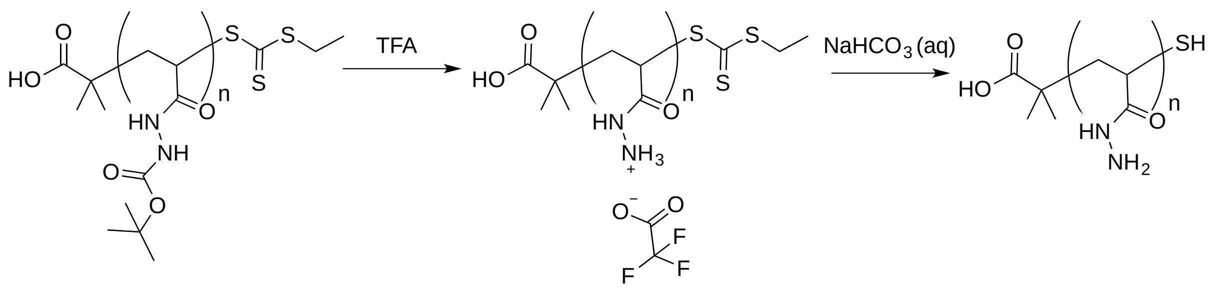

Scheme 1.13: Cascade deprotection and neutralisation from Boc-**P1** to achieve target poly(acryloyl hydrazide) **P1**.

in systems with at least 5% H_2O content in DMSO. As a consequence, all ^1H NMRs spectrums with **P1** and subsequent functionalisations were carried out in D_2O or DMSO with D_2O as co-solvent resulting in proton exchanges with the N-H protons so these were not visible. The alkyl polymer backbone represented by three broad peaks between 2.25-1.30 ppm closely resembles the same features displayed by poly(acryloyl hydrazide) synthesised by Bertozzi's Lab.[17] Furthermore, the two methyl groups from the carboxylic acid end at 1.00 and 0.94 ppm were also observed (**Fig. 1.12**). By comparing the intensity of these peaks versus the broad alkyl signals, the DP of the polymer sample could be estimated. Because there are 6H from the two methyl groups at the terminus, and every repeating unit in the polymer chain has 3H, the integration of the broad alkyl region is a function of 3n where n should be the DP.

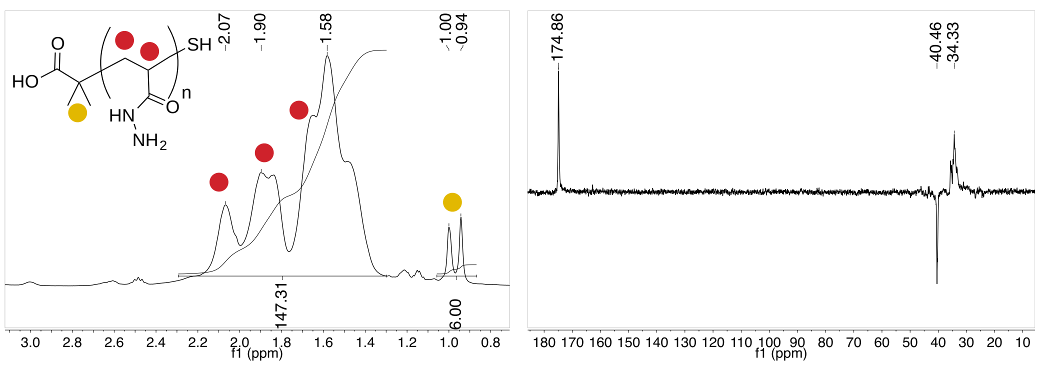

Figure 1.12: ^1H NMR (left) and PENDANT ^{13}C NMR (right) spectra of a sample of **P1**$_{40}$.

Using this integration method, DP values for **P1**$_x$ were obtained, which were in accordance to the approximated values obtained for Boc-**P1**$_x$ in the previous step, and the difference between samples of different molecular weights was correctly reflected (**Fig. 1.13**, **Table 1.2**).

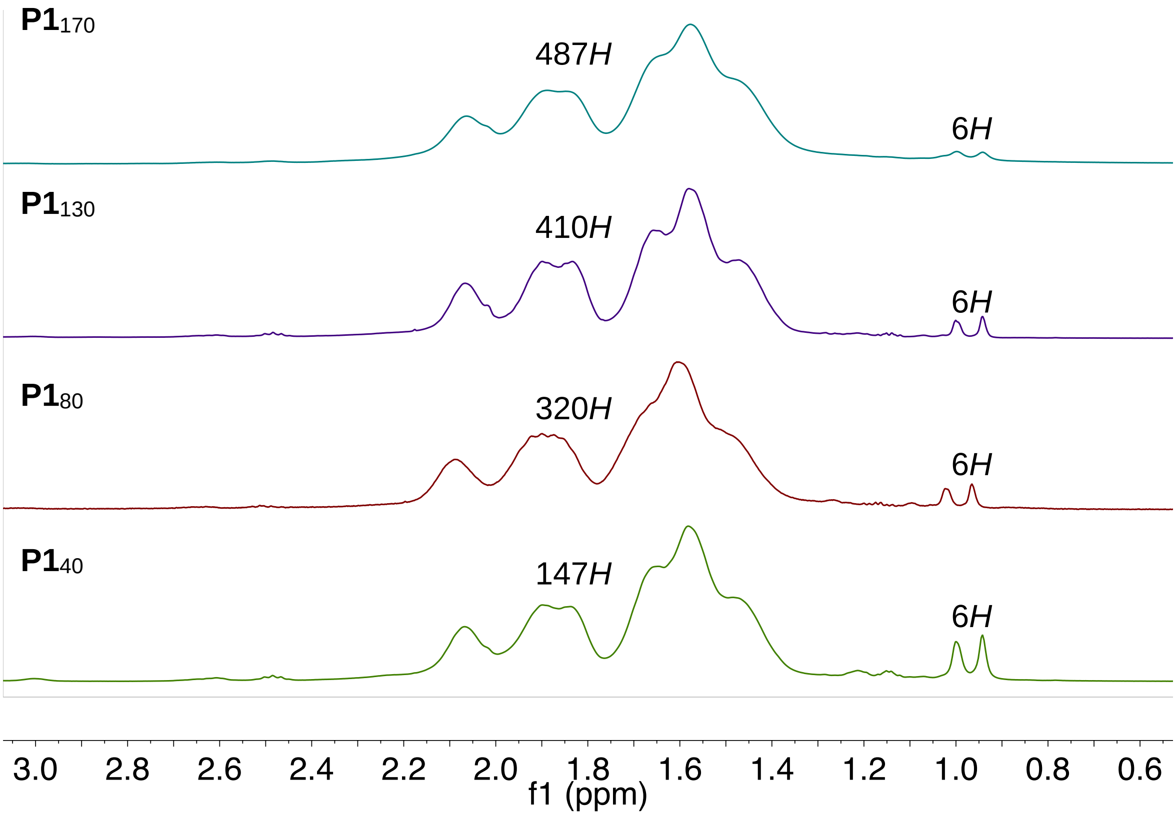

Figure 1.13: ^{1}H NMR spectra of four samples of **P1** with different DPs and molecular weights.

Polymer	DP_{NMR}[a]	Mn[b]	Đ[b]
P1$_{40}$	49	10918	1.37
P1$_{80}$	106	18446	1.33
P1$_{130}$	136	—[c]	—[c]
P1$_{170}$	162	—[c]	—[c]

Table 1.2: Poly(acryloyl hydrazide)s (**P1**$_x$) described in this research. [a]calculated from ^{1}H NMR peak integration of methyl signals versus alkyl backbone signals. [b]calculated by SEC/GPC and calibrated against PEG standards, [c]samples were not soluble in DPBS.

Aqueous SEC/GPC was carried out using two PL-aquagel-OH columns and Lonza™ DPBS (pH 7.4) as eluent. The molecular weights obtained were based on a calibration curve with PEG standards, however **P1**$_{130}$ and **P1**$_{170}$ were not soluble in this buffer and no data was obtained for them. In other buffer conditions no sample of **P1** was visible regardless of molecular weight.

The polymers were also analysed by SEC/GPC using two Shodex Asahipak columns, 100 mM AcOH as the eluent. The polymers were not detectable by neither the UV-Vis nor the RI detectors, however, it was decided to use the hydrazide side-chain to attach an aldehyde with a strongly UV-Vis active group. The choice was made to react **P1** (**Scheme 1.14**) with 4–imidazolecarboxaldehyde (**A1**) in the same solvent as the eluent and inject the crude. The resulting functionalised polymers **P1A1** were detectable by SEC/GPC.

A1

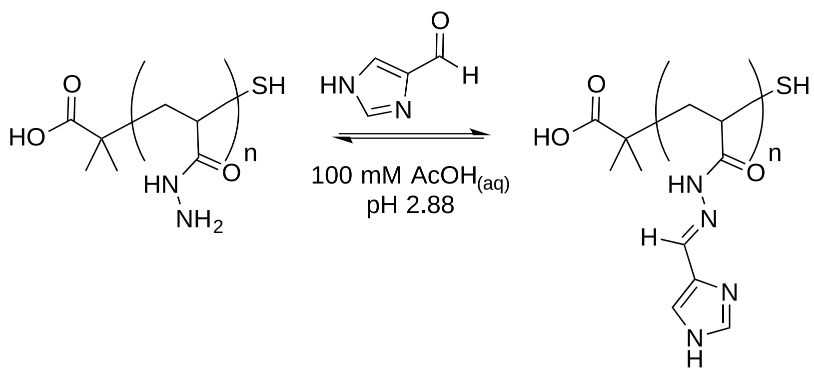

P1 **P1A1**

Scheme 1.14: Functionalisation of **P1** with imidazole **A1** for SEC/GPC analysis.

Furthermore, it was also observed (**Fig. 1.14**) that there was limit to the number of aldehydes that could be attached to the scaffold. At levels above 0.75 equiv. unbounded imidazole **A1** (31 min) was observed in the SEC/GPC spectra. The intensity of the **P1A1** peak (18 min) also stopped increasing beyond 0.75 equiv. This

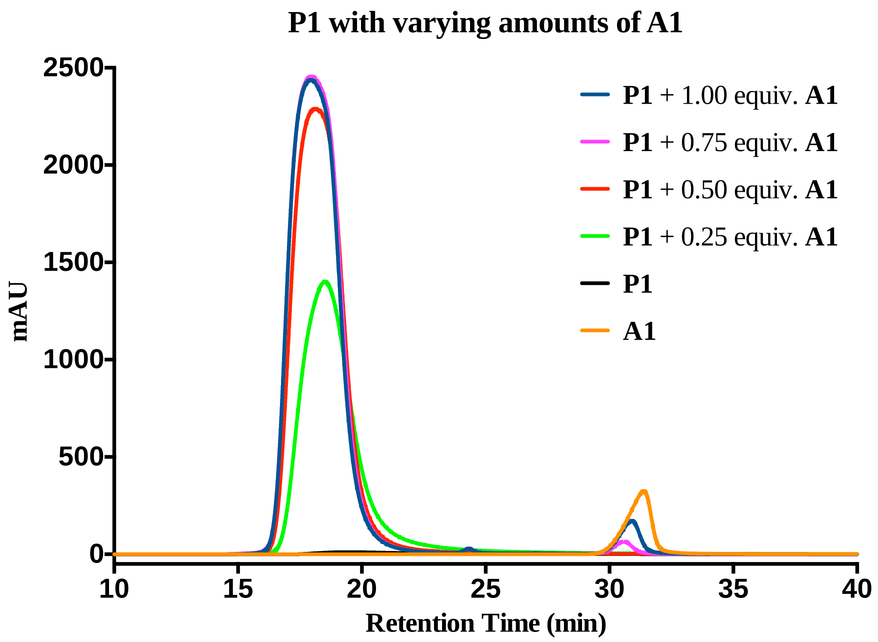

Figure 1.14: SEC/GPC chromatogram showing the functionalisation of **P1** with imidazole aldehyde **A1** at different equivalence values.

was not unexpected, as it is believed the side-chains are becoming increasingly sterically hindered. Similar levels of functionalisation were reported by Bertozzi's group during their synthesis of glycopolymers using a similar scaffold to **P1**.[17]

Functionalisation of poly(acryloyl hydrazide) P1 with aldehydes

To investigate the functionalisation of poly(acryloyl hydrazide) under aqueous conditions we used 4–imidazolecarboxaldehyde **A1** as a model hydrophilic aldehyde and **P1**$_{40}$ as the polymer scaffold. As reported before, by SEC/GPC the coupling of **A1** in 100 mM $AcOH_{(aq)}$ was complete up to ~0.75 equiv. aldehyde. This was investigated further by ^{1}H NMR spectroscopy in a 100 mM $AcOH/D_2O$ buffer. It was observed that the duration of the coupling was not dependent on the number of equivalents added, with 0.3 and 0.6 equiv. of **A1** requiring one hour for complete coupling to be observed (**Fig. 1.15**). For 0.9 equiv., no full consumption of aldehyde was observed even after 24 h. (**Table 1.3**), however the amount of free aldehyde

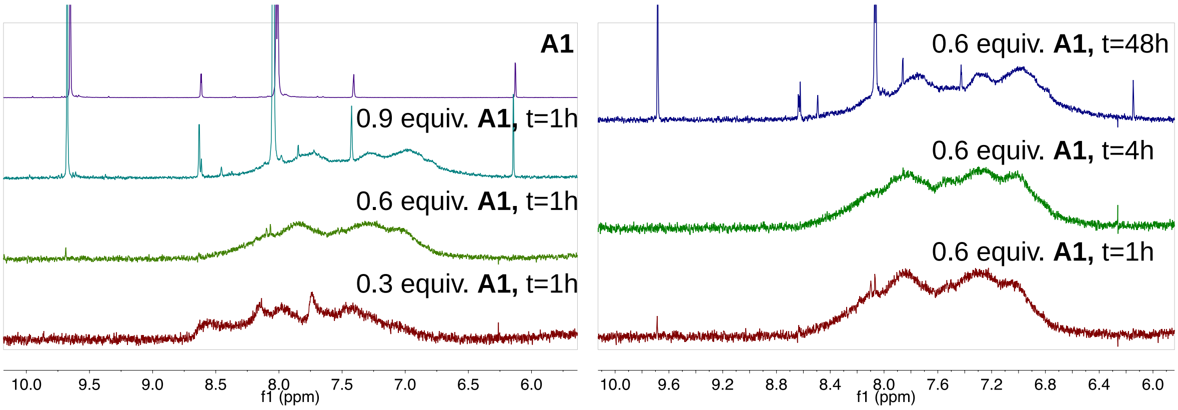

Figure 1.15: ^{1}H NMR spectra of **A1** (Top) and **P1**$_{40}$ in the presence of decreasing amounts of **A1** (left). ^{1}H NMR spectra of **P1**$_{40}$ in the presence of 0.6 equiv. **A1** at different time intervals.

(~27%) was generally constant at measured time intervals, suggesting that ~66% of the hydrazide side-chains had reacted. For 0.6 equiv., despite initially observing full aldehyde consumption, it was observed that after 48 hours 7% of the aldehyde had been regenerated (**Fig. 1.15**) suggesting that the hydrazones formed are not completely stable under these conditions.

Further coupling under aqueous conditions was investigated by reacting **P1**$_{40}$ with a series of hydrophilic aldehydes including glyceraldehyde (**A2**), anionic glyoxylic acid

Equivalence of 4−imidazolecarboxaldehyde (A1)	Reaction Time (h)	% conjugation
0.3	1	30.0
	4	30.0
0.6	1	59.9
	4	60.0
	48	55.8
0.9	1	65.7
	4	65.7
	24	65.7

Table 1.3: Percentage loading of **P1**$_{40}$ with 4-imidazolecarboxaldehyde (**A1**) using different equivalents and different incubation times.

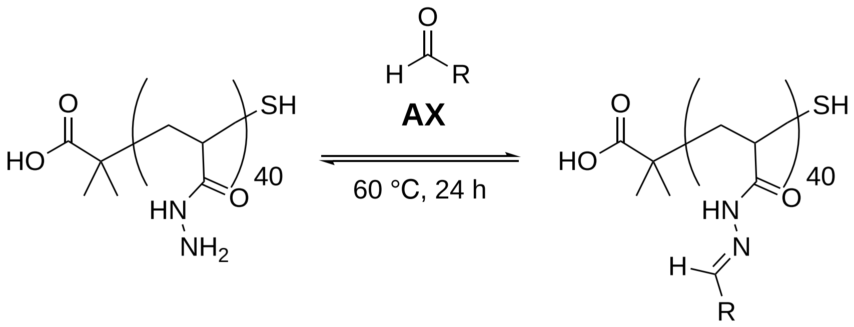

P1$_{40}$ **P1$_{40}$AX**

A1 **A2** **A3** **A4** **A5** **A6**

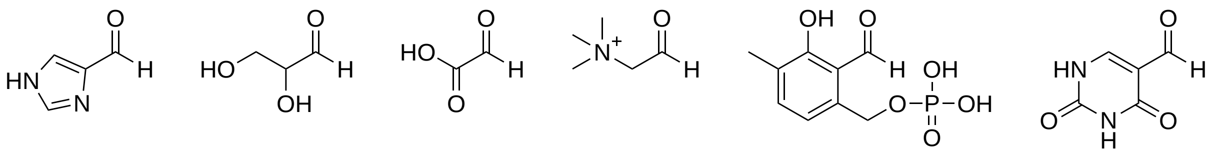

Entry	Polymer	5% AcOH in D_2O pH 2.88	100 mM Na_2HPO_4 in D_2O pH 9.11	95% DMSO-*d6* 5% AcOH in D_2O
1	**P1$_{40}$A1**	66	-	74
2	**P1$_{40}$A2**	65	13	20
3	**P1$_{40}$A3**	3	63	68
4	**P1$_{40}$A4**	80	-	30
5	**P1$_{40}$A5**	—[a]	86	—[a]
6	**P1$_{40}$A6**	—[a]	—[a]	65

Table 1.4: Percentage loading in coupling reactions of **P1$_{40}$** with different water soluble aldehydes under different aqueous conditions. All experiments characterised after 24 h incubation at 60 ℃. Percentage functionalisation calculated by ^{1}H NMR signal integration. [a]Insoluble aldehyde and insoluble products.

(**A3**) or aldehydes which contain biologically important motifs such as betaine aldehyde chloride (**A4**), pyridoxal-5'-phosphate (**A5**) and 5-formyluracil (**A6**) (**Table 1.4**). As expected, the coupling was highly dependent on the solubility of both the aldehyde and functionalised polymer in the buffer used. When acidic conditions were used (5% AcOH, 24 h incubation time) only the neutral (**A2**) and the cationic aldehydes (**A4**) gave similar degrees of functionalisation to that reported for the imidazole derivative (**A1**). The anionic phosphate aldehyde (**A5**) and the uracil derivate (**A6**) were insoluble in this acidic buffer while glyoxylic acid (**A3**) resulted in insoluble polymers that compromised the characterisation of the degree of functionalisation. Switching to a basic phosphate buffer (100 mM Na_2HPO_4) compromised the overall coupling, and in this case, only the anionic derivatives gave satisfactory degree of functionalisation. Indeed a good 63% coupling was observed for glyoxylic acid (**A3**) and a very good 86% coupling for pyridoxal-5'-phosphate (**A5**). 5–Formyluracil (**A6**) remained insoluble in both acid and basic media so a polar organic solvent like DMSO was opted for, to carry out the coupling. However, due to the solubility properties of **P1** mentioned before, the functionalisations of **P1** in 100% DMSO could not be carried out, instead the polymer had to be dissolved in an aqueous AcOH buffer first and diluted in DMSO up to 95% DMSO content. Using a co-solvent like DMSO in the coupling reactions facilitated the comparison of percentage functionalisation between different aldehydes in the same solvent. Investigation of the kinetics of the reactions with our model aldehyde **A1** revealed that although similar degrees of functionalisation could be achieved, often longer incubation times (24 h) and temperatures of 60 ℃ were required. This observation seems to be in accordance to one of the fundamental principles of click-chemistry, which states that when water is used in reactions as a solvent, it can act as a powerful catalyst.[18] Using a 1:1 mixture of aqueous buffer (5% AcOH in D_2O) and DMSO-*d6*, less than half of the imidazole (**A1)** had coupled after incubation for 24 h at 60℃ (**Fig. 1.16**). Surprisingly, however, using a 5% of the aqueous buffer and 95% DMSO-*d6* solvent mixture, functionalisation of 74% of side-chains was achieved. In light of this observation, all coupling reactions with the remaining aldehydes (**A2**-**A6**)

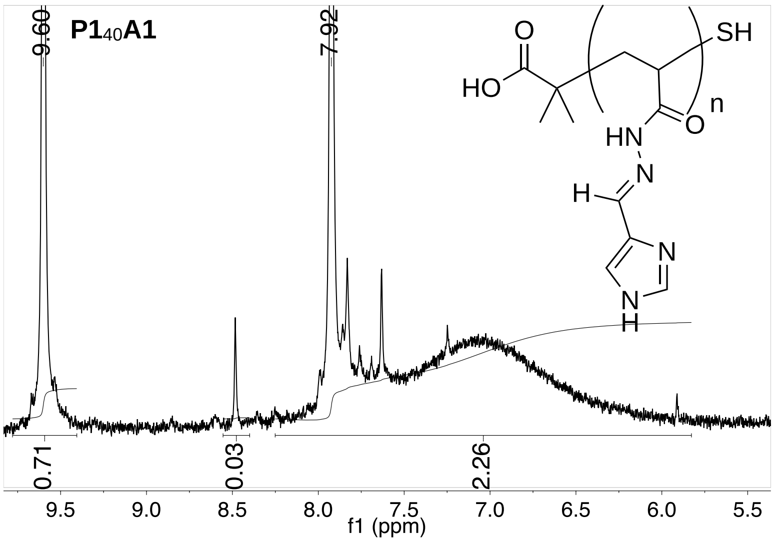

Figure 1.16: ^{1}H NMR spectrum of the functionalisation of **P1**$_{40}$ with 4–imidazolecarboxaldehyde (**A1**) in a 1:1 mixture of 5% AcOH in D_2O and DMSO–*d6*.

were carried out in this solvent mixture (95% DMSO-*d6* / 5% AcOH in D_2O) and reaction conditions (24 h incubation time at 60 ℃). Under these conditions, **P1**$_{40}$ was successfully functionalised up to 65% with the uracil derivative (**A6**), which was previously not determined due to its insolubility in the aqueous buffers used. All aldehydes apart from pyridoxal-5'-phosphate (**A5**) were soluble and coupled with varying results. Glyceraldehyde (**A2**) showed a low degree of functionalisation (20%) as evidenced by the hydrazone peak at 7.38 ppm, mainly, believed to be, due to competing self-polymerisation reactions via cyclic ketal formation as evidenced by the disappearance of the aldehyde peak and the appearance of a new signal at 3.53 ppm (**Fig. 1.17**).

In biological applications such as antimicrobial polymers and gene delivery vectors there is often the need for hydrophobic components.[19-24] Using DMSO in the coupling reactions allowed the investigation of the coupling of a series of commercially available hydrophobic molecules ranging from aromatic to aliphatic

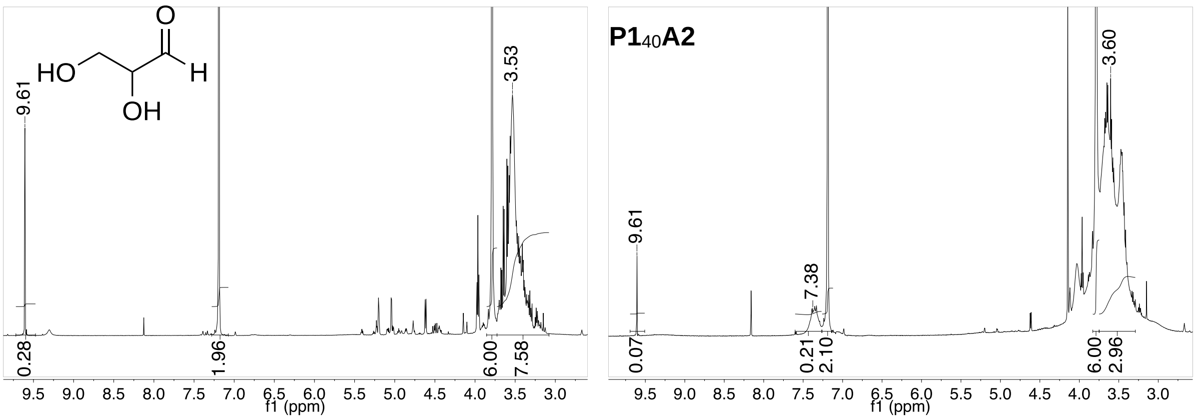

Figure 1.17: ^1H NMR spectra of the glyceraldehyde (**A2**) control reaction (left). ^1H NMR of **P1**$_{40}$ functionalisation with glyceraldehyde (**A2**) (right). Both samples were incubated for 24 h at 60 ℃ in 5% aqueous buffer (5% AcOH in D_2O) 95% DMSO-*d6*. Samples were spiked with equimolar amounts of syringic acid (7.19 and 3.79 ppm).

aldehydes. Among these, it was experimented with unsubstituted aromatics like benzaldehyde (**A7**) and naphthaldehyde (**A8**), hydroxy or fluoro-substituted aromatics such as 4−hydroxybenzaldehyde (**A9**), 2,3−dihydroxybenzaldehyde (**A10**), and 2,4,6−trihydroxybenzaldehyde (**A11**), 2,4,6−trifluorobenzaldehyde (**A14**) and 2,3,4,5,6-pentafluorobenzaldehyde (**A15**), carboxylated aromatic aldehydes such as 5−formylsalicylic acid (**A12**), heteroaromatic aldehydes such as 4−imidazole carboxaldehyde (**A1**) and indole-3-carboxaldehyde (**A13**), as well as aliphatic linear and branched aldehydes such as acetaldehyde (**A16**), isovaleraldehyde (**A17**), 2−ethylhexanal (**A18**), octanal (**A19**) and decanal (**A20**).

Initially the coupling was investigated in a 1:1 mixture of aqueous buffer (5% AcOH in D_2O) and DMSO-*d6* to mimic the conditions used in the work on siRNA delivery (see **Chapter 3**). The experiments were carried out by dissolving the aldehyde in DMSO and adding the polymer solubilised in the aqueous buffer. For most samples immediate precipitation of aldehyde or functionalised polymer was observed (**Fig. 1.18**), but most samples dissolved after stirring and heating to 60 ℃ for 4 h. Upon

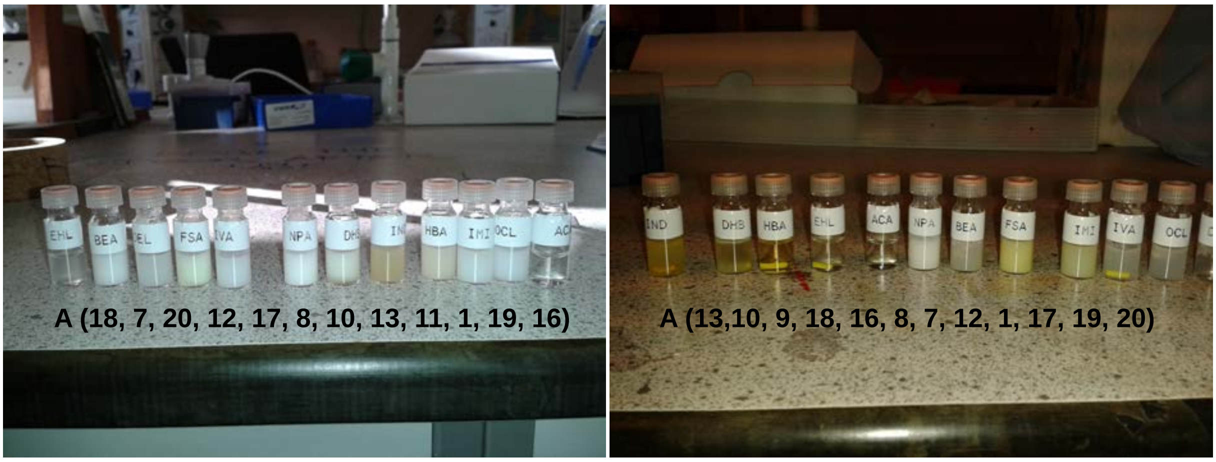

Figure 1.18: Photographs showing: Reactions of poly(acryloyl hydrazide) **P1**$_{40}$ with different aromatic and aliphatic aldehydes at t=0 (left) and t=4 h (right) in 1:1 mixture aqueous buffer (5% AcOH in D_2O) and DMSO-*d6*.

cooling, however, most samples precipitated out of solution. Interestingly, the precipitates formed did display different colours than the original precipitates suggesting that coupling to poly(acryloyl hydrazide) had occurred. Further evidence towards functionalisation is that the ^{1}H NMR spectra showed complete absence of polymer but presence of free aldehyde, quantification of coupling was not obtained however.

The coupling reactions were repeated in 5% aqueous buffer and 95% DMSO-*d6* and overall the coupling efficiency for aromatic aldehydes was around the 70% expected benchmark regardless of the molecule size (**Table 1.5**, **Entry 1** vs **Entry 2**) or substitution at the aromatic centre (**Entry 3** vs **Entry 4** vs **Entry 6**, vs **Entry 8**). Short aliphatic aldehydes showed very good coupling efficiencies (**Entry 10** vs **Entry 11**) while for the bulkier molecules (**Entry 12** vs **Entry 13** vs **Entry 14**) the couplings are estimative since turbid solutions were observed suggesting insoluble products or micelle formation. Percentage functionalisation was determined by ^{1}H NMR spectroscopy signal integration (**Fig. 1.19**) by comparing the sharp aldehyde peak against the other peaks and the newly formed broad hydrazone peak (usually ~7.40

AX

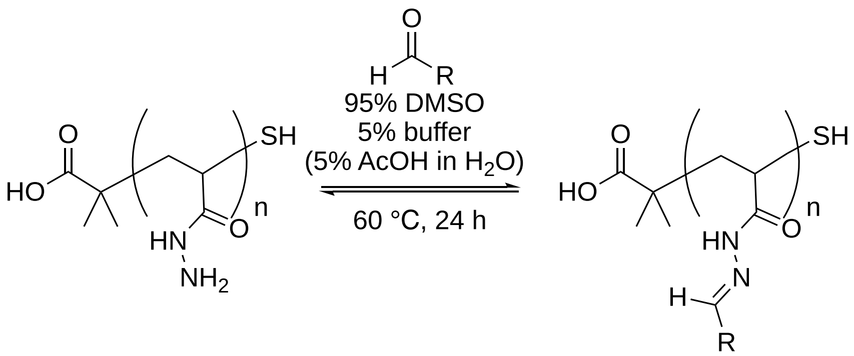

P1$_{40}$ **P1$_{40}$AX**

A7 **A8** **A9** **A10** **A11** **A12** **A13**

A14 **A15** **A16** **A17** **A18** **A19** **A20**

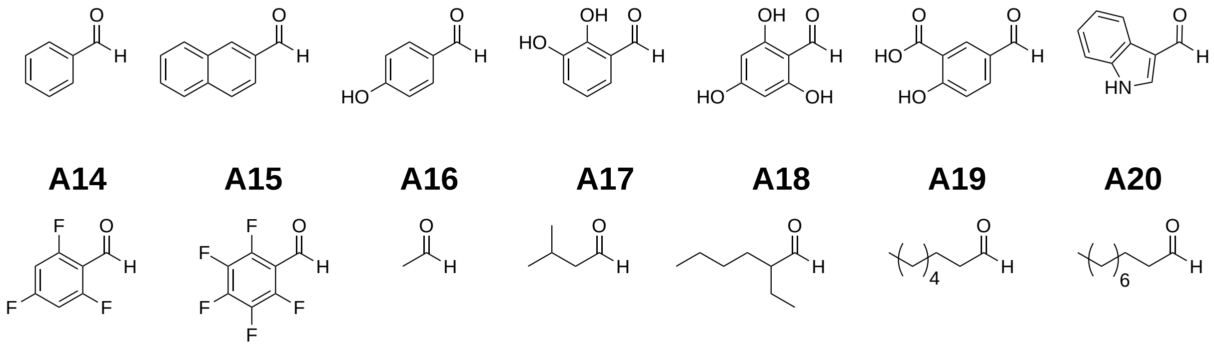

Entry	Polymer	%loading	Entry	Polymer	%loading
1	**P1$_{40}$A7**	64	**8**	**P1$_{40}$A14**	72
2	**P1$_{40}$A8**	73	**9**	**P1$_{40}$A15**	56
3	**P1$_{40}$A9**	71	**10**	**P1$_{40}$A16**	96
4	**P1$_{40}$A10**	85	**11**	**P1$_{40}$A17**	75
5	**P1$_{40}$A11**	50	**12**	**P1$_{40}$A18**	—[a]
6	**P1$_{40}$A12**	75	**13**	**P1$_{40}$A19**	62[a]
7	**P1$_{40}$A13**	52	**14**	**P1$_{40}$A20**	59[a]

Table 1.5: Percentage loading in coupling reactions of **P1$_{40}$** with different hydrophobic aldehydes. All experiments characterised after 24 h incubation at 60 ℃ in 5% aqueous buffer and 95% DMSO-*d6*. Percentage functionalisation calculated by ^{1}H NMR signal integration. [a]insoluble products.

ppm, generally not clearly identified with aromatic aldehydes due to broadening of aromatic signals). The integration was compared against control reactions in which the aldehydes were incubated in the absence of poly(acryloyl hydrazide) and both

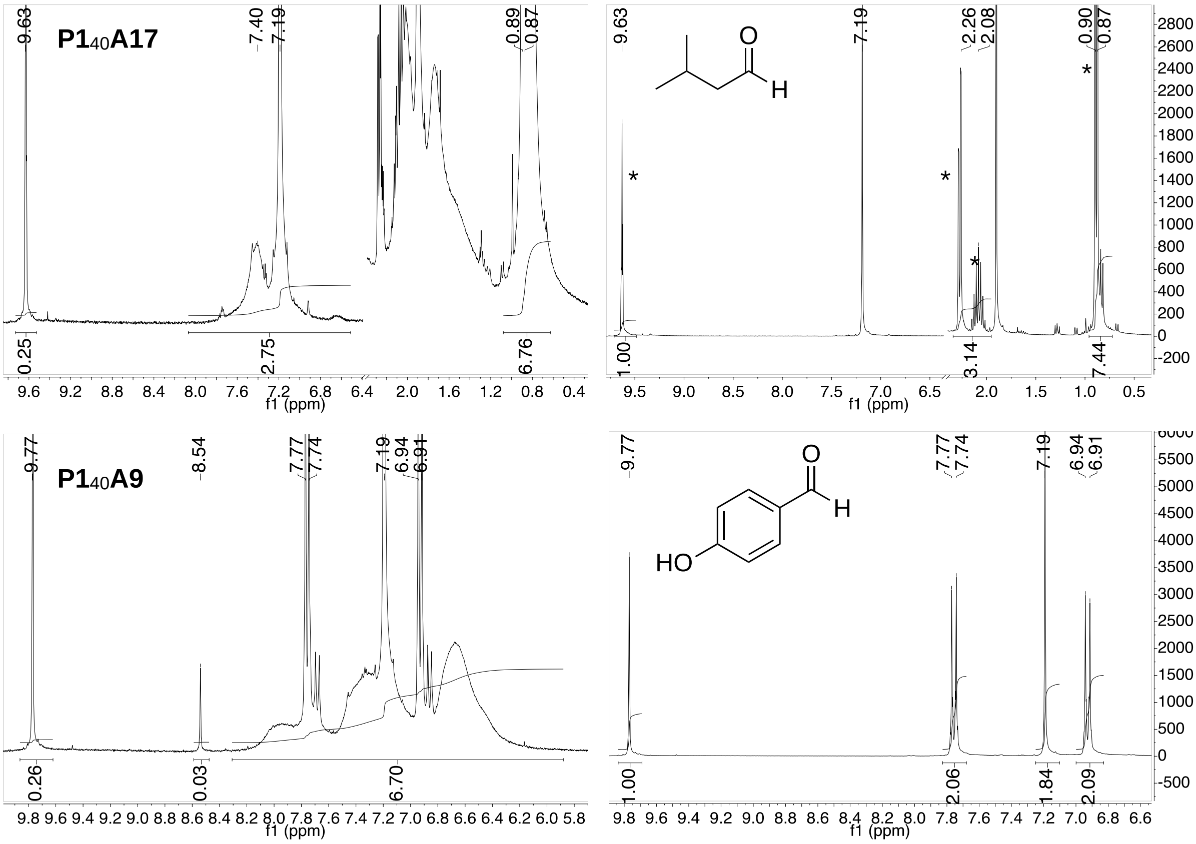

Figure 1.19: ^{1}H NMR spectra of the reaction of **P1**$_{40}$ with isovaleraldehyde (**A17**) (top left) and 4−hydroxybenzaldehyde (**A9**) (bottom left) and their controls (top right, bottom right), showing the determination of percentage loading. Samples were incubated for 24 h at 60 ℃ in 5% aqueous buffer (5% AcOH in D_2O) 95% DMSO-*d6*. Samples were spiked with equimolar amounts of syringic acid (7.19 ppm).

reaction and control were spiked with equimolar amounts of syringic acid prior to running ^{1}H NMR spectroscopy. Furthermore, broadening of the signals belonging to the aldehyde was a clear indication that coupling was occurring. Several aldehydes (**A11**, **A13**, **A15**) displayed degrees of functionalisation visibly lower than the overall average. It is believed that 2,4,6−trihydroxybenzaldehyde (**A11**) has a less electrophilic carbonyl centre as a result of electron delocalisation due to the three hydroxy groups. Furthermore, in the control reaction, the peak at 5.80 ppm (**Fig. 1.20**), which was assigned to the two aromatic protons, integrates to only 33% expected value compared to the aldehyde signal (1:0.66 instead of 1:2). This could

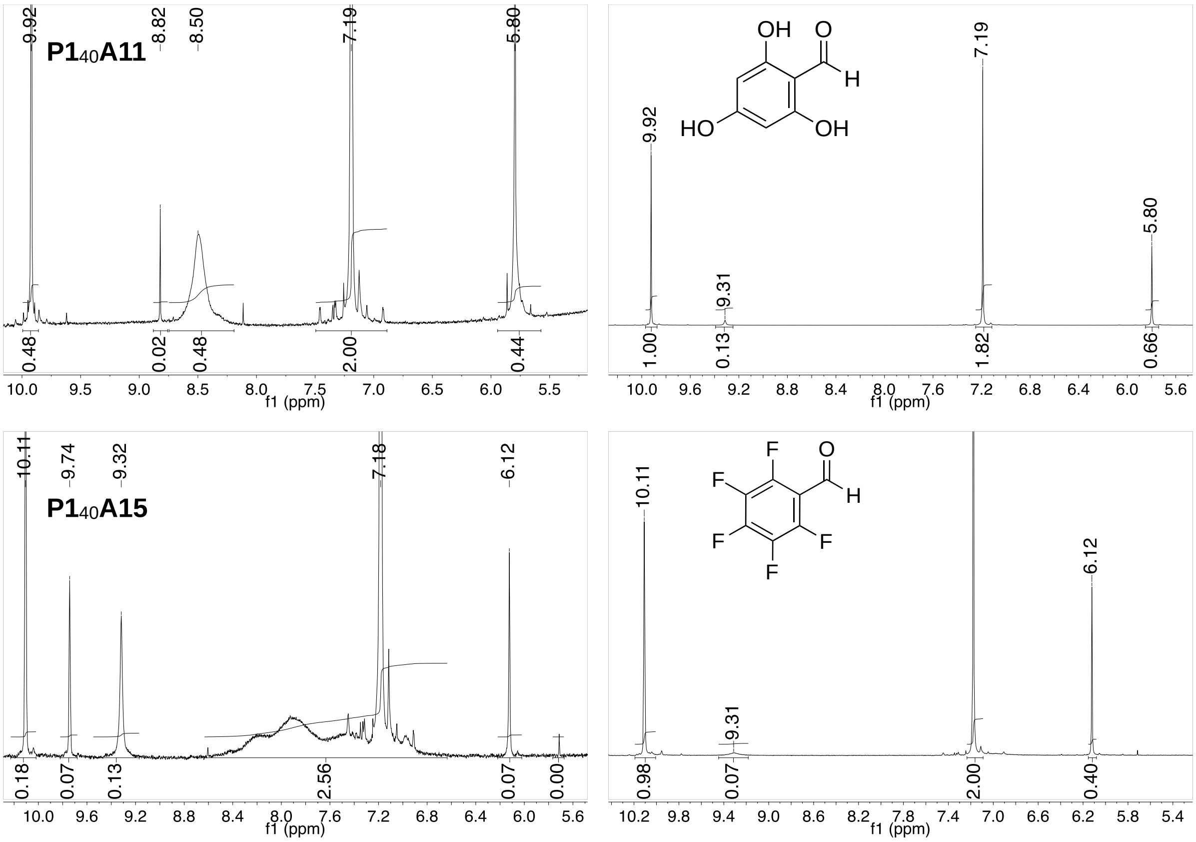

Figure 1.20: ^{1}H NMR spectra of the reaction of **P1**$_{40}$ with 2,4,6-trihydroxybenzaldehyde (**A11**) (top left) and pentafluorobenzaldeyde (**A15**) (bottom left) and their controls (top right, bottom right) showing the determination of percentage loading and by-products. Samples were incubated for 24 h at 60 ℃ in 5% aqueous buffer (5% AcOH in D_2O) 95% DMSO-*d6*. Samples were spiked with equimolar amounts of syringic acid (7.19 ppm).

be due to longer relaxation time of the aromatic protons, although ^{1}H NMR spectroscopy experiments carried out with longer scans and longer relaxation times always resulted in similar results as the normal conditions. Alternatively, there is a possibility that in this acidic solvent mixture proton exchange with the aromatic protons could be occurring.[25] This made the accurate determination of percentage loading more difficult. The pentafluorobenzaldehyde (**A15**) similarly displayed peculiarities in its ^{1}H NMR spectra (**Fig. 1.20**). The spectra of the control displayed an unexpected singlet peak at 6.12 ppm which had an integration of 0.40 compared to the aldehyde peak. A plausible explanation is the formation of the relatively stable pentafluorophenylmethanediol due to the presence of strong electron withdrawing group (i.e. pentafluorobenzene). This could potentially mean that a longer reaction time is needed to achieve similar similar couplings efficiency to the other aldehydes. Furthermore, during the reaction with poly(acryloyl hydrazide) **P1** two new sharp singlets were observed in the aldehyde region at 9.74 and 9.31 ppm suggesting additional by-products.

Especially in the case of reactions with aromatic aldehydes the formation of new impurities was observed. The ^{1}H NMR spectra (**Fig. 1.21**) of these impurities bear resemblance to their aldehyde counterparts in the sense that they showed the same number of peaks and multiplicity. The major difference is that the impurities showed a characteristic sharp singlet between 9.0-8.5 ppm (**Fig. 1.21**) instead of the 10.1-9.7 observed for the aldehyde peak. These impurities could be identified in all the functionalisations with aromatic aldehydes, but their overall content was generally around 1-3% of total amount of aldehyde used (**Table 1.6**). These chemical shift seemed to be consistent with *H*-C(R)=X environments where it was hypothesised that X could be N-R or N-NHR, meaning that the impurity observed would be as a result from imine or hydrazone formation. To prove this hypothesis, reactions were carried out in conditions similar to those used for functionalisation of **P1**, using ammonia and hydrazine monohydrate. None of the conditions tested with ammonia resulted in compounds whose NMR spectra matched that of the observed impurities. Coupling between hydrazine and benzaldehyde (**A7**) and between hydrazine and 4−hydroxybenzaldehyde (**A9**), however, resulted in the formation of hydrazones with NMR spectra (**Fig. 1.22**) that matched those of the impurities observed. In the presence of only 1 equiv. of hydrazine, two distinct hydrazones could be formed with

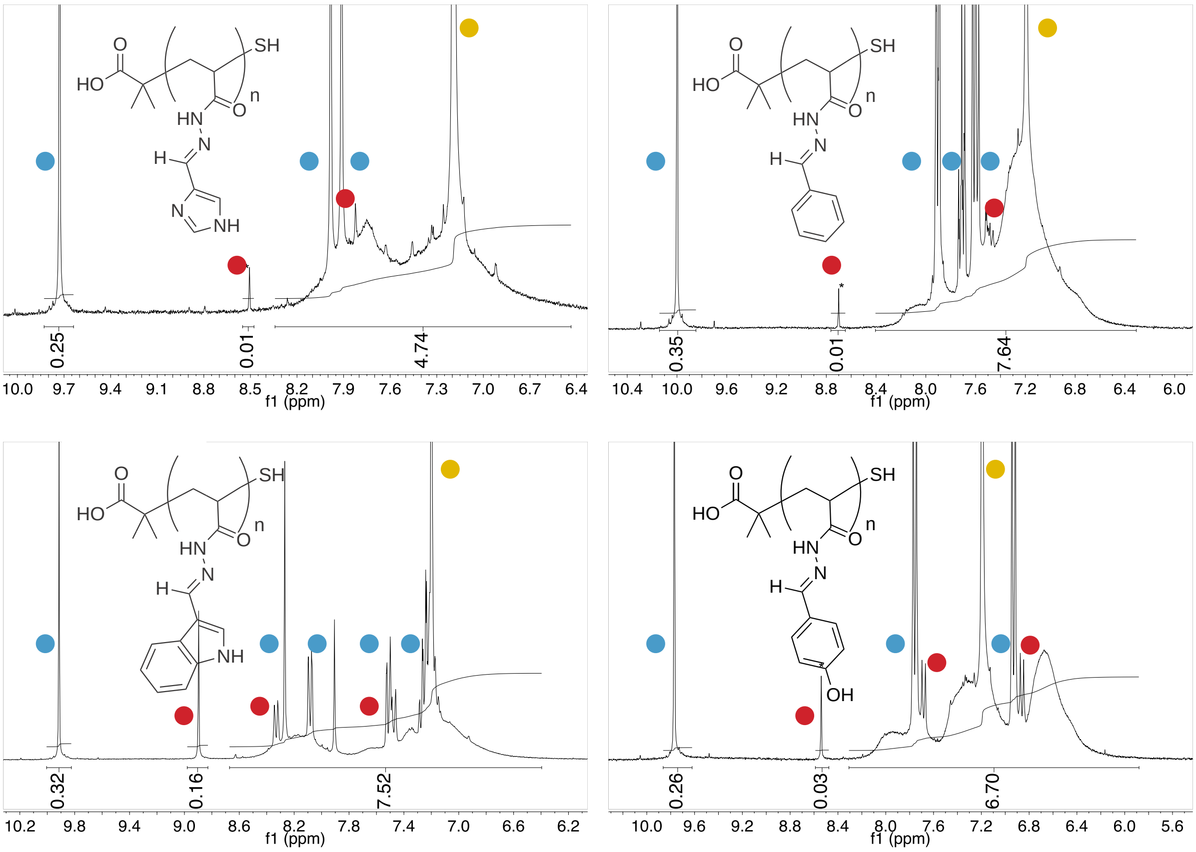

Figure 1.21: ^{1}H NMR spectra of the reactions of **P1**$_{40}$ with representative aromatic aldehydes, showing broad hydrazone signals from the functionalised polymer, signals from unreacted aldehydes [blue circles] and signals from small molecule hydrazone impurities (sharp hydrazone singlets between 9.0-8.5 ppm and sharp aromatic signals (some are concealed underneath the broad aromatic peaks) [red circles]. All samples were spiked with equimolar amounts of syringic acid (7.19 ppm) [yellow circle]. The integration values of the aldehyde and hydrazone signals represent the percentage unreacted aldehyde and impurity formed.

Entry	Polymer	%Impurity	Entry	Polymer	%Impurity
1	**P1$_{40}$A7**	1	8	**P1$_{40}$A14**	3
2	**P1$_{40}$A8**	2	9	**P1$_{40}$A15**	27
3	**P1$_{40}$A9**	3	10	**P1$_{40}$A16**	—
4	**P1$_{40}$A10**	1	11	**P1$_{40}$A17**	—
5	**P1$_{40}$A11**	2	12	**P1$_{40}$A18**	—
6	**P1$_{40}$A12**	3	13	**P1$_{40}$A19**	—
7	**P1$_{40}$A13**	16	14	**P1$_{40}$A20**	—

Table 1.6: Percentage impurity formed in coupling reactions of **P1**$_{40}$ with different hydrophobic aldehydes. All experiments characterised after 24 h incubation at 60 ℃ in 5% aqueous buffer and 95% DMSO-*d6*. Impurity formation calculated by ^{1}H NMR peak integration.

benzaldehyde (**Fig. 1.22**, **C**), which were attributed to the mono- and di-hydrazone. This was confirmed by treating the aldehyde (**A7**) with excess amounts of hydrazine (4.0 equiv.) so that formation of the monohydrazone was favoured (**Fig. 1.22**, **B**). Conversely, 4-hydroxybenzaldehyde reacted with 1 equiv. hydrazine to form only the mono-hydrazone product (**Fig. 1.22**, **F**), while excess aldehyde (2.0 equiv.) lead to the formation of both the mono- and di−hydrazone products (**Fig. 1.22**, **G**). To further

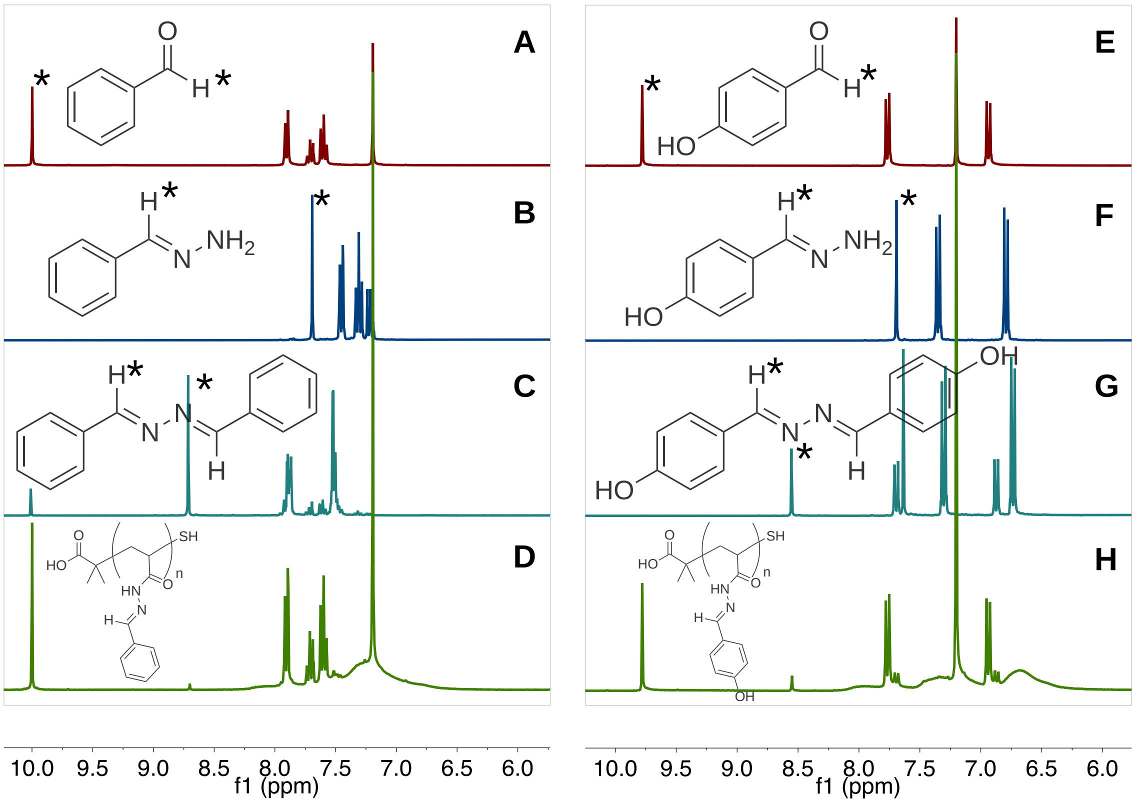

Figure 1.22: ^{1}H NMR spectra of (A) benzaldehyde (**A7**); (B) reaction between benzaldehyde and 4 equiv. hydrazine to afford monobenzylidenehydrazine; (C) reaction between benzaldehyde and 1 equiv. hydrazine to afford mostly dibenzylidenehydrazine; (D) the reaction of **P1**$_{40}$ with 1 equiv. **A7**; (E) 4−hydroxybenzaldehyde (**A9**); (F) reaction between 4−hydroxybenzaldehyde and 1 equiv. hydrazine monohydrate to afford mono(4−hydroxybenzylidenehydrazine); (G) reaction between benzaldehyde and 0.5 equiv. hydrazine monohydrate to afford a mixture of mono- and di (4−hydroxybenzylidenehydrazine; (H) the reaction of **P1**$_{40}$ with 1 equiv. **A9** (D) All samples were incubated for 24 h in 95% DMSO-*d6* / 5% AcOH in D_2O. Samples A, D, E, and H contain 1 equiv. syringic acid as internal standard.

investigate the formation of the mono- and di-hydrazones, kinetic studies were carried out with substoichiometric (0.25 equiv.) amounts of benzaldehyde (**A7**) and **P1** in the established conditions. It was observed that even before all the aldehyde had coupled to the polymer (~4 h) (**Fig. 1.23**, **F**), both the mono- and di-hydrazone impurities could be identified by ^{1}H NMR spectroscopy. Following the full consumption of the aldehyde, a steady increase in the concentration of the mono-hydrazone (benzylidenehydrazine) was observed, with up to 15% content (compared

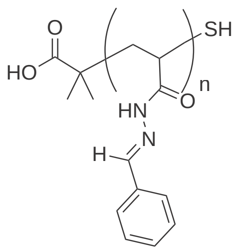

P1$_{40}$A7

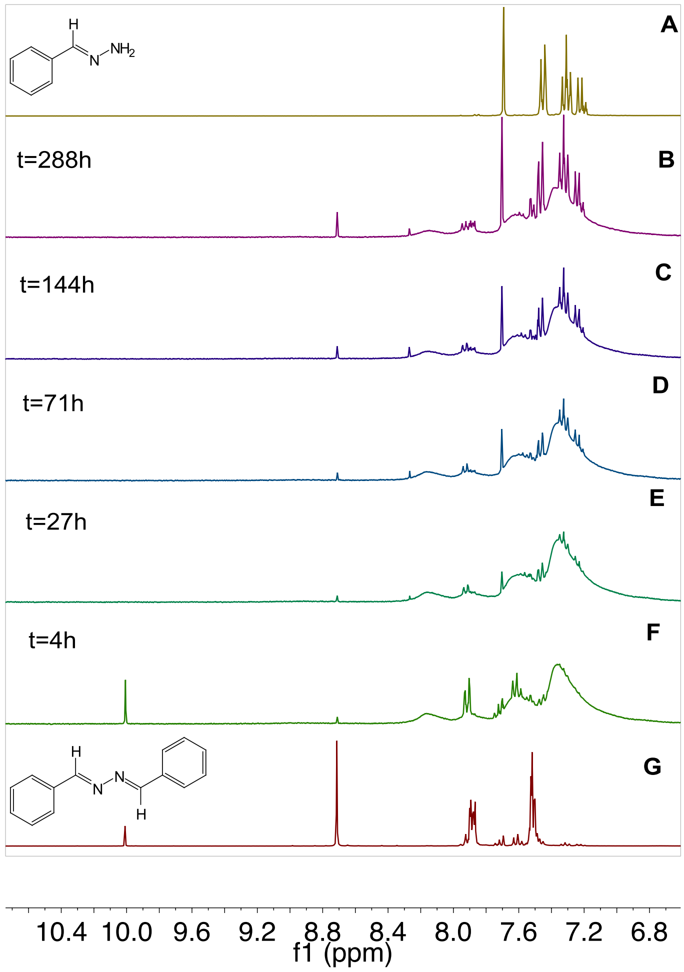

Figure 1.23: ^{1}H NMR spectra of the reaction of **P1**$_{40}$ with 0.25 equiv. benzaldehyde (**A7**) monitored at different time intervals (B-F). ^{1}H NMR spectra of monobenzylidenehydrazine (A), dibenzylidenehydrazine (G) are shown for comparison. All samples were incubated for 24 h in 95% DMSO-*d6* / 5% AcOH in D_2O.

to original aldehyde content) after 12 days (**Fig. 1.23**, **B**). No significant increase in the concentration of the di-hydrazone (1,2−dibenzylidenehydrazine) (~3%) was observed even after 12 days. Mechanistically, this would suggest that the mono-hydrazone forms first through the cleaving of the C-N bond from the polymer's hydrazide chains. The di−hydrazone would then be formed through the subsequent reaction between the mono-hydrazone and any free aldehyde left in solution. As far as it was ascertained, there are no clear examples of such reactivity occurring in small molecule organic chemistry. Instead, it is believed that a macromolecular effect may be responsible, similar to a protease type mechanism[26] (**Fig. 1.24**). It remains to be elucidated whether H_2O/D_2O in the solution, or any nucleophile for that matter,

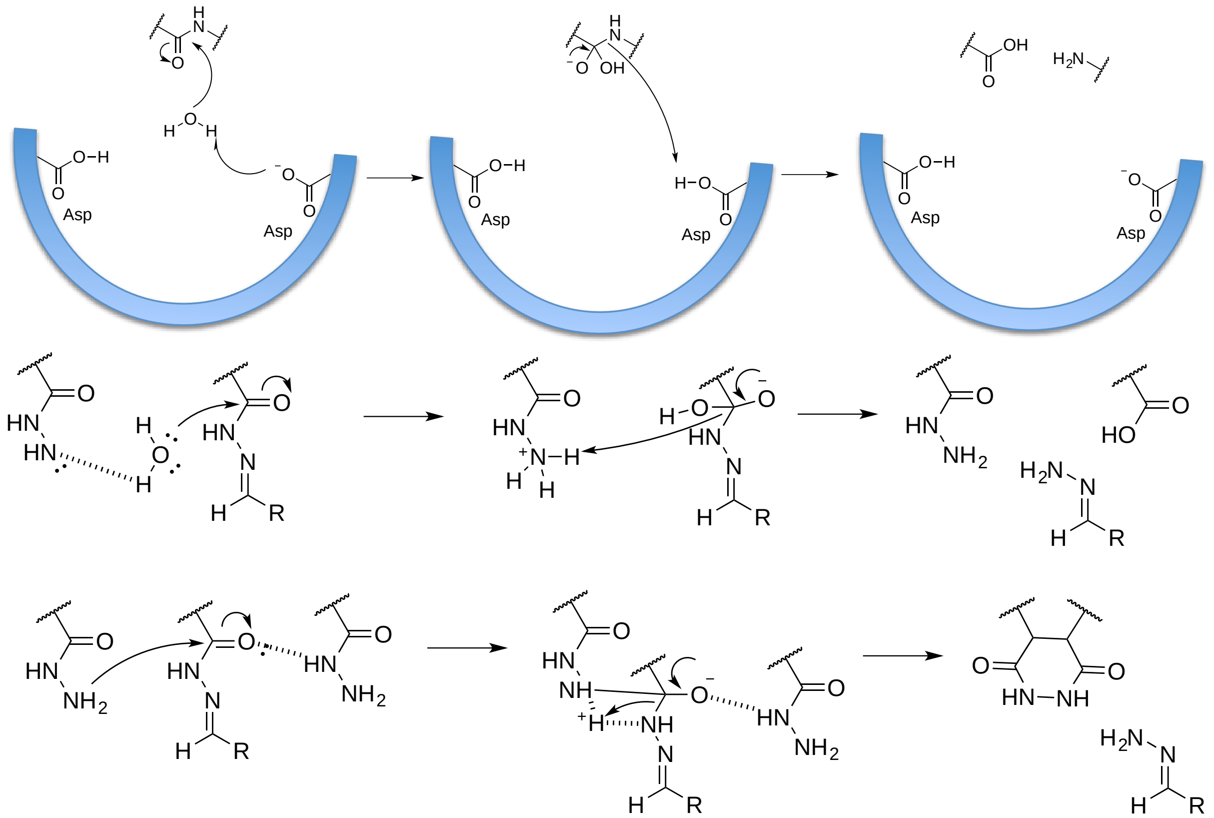

Figure 1.24: Aspartyl protease mechanism, one of many types of proteases (top); proposed mechanism responsible for mono-hydrazone formation driven by an external nucleophile (e.g. water) (middle); proposed mechanism responsible for mono-hydrazone formation driven solely by unreacted hydrazide side-chains (bottom).

take part in the formation of the impurity, or the whole process is driven intramolecularly by neighbouring, non-functionalised side-chains. Nonetheless, the data suggests that the larger the number of non-functionalised side-chains the higher the extent of impurities formed. This was evidenced by the lower amount of impurity formed when **P1**$_{40}$ was reacted with 1.0 equiv. compared to its reaction with 0.25 equiv. benzaldehyde (**A7**). Attempts were made to identify the mechanism responsible through two means; one set of experiments attempted to disprove that water plays a role in the reaction which would indicate a mechanism driven solely by the free hydrazide side-chains. Solid-liquid coupling reactions were carried out, in which the solid poly(acryloyl hydrazide) **P1** was stirred at 60 ℃ with solutions of **A7** or **A9** in dry DMSO with AcOH. It was observed that eventually the functionalised polymer does dissolve in the solution, but the characteristic ^{1}H NMR signals from the trace impurities were also observed (**Fig. 1.25**, red circles). However, since complete absence of water from the system could not be guaranteed (i.e. water content in dry DMSO is only as low as 100 ppm), the experiment did not prove with a certainty that water does not play a role in the formation of the impurity.

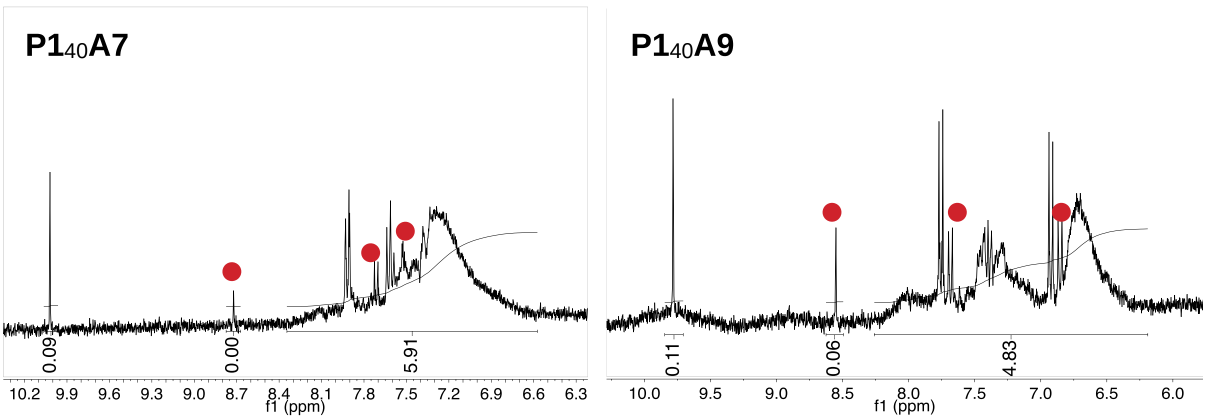

Figure 1.25: ^{1}H NMR spectra of the reaction of **P1**$_{40}$ with 1.0 equiv. benzaldehyde (**A7**) (left) and 4-hydroxybenzaldehyde (**A9**) (rigtht). Both samples were incubated for 24 h in dry DMSO with 0.025% AcOH and spiked with DMSO-*d6* for signal acquisition.

The purpose of the second set of experiments was to see if other nucleophiles in the reaction would be incorporated into the polymer as part of the cleaving process. In three separate experiments, **P1** was reacted with with 0.25 equiv. of **A7** and then 0.25 equiv. of ethanol, piperidine or cysteamine were added to monitor the possible formation of the ethyl ester, the amide or the thioester (**Scheme 1.15**). The results were overall inconclusive. Even after 10 days, formation of new peaks (broad or sharp), that would suggest formation of the proposed species, were not observed.

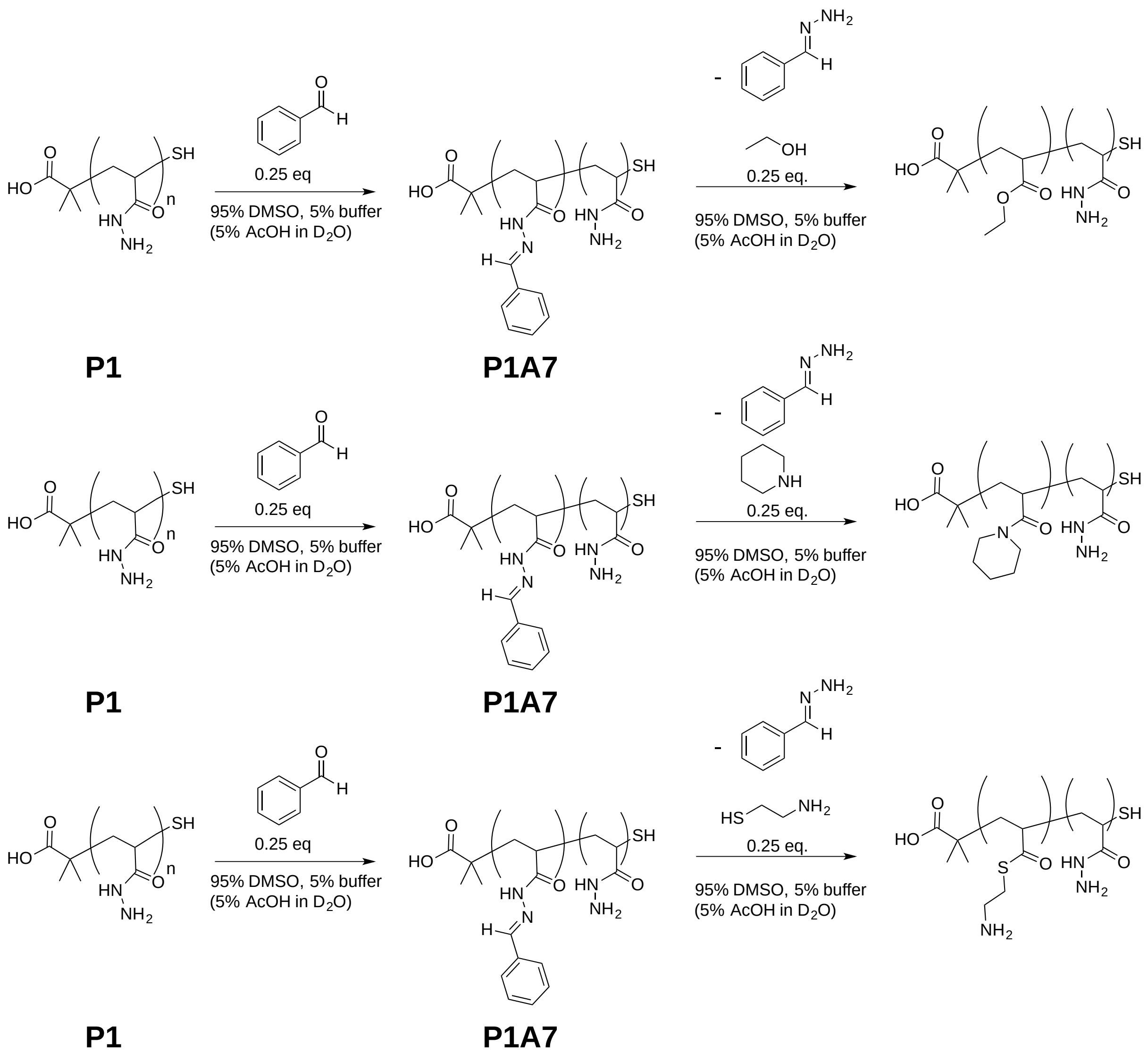

Scheme 1.15: Functionalisation of **P1** with benzaldehyde **A7** followed by reaction with a nucleophile to investigate the mechanism of monobenzylidenehydrazine formation.

This could be because under these conditions water is greatly in excess compared to the added nucleophile, or because the mechanism is indeed independent of external nucleophiles. Nonetheless, at this stage, there is not enough evidence to confirm either of the two hypotheses.

To further probe the scope of functionalisation of **P1** with aldehydes, the effect of excess amounts of aldehyde on the percentage loading was investigated. Functionalisations with three aromatic aldehydes, basic 4−imidazolecarboxaldehyde (**A1**), neutral benzaldehyde (**A7**) and acidic 5−formylsalicylic acid (**A12**), as well as two aliphatic aldehydes: acetaldehyde (**A16**) and isovaleraldehyde (**A17**) were carried out. In all cases, an increase in percentage loading was observed (**Table 1.7**). In some cases full conversion was almost observed, but no significant changes in the

Entry	Aldehyde	Loading 1.0 equiv.	%Impurity	Loading 2.0 equiv.	%Impurity
1	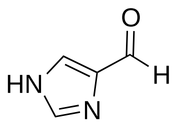	74	1	76	1
2	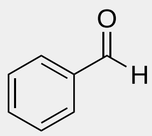	64	1	84	3
3	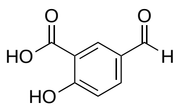	75	3	87	1
4	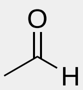	89	—	95	—
5	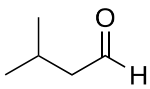	82	—	97	—

Table 1.7: Percentage loading in coupling reactions of **P1**$_{40}$ with selected aldehydes and the amount of impurity formed. Loading and impurity calculated from ^{1}H NMR integration. Samples were incubated for 24 h at 60℃ in 5% aqueous buffer (5% AcOH in D_2O) 95% DMSO-*d6*. Samples were spiked with equimolar amounts of syringic acid (7.19 ppm).

level of impurities formed was observed. The overall increase in percentage loading was not surprising considering that the hydrazone formation is an equilibrium and given Le Chatelier's principle on equilibrium repositioning to counteract the increase in concentration of one of the reactants.

To develop a truly useful tool for investigating structure-activity relationships, the effects on percentage loading as a function of polymer size was explored. As such, functionalisation experiments with **P1**$_{80}$ and aldehydes **A1**, **A7**, **A8**, **A9**, **A10**, **A12**, **A13**, **A16** and **A17** (**Table 1.8**) were carried out. Overall, the trend shows either similar level of coupling like **P1**$_{80}$**A7** and **P1**$_{80}$**A12**, slightly lower (**P1**$_{80}$**A13**, **P1**$_{80}$**A17**) or percentage loadings lower than 10% to the initial aldehyde content (**P1**$_{80}$**A1**, **P1**$_{80}$**A8**, **P1**$_{80}$**A9**, **P1**$_{80}$**A10**, **P1**$_{80}$**A13**, **P1**$_{80}$**A16**) compared to **P1**$_{40}$. Similarly to **P1**$_{40}$, improved side-chain functionalisation could be achieved for **P1**$_{80}$ by reacting the polymer scaffold with 2 equiv. of the aldehyde. This suggested that the lower percentage loadings observed for reactions between **P1**$_{80}$ and 1 equiv. of aldehyde was probably due to slower kinetics due to increased steric hinderance. To gain a better understanding how fast particular aldehydes react with **P1**$_{80}$ a series of kinetic experiments were carried out. ^{1}H NMR spectroscopy was used to monitor the reactions between **P1**$_{80}$, **A7**, **A9**, **A10**, **A12**, **A13** and **A17** after different time intervals at 60 ℃ (**Fig. 1.26**). The data showed that while 5-formylsalicylic acid (**P1**$_{80}$**A12**) and isovaleraldehyde (**P1**$_{80}$**A17**) achieved close to their limiting percentage loading for **P1**$_{80}$ within the first 2 hours of incubation at 60 ℃, benzaldehyde (**P1**$_{80}$**A7**) and 2,3−dihydroxybenzaldehyde (**P1**$_{80}$**A10**) achieved that point after 4-6 h incubation. In the case of the reaction between **P1**$_{80}$ and 4−hydroxybenzaldehyde (**P1**$_{80}$**A9**) and indole-3-carboxaldehyde (**P1**$_{80}$**A13**) respectively, the data shows a continuous increase in percentage loading over 48 hours incubation and no clear evidence of plateauing, suggesting that their limiting percentage loading had not yet been achieved. In the case of the previous four aldehydes, no significant increase was

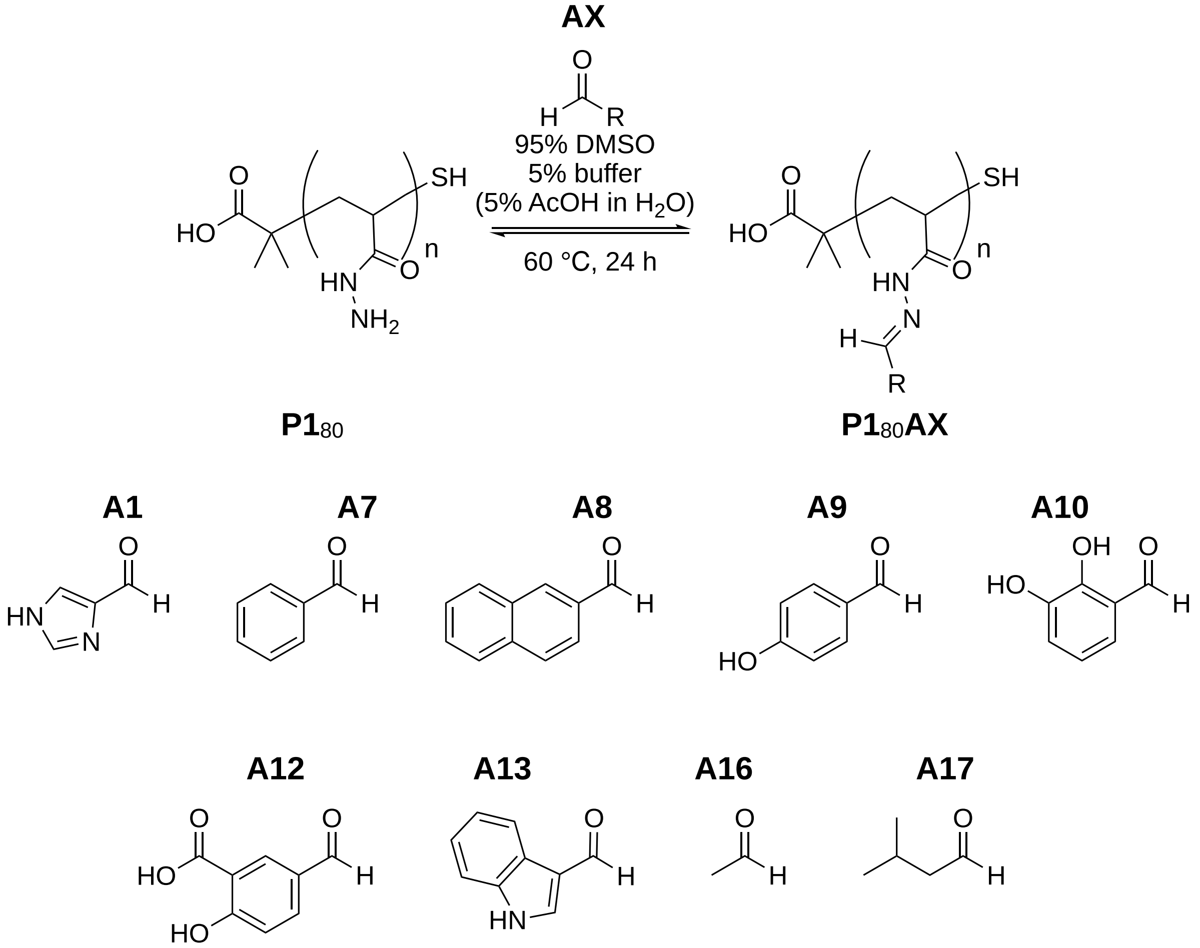

Entry	Polymer	Loading	Impurity	Entry	Polymer	Loading	Impurity
1	**P1**$_{80}$**A1**	60	1	**6**	**P1**$_{80}$**A12**	72	2
2	**P1**$_{80}$**A7**	66	1	**7**	**P1**$_{80}$**A13**	46	12
3	**P1**$_{80}$**A8**	50	1	**8**	**P1**$_{80}$**A16**	65	—
4	**P1**$_{80}$**A9**	59	7	**9**	**P1**$_{80}$**A17**	78	—
5	**P1**$_{80}$**A10**	62	1				

Table 1.8: Percentage loading and percentage impurity in coupling reactions of **P1**$_{80}$ with different hydrophobic aldehydes. All experiments characterised after 24 h incubation at 60 ℃ in 5% aqueous buffer and 95% DMSO-*d6*. Percentage functionalisation calculated by ^{1}H NMR peak integration.

observed after 48 hours incubation. These experiments have shown that, by adjusting reaction time and equivalent amounts of aldehyde used, functional polymers with similar levels of percentage loading could be achieved for a variety of diverse aldehydes onto poly(acryloyl hydrazide) with varied molecular weights. Further experiments could be carried out such as investigating the dynamic aspect of the hydrazone bonds or assessing the stability of the polymers post-functionalisation under different conditions, but at this stage a working model for rapidly testing a

A7 **A9** **A10** **A12** **A13** **A17**

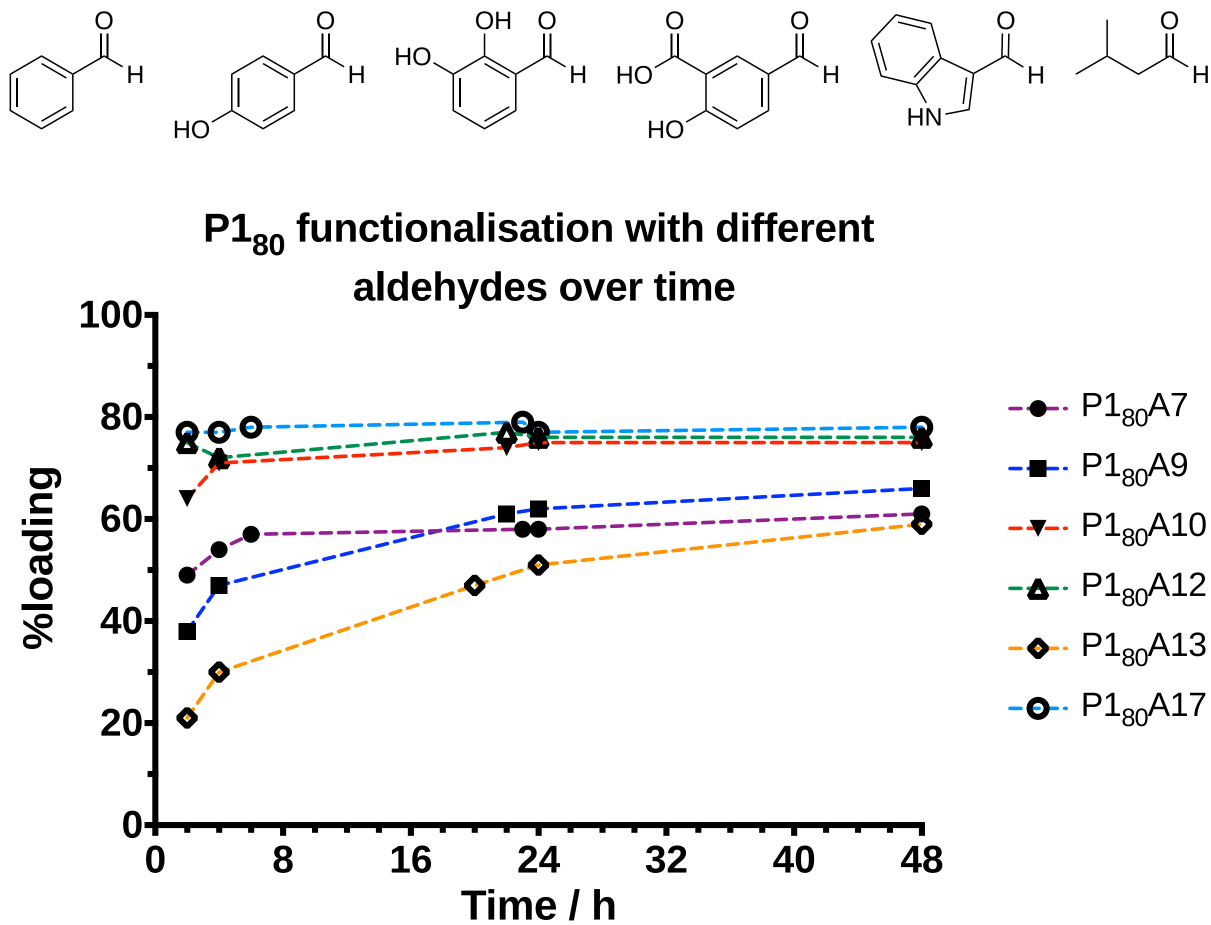

Figure 1.26: Graphs showing percentage loading for six aldehydes with **P1**$_{80}$ at different incubation times. All experiments characterised after incubation at 60 ℃ in 5% aqueous buffer and 95% DMSO-*d6*. Percentage functionalisation calculated by ^{1}H NMR signal integration.

series of functional polymers for different biomedical applications was achieved. In parallel, different hydrazone reduction chemistries were explored, with the view that once useful functional polymer formulations had been discovered, functionalised hydrazone polymers could be reduced. This would potentially allow comparison of biological activity between a polymer with dynamic functionality versus a fixed counterpart but it would also present the potential for long term storage of viable hits.

Reduction of hydrazone bonds in functionalised poly(acryloyl hydrazide) P1

Reduction of hydrazones[27-30] is generally carried out using sodium cyanoborohydride ($NaBH_3CN$) as the reducing agent. This is a useful reagent as it is a mild reducing agent, and can be used selectively to reduce imines in mildly basic solutions (pH 7-10). Under acidic conditions, however, $NaBH_3CN$ can release the toxic cyanide gas. Since the scope of the research was to develop a 'tool' for biomedical applications, chemistries that could potentially be applied outside a chemistry lab or at least with minimal training (i.e. by a microbiologist) were preferred. The functionalisations of **P1** were carried out at mild acidic pH, as such there was a risk of formation of cyanide gas. The pH of the reaction solution could have been adjusted before reduction, however, since hydrazones are unstable under basic conditions, this could have potentially affected the equilibrium of the reaction and change the percentage loading. To identify potentially useful hydrazone reduction chemistries, imine and oxime reduction conditions were explored. Although imine reduction is extensively documented and used in industry to produce amines, reactions involving mild reducing agents were considered, in order to avoid reductions of other functional groups included in the aldehyde molecule.

Initially, $NaBH_4$ and $NaBH(AcO)_3$ were tested as safer alternatives to $NaBH_3CN$, using benzaldehyde (**A7**) and *tert*-butyl carbazate to form a model hydrazone on which the reduction conditions were investigated (**Scheme 1.16**). In a typical reaction, the aldehyde was reacted with 1.1 equiv. of *tert*-butyl carbazate to form the hydrazone in quantitative yields within minutes, followed by the addition of the reducing agent without further purification. The purpose was to identify suitable reduction conditions with minimal required purification steps towards a scaffold that could be functionalised and then reduced *in-situ*.

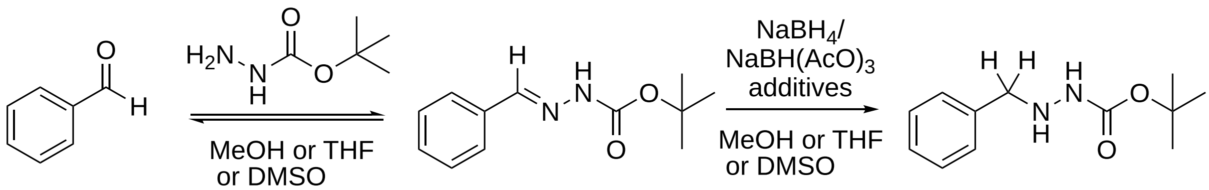

Scheme 1.16: Model experiment used to probe hydrazone reduction.

Of the several different conditions tested (**Table 1.9**) including variations in solvent, additives or using in-situ formed $NaBH(AcO)_3$ versus commercially purchased $NaBH(AcO)_3$, only the reduction using $NaBH_4$ with acetic acid (Entry **4**, **Table 1.9**) (i.e. formation of $NaBH(AcO)_3$ in-situ) gave satisfactory results. In several cases, particularly those in which iodine was used as an additive, there was a clear decrease in the hydrazone signal, but many unidentified by-products were observed (Entries **3**, **7**, **Table 1.9**). Although the reduction was successful as it could be observed from the disappearance of the hydrazone peak at 8.00 ppm (**Fig. 1.27**) and the appearance of the expected CH_2 peak at 3.84 ppm, the presence of a quartet and a triplet at 2.72 ppm and 0.99 ppm respectively (i.e. a X−CH_2−CH_3 group) demanded further investigation. It was established that the peaks were not due to any solvent impurities (e.g. reduction of AcOH to EtOH) as their NMR spectra didn't not match the

Entry	Reducing Agent	Solvent	Additives	Remaining Hydrazone	Byproducts
1	$NaBH_4$	MeOH	—	100%	No
2	$NaBH_4$	THF	—	100%	No
3	$NaBH_4$	THF	I_2	3%	Yes
4	$NaBH_4$	THF	AcOH	11%	No
5	$NaBH(AcO)_3$	THF	—	100%	No
6	$NaBH(AcO)_3$	THF	AcOH	62%	Yes
7	$NaBH(AcO)_3$	THF	I_2	10%	Yes
8	$NaBH_4$	DMSO	AcOH	58%	No

Table 1.9: Results from different experiments probing the reduction of *tert*-butyl 2−benzylidenehydrazine-1-carboxylate.

chemical shifts observed, and the signals' integration were related to that of the Boc-group and the newly formed CH_2 peak (9:3:2:2). This was attributed to the ethylation of the hydrazine at the former hydrazone centre, a process which has been reported in the past for imines and enamines and used strategically to reduce and *N*-alkylate in a one-pot reaction. Although, in itself, this would be an interesting concept to use towards increasing the complexity of functionalised poly(acryloyl hydrazide) scaffolds,

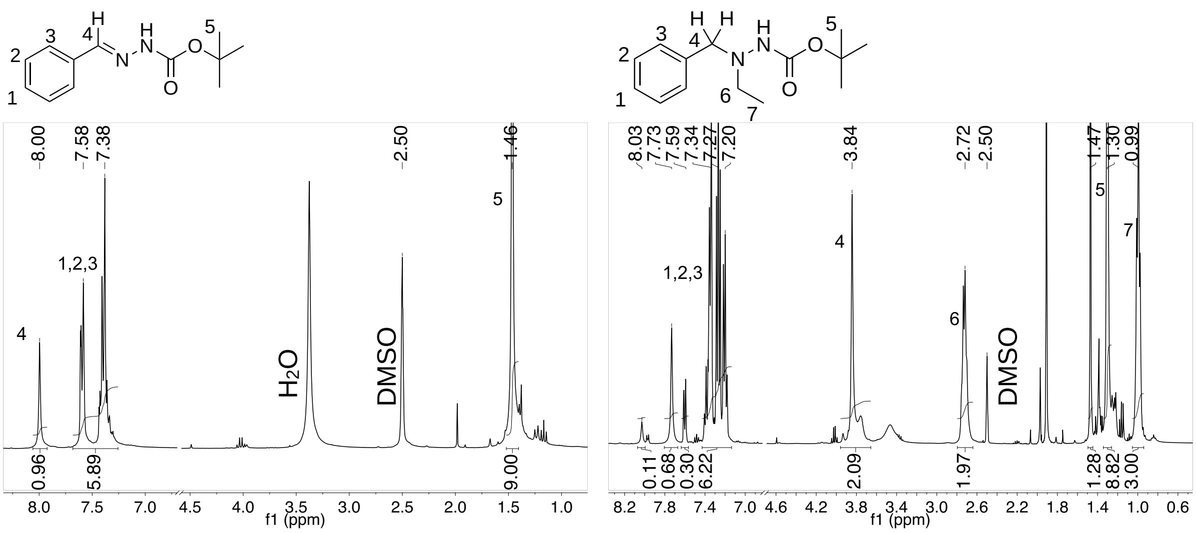

Figure 1.27: ^{1}H NMR spectra of *tert*-butyl 2−benzylidenehydrazine-1-carboxylate (left) and the products after its reduction with $NaBH_4$ and AcOH (right).

alternative reduction methods were explored, especially those used successfully in the reduction of oximes.

Oxime reduction methods are generally centred around the use of diborane or amino-boranes[31-33] reducing agents, especially borane-pyridine (BAP) in acidic media. Kikugawa *et al*.[34,35] showed that oximes can be reduced to hydroxylamines in the presence of a variety of functional groups which were unaffected by the reagent. Starting from Kikugawa's conditions ($BH_3 \cdot$pyridine, 10% $HCl_{(aq)}$, EtOH), the method was adapted in the laboratory to suit the conditions used during the post-polymerisation modification reaction (**Scheme 1.17**).

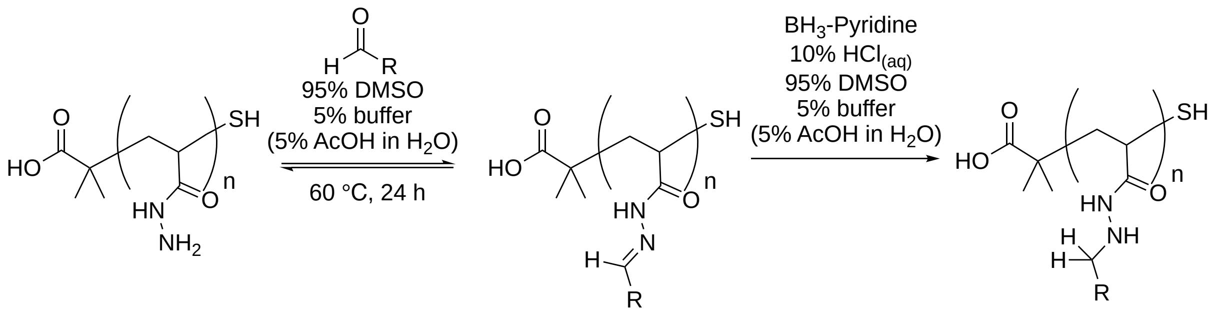

P1

Scheme 1.17: Functionalisation of poly(acryloyl hydrazide) **P1** with aldehydes and reduction to permanently immobilise the functionality.

The disappearance of the hydrazone signal in ^{1}H NMR spectra of **P1** functionalised with aromatic aldehydes was difficult to prove due to the overlapping broad signals (**Fig 1.21**) around the 8.2-6.0 ppm area (i.e. hydrazone and aromatic protons). As a consequence, **P1** was reacted with acetaldehyde (**A16**) and isovaleraldehyde (**A17**), as the hydrazone signals in the ^{1}H NMR spectra of these reactions were clearly visible (7.58 and 7.42 ppm respectively) For each aldehyde, two functionalisation experiments were set up, in one of which the hydrazone was reduced using the conditions explained above, while the in the other the hydrazone was not reduced.

Both samples were then purified by dialysis against water and the isolated products compared by ^1H NMR spectroscopy.

For **P1A16** (**Fig. 1.28**) the reduction was evidenced by both the disappearance of the hydrazone peak at 7.58 ppm and the appearance of the CH_2 peak at 2.74 ppm, but also in the change in chemical shift of the aldehyde's CH_3 peak. While as a hydrazone, this peak appears at 1.94 ppm, in the expected region for groups directly bound to C=X groups. After reduction, this peak had shifted to 1.02 ppm denoting a change from hydrazone to hydrazine. From the integration of the hydrazone signal against the backbone and methyl peaks, it was estimated, that after dialysis, only ~45% of side-chains were still functionalised. This was not unexpected, as dialysis against a large volume of water was expected to favour the backwards reaction (i.e. regeneration of the aldehyde and **P1**). For the reduced product of **P1A16** however, determination of the functionalisation was inaccurate. When the polymer backbone signals were integrated for the three corresponding, the -HN-CH_2-CH_3 peaks gave integration values of 4H and 7H respectively instead of 2H and 3H respectively. This would suggest that due to several factors including shielding and different relaxation times, the backbone protons do not integrate correctly when the

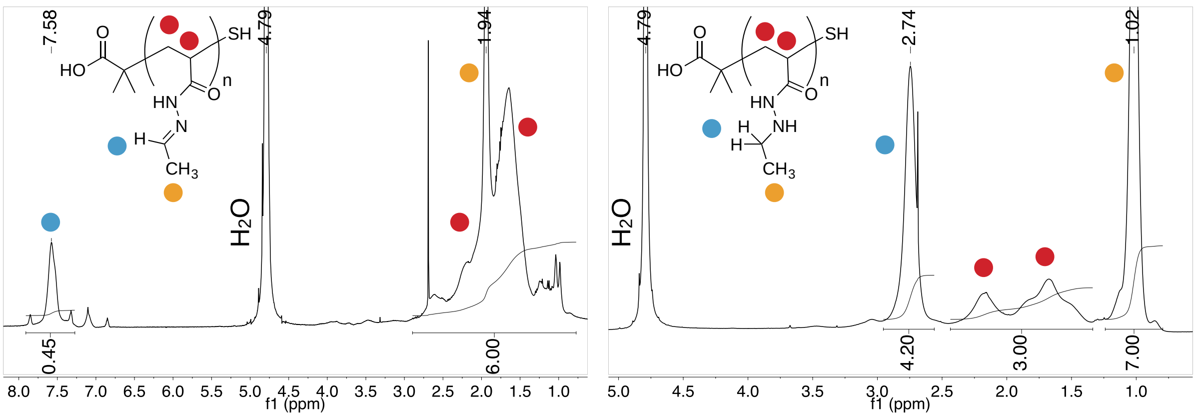

Figure 1.28: ^1H NMR spectra in D_2O of non-reduced **P1A16** (left) and reduced **P1A16** (right) after purification by dialysis.

scaffold is functionalised. Although, no hydrazone species bound to the polymer were observed, that does not completely prove that the reduction goes to completion (i.e. unreduced hydrazones could be hydrolysed during dialysis).

Similarly for **P1A17** the disappearance of the hydrazone peaks at 7.42 and 7.23 ppm and the presence of a new peak at 2.68 ppm (**Fig. 1.29**) was observed. Furthermore chemical shift changes for the -N=C(H)-CH_2-CH-(CH3)$_2$ environments from 2.03 and 1.77 ppm in the non-reduced **P1A17** were observed, to 1.25 and 1.62 ppm respectively in the reduced product. Due to the close proximity and overlap of the DMSO signal to the new -N-CH_2- signal, ^{1}H NMR spectroscopy was carried out in $CDCl_3$ to definitely prove that reduction had occurred as evidenced by the peak at 2.68 ppm. Although it was evident that there were no unreduced hydrazones attached to the polymer, quantification of percentage loading post-reduction proved again inconclusive. The solubility of the non-reduced **P1A17** in DMSO-*d6* was good compared to the reduced product. This meant that even with an internal standard (i.e. syringic acid), accurate percentage loading could not be determined. After dialysis, the non-reduced **P1A17** seems to display around ~51% functionalisation. Conversely, in $CDCl_3$ the reduced **P1A17** was soluble while the non-reduced was a turbid solution. After spiking the sample with DCM as an internal standard, 82% loading for both the reduced and non-reduced products was obtained. The analysis was made by integrating either the DCM signal or the syringic acid aromatic signal and comparing against isovaleraldehyde's two methyl groups, knowing both the amount of product in the sample and the exact amount of standard used to spike the sample. The accuracy of this method was compromised by factors such as poor solubility and the presence of water (after freeze drying and vacuum with P_2O_5) in the

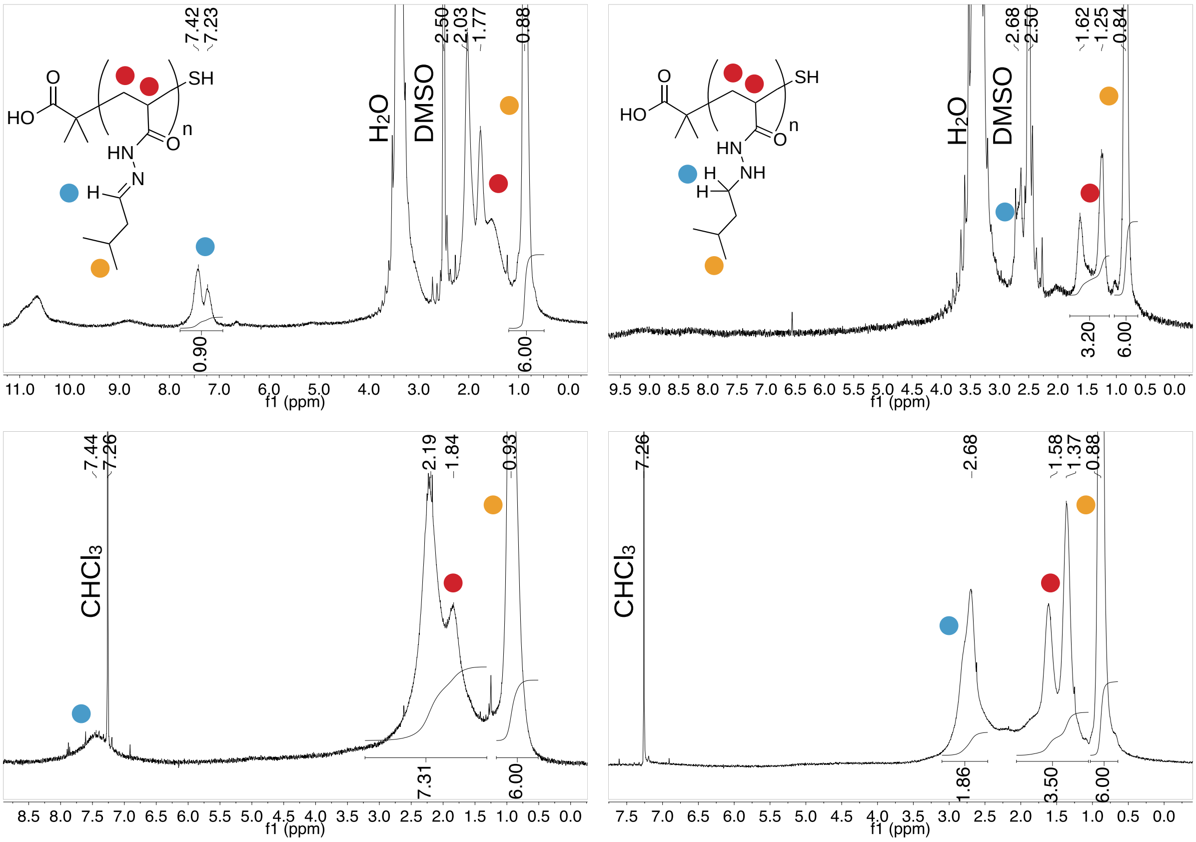

Figure 1.29: ^{1}H NMR spectra in DMSO-*d6* of non-reduced **P1A17** (top-left) and reduced **P1A17** (top-right) and in $CDCl_3$ of non-reduced **P1A17** (bottom-left) and reduced **P1A17** after purification by dialysis.

sample as these could affect the real mass of product in the sample. Investigation of the percentage loading using fluorescence by analysing the percentage free-hydrazides using the Fluorescamine Assay was considered, by comparing against non-functionalised **P1**, but this method too suffers from many variables. Firstly, Fluorescamine is a bulky molecule, and the chances of probing all side-chains are minimal. Secondly, it is likely that quenching effects will be observed as more and more side-chains are probed. Also, there are no indications as to how the fluorescence would be affected by different neighbouring residues. As such, in the absence of better available characterisation techniques, the only conclusions that were drawn at this stage was that BH_3-pyridine seems to be a reducing agent worth investigating further.

Synthesis of fluorescent poly(acryloyl hydrazide) P1 scaffolds

Driven by the successful collaboration with Dr Javier Montenegro and his laboratory and the encouraging results on the use of functionalised **P1** for the delivery of siRNA (see **chapter 3**), the development of a synthetic route towards a fluorescent poly(acryloyl hydrazide) was pursued as a scaffold towards fluorescent functional polymers. It was envisaged using these polymers to investigate cell internalisation mechanisms as well as investigating the mechanism of siRNA delivery.

In the initial approach it was decided to target the terminal free thiol on **P1** and functionalise it with model maleimides (**Scheme 1.18**) with a view to functionalise with fluorescein-maleimide or other fluorescent-maleimide tags. It was quickly determined however that even at optimal pH conditions (i.e. 6.5-7.5) selective addition at the thiol end in the presence of such a large excess of free hydrazides could not be achieved. Furthermore, studies with a model thiol and a hydrazide showed that even in a 1:1 ratio selective binding of the maleimide to the thiol could not be obtained.

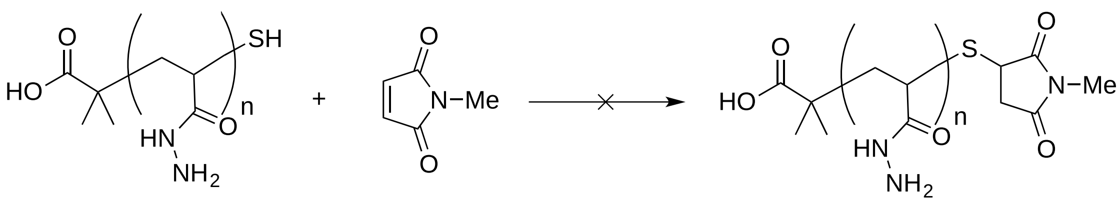

P1

Scheme 1.18: Functionalisation of poly(acryloyl hydrazide) **P1** with *N*-methyl maleimide

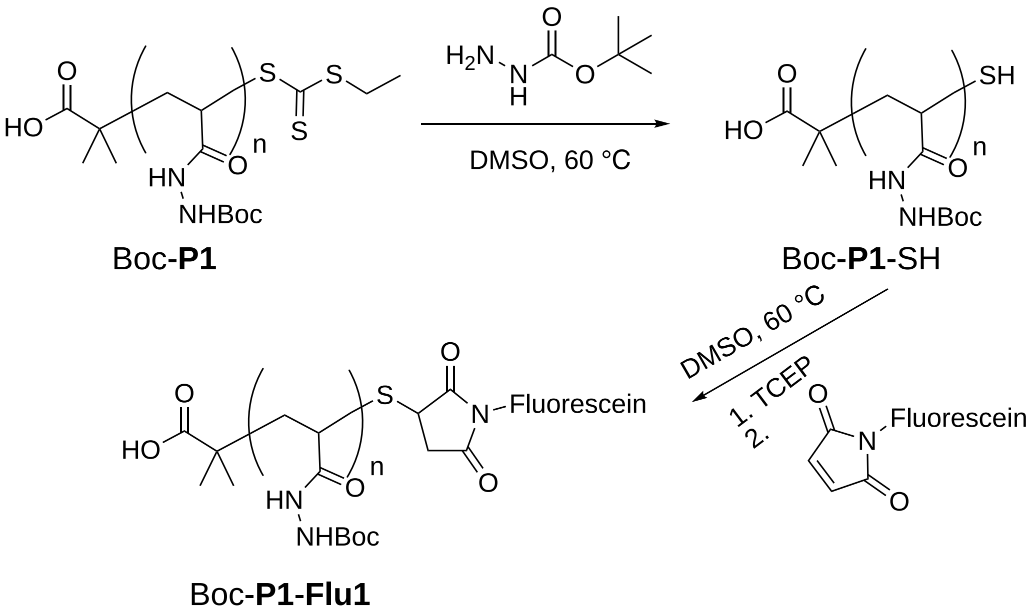

Scheme 1.19: 2 steps reaction towards the functionalisation of poly(acryloyl hydrazide) **P1** with fluorescent maleimides.

The thiol-maleimide coupling on the protected poly(acryloyl hydrazide) Boc-**P1** was explored. To transform the trithio group into a thiol Boc-**P1** was reacted with a large excess of *tert*-butyl carbazate in DMSO at 60 ℃ (**Scheme 1.19**) and purified by dialysis. The product (Boc-**P1**-SH) was analysed by UV-Vis (**Fig. 1.30**) to show the loss of the peak at λ_{300} nm and prove the presence of the thiol by Ellman's Assay. SEC/GPC was used to investigate if any thiol oxidation was occurring. This would

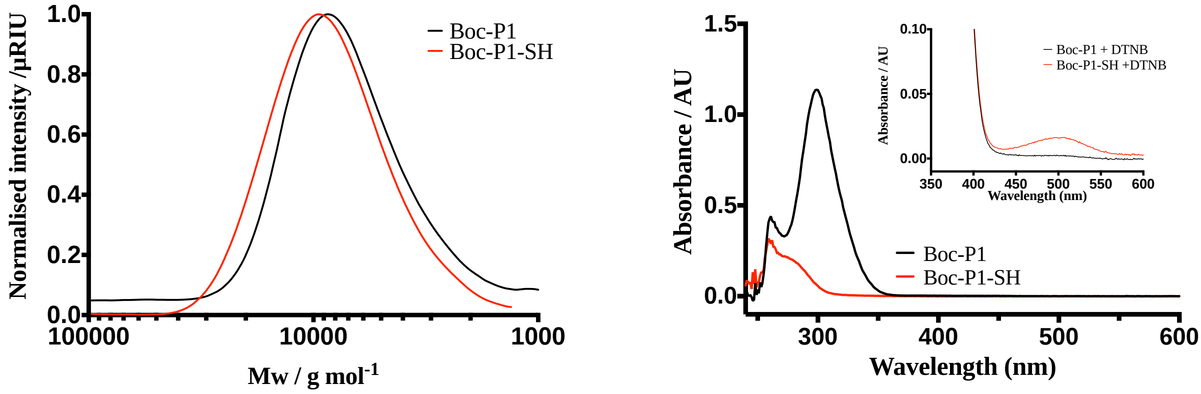

Figure 1.30: Normalised SEC/GPC spectra of Boc-**P1** and Boc-**P1**-SH (left). UV-Vis spectra of Boc-**P1** and Boc-**P1**-SH (main right) and the UV-Vis of the two samples after treatment with DTNB (inset right).

have been evident by significant changes in the retention time, Mn and Đ as well as the presence of a small ‘shoulder’ at lower retention time. Looking at the data obtained, an increase of ~1.1kDa in Mn and ~0.017 in Đ was observed (**Fig. 1.30**). This difference was below what would have been expected if thiol oxidation was occurring (i.e. 2 x Mn increase), but it was concluded that it may be useful to treat the sample with a thiol reducing agent prior to maleimide addition. Reported protocols[36,37] for the functionalisation of proteins with fluorescent maleimides describe using at least a 10-fold excess fluorescent tag per thiol. In order to synthesise sufficient fluorescent polymer scaffold for biological studies, the labelling reaction had to be carried out with ~200 mg Boc-**P1**-SH to compensate for the material lost during the succeeding purifications by dialyses and deprotection. Due to

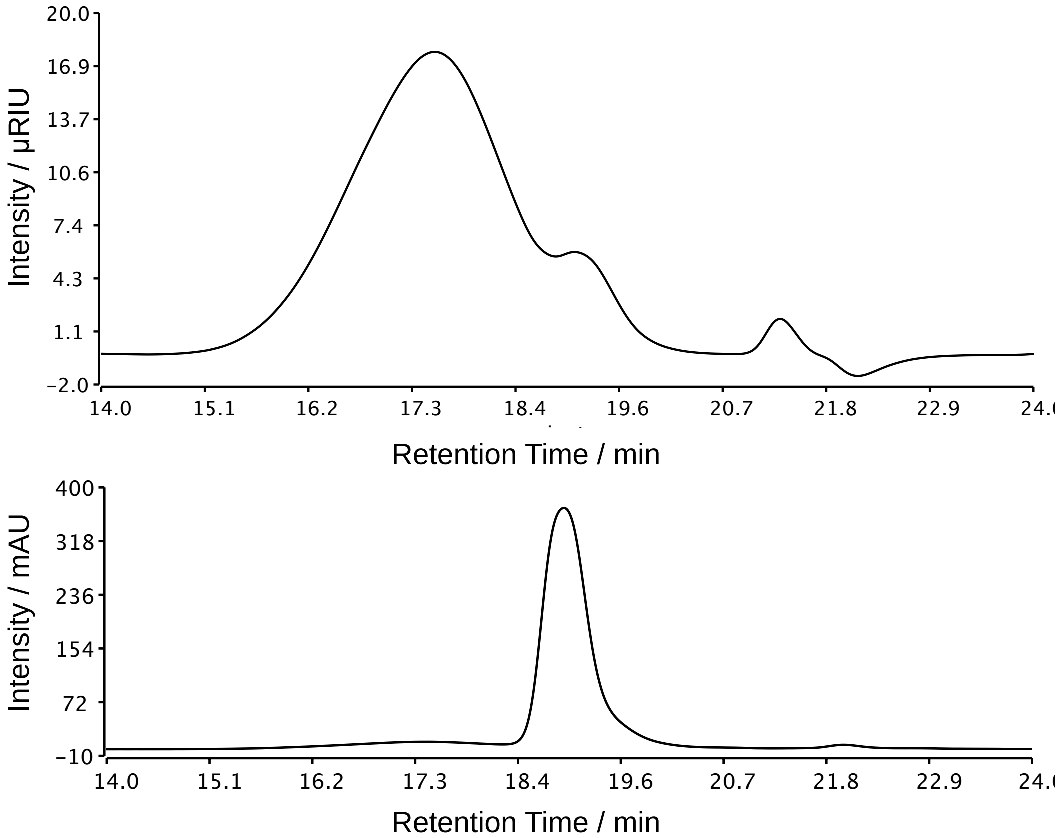

Figure 1.31: SEC/GPC chromatograms of **P1-Flu1** visualised by RI (top) and UV-Vis at λ_{300} nm (bottom).

the prohibitive cost of fluorescein-maleimide the labelling reaction was carried out using only a 4-fold excess of maleimide to thiol. Unfortunately, analysis of the deprotected polymer **P1-Flu1** by SEC/GPC (**Fig. 1.31**) suggested that most of the fluorescent label was not attached to the polymer but rather to some oligomeric species as indicated by the more intense sharp signal (according to UV-Vis at 455 nm) with retention time 18.9 min instead of the broad peak at 17.5 min which is the main product according to the RI detector. Separation of the two peaks was attempted by purification by chromatography using Sephadex-G10 as the stationary phase, but only ~15 mg (out of a maximum possible 92 mg) of a 80% pure fluorescent polymer scaffold was isolated and confirmed by ^{1}H NMR spectroscopy (**Fig. 1.32**).

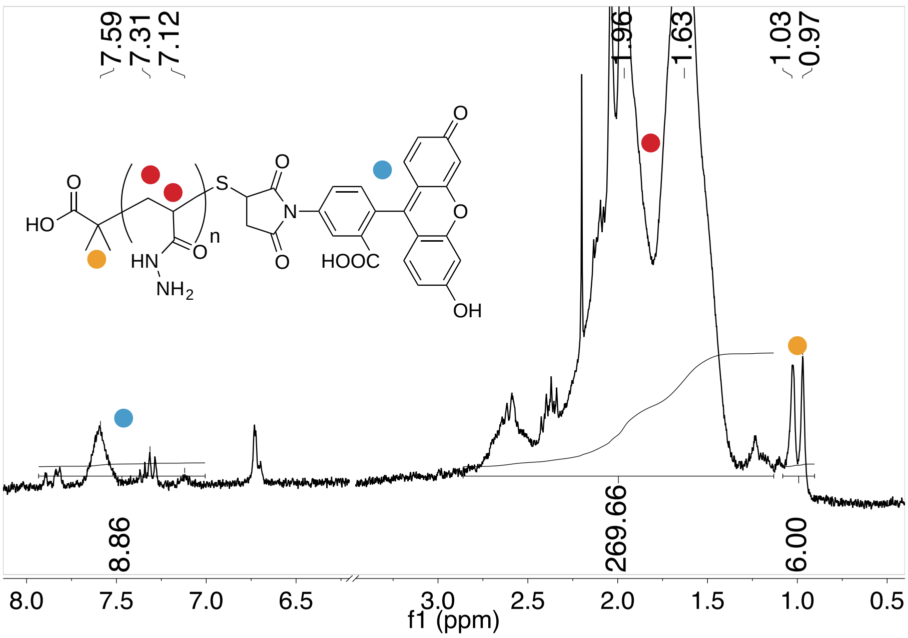

Figure 1.32: ^{1}H NMR spectrum of **P1-Flu1** in D_2O.

Because of the problems encountered during the synthesis of **P1-Flu1** and high cost of the maleimide dye and even higher costs of other fluorescent tags it was decided to explore alternatives involving the carboxylic acid terminus of the polymer.

As far as it was ascertained during this research, there were no cheap alternatives (i.e. amine, hydrazine or hydroxylamine probes) available for labelling carboxylic acids. However, one of the cheaper labelling dyes available is fluorescein isothiocyanate (FITC), which is used extensively as a label for reactive nucleophiles especially amines. As a consequence, it was decided to derivatise the carboxylic acid with 1,2-ethylenediamine (**Scheme 1.20**) to afford Boc-**P1** with a nucleophilic terminus capable of reacting with FITC in a click-chemistry reaction. The polymer was dissolved in a 1:1 mixture of DMSO and 1,2-ethylenediamine and EDC was added in portions to activate the carboxylic acid. The product (Boc-**P1**-NH_2) was isolated and characterised by ^{1}H NMR and fluorescence spectroscopy after purification by dialysis against water. The ^{1}H NMR spectrum (**Fig. 1.33**) in $CDCl_3$ showed a new broad peak at 3.25 ppm which were attributed to one of the two CH_2 environments from the attached 1,2−ethylenediamine, however signal integration could not be used to calculate the extent of carboxylic acid converted.

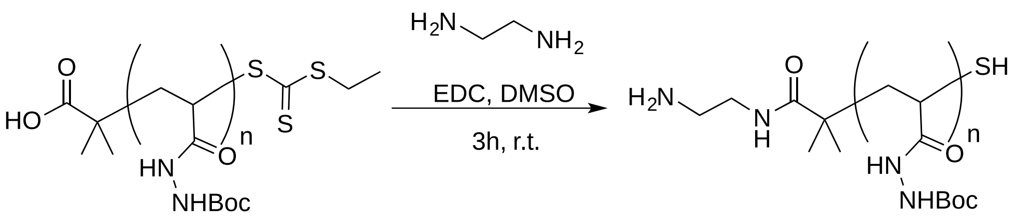

Boc-**P1** Boc-**P1**-NH_2

Scheme 1.20: Derivatisation of Boc-**P1** with 1,2-ethylenediamine to afford Boc-**P1**-NH_2, a scaffold capable to reacting with FITC.

Instead fluorescence spectroscopy was used to quantify the amounts of amine groups using the Fluram Assay from known samples of Boc-**P1**-NH_2. Analysis of *N*−Boc−ethylenediamine as a model substrate with fluorescamine (**Fig. 1.34**) was carried out in order to determine the optimum, saturation and quenching

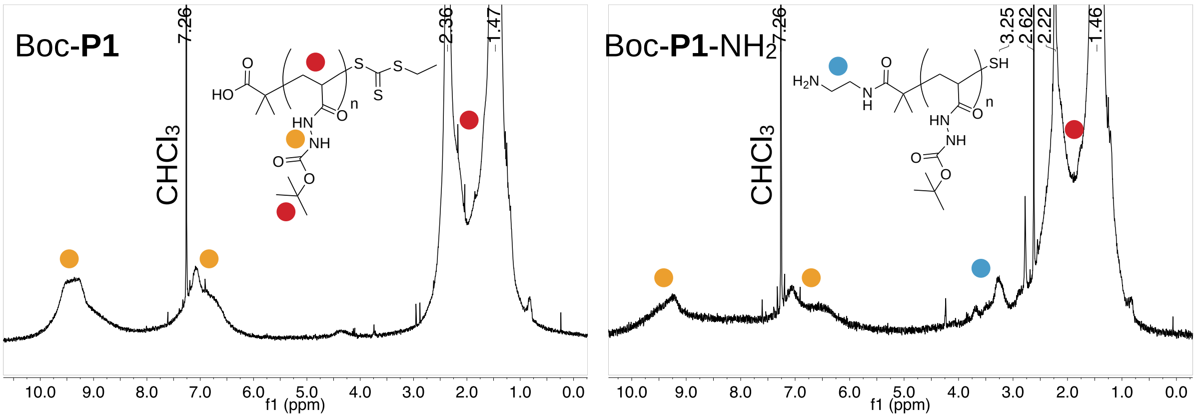

Figure 1.33: ^{1}H NMR spectra of Boc-**P1** (left) and Boc-**P1**-NH_2 (right) in $CDCl_3$.

concentrations for the experiment, and the data obtained was used to calculate the ratio of amines to repeating units. An average of 54 monomers was per amine group detected was calculated (from the mass of polymer weighed and concentration of amines in solution), which is in agreement with DPs calculated for the parent Boc-**P1** polymer.

To synthesise the protected fluorescent polymer (Boc-**P1-Flu2**) 400 mg Boc-**P1**-NH_2 in DMF was reacted with DIPEA and 4-fold excess FITC (**Scheme 1.21**) for 24 hours, and the material was purified by removing the solvent and running the

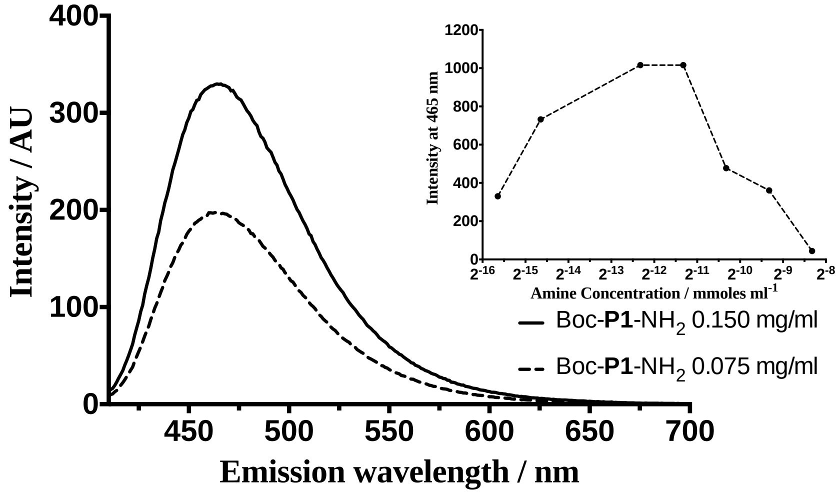

Figure 1.34: Fluorescence spectra showing the results of the Fluram Assay for known concentrations of Boc-**P1**-NH_2 (main), and fluorescence intensity at λ_{465} nm vs varying concentrations of *N*-Boc-ethylenediamine (inset).

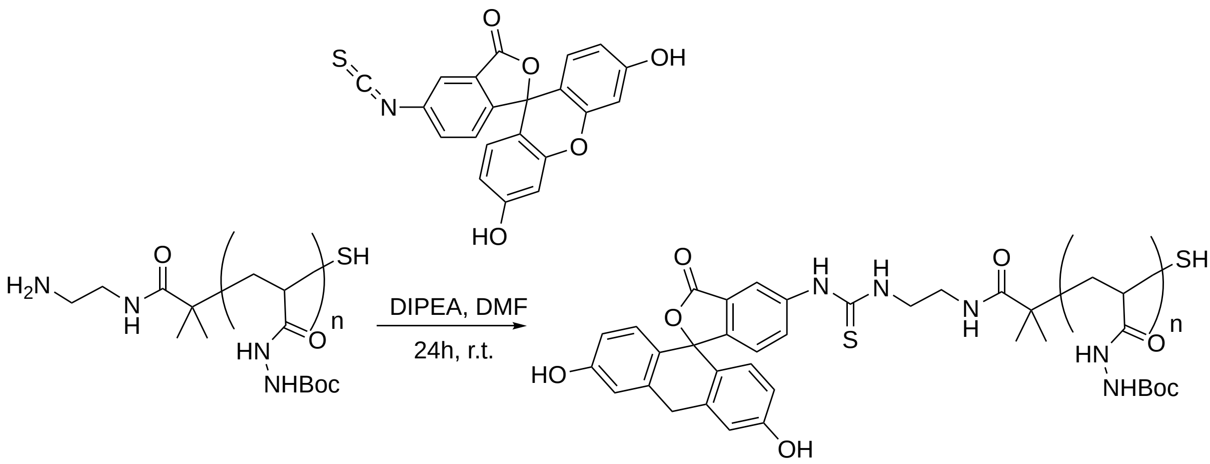

Boc-**P1**-NH_2 Boc-**P1-Flu2**

Scheme 1.21: Click-chemistry reaction between the amine on Boc-**P1**-NH_2 and FITC to afford fluorescent Boc-**P1-Flu2**.

crude through a Sephadex LH-20 column to obtain Boc-**P1-Flu2** with a purity of around 97% according to the RI detector and 80% according to the fluorescent detector (i.e. two molecules containing a fluorescent label will be detected as having similar intensities by the SEC/GPC fluorescence detector but this fails to account that in the polymer for every fluorescent tag there are 40-50 repeating units which make up most of the mass).

P1-Flu2 was synthesised by deprotecting Boc-**P1-Flu2** in neat TFA, neutralising the acid and purifying by dialysis. The resulting orange powder was analysed by ^{1}H NMR spectroscopy (**Fig. 1.35**), which according to the signal integration confirmed that there is one dye per 51 monomers, in accordance with the expected DP (i.e. integrating the aromatic area for the 9H in the dye and dividing by 3 the integration value of the alkyl backbone (154 H), the ratio of dye to repeating units 1:51) was obtained.

SEC/GPC using a fluorescence detector showed a broad peak (**Fig. 1.36**) at the expected retention time (i.e. ~16.5 min) but also showed some recurring broad

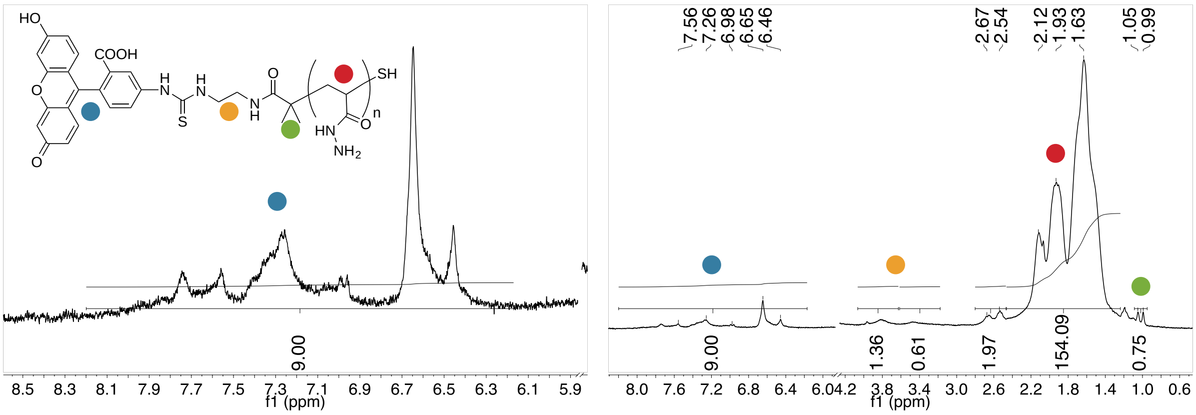

Figure 1.35: ^{1}H NMR spectrum of **P1-Flu2** in D_2O(right) and expanded on the aromatic area (left).

fluorescent peaks past usual void time (~21.5 min). This may suggest some solubility issues with **P1-Flu2** or the presence of some by-products. Nonetheless, the peak associated with **P1-Flu2** accounts for 87% of the integrated areas by fluorescence and 90% by RI. Using this method more than 50 mg of fluorescent poly(acryloyl hydrazide) were isolated, and the coupling with a couple of aldehydes was investigated in order to verify that the percentage loading with **P1-Flu2** remains similar to **P1**. The coupling reaction of **P1-Flu2** in acidic aqueous conditions with imidazole **A1** was carried out, observed 75% loading was observed by ^{1}H NMR spectroscopy (**Fig. 1.37**) after 4 h, by integrating the signals and comparing the

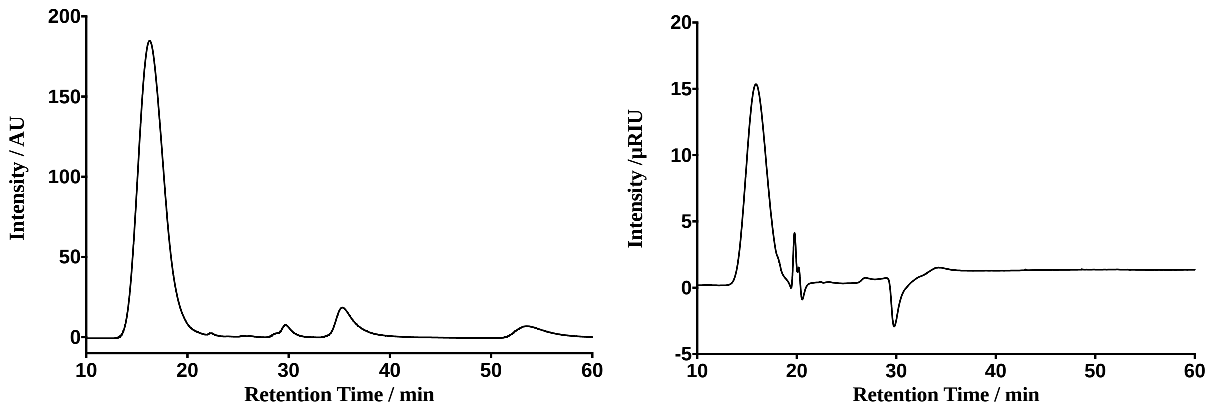

Figure 1.36: SEC/GPC chromatograms of **P1-Flu2** detected by fluorescence emission at λ_{510} nm (left) and by RI (right).

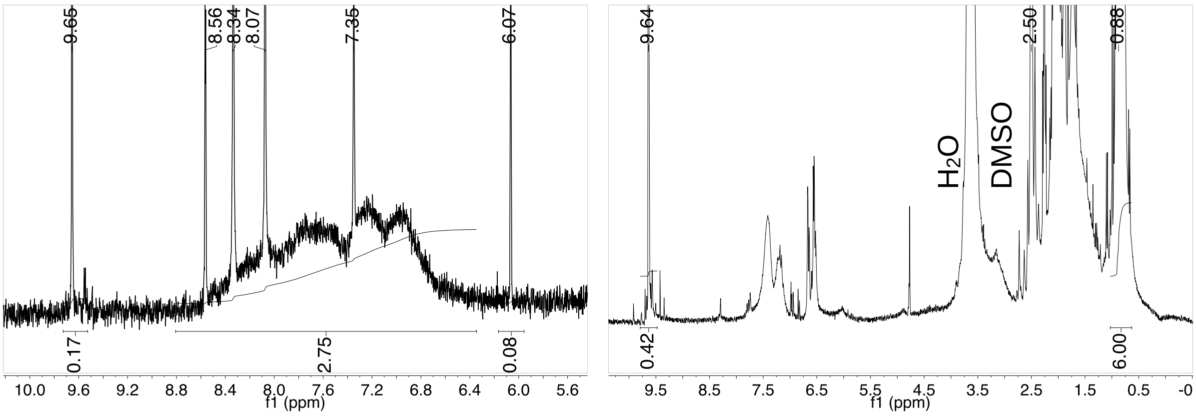

Figure 1.37: [1]H NMR spectra the reaction of **P1-Flu2** with imidazole **A1** in 100mM AcOH in D_2O after 4 h (left) and the reaction of **P1-Flu2** with isovaleraldehyde **A17** in a mixture of 95% DMSO-*d6* and 5% acidic buffer (5% AcOH in D_2O) after 2 h (right).

aldehyde signal (9.65 ppm) and the broad aromatic and hydrazone signals (8.8 - 6.4 ppm). Experiments with isovaleraldehyde **A17** in the usual mixture of DMSO and acidic buffer showed a coupling of 58% after 2 h incubation at 60 ℃ (**Fig. 1.37**). SEC/GPC experiments using the Shodex column system and varied amounts of imidazole **A1** were also carried out. It was previously determined that poly(acryloyl hydrazide)

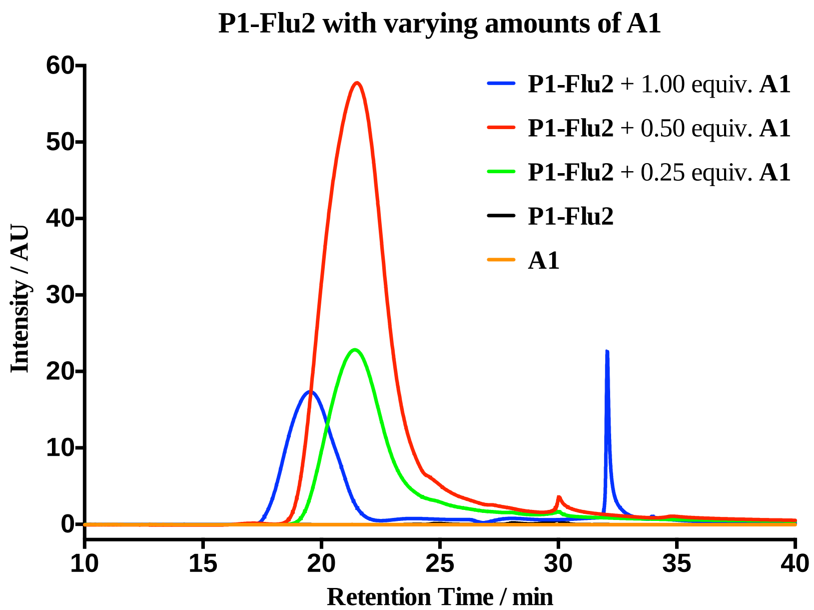

Figure 1.38: SEC/GPC chromatogram showing the functionalisation of **P1-Flu2** with imidazole aldehyde **A1** at different equivalence values.

P1 does not run through this column, however when it is functionalised with **A1** it is detected (**Fig. 1.14**). A similar experiment using the fluorescence detector was carried out, to show that similar levels of aldehyde loading could be achieved for **P1−Flu2** compared to **P1** (**Fig.1.38**). A decrease in retention time with increasing equiv. **A1** was observed suggesting that and increase in the molecular weight was occurring with increased percentage functionalisation. Overall, the studies carried out show that **P1-Flu2** can be used a fluorescent polymer scaffold for functionalisation with aldehydes.

1.4 Summary

A reliable route towards the synthesis of relatively large amounts of Boc-protected acryloyl hydrazide monomer was successfully developed. Using RAFT methodology and a simple deprotection step the polymerisation of this monomer to afford poly(acryloyl hydrazide) **P1** scaffolds, with varying molecular weights was achieved. The scaffold was investigated as a tool towards the synthesis of libraries of functional polymers through its click-chemistry reaction with aldehydes. Using the knowledge gained, **P1** was successfully used to develop a platform for quickly analysing the siRNA delivery ability of functional polymers derivatised from **P1** (see **Chapter 3**).

Furthermore, experiments with a series of hydrazone reduction reagents were carried out to identify suitable reaction conditions to permanently bind the functional groups to the backbone. Borane-pyridine was identified as a mild suitable reducing reagent, however, accurate determination of the percentage loading after reduction and purification proved challenging.

Finally, a route towards the synthesis of poly(acryloyl hydrazide) labelled with fluorescein (**P1-Flu2**) was developed, as a tool towards investigating different biological processes using fluorescent functional polymers. Although further optimisation of the process is required, and further functionalisation experiments with different aldehydes are needed to assess the suitability of **P1-Flu2** as a scaffold, the explored chemistry could be suitable towards the synthesis of libraries of **P1** scaffolds, which could incorporate a variety of fluorescent dyes for diverse applications.

1.5 Future work

From a synthetic point of view, the RAFT polymerisation to synthesise Boc-**P1** could be optimised further to produce poly(acryloyl hydrazide) with narrower dispersities such that the structure-activity relationship of functional polymers could be evaluated with increased confidence (i.e. prove that any observed physicochemical benefits of a sample of functionalised **P1** is not due solely to a subset of a particular molecular weight).

With regards to the functionalisation of **P1**, it is believed there are three key aspects worth investigating. The first feature is related to functionalisation with multiple aldehydes at the same time. This was investigated briefly as part of the work on siRNA delivery (see **Chapter 3**) but more thorough experiments could be carried out to determine if loading of different types of aldehyde affects the structure of final polymer (i.e. randomisation of side-chains, block-functionalisation, facial segregation etc.). The second feature worth determining is related to the dynamic aspect of the hydrazone bonds and re-equilibration between functional polymers with different hydrazone side-chains. Also re-equilibration in the presence of a template is important to understand processes involved in the formation of polyionic complexes such as those with siRNA or plasmids. Finally, a thorough investigation of the products obtained after the reduction of hydrazone bonds in functionalised **P1** could be a valuable addition to this scaffold's toolbox, but this is conditioned by the availability of better analytical methods.

Finally, the synthesis of **P1-Flu2** has opened the way towards the synthesis of similar fluorescent **P1** scaffolds. Both the reaction with 1,2-ethylenediamine and the subsequent reaction with the dye need optimising to minimise wastage especially of expensive fluorescent dyes.

1.6 Experimental

Cyanomethyl methyl(4-pyridyl)carbamodithioate (**CTA2**) was purchased from Sigma-Aldrich® and used without further purification. All other chemicals were purchased from Sigma-Aldrich®, Fisher Scientific®, VWR® or Acros® and used without further purification. All solvents were Reagent grade or above, purchased from Sigma-Aldrich®, Fisher Scientific® or VWR® and used without further purification.

Nuclear Magnetic Resonance (NMR) spectra were recorded on either a Bruker Avance III 300 MHz or a Bruker Avance III 400 MHz spectrometer. Chemical shifts are reported in ppm (δ units) referenced[40] to the following solvent signals: residual DMSO in DMSO-*d6* at δH 2.50, H_2O in D_2O at δH 4.79, $CHCl_3$ in $CDCl_3$ at δH 7.26. Infrared (IR) spectra were recorded on a Perkin Elmer Spectrum Two FT−IR spectrometer. Peaks are reported as strong (s), medium (m) or weak (w), sharp (sh) or broad (br). Ultraviolet-visible (UV-vis) spectra were recorded on a Cary 50 Spectrophotometer. Fluorescence spectra were recorded on a Shimadzu RF-5301PC Spectrofluorophotometer. Mass spectra were recorded on a Waters Xevo G2-XS ToF using electrospray ionisation (ESI) and time-of-flight (ToF) in positive or negative ion mode. Thin-layer chromatography was carried out on sheets coated with silica gel. Size Exclusion Chromatography/Gel Permeation Chromatography (SEC/GPC) were recorded on a Shimadzu Prominence LC-20A fitted with a Thermo Fisher Refractomax 521 Detector and a Shimadzu SPD20A UV-vis Detector or fitted with a Shimadzu SPD-M20-A Photodiode Array Detector and a Shimadzu RF-10A Fluorescence Detector. Boc-**P1**$_X$ was analysed using 0.05 M LiBr in DMF at 60 ℃ as the eluent and a flow rate of 1 mL·min^{-1}. The instrument was fitted with a Polymer

Labs PolarGel guard column (50 × 7.5 mm, 5 µm) followed by two PLGel PL1110-6540 columns (300 × 7.5 mm, 5 µm). Molecular weights were calculated based on a standard calibration method using polymethylmethacrylate. **P1** was analysed using Lonza® DPBS at 35 ℃ as the eluent and a flow rate of 1 mL·min^{-1}. The instrument was fitted with a Polymer Labs PL-aquagel-OH guard column (50 x 7.5 mm, 8 µm) followed by a PL-aquagel-OH 30 column (300 x 7.5 mm, 8 µm) and a PL-aquagel-OH 40 column (300 x 7.5 mm, 8 µm). Molecular weights were calculated based on a standard calibration method using PEG. Activation of **P1**$_X$ was analyzed using 100 mM acetic acid at pH 2.9 at 40 ℃ as the eluent and a flow rate of 0.6 mL·min^{-1}. The instrument was fitted with a Shodex Asaphipak GF-510 HQ column and a Shodex Asaphipak GF-310 HQ column (300 × 7.5 mm, 5 µm). All dialyses were carried out using Spectrum Labs SpectraPor® Dialysis Tubing MWCO 1000 in water unless specified otherwise for a minimum of 24 hours and at least 3 changes of solvent.

***tert*-Butyl 2-acryloylhydrazine-1-carboxylate (1.3)**

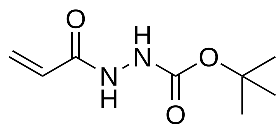

Acrylic acid (3.81 mL, 54.95 mmol) and *tert*-butyl carbazate (8.89 g, 65.95 mmol) were dissolved in a H_2O/THF mixture (2:1, 180 mL) at RT. *N*−(3−dimethylaminopropyl)-*N'*-ethylcarbodiimide hydrochloride (EDC) (11.75 g, 61.29 mmol) was added in portions to the solution over 15 minutes and left stirring for 3 h. The crude reaction was extracted with EtOAc (3 x 75 mL) and the organic layer was washed with 0.1 M HCl (3 x 75 mL), H_2O (50 mL) and brine (2 x 50 mL). The organic phase was dried with anhydrous Na_2SO_4 and the solvent was removed under reduced pressure to afford the crude product as a white solid. The crude product was purified by recrystallization from EtOAc (70 ℃ to RT, followed by cooling in freezer) to afford (5.05 g, 50% yield) of a white crystalline powder identified as **1.3**. R_f = 0.87 (100% EtOAc); ν_{max} (neat)/cm^{-1} 3311m sh (N-H), 3221m sh (N-H), 2981w sh (C-H), 1715s sh (C=O), 1668s sh (C=O); δ_H(300 MHz, DMSO-*d6*) [calibrated using (C*H*D_2)(CD_3)SO resonance at 2.50 ppm] 1.40 (s, 9H, C(CH_3)$_3$), 5.69 (dd, 1H, CH_2C*H*), 6.17-6.20 (m, 2H, CHCH_2), 8.84 (s, 1H, OC(O)N*H*), 9.79 (s, 1H, CHC(O)N*H*); δ_C(100 MHz, DMSO–*d6*) [calibrated using (*C*D_3)$_2$SO resonance at 39.52 ppm] 28.1 (C(*C*H_3)$_3$), 79.2 (*C*(CH_3)$_3$), 126.2 (*C*H_2CH), 129.4 (CH_2*C*H), 155.3 (O*C*(O)NH), 164.3 (CH*C*(O)NH). The characterisation data is in accordance to literature.[41]

Acryloylhydrazide hydrochloride (1.4)

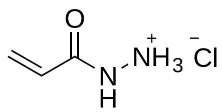

Hydrazide **1.3** (2.00 g, 10.73 mmol) in 1 M $HCl_{(aq)}$ (80 mL) was stirred at 0 ℃ for 24 h and stirred a further 48 h at RT. Excess HCl was removed under reduced pressure while keeping the solution cold. Water was removed by lyophilisation to afford (0.9 g, 68% yield) of a white crystalline powder identified as **1.4**. ν_{max} (neat)/ cm^{-1} 3345s br (N-H), 3170s br, 2911w sh (C-H), 1684s sh (C=O); δ_H(300 MHz, DMSO-*d6*) [calibrated using (C*H*D_2)(CD_3)SO resonance at 2.50 ppm] 4.35 (br, 3H, $^+NH_3$), 5.85 (dd, 1H, CH_2C*H*), 6.26-6.39 (m, 2H, CHCH_2), 11.44 (s, 1H, CHC(O)N*H*); δ_C(100 MHz, DMSO-*d6*) [calibrated using (*C*D_3)$_2$SO resonance at 39.52 ppm] 127.7 (CH_2*C*H), 129.1 (*C*H_2CH), 163.9 (CH*C*(O)NH); MS (TOF ES+) 87.10 ($[M-H]^+$ 100%).

2-(((Ethylthio)carbonothioyl)thio)-2-methylpropanoic acid (CTA1)

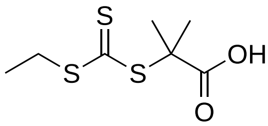

Ethane thiol (3.6 ml, 47.64 mmol) was added to a suspension of tripotassium phosphate (15.4 g, 71.46 mmol) in acetone (150 mL) and stirred for 10 min. Carbon disulfide (7.2 ml, 119.10 mmol) and 2-bromoisobutyric acid (7.3 g, 42.88 mmol) were added to the above suspension in quick succession and left stirring overnight. The solution was concentrated by purging with argon and filtered. The cream coloured solid residue was dissolved in 1 M HCl (150 mL) and extracted with DCM (3 x 100 mL). The organic layer was collected and washed further with 0.1M HCl (2 x 100 mL), water (2 x 100 mL) and brine (2 x 100 mL) and dried with anhydrous Na_2SO_4. The solution was concentrated under reduced pressure to afford an orange oil. The crude product was purified by recrystallisation from hexane (55 ℃ to 0 ℃ followed by overnight cooling in freezer) to afford a bright yellow powder (3.5 g, 36% yield). UV (DMSO) λ_{max} 310 nm; δ_H(300 MHz, DMSO-*d6*) [calibrated using (CHD_2)(CD_3)SO resonance at 2.50 ppm] 1.25 (t, $^3J_{H,H}$ = 7.36 Hz, 3H, CH_2CH_3), 1.62 (s, 6H, $C(CH_3)_2$), 3.29 (q, $^3J_{H,H}$ = 7.36, 2H, CH_2CH_3), 12.95 (s, 1H, COO*H*); δ_C(100 MHz, DMSO-*d6*) [calibrated using $(CD_3)_2SO$ resonance at 39.52 ppm] 12.9 (CH_2CH_3), 25.1 ($C(CH_3)_2$), 30.7 (CH_2CH_3), 56.1 ($C(CH_3)_2$), 173.2 (*C*OOH), 221.6 (S*C*(S)S). The characterisation data is in accordance to literature.[12]

Poly(*tert*-butyl 2-acryloylhydrazine-1-carboxylate) (Boc-P1$_x$)

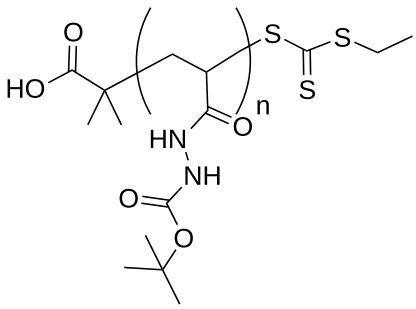

In a typical experiment, a solution of 4,4'-azobis(4-cyanovaleric acid) (ACVA) (18.4 mg, 0.064 mmol) in DMSO (1.5 ml) and a solution of CTA (72.3 mg, 0.322 mmol) in DMSO (1.5 mL) were added sequentially to a solution of *tert*-butyl 2-acryloylhydrazine-1-carboxylate (3.00 g, 16.095 mmol) in DMSO (14.88 mL). A 50 μL aliquot of this solution was taken at this stage to aid in the calculation of conversion. The reaction mixture was then sealed and degassed with argon for 30 min. The degassed solution was left to react at 70 ℃ for 7 h. The reaction was stopped by allowing it to cool down to room temperature and by exposing it to air. A 50 μL aliquot of this solution was taken at this stage to aid in the calculation of conversion. The polymer was purified by dialysis against water. The water was removed by lyophilisation and by drying in a desiccator with P_2O_5 to afford Boc-**P1**$_{40}$ as an off-white powder (2.2 g, 73% yield). UV (DMSO) λ_{max} 300 nm; ν_{max} (neat)/cm^{-1} 3244m br (N-H), 2916w sh (C-H), 1642s br (C=O), 1523m sh (C=O); δ_H(300 MHz, DMSO-*d6*) [calibrated using (C*H*D$_2$)(CD$_3$)SO resonance at 2.50 ppm] 1.41 (br, 11H, 9H in C(C*H*$_3$)$_3$, 2H in CHC*H*$_2$), 2.03 (br, 1H, C*H*CH$_2$), 8.60 (br, 1H, OC(O)N*H*), 9.22 (br, 1H, CHC(O)N*H*); Conversion 86%; DP (UV-Vis) 45; Mn (DMF GPC) 10270; Đ (DMF GPC) 1.36.

Poly(acryloyl hydrazide) ($P1_x$)

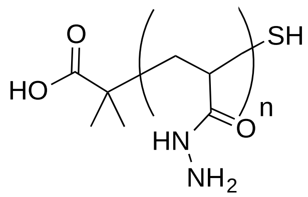

In a typical experiment, trifluoroacetic acid (TFA) (15 mL) was added dropwise to poly(*tert*-butyl-2-acryloylhydrazine-1-carboxylate) (Boc-$\mathbf{P1}_{40}$) (1.5 g) and the yellow solution was stirred at RT for 2 h. Excess of TFA was removed by blowing a steady stream of argon and the resulting oil was diluted in water (15 mL). The $\mathbf{P1}_{40}$·TFA salt formed was neutralised by adding $NaHCO_3$ until no foaming was observed. The colourless solution was allowed to stir overnight. The crude polymer was purified by dialysis against water. The water was removed by lyophilisation and by drying in a desiccator with P_2O_5 to afford $\mathbf{P1}_{40}$ as a white powder (650 mg, 92% yield). ν_{max} (neat)/cm^{-1} 3254w br (N-H), 1609m br (C=O), 1428s sh (C-C); δ_H(300 MHz, D_2O) [calibrated using *H*DO resonance at 4.79 ppm] 0.95 (s, 3H, C(C*H*$_3$)), 1.01 (s, 3H, C(C*H*$_3$)), 1.59-2.08 (br m, 3H x DP, C*H*C*H*$_2$); δ_C(100 MHz, D_2O) 34.3 (CH*C*H$_2$), 40.5 (*C*HCH$_2$), 174.9 (CH*C*(O)NH); DP (^{1}H NMR) 49; Mn (DPBS GPC) 10918; Đ (DPBS GPC) 1.37.

Functionalisation of poly(acryloyl hydrazide) ($P1_x$) with aldehydes (RCHO)

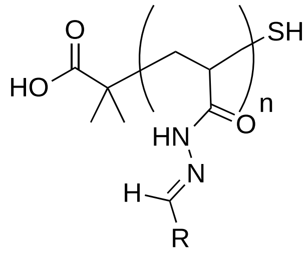

In a typical experiment, poly(acryloyl hydrazide) **P1**$_x$ (5 mg, 0.058 mmol) was dissolved in D_2O (35.63 µL) with 5% AcOH (1.87 µL). DMSO-*d6* (337.5 µL) was added to the above solution while vortexing. In a separate vial fitted with a magnetic stirrer, DMSO-*d6* (375 µL) was added to the aldehyde (0.058 mmol, 1.0 equiv.). The polymer solution was added to the aldehyde solution and the reaction was incubated at 60 ℃ for 24 h and analysed by ^{1}H NMR spectroscopy.

Hydrazone reduction in functionalised poly(acryloyl hydrazide)

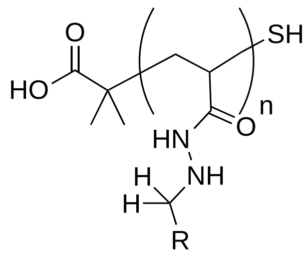

In a typical experiment, to an incubated solution (4.5 mL) of polymer (30 mg, 0.348 mmol) and aldehyde (0.348 mmol, 1.0 equiv.), 8 M borane-pyridine was added (1.16 mmol, 145 µL, 3.33 equiv.) at RT. 10% (3 M) $HCl_{(aq)}$ (387 µL, 3.33 equiv.) was added dropwise over 5 min. and the solution was stirred for 2 h. The crude polymer was purified by dialysis against water. The water was removed by lyophilisation and by drying in a desiccator with P_2O_5.

Modification of poly(*tert*-butyl 2-acryloylhydrazine-1-carboxylate) with 1,2−ethylenediamine (Boc-P1-NH$_2$)

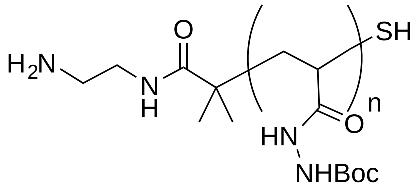

In a typical experiment, DMSO (5 mL) and 1,2-ethylenediamine (5 mL) were added successively to Boc-**P1** (0.5 g, 2.69 mmol). To this solution, EDC (1.0 g, 5.22 mmol) was added in three portions over 2 h. and stirred for a further 2 h. The polymer was purified by dialysis against water. The water was removed by lyophilisation and by drying in a desiccator with P_2O_5 to afford Boc-**P1-**NH$_2$ as a white powder (0.35 g, 70% yield). δ_H(300 MHz, CDCl$_3$) [calibrated using C*H*Cl$_3$ resonance at 7.26 ppm] 1.46 (br, 11H x DP, 9H in C(CH_3)$_3$, 2H in CHCH_2), 2.22 (br, 1H, C*H*CH$_2$), 3.25 (br, 4H, NH2CH_2CH_2), 7.17 (br, 1H x DP, OC(O)N*H*), 9.35 (br, 1H x DP, CHC(O)N*H*); DP (Fluorescence, Fluram Assay) 51.

Fluorescent poly(acryloyl hydrazide) (P1-Flu2)

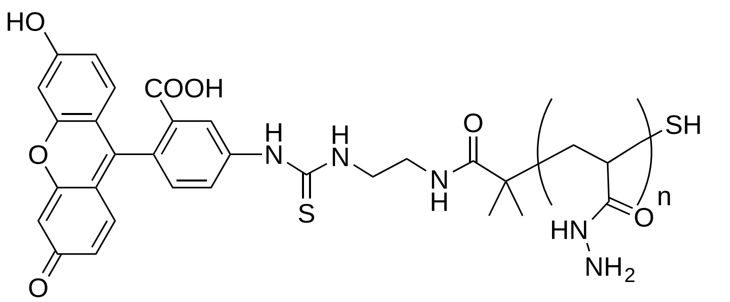

In a typical experiment, DMF (5 mL) and DIPEA (100 µL) were a added to Boc-**P1**-NH$_2$ (200 mg, 1.07 mmol). To this, FITC (100 mg) in DMF (5 mL) was added, and the solution was stirred overnight protected from light. A 100 µL aliquot was used to prepare a 4 mg mL^{-1} sample for SEC/GPC to verify a successful reaction using a fluorescence detector. The solution was concentrated under reduced pressure to afford a thick oil. The crude oil was diluted in DMF and purified by chromatography (Sephadex LH-20, EtOH) to afford Boc−**P1**−**Flu2** as an orange oil. To this oil, TFA (5 mL) was added and stirred for 3 h. Excess of TFA was removed by blowing a steady stream of argon and the resulting oil was diluted in water (10 mL). The **P1-Flu2**·TFA salt formed was neutralised by adding $NaHCO_3$ until no foaming was observed. The crude polymer was purified by dialysis against water. The water was removed by lyophilisation and by drying in a desiccator with P_2O_5 to afford **P1-Flu2** as an orange powder (70 mg, 76% yield). δ_H(300 MHz, D_2O) [calibrated using *H*DO resonance at 4.79 ppm] 1.00 (s, 3H, C(CH_3)), 1.05 (s, 3H, C(CH_3)), 1.62-2.10 (br m, 3H x DP, C*H*CH_2) 6.27-7.94 (br m, 9H, FITC Ar-*H*); DP (^{1}H NMR) 50.

1.7 References

1. J. Chiefari, Y. K. Chong, F. Ercole, J. Krstina, J. Jeffery, T. P. T. Le, R. T. A. Mayadunne, G. F. Meijs, C. L. Moad, G. Moad, E. Rizzardo and S. H. Thang, *Macromolecules*, 1998, **31**, 5559–5562.
2. C. Barner-Kowollik, *Handbook of RAFT Polymerization*, *Wiley-VCH*, 2008.
3. J. Chiefari, R. T. A. Mayadunne, C. L. Moad, G. Moad, E. Rizzardo, A. Postma and S. H. Thang, *Macromolecules*, 2003, **36**, 2273–2283.
4. D. J. Keddie, G. Moad, E. Rizzardo and S. H. Thang, *Macromolecules*, 2012, **45**, 5321–5342.
5. S. Perrier, T. P. Davis, A. J. Carmichael and D. M. Haddleton, *Chem. Commun.*, 2002, 2226–2227.
6. C. A. G. N. Montalbetti and V. Falque, *Tetrahedron*, 2005, **61**, 10827–10852.
7. E. Valeur and M. Bradley, *Chem. Soc. Rev.*, 2009, **38**, 606–631.
8. G. Yaşayan, M. Redhead, J. P. Magnusson, S. G. Spain, S. Allen, M. Davies, C. Alexander and F. Fernández-Trillo, *Polym. Chem.*, 2012, **3**, 2596–2604.
9. N. Nakajima and Y. Ikada, *Bioconjugate Chem.*, 1995, **6**, 123–130.
10. M. Benaglia, J. Chiefari, Y. K. Chong, G. Moad, E. Rizzardo and S. H. Thang, *J. Am. Chem. Soc.*, 2009, **131**, 6914–6915.
11. T. Ta, E. Bartolak-Suki, E.-J. Park, K. Karrobi, N. J. McDannold and T. M. Porter, *J. of Controlled Release*, 2014, **194**, 71–81.
12. J. Skey and R. K. O'Reilly, *Chem. Commun.*, 2008, 4183.
13. R. Hinman, *J. Org. Chem.*, 1958, **23**, 1587–1588.
14. C. R. Lindegren and C. Niemann, *J. Am. Chem. Soc.*, 1949, **71**, 1504–1504.
15. Y. K. Chong, J. Krstina, T. P. T. Le, G. Moad, A. Postma, E. Rizzardo and S. H. Thang, *Macromolecules*, 2003, **36**, 2256–2272.
16. D. J. Keddie, C. Guerrero-Sanchez, G. Moad, E. Rizzardo and S. H. Thang, *Macromolecules*, 2011, **44**, 6738–6745.
17. K. Godula and C. R. Bertozzi, *J. Am. Chem. Soc.*, 2010, **132**, 9963–9965.
18. H. C. Kolb, M. G. Finn and K. B. Sharpless, *Angew. Chem. Int. Ed*, 2001, **40**, 2004–2021.
19. T. L. Raguse, E. A. Porter, B. Weisblum and S. H. Gellman, *J. Am. Chem. Soc.*, 2002, **124**, 12774–12785.
20. J. M. Priegue, J. Montenegro and J. R. Granja, *Small*, 2014, **10**, 3613–3618.
21. E.-R. Kenawy, S. D. Worley and R. Broughton, *Biomacromolecules*, 2007, **8**, 1359–1384.
22. G. J. Gabriel, A. Som, A. E. Madkour, T. Eren and G. N. Tew, *Mater. Sci. Eng. R.,* 2007, **57**, 28–64.
23. G. N. Tew, D. Liu, B. Chen, R. J. Doerksen, J. Kaplan, P. J. Carroll, M. L. Klein and W. F. DeGrado, *Proc. Natl. Acad. Sci. U.S.A.*, 2002, **99**, 5110–5114.

24. Y. Ishitsuka, L. Arnt, J. Majewski, S. Frey, M. Ratajczek, K. Kjaer, G. N. Tew and K. Y. C. Lee, *J. Am. Chem. Soc.*, 2006, **128**, 13123–13129.
25. G. J. Köves, *J. Labelled Comp. Radiopharm.*, 1994, **34**, 255–262.
26. E. Erez, D. Fass and E. Bibi, *Nature*, 2009, **459**, 371–378.
27. J. M. Khurana, B. M. Kandpal, P. Sharma and M. Gupta, *Monatsh. Chem.*, 2014, **146**, 187–190.
28. R. L. Augustine, *Reduction: Techniques and Applications in Organic Synthesis* 1968.
29. M. Hudlicky, *Reductions in Organic Synthesis*, *Ellis Horwood Ltd.*,1984.
30. C. S. Mahon, M. A. Fascione, C. Sakonsinsiri, T. E. McAllister, W. Bruce Turnbull and D. A. Fulton, *Org. Biomol. Chem.*, 2015, **13**, 2756–2761.
31. R. O. Hutchins, K. Learn, B. Nazer, D. Pytlewski and A. Pelter, *Org. Prep. Proc. Int.*, 1984, **16**, 335–372.
32. M. Kawase and Y. Kikugawa, *J. Chem. Soc., Perkin Trans. 1*, 1979, 643.
33. A. Pelter, R. M. Rosser and S. Mills, *J. Chem. Soc., Perkin Trans. 1*, 1984, **0**, 717–720.
34. Y. Kikugawa and M. Kawase, *Chem. Lett.*, 1977, **6**, 1279–1280.
35. Y. Kikugawa and M. Kawase, *Synth. Commun.*, 1979, **9**, 49–52.
36. M. Brinkley, *Bioconjugate Chem.*, 1992, **3**, 2–13.
37. J. G. Cannon, *J. Med. Chem.*, 1997, **40**, 631–631.
38. E. A. Hoff, B. A. Abel, C. A. Tretbar, C. L. McCormick and D. L. Patton, *Polym. Chem.*, 2017, **128**, 15602–5.
39. D. Held, *Tips & Tricks GPC/SEC: Mobile Phase Considerations*, PSS Polymer standards Service GmbH, 12-15.
40. H. E. Gottlieb, V. Kotlyar and A. Nudelman, *J. Org. Chem*., 1997, **62**, 7512–7515.
41. T. Flagstad, M. R. Hansen, S. T. Le Quement, M. Givskov and T. E. Nielsen, *ACS Comb. Sci*., 2015, **17**, 19–23.

Chapter 2

Acetylene Polymer Scaffolds via Metal Catalysed Polymerisation

2.1 Background

In comparison with alkene substrates, attempts of using radical addition methods in alkyne polymerisation have been mostly unsuccessful.[1] Instead, most focus has gone into polymerisation of alkyne substrates using transition metal catalysts, in which Mo, W and Rh catalysts have proven most efficient. The metal catalysed polymerisation of alkynes can be described through either of two mechanisms: metathesis (metal carbene) or insertion (metal alkyl) (**Scheme 2.1**).[2]

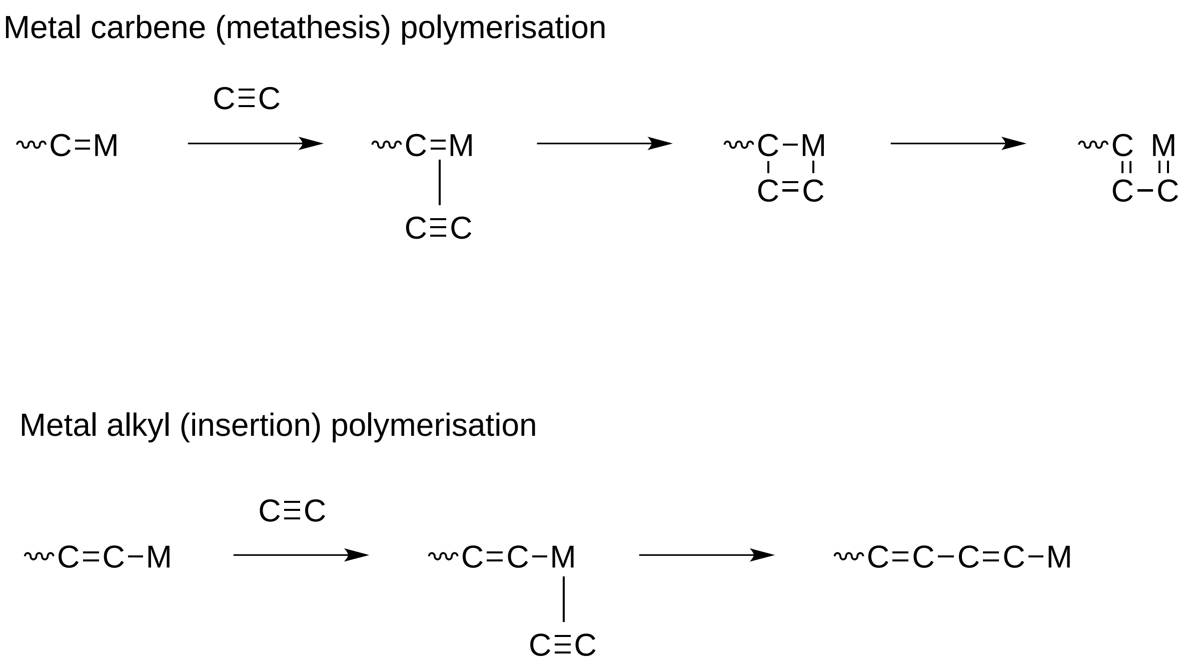

Scheme 2.1: The propagating mechanisms and propagating species of metal catalysed alkyne polymerisation. (M=metal)

The main issues associated with these types of polymerisation reactions are the high substrate specificity. Group 6 metal-halides such $MoCl_5$ and WCl_6, have been shown[1] to be suitable catalysts for the polymerisation of various bulky monosubstituted alkyne substrates but their tolerance for polar substituents is relatively poor. As a consequence it is unlikely that this chemistry would prove useful for the polymerisation of hydrazide containing alkynes. Rh based catalysts however, have been shown to tolerate polar substituents remarkably well, as evidenced by the results obtained in the polymerisations of propiolic acid esters, *N*–propargylamides and other polar substituents.[3,4] The bicyclo[2.2.1]hepta-2,5-diene-rhodium(I) chloride dimer $[Rh(nbd)Cl]_2$ has proven particularly efficient in acetylene polymerisations with a high yield in cis-transoid conformation (**Fig. 2.1**). This conformation is a direct consequence of the insertion-type mechanism[5,6] through which Rh catalysed polymerisations proceed. Mechanistically, all polymers synthesised through this mechanism should have a 100% *cis*-content, however, due to molecular rotation in solution, the *cis*-content can be lost.[7-10] The geometry of such conformations resemble the helicity of naturally occurring moieties (i.e. antimicrobial peptides), which can prove a useful tool in some of the proposed bio-medical applications.

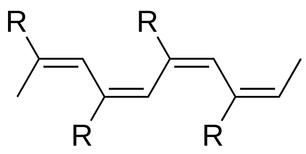

cis-transoidal

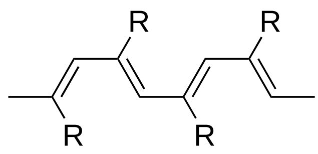

trans-cisoidal

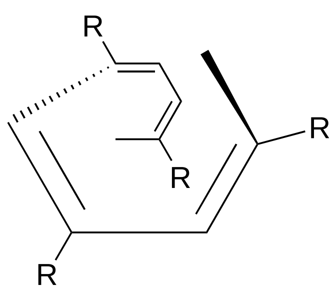

cis-cisoidal

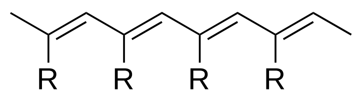

trans-transoidal

Figure 2.1: Four possible helical stereoisomers of acetylene polymers.

This rhodium catalyst and variants have generally shown particularly high potential in the polymerisation of phenyl-bearing acetylene monomers that incorporate polar groups such as carboxylic acids.[1] However, to the best of the author's knowledge, no current research exists into the polymerisation of acetylene moieties bearing hydrazide, hydrazine or *O*-hydroxylamine substituents. The closest similarity to such substrates are a series of *N*−substituted and *N*-unsubstituted 2−propynamides.[11,12] Polymerisation of these substrates has proved difficult with commonly used metal catalysts based on Mo or W and even with the $[Rh(nbd)Cl]_2$ catalyst. Two palladium based catalysts, $[Pd(CH_3CN)_4](BF_4)_2$ and $PdCl_2(PhCN)_2$, have shown promising results with the polymerisation of *N*-butyl-2-propynamide. As a consequence, these are likely to be potential candidates for obtaining a scaffold with a simple acetylenenic backbone (i.e. an analogue of poly(acryloyl hydrazide)) that incorporates our target hydrazide side-chains.

Due to their versatility in polymerising phenyl-bearing acetylenes[1,13-19] with polar substituents it is worth considering Rh catalysts as viable candidates for polymerising phenylacetylene substrates that incorporate hydrazides in the *para*-position. Rh-catalysed polymerisations can be carried out in most common organic solvents, polar and non-polar, but water has also been explored as possible solvent.

Several examples[16,20] exist in which organorhodium catalysts were used in aqueous media to afford rapid, high yielding and highly stereoregular polyphenylacetylenes. Patented research by Tang *et al*.[21] showed that the polymerisation of phenylacetylene and *p*−(methylphenyl)acetylene can be carried out in water both in the presence and absence of additives, with a variety of rhodium catalysts (e.g.) $[Rh(nbd)Cl]_2$, $[Rh(cod)Cl]_2$, $Rh(nbd)(tos)(H_2O)$ or $Rh(cod)(tos)(H_2O)$.

It was observed, that generally, rhodium catalysed polymerisations of phenylacetylenes are strongly affected by the presence of polar molecules in solution. Polymerisation yields in non–polar solvents such as toluene were significantly lower compared to those in polar solvents (i.e. MeOH, THF, H_2O) or in non-polar solvents with polar additives (i.e. Toluene with H_2O, MeOH, Et_3N). Addition of Et_3N as a co-catalyst is common practice throughout many examples of polymerisation using $[Rh(nbd)Cl]_2$ and it is suggested that the amine coordinates to the metal, breaking the dimer into the active catalytic rhodium species.

Compared to vinyl or acrylate based polymers, acetylene based polymers, although possessing important useful properties (e.g. high conductivity), have found very little use in commercial applications. The polymer backbone is highly susceptible to oxidation when exposed to air,[22] and formation of carbonyls, epoxides and peroxides has been reported. Furthermore thermal *cis*-*trans* isomerization of *cis*-transoidal polyacetylenes in solution, has been shown to accompanied by cyclisation and chain scission reactions,[9,10,23] leading to the degradation of the backbone (**Fig. 2.2**). This is driven by the formation of aromatic rings, which are energetically more stable. The isomerization process occurs more rapidly at higher temperatures (> 120 ℃) and as a consequence, it is believe that, for biological applications this property could be advantageous (e.g. degradation of antimicrobial polymers to minimise antimicrobial resistance due to antibiotic waste).

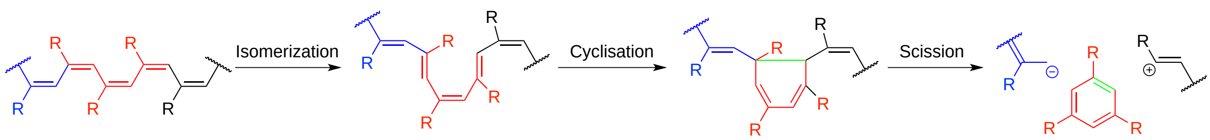

Figure 2.2: Mechanism of *cis*-*trans* isomerization of polyacetylenes, which can alternatively lead to cyclisation and aromatisation. This causes chain scission resulting in aromatic small molecules and shorter chain fragments.

2.2 Objectives

The first objective was to synthesise Boc-protected- (**2.1)** and unprotected propiolohydrazide monomers (**2.2)** and to attempt their polymerisation using Pd and Rh catalysts to achieve poly(propiolohydrazide) **P2** (**Scheme 2.2**) as a direct comparison with poly(acryloyl hydrazide) **P1** (see **Chapter I**).

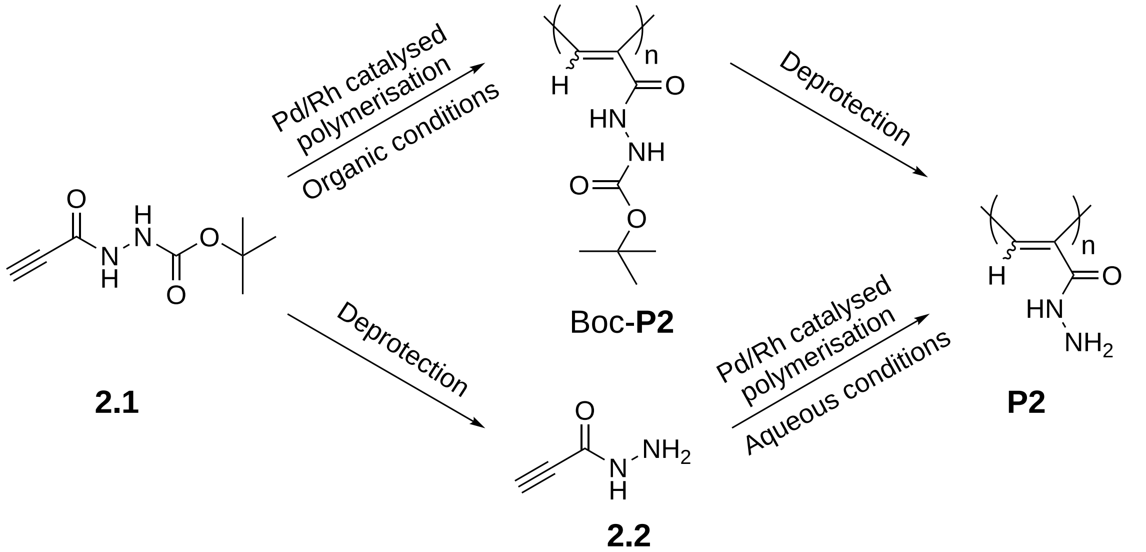

Scheme 2.2: First objective. The synthesis of poly(propiolohydrazide) **P2** via direct polymerisation of propiolohydrazide **2.2** or via the Boc-protected alternative Boc-**P2**.

Given the proven record in the polymerisation of monosubstituted phenylacetylene, as a second objective, it was aimed to synthesise Boc-protected- (**2.3**) and unprotected 4−ethynylbenzohydrazide (**2.4**), and polymerise these monomers to achieve poly(4−ethynylbenzohydrazide) (**P3**) (Scheme **2.3**). Following the synthesis and characterisation of these polymers the it was aimed to explore the functionalisation of these acetylene hydrazide scaffolds with aldehydes and investigate their possible degradation.

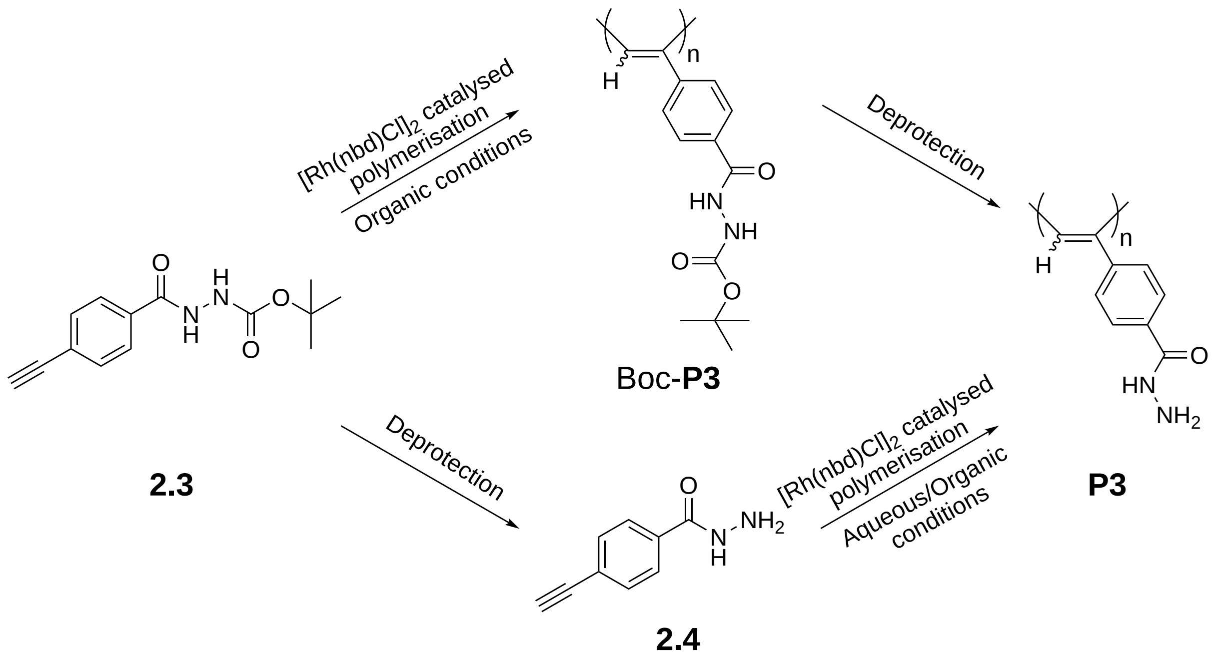

Scheme 2.3: Second objective. The synthesis of poly(4-ethynylbenzohydrazide) **P3** via direct polymerisation of 4-ethynylbenzohydrazide **2.4** or via the Boc-protected alternative Boc-**P3**.

2.3 Results and Discussion

The Boc-protected propiolohydrazide precursor **2.1** was synthesised in a similar fashion as the Boc-protected acryloyl precursor **1.3**. In this situation however (**Scheme 2.4**) there was no requirement for THF as a co-solvent, as both the reagents and the product were water-soluble.

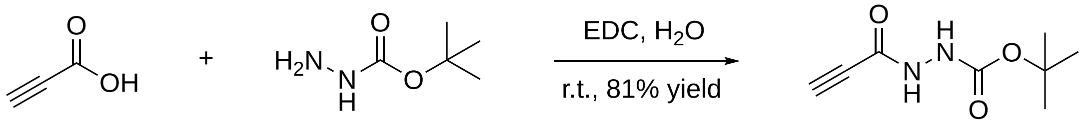

2.1

Scheme 2.4: Reaction scheme showing the synthesis of the target precursor *tert*−butyl−2−propiolohydrazine−1−carboxylate compound (**2.1**).

Depending on the excess reagent, purification was performed either via an acidic (i.e. excess *tert*-butyl carbazate) or a basic (i.e. excess propiolic acid) work-up. In comparison to the synthesis of the Boc-protected acryloyl hydrazide **1.3** the purification of compound **2.1** required no recrystallization step. The reaction was very efficient in the sense that on a small scale (up to 0.5 g propiolic acid), reaction completion occurs within 15 minutes. Additionally, the reaction was successfully scaled up to afford a quick route to large quantities of this intermediate.

Characterisation of the product revealed a series of unexpected results. Although thin layer chromatography indicates a single product present, ^{1}H and PENDANT ^{13}C NMR (**Fig. 2.3**) showed a “duplication” of the expected peaks ((i.e. four N-*H* peaks, two alkyne H and two Boc $(CH_3)_3$ peaks in the ^{1}H NMR spectrum) , with the duplicates accounting for ~20% of the integration total. Possible explanations include the presence of rotamers, but high temperatures ^{1}H NMR spectroscopy analysis was overall inconclusive (**Fig. 2.4**). The four N-*H* peaks (10.29 - 8.92 ppm) and the two

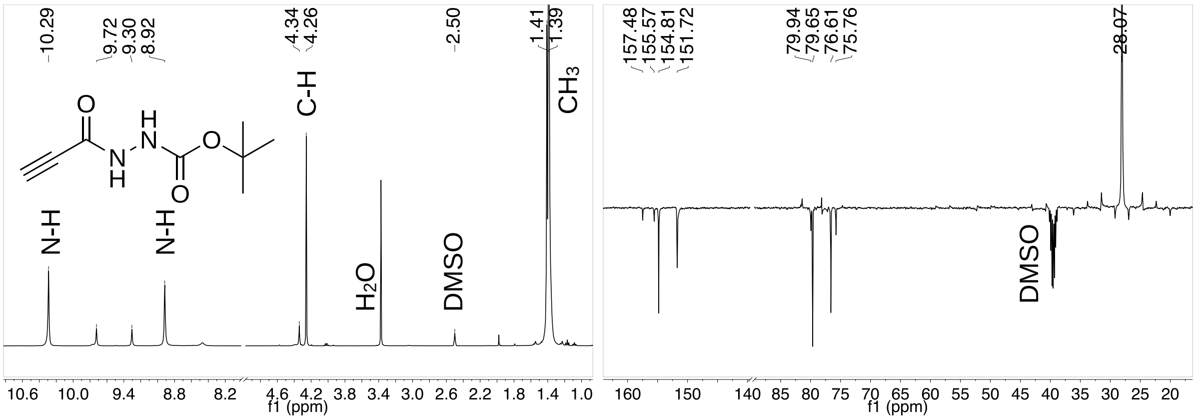

Figure 2.3: (left) ¹H NMR and (right) PENDANT ¹³C NMR spectra of *tert*-butyl-2-propiolohydrazine-1-carboxylate (left) **2.1**. The expected peaks at 10.29, 8.92, 4.26 and 1.39 ppm are accompanied by "duplicates" at 9.72, 9.30, 4.34 and 1.41 ppm respectively.

alkyne peaks (4.34 and 4.26 ppm) showed a decrease in the chemical shift value with increasing temperature (from 30 ℃ to 110 ℃) while the $(CH_3)_3$ peak showed an increase in chemical shift and a coalescence between the two peaks. Furthermore, all peaks showed broadening with increasing temperature, but the evidence is not sufficient to conclude the presence of rotamers. Alternatively, the "duplication" could in fact be a seemingly identical unidentified derivative of the target hydrazide.

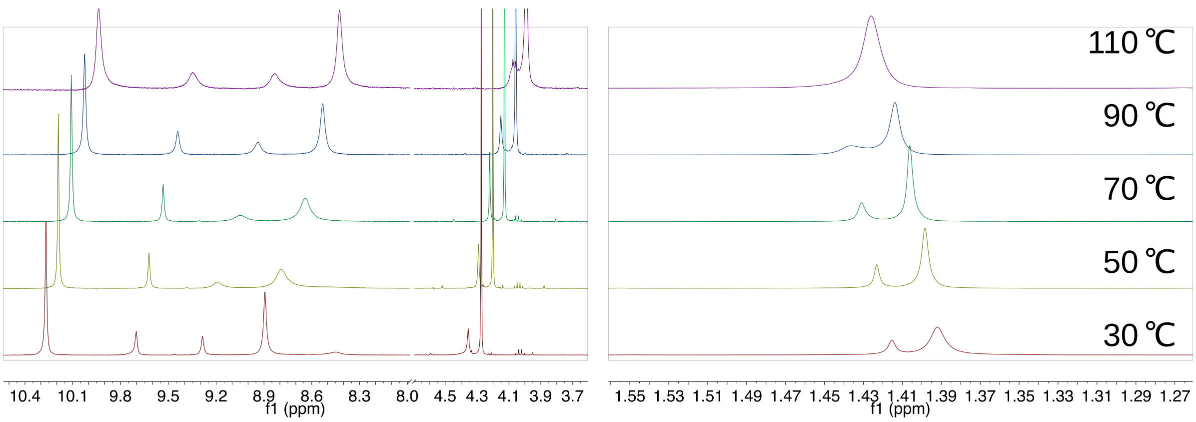

Figure 2.4: Variable temperature ¹H NMR spectra of **2.1**.

Deprotection of *tert*-butyl-2-propiolohydrazine-1-carboxylate proved challenging and was largely unsuccessful. Despite attempting several well-known

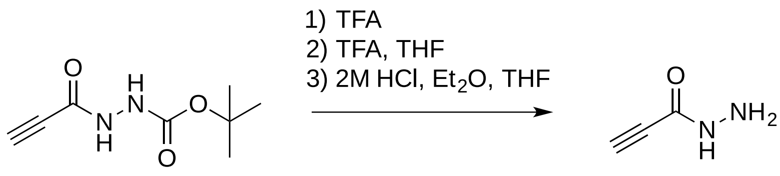

2.1 **2.2**

Scheme 2.5: Conditions attempted for substrate **2.1** deprotection.

Boc-group removal strategies (**Scheme 2.5**), the target monomer **2.2** could not be isolated.

Attempts with TFA, as a reagent and solvent, could be seen by ^{1}H NMR spectroscopy (**Fig. 2.5**) to have been the only conditions to afford the desired target molecule. In the purification process however, the impure oil obtained could not be precipitated successfully, and multiple alkyne environments could be detected.

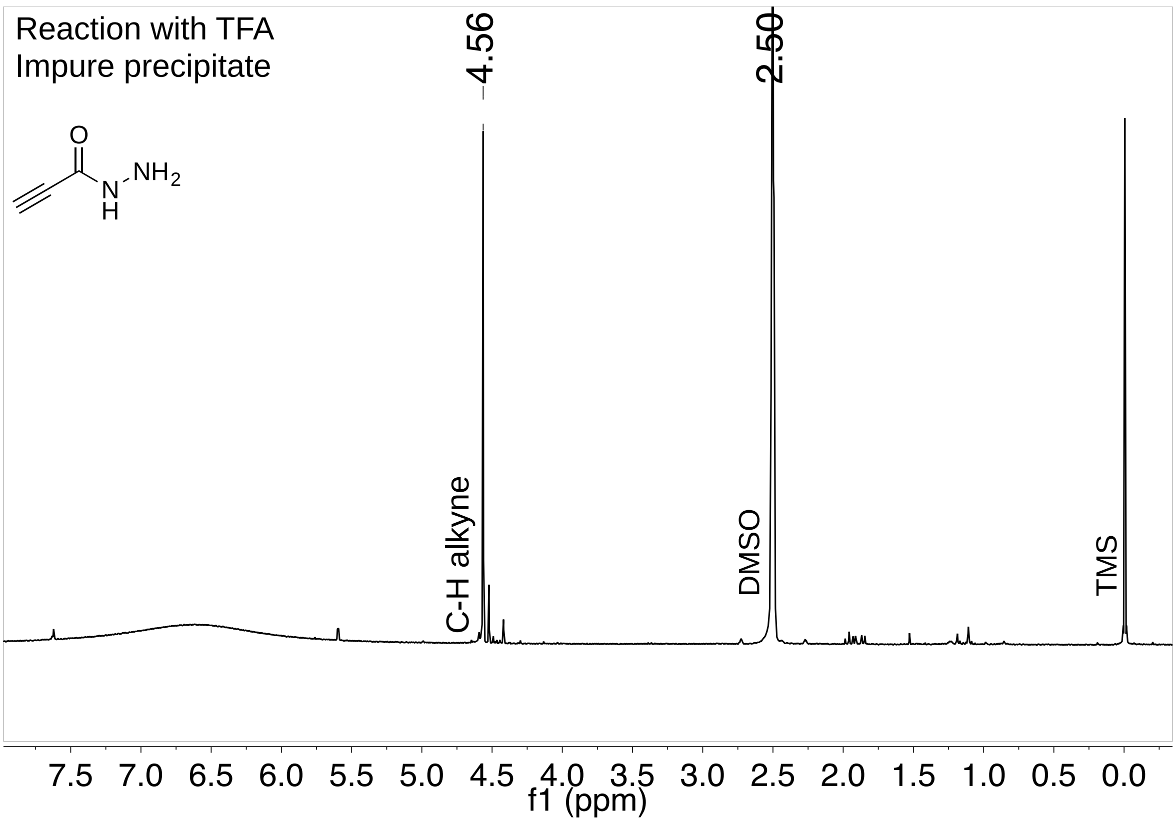

Figure 2.5: ^{1}H NMR spectrum of impure **2.2** isolated after precipitating the crude from the reaction with TFA. Multiple H-C alkyne peaks are seen.

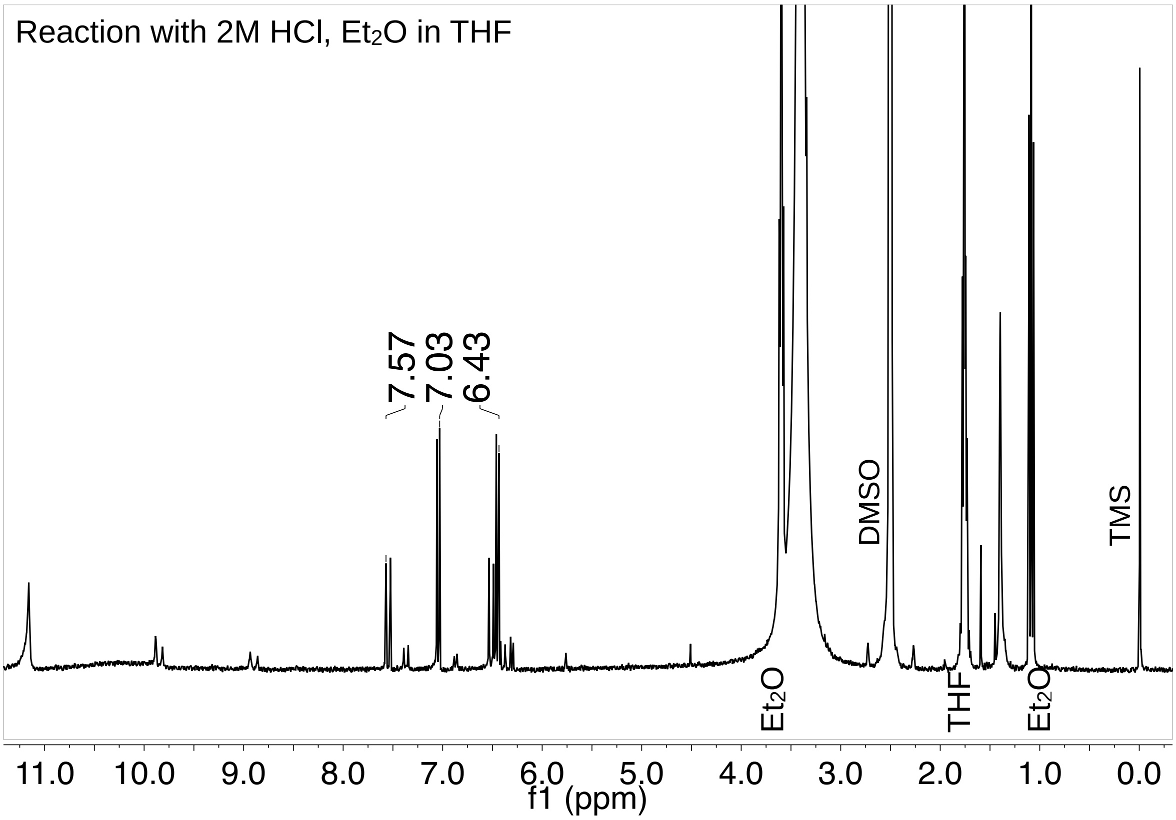

Figure 2.6: [1]H NMR spectrum of the precipitate isolated from the deprotection of **2.1** using 2M HCl in Et_2O and THF. Several pairs of doublets with different intensities can be observed between 6.3-10.0 ppm. These are believed to be products caused by Michael addition.

Furthermore, consecutive attempts at precipitation seemed to introduce even more impurities. Deprotection using 2 M HCl in Et_2O was also unsuccessful. The expected Boc-group removal was observed, but this was accompanied most likely by Michael addition reactions (**Fig. 2.6**). No alkyne signals were observed in the 4.3 ppm region, instead, several pairs of doublets in the alkene region (i.e. 6.4 - 7.6 ppm) were observed. Curiously, this pattern of reactivity seems to be also observed during the polymerisation reactions as likely side-products. Due to the repeated failures in isolating the deprotected monomer it was decided to attempt the synthesis of Boc-**P2** by polymerising Boc-protected propiolohydrazide **2.1**.

The polymerisation of **2.1** was explored under three different metal catalysts and different reaction conditions (**Table 2.1**). The first attempts using the [Rh(nbd)Cl]$_2$ catalyst proved generally ineffective (**Table 2.1**, **Entry 1,2**). Although full monomer consumption was observed (**Fig. 2.7**), conversion to polymer seems to be small. Initially it was thought that likely by-products were small size oligomers or possibly [2+2+2] cyclisation products. To rule out the [2+2+2] cyclisation product the possible [2+2+2] product **2.5** (**Fig. 2.7**) was synthesised, using the same EDC, H_2O/THF protocol from trimesic acid and *tert*-butyl carbazate. The ^{1}H NMR spectrum of this product (**Fig. 2.7**) was inconsistent with any features of the ^{1}H NMR spectra that were obtained for the polymerisation reactions. The quartet at 3.93 ppm (2*H*) and the triplet at 1.15 ppm (3*H*), may be evidence of Et_3N undergoing Michael addition to the monomer.[24] The alkene signals at 5.85 and 5.55 ppm showed an integration with respect to the former quarter and triplet of (1:1:6:9) suggesting three ethyl groups per alkene further encouraging this hypothesis. Further attempts at polymerisation with

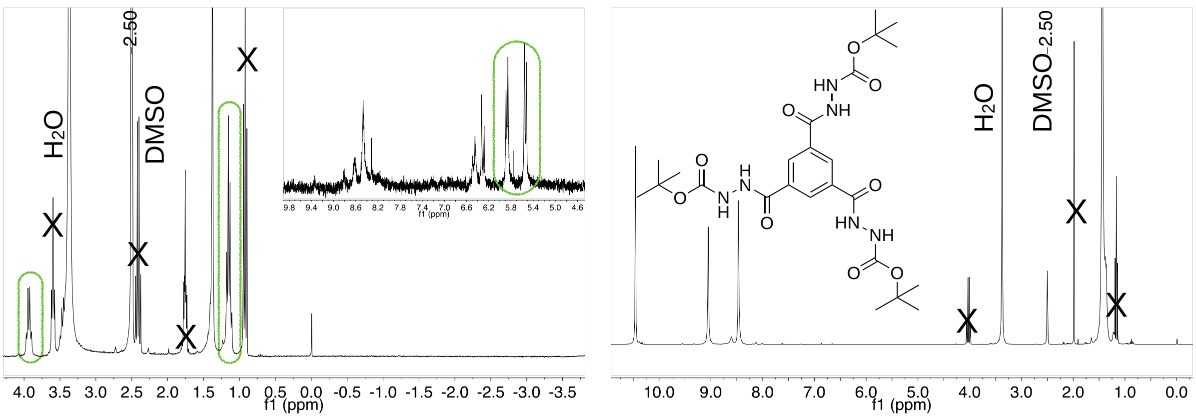

Figure 2.7: ^{1}H NMR spectrum of polymerisation crude of **2.1** with [Rh(nbd)Cl]$_2$ in TEA/THF (crosses) showing the consumption of monomer and the suspected presence of the Michael addition product of **2.1** with TEA (left). Expanded region 9.8 - 4.6 ppm (inset). ^{1}H NMR spectrum of tri-*tert*-butyl 2,2',2''-(benzene-1,3,5-tricarbonyl) tris(hydrazine-1-carboxylate) **2.5** (i.e. the expected product of the [2+2+2] cyclisation of **2.1** or chain scission product of Boc−**P2**) (right).

the Rh catalyst were similarly futile. As a consequence, it was decided to explore palladium based catalysts. Due to its moderate success in polymerising *N*-butyl-2-propynamide,[11] $[Pd(CH_3CN)_4](BF_4)_2$ was considered as an appropriate catalyst for these type of substrates. Monomer conversion to polymer rather than by-products seemed to occur in prevalence at higher temperatures (**Table 2.1**, **Entry 3,4 vs 5**), but full monomer consumption was not obtained even after reacting for a couple of weeks (**Table 2.1**, **Entry 5**). The polymerisation of **2.1**, using $PdCl_2(PhCN)_2$ as a catalyst in toluene, lead to full monomer consumption with polymeric compounds as the predominant product within 48 hours, but only at elevated temperatures (**Table 2.1, Entry 6,7**). Characterisation of the products obtained proved challenging. Proton NMR spectra of reaction crudes containing toluene were particularly difficult to analyse due to the aromatic protons blocking an area where most new signals are observed and expected. A common feature among most "polymeric" products

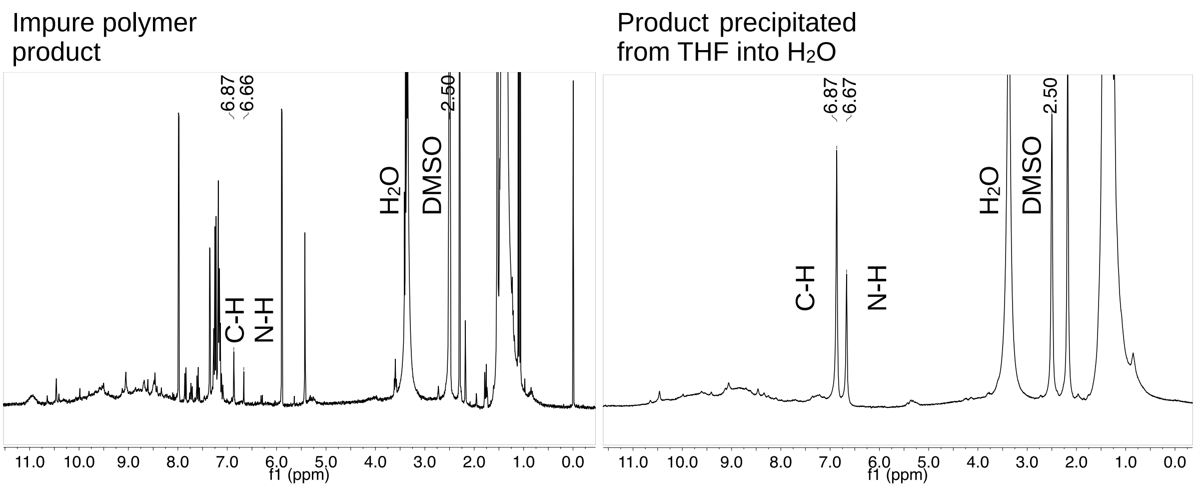

Figure 2.8: ^1H NMR spectra of a Boc-**P2** polymer sample before (left) and after (right) purification by precipitation. The peak at 6.67 ppm was identified as an N-H peak as it was shown to be an exchangeable proton in the presence of MeOD. The small broad peak at 7.24 ppm integrates to ~10% of the integration value of the peak at 6.87 ppm, and only 2% of the integration value of the CH_3 in the Boc-group. This suggested that there could be small quantities of a polymeric species (i.e. Boc-**P2**), but the main product is either a small molecule or a short oligomer of Boc-P**2**.

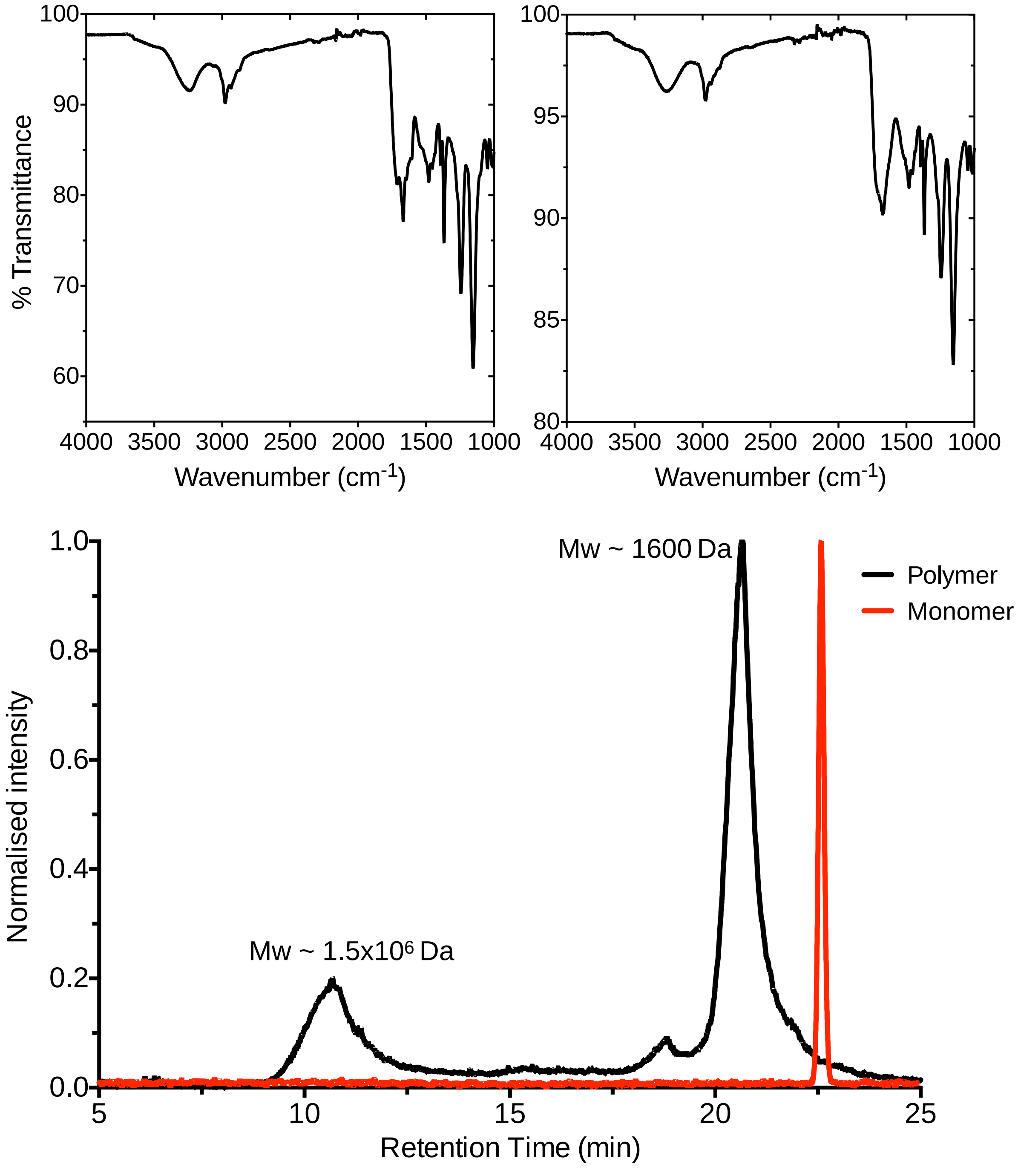

Figure 2.9: (Top) FT-IR spectra of polymer products isolated after reactions of **2.1** with $[Pd(CH_3CN)_4](BF_4)_2$ (left) and $PdCl_2(PhCN)_2$ (right) respectively. The absence of alkyne vibrational stretch, and broadening of the hydrazide and Boc-group carbonyl peaks suggests presence of polymeric or oligomeric products. (Bottom) SEC/GPC chromatograms of products of the polymerisation of **2.1** showing polymeric (10.8 min) and oligomeric (20.7 min) specific peaks in the isolated product. Molecular weight are calculated based on PMMA calibration standards.

identified were a pair of singlets at ~6.87 and ~6.67 ppm assigned as C-H and N−H environments (**Fig. 2.8**). These peaks did not show the characteristic broadening expected of polymer species. FT-IR spectra showed (**Fig. 2.9**) the disappearance of the alkyne vibrational stretch and a coalescence of the two carbonyl stretches into a single broader peak. SEC/GPC (**Fig. 2.9**) suggested the presence of small amounts of a relatively large polymeric species, but the main peak is characteristic of several

Entry	Monomer: *tert*-butyl 2-propiolohydrazine-1-carboxylate						
	Solvent	[M]/ [cat.]	[M]	Temp. (℃)	Time (h)	% monomer consumption[a]	% product recovered
	Catalyst: $[Rh(nbd)Cl]_2$						
1	THF/ Et_3N[b]	100	0.201	30	24	100	17[f]
2	MeOH/ Et_3N[c]	110	0.220	30	124	100	32[f]
	Catalyst: $[Pd(CH3CN)_4](BF_4)_2$						
3	Toluene /THF[d]	83	0.163	30	432	84	14[f]
4	THF	91	0.443	30	192	25	9[g]
5	Toluene /THF[e]	95	0.159	70	72	75	20[g]
	Catalyst: $PdCl_2(PhCN)_2$						
6	Toluene	107	0.486	70	48	100	34[g]
7	Toluene	187	0.868	70	48	100	58[g]
8	DMSO	49	0.904	70	24	100	25[f]

Table 2.1: Summary of key polymerisation reaction attempts with monomer **2.1**. [a]According to ^{1}H NMR; [b]Volume ratio: 2:1; [c]Volume ratio: 1:1; [d]Volume ratio: 2.5:1; [e]Volume ratio: 6:1; [f]Isolated after dialysis; [g]Isolated after precipitation from THF to H_2O at 80 ℃.

discrete oligomeric moieties. After these failed attempts to synthesise larger molecular weight Boc-**P2**, in which different catalysts, temperatures and solvent conditions were considered, the work these types of polymers was halted and research was diverted towards phenylacetylene type monomers as the literature suggested that they were more likely to have a higher chance of success.

The phenylacetylene hydrazide monomer **2.4** was synthesised in three steps. In the first step 4-iodobenzoic acid was reacted with *tert*-butyl carbazate under the previously reported conditions (i.e. EDC, water, THF) (**Scheme 2.6**) in high yields to afford the Boc-protected iodobenzylhydrazide **2.6**.

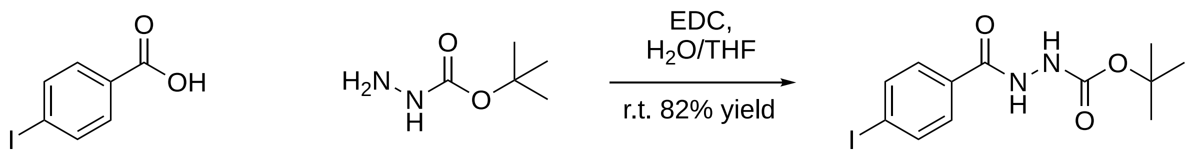

2.6

Scheme 2.6: Synthetic route towards *tert*-butyl 2-(4-iodobenzoyl)hydrazine-1-carboxylate **2.6**.

The alkyne functionality was inserted via the Sonogashira coupling between the aforementioned iodobenzoyl (**2.6**) and trimethylsilylacetylene (**Scheme 2.7**). The expected product was isolated in good yields after purification via column chromatography and the characterisation data obtained via ^{1}H, ^{13}C NMR and IR

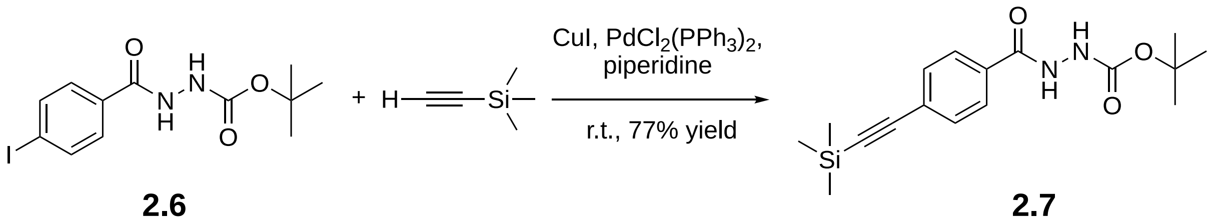

2.6 **2.7**

Scheme 2.7: *tert*–butyl–2–((4–trimethylsilyl)ethynyl)benzoyl)hydrazine–1–carboxylate **2.7** synthesised via the Sonogashira coupling of compound **2.6** and trimethylsilylacetylene.

spectroscopy and mass spectremetry confirmed the expected structure **2.7** (**Fig. 2.10**).

The new alkyne bond was evidenced by both the stretch at ~2170 cm^{-1} in the FT-IR spectrum and two new quaternary carbon centres in the ^{13}C NMR spectrum, while the trimethylsilyl (TMS) group was also evident from the ^{1}H NMR spectrum.

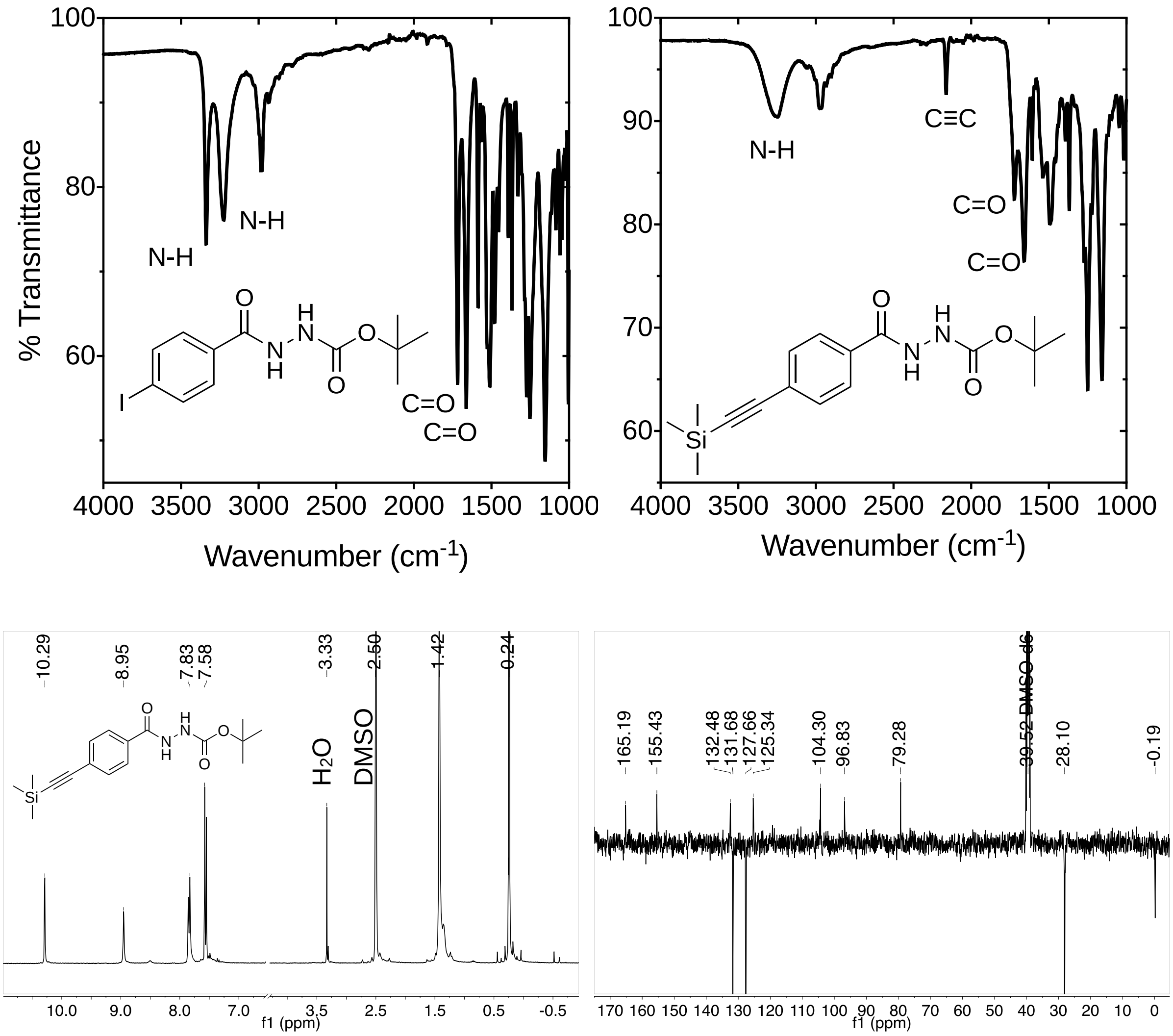

Figure 2.10: (Top) FT-IR spectra of compounds **2.6** (left) and **2.7** (right) showing the newly introduced alkyne functionality characterised by the C≡C stretch at 2159 cm^{-1}. (Bottom) ^{1}H (left) and PENDANT ^{13}C (right) NMR spectra of alkyne **2.7** confirming the structure of the molecule. The trimethylsilyl (TMS) group is evidenced by the peak at 0.24 ppm in the ^{1}H NMR and -0.19 ppm in the ^{13}C NMR spectra, and the alkyne peak is evidence by the peaks at 104.30 and 96.83 ppm in the ^{13}C NMR spectrum.

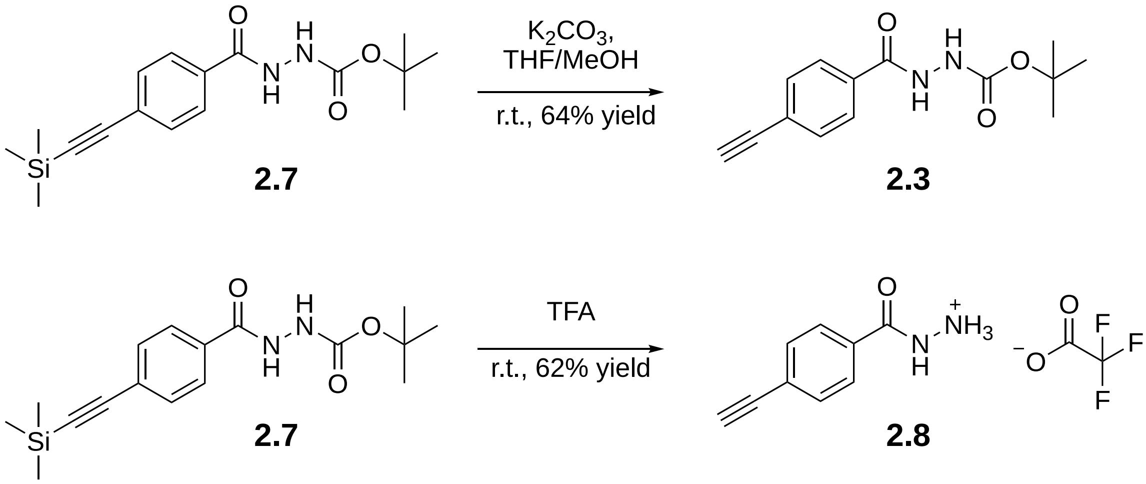

Scheme 2.8: Selective removal of the TMS group (top) or dual removal of the TMS and Boc groups to afford phenylacetylenes **2.3** and **2.8** respectively (bottom).

At this stage two distinct deprotection strategies (**Scheme 2.8**) were explored. Selective deprotection of the alkyne was achieved using K_2CO_3 in a 1:1 THF/MeOH mixtures, to afford *tert*–butyl 2-(4-ethynylbenzoyl)hydrazine-1-carboxylate **2.3**. Alternatively, a dual deprotection to remove both the TMS and the Boc group was carried out to afford the TFA salt **2.8** of our target molecule **2.4**. Both products were purified either by work-ups, precipitation or trituration. In both cases ^{1}H NMR spectroscopy (**Fig. 2.11**) confirmed the loss of the TMS group at 0.24 ppm and the presence of the alkyne proton at 4.41 and 4.47 ppm respectively.

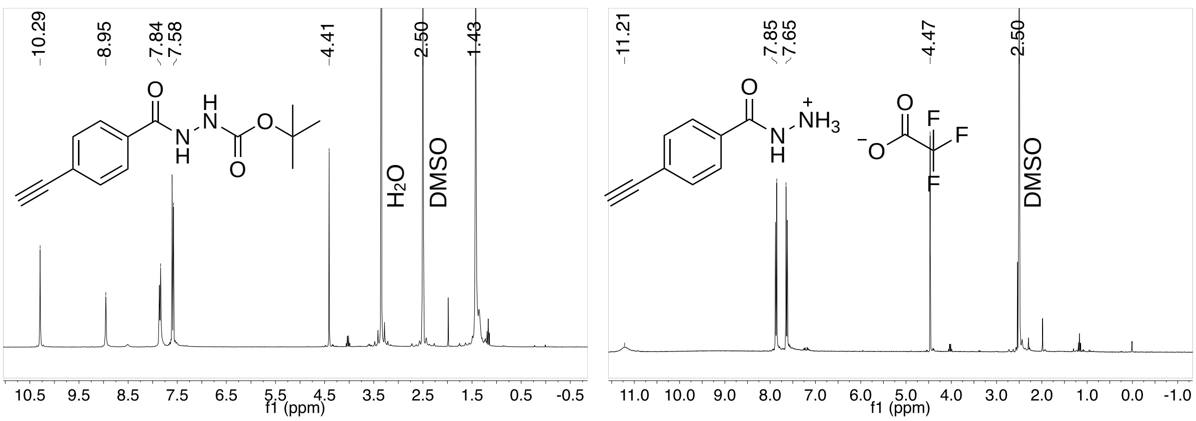

Figure 2.11: ^{1}H NMR spectra of Boc-protected 4-ethynylbenzohydrazide **2.3** (left) and the TFA salt of 4-ethynylbenzohydrazide **2.8** (right) in DMSO-*d6*.

Initially the polymerisation of the TFA hydrazide salt **2.8** was explored using the $[Rh(nbd)Cl]_2$ catalyst with Et_3N in H_2O, DMSO or H_2O/DMSO mixtures (**Scheme 2.9**). Regardless of whether the concentration of monomer in solution was high (1.0 M) or low (0.2 M), polymerisation occurred rapidly as suggested by the immediate increase in viscosity upon the addition of the catalyst.

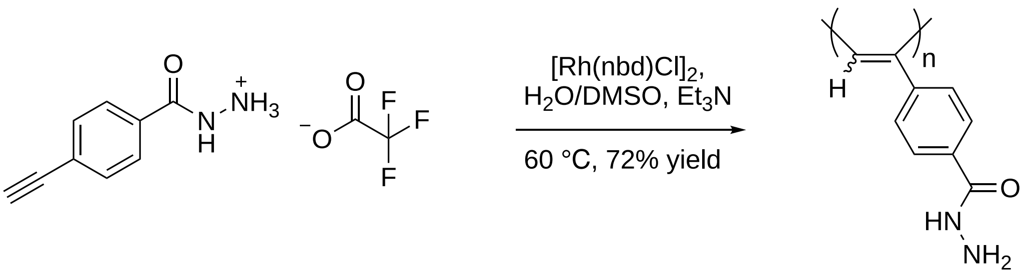

2.8 **P3**

Scheme 2.9: Attempted polymerisation conditions for phenylacetylene **2.8**, the TFA salt of monomer **2.4**.

Unfortunately, the polymers isolated were insoluble despite attempts at using varied combinations of aqueous, organic or acidic media as well as H-bonding-disrupting additives such as urea. It is believed that the polymer molecules H-bond to each other via the hydrazide side-chains to create unbreakable networks. As a consequence of its insolubility, the only characterisation information obtained was from IR-spectroscopy (**Fig. 2.12**). The data suggested that a structure high in *cis*-transoid content is present according to Simionescu *et al*.[8,25] According to the literature, *cis*-transoid specific peaks are at 740, 895 and 1380 cm^{-1} for poly(phenylacetylene). In the FT-IR spectra of **P3** peaks at 755, 896 and 1373 cm^{-1} were observed, which could be considered within a margin of error due to poor resolution and the fact that the reported values are for unsubstituted poly(phenylacetylene) as opposed to **P3**, which has a hydrazide substituent.

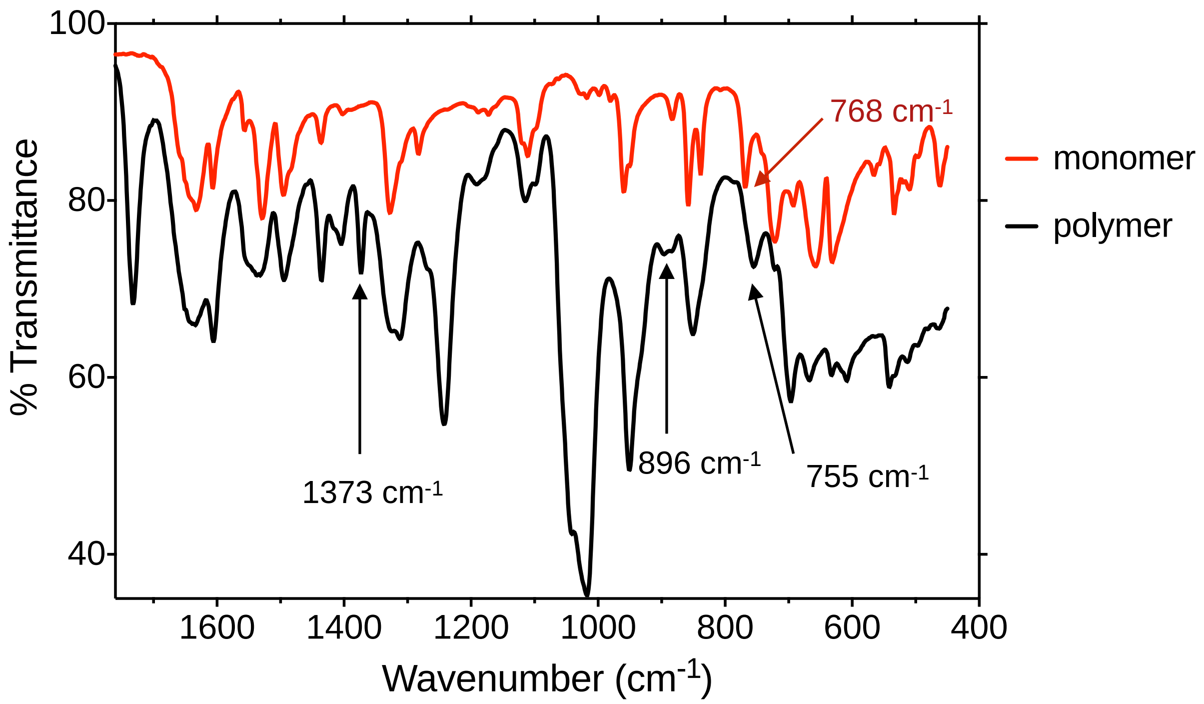

Figure 2.12: FT-IR spectra of monomer **2.8** and the insoluble polymer **P3**. The highlighted peaks could be consistent with the reported values for poly(phenylacetylene) and the small deviations could be attributed to poor resolution and the presence of the hydrazide group.

As a consequence of the insolubility issues encountered, it was decided to attempt the polymerisation of the Boc-protected monomer **2.3** (**Scheme 2.10**), with a view to deprotect post–polymerisation and isolate the TFA or chloride salt of **P3**.

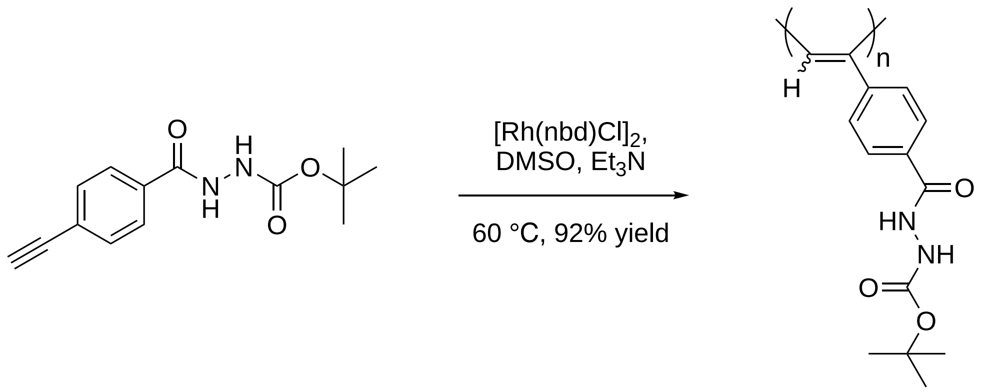

2.3 Boc-**P3**

Scheme 2.10: Polymerisation conditions for Boc-protected phenylacetylene hydrazide **2.3** to afford Boc-**P3**.

Polymerisation of this substrate proved efficient and the obtained Boc-**P3** polymers showed solubility in organic polar solvents such as THF, MeOH and DMSO. The effects of monomer concentration on the reaction kinetics and polymer size were investigated by analysing by SEC/GPC in MeOH three reaction crudes at [0.5], [1.0] and [1.5] monomer concentration after 2 hours. As expected, monomer conversion was higher with increased concentration, but larger molecular weight polymers were also observed while less oligomers were present (**Fig. 2.13**).

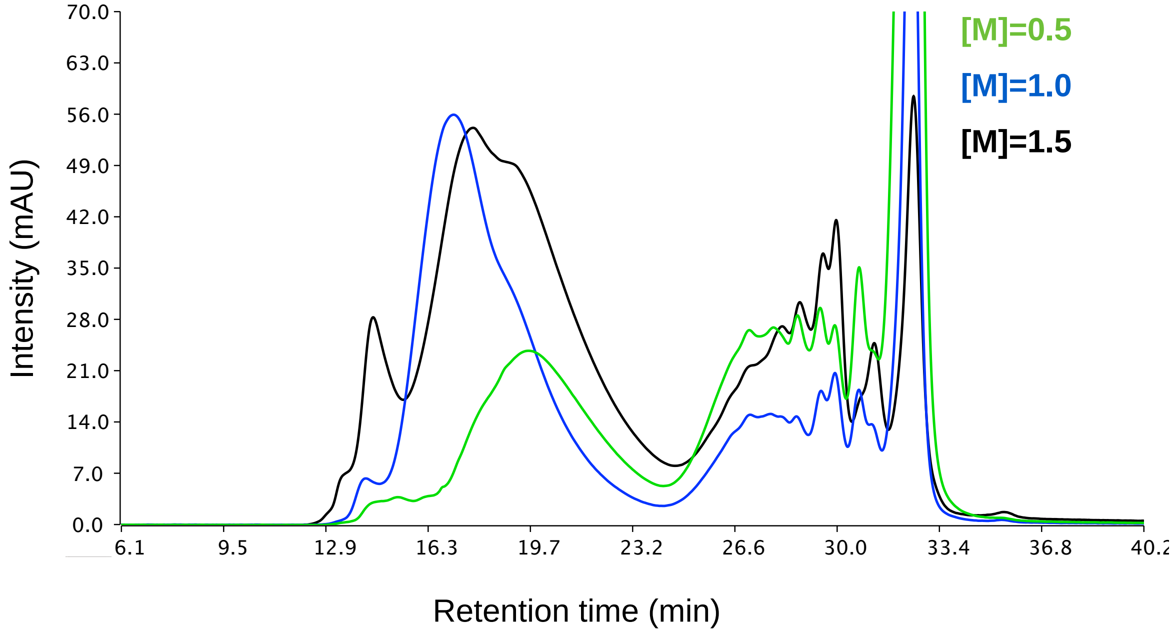

Initial Monomer conc.	%Area under curve (AUC) at retention time x (min)*:							
	14.3 -15.5	16.8 -17.3	19.22	27.8	28.6	29.9	30.70	32.4
[M]=0.5	-	-	28.01	4.17	0.35	2.18	2.83	62.46
[M]=1.0	0.54	72.09	-	3.10	-	0.75	1.43	22.09
[M]=1.5	7.6	55.37	-	-	0.45	23.88	4.20	8.52

Figure 2.13: (Top) SEC/GPC chromatogram showing the difference in reaction profiles of polymerisations of **2.3** at different monomer concentrations after 2h. (Bottom) Table summarising the area under the curve for each peak observed.

In the figure above, the retention time at 32.4 min. is due to the monomer, peaks between 27.8-30.70 are suspected to be oligomers while peaks between 14.3-19.22 are target polymers. It could be seen that for [M]=1.5 a rapid consumption of monomer is observed. Because the area under the curve is dependent on the absorption profile at 275 nm, a 8.52% AUC for the monomer does not necessarily mean that a conversion of 91% has occurred, as the polymer could be a better UV-Vis absorber. However, these values can be used to compare the reactions at different concentrations.

With these findings in mind, the monomer was polymerised at [M]=1.5 on a 250 mg scale to successfully obtain 230 mg of a polymer/oligomer mixture as evidenced by the SEC/GPC chromatogram (**Fig. 2.14**). The chemical shifts and shape of the peaks in the ^{1}H NMR spectrum (**Fig. 2.15**) of this sample were consistent with the literature

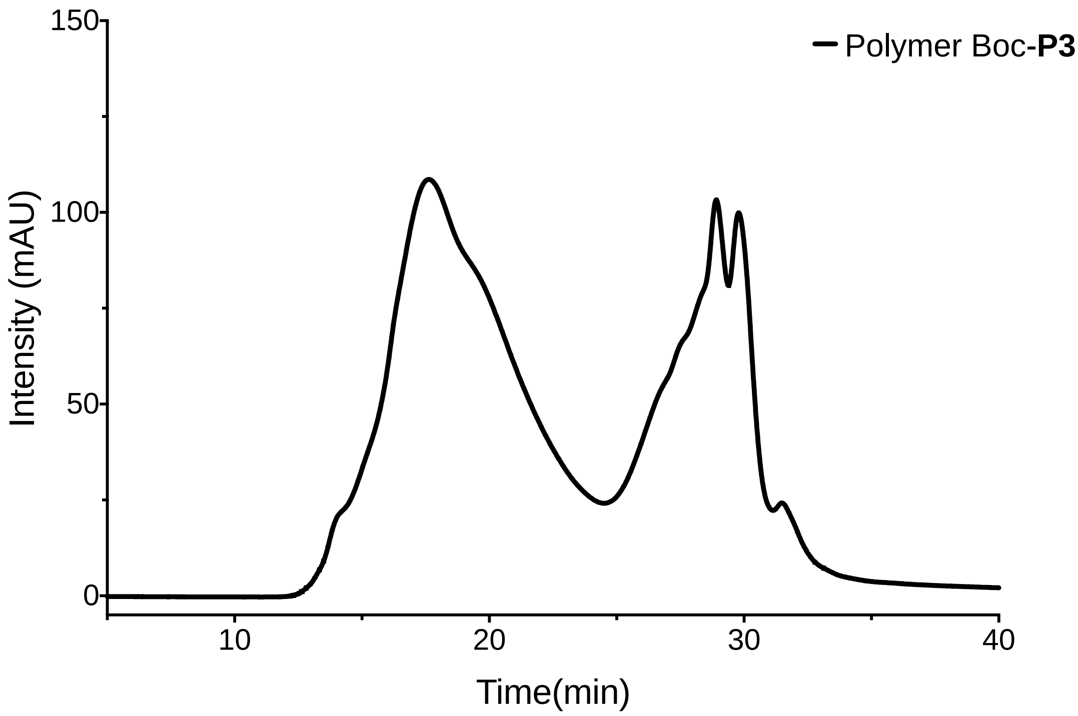

Figure 2.14: SEC/GPC chromatogram of polymer Boc-**P3**. According to the area under curve, the area peaking at 17.4 min represents 60% of the total, while the oligomers account for the rest of the sample.

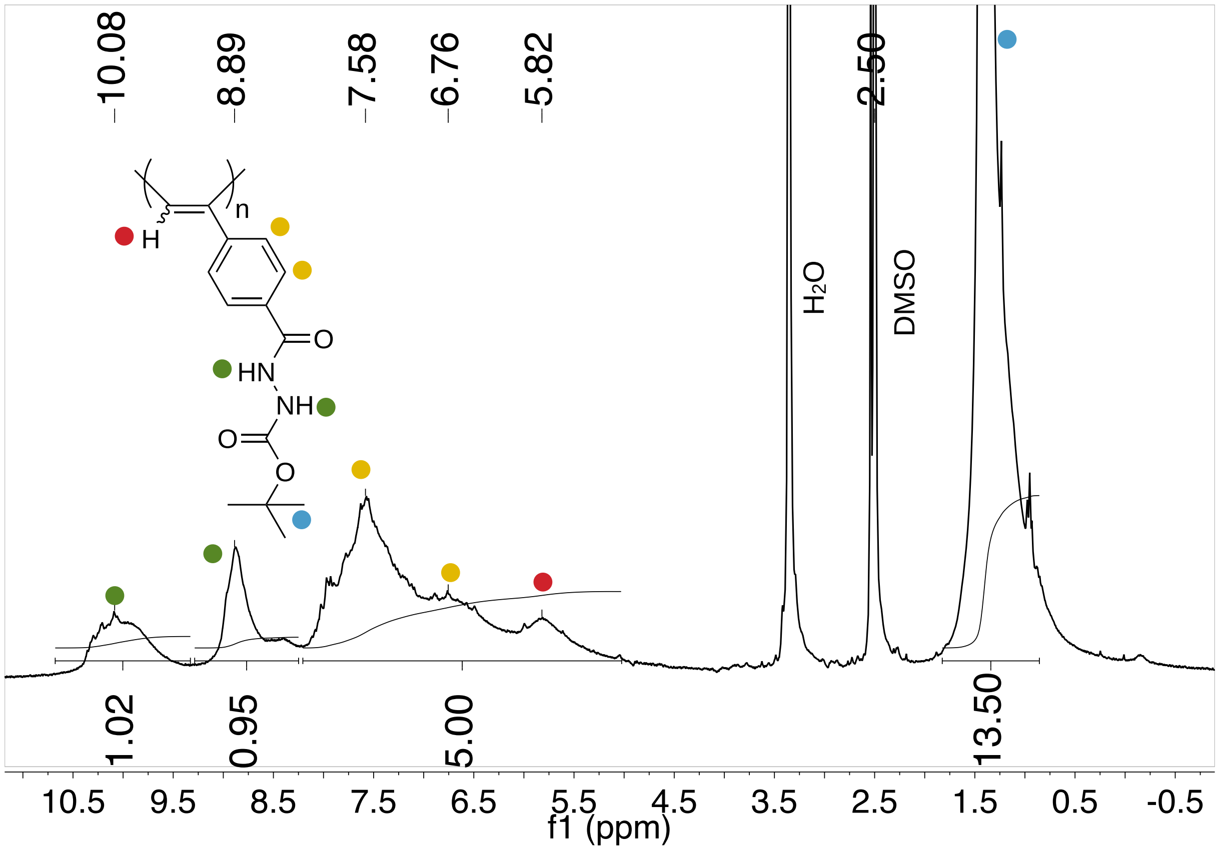

Figure 2.15: ^{1}H NMR spectrum of polymer Boc-**P3** showing the expected broad peaks. The peaks at 10.08 and 8.89 ppm are consistent with the N-H peaks, 7.58, 6.76 and 5.82 ppm with the aromatic peaks and vinyl peak respectively, while the broad peak at 1.42 ppm is due to the Boc group.

prediction[9,10,26] for poly(phenylacetylene): alkene proton around 5.82 and broad aromatic protons between 6.70 and 7.50 ppm. The sharper features hidden underneath the broad peaks could be due to the oligomers present as evidenced by the SEC/GPC.

To obtain the target polymer scaffold **P3**, the deprotection of polymer Boc-**P3** with TFA in DMSO was attempted. In all experiments where the content of TFA was lower than that of DMSO, no deprotection was observed. This could be attributed to the protonation of DMSO in solution. When the deprotection was carried out in 3:1 TFA/DMSO, successful removal of the Boc group was observed. Isolation of the compound proved difficult however. Removal of DMSO using solvent removal techniques was unsuccessful and dialysis under basic conditions, to deprotonate the TFA hydrazide, lead to the insoluble polymer **P3**. The deprotection was successfully repeated in 3:1 TFA/THF (**Scheme 2.11**). The solvent was removed by a series of dissolutions in Et_2O and evaporation through blowing a stream of argon. An orange precipitate (TFA-**P3**) was isolated and dried further under vacuum to afford the TFA salt of polymer **P3**.

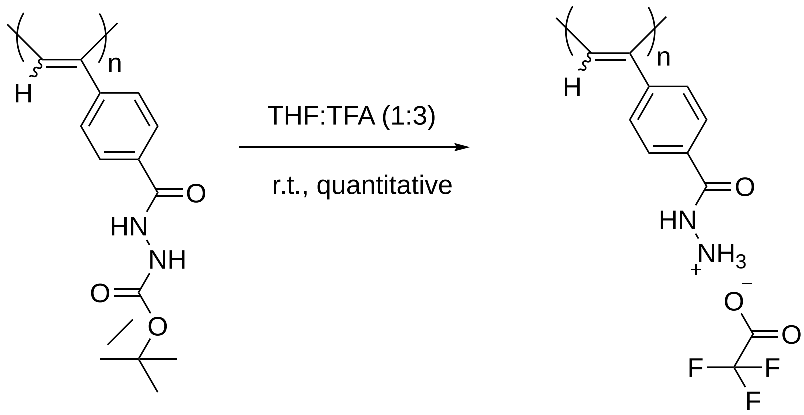

Boc-**P3** TFA-**P3**

Scheme 2.11: Reaction scheme showing the deprotection of polymer Boc-**P3** to afford the target hydrazide scaffold **P3** as a TFA salt.

Polymer TFA-**P3** was analysed by ^{1}H NMR spectroscopy in DMSO-*d6* (**Fig. 2.16**), but the solubility of the polymer was poor. Heating was required to achieve dissolution and a viscous solution was obtained. The spectrum showed the expected broad aromatic and the alkene peak at 7.49, 6.70 and 5.75 ppm respectively. No peak was observed in the expected region of for the Boc-group, while the NH_3^+ is believed to be masked by the excess TFA solvent at 4.34 ppm. To determine if the scaffold is reactive towards aldehydes, 0.45 equiv. benzaldehyde (**A7**) were added to the NMR sample. Immediate and complete coupling was observed as evidenced by the absence of both the aldehyde signal and sharp aromatic signals. However, because of the overlap between the aromatic signals of the phenylhydrazide side-

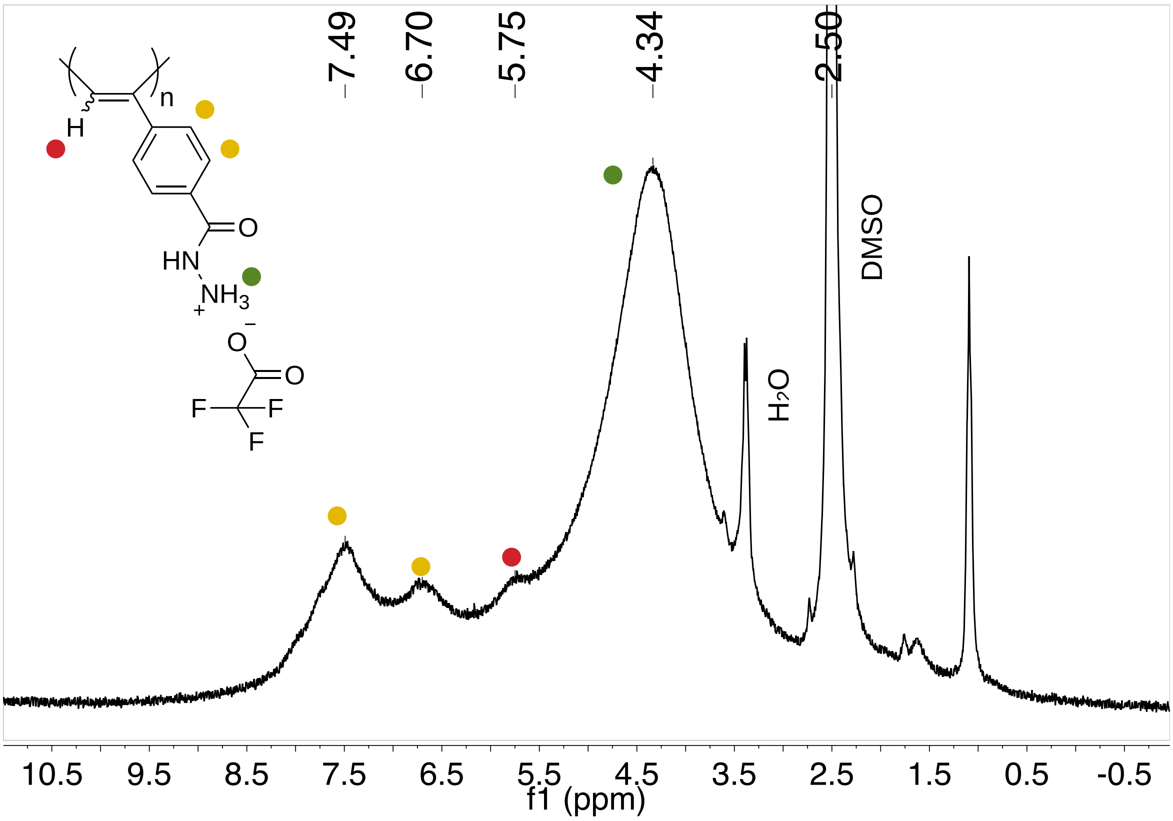

Figure 2.16: ^{1}H NMR spectrum of polymer TFA-**P3** showing similar broad peaks as polymer Boc-**P3** but no Boc-group peak. The peak at 4.34 ppm could be accounted for by the NH_3^+ and excess TFA in the sample.

chains and aromatic signals of the aldehyde, it was difficult to assign and integrate peaks in that region. As such, analysis of the conjugation with aromatic aldehydes to poly(4−ethynylbenzohydrazide) was significantly more challenging compared to poly(acryloyl hydrazide) **P1**. Further functionalisation with 1.35 equiv. benzaldehyde resulted in ~70% loading immediately after addition, which increased to ~75% after 22 hours. Further monitoring over 4 days, showed a slight decrease in the percentage conjugation (**Fig. 2.17**). This could potentially be attributed to increased amounts of water in the sample over time (due to the hygroscopic nature of DMSO), which could alter the equilibrium of hydrazone formation. It could also be observed that in these experiments compared to poly(acryloyl hydrazide) no mono- and

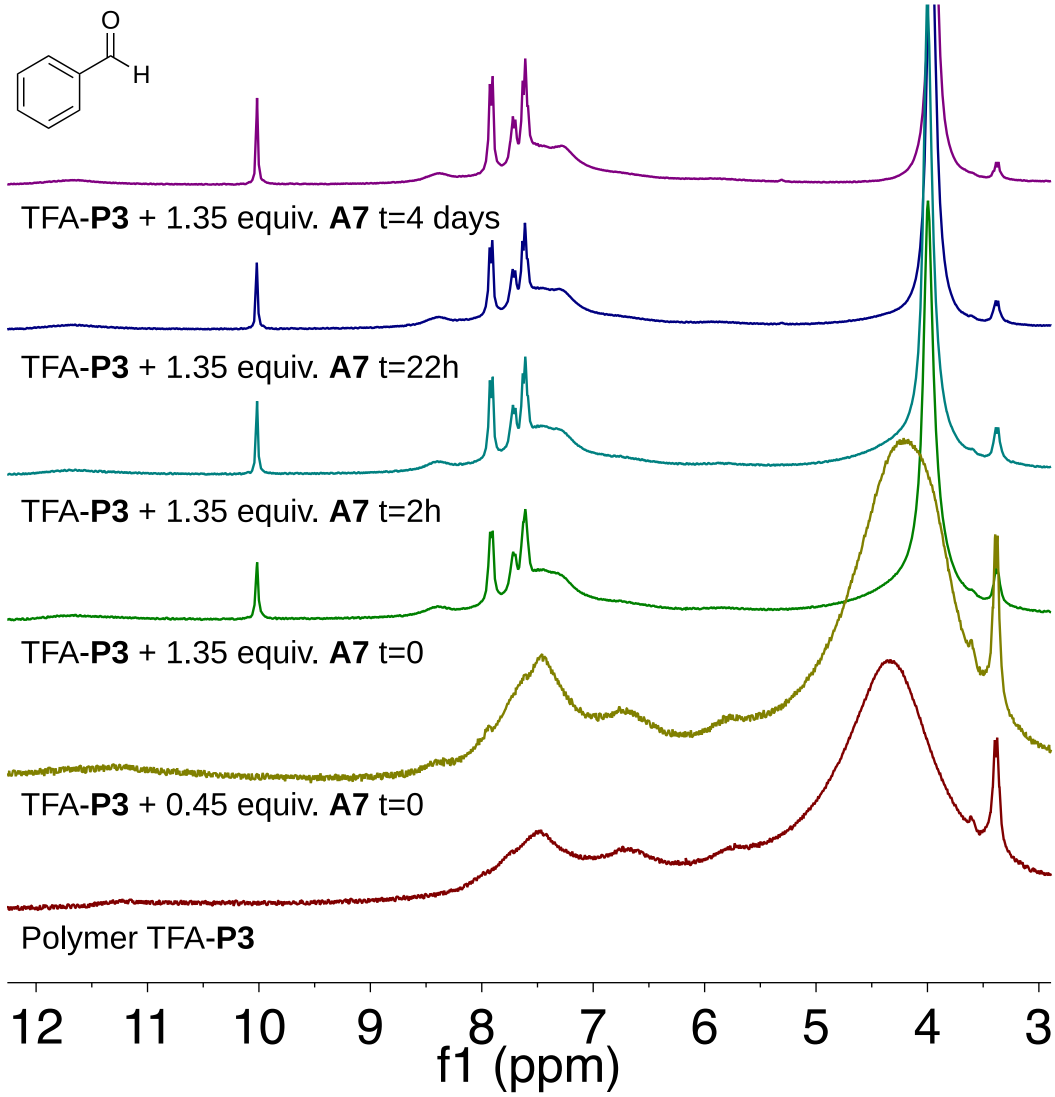

Figure 2.17: ^{1}H NMR spectra of polymer TFA-**P3** and its conjugation to benzaldehyde (**A7**). Immediate coupling is occurring upon addition of **A7**. Maximum coupling is observed within 22h, after which a slight decline in bound **A7** is observed.

dihydrazone impurities were formed. One possible reason behind this lies in the highly arranged helical structure of this scaffold. If the hypothesis (see **Chapter 1**) behind the impurity forming mechanism is true, neighbouring hydrazide chains are required in close proximity to catalyse the system. This should be easier achieved in a random coil polymer than a highly structured helical polymer in which the hydrazide side chains are further apart and with limited flexibility.

Further coupling experiments with ~0.8 equiv. isovaleraldehyde (**A17**) showed a similar pattern to benzaldehyde. Rapid and almost complete conjugation of the

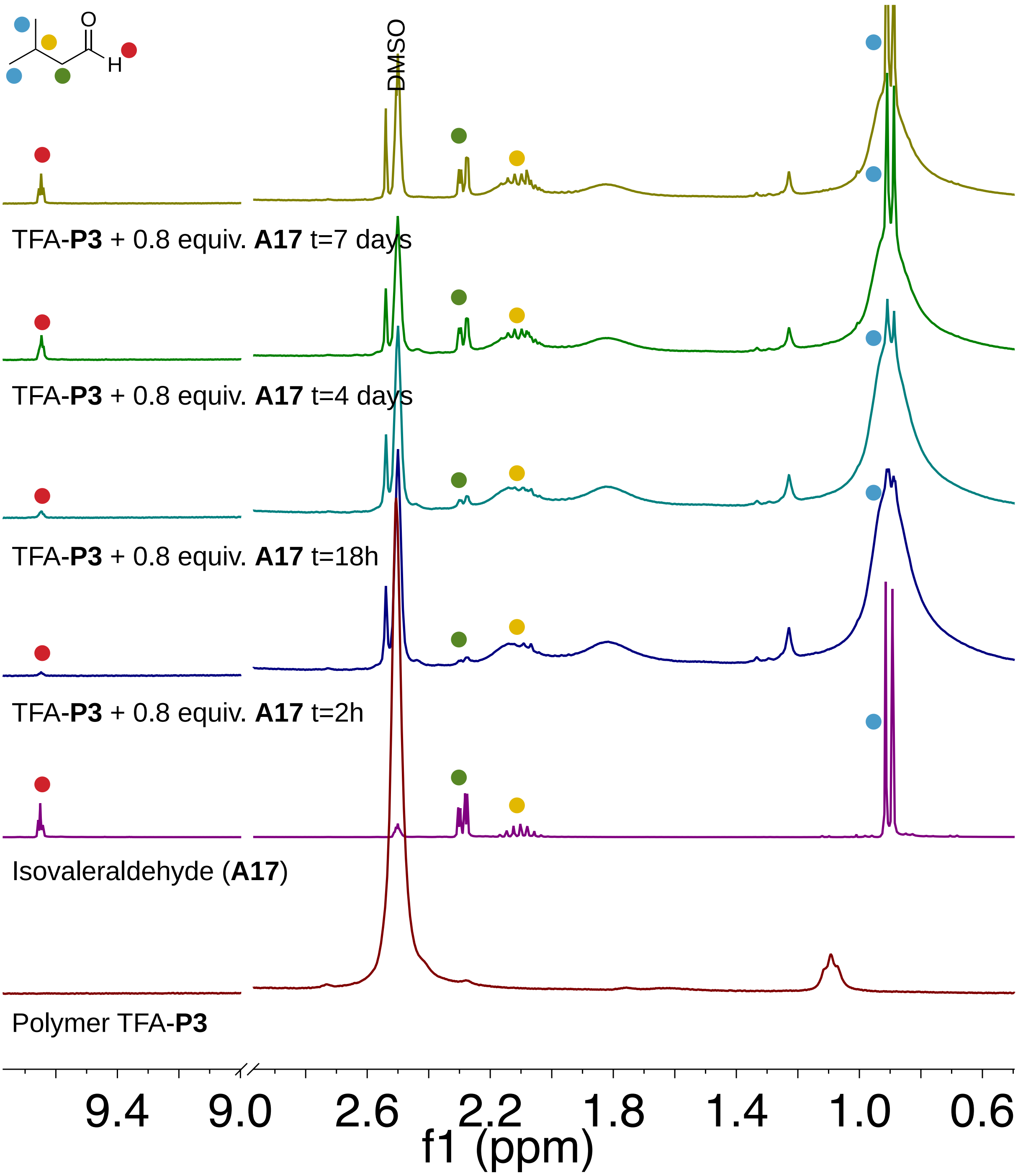

Figure 2.18: ^{1}H NMR spectra of polymer TFA-**P3** and its conjugation to isovaleraldehyde (**A17**). Almost all of the 0.8 equiv. **A17** has coupled within 2h. Over the next 7 days ~11% of the bound **A17** decouples from the scaffold. This is seen by the increasing size of the sharp peaks at 0.91 and 0.89 ppm, the doublet of doublets at 2.29 ppm and the septet at 2.10 ppm.

aldehyde to the scaffold was observed within 2 hours. Analysis of the sample over 7 days shows that some of the aldehyde is being slowly regenerated. The broad alkyl signals at 2.14, 1.80 and 0.90 ppm (**Fig. 2.18**) became sharper over time and recovered the original splitting pattern observed for isovaleraldehyde. There are no further changes between 4 and 7 days, suggesting equilibrium had been reached by that time. Overall, only about 11% of the aldehyde was in the unconjugated form. These two experiments showed that functionalisation of **P3** was less predictable compared to P1, despite achieving similar percentage functionalisation with **A7** and **A17**.

As mentioned before, poly(phenyl acetylene)s synthesised via rhodium catalysed polymerisation mechanistically produce 100% *cis*-containing conformers. Loses in *cis*-content is due to molecular rotation in the backbone and it can be highly dependent on solvent, temperature and pendant side-chains. The stability of the protected polymer Boc-**P3** was investigated via SEC/GPC, UV-Vis and fluorescence spectroscopy

Stability studies via SEC/GPC (**Fig. 2.19**) were carried out by re-injecting at 45 min intervals a sample of polymer Boc-**P3** dissolved in the MeOH. At t0 the spectra showed a sharp intense peak at retention time ~11.1 min flanked by much smaller peaks at 8.7 and 9.7 min. In the first 18h significant changes were observed at every interval. The main peak at ~11.1 min decreased in intensity and broadened towards longer retention times, while the peaks at 8.7 and 9.7 min increased in intensity until they plateaued. The shorter retention time suggested polymeric species with larger hydrodynamic radius. Since the length of a helical polymer can be thought of as the radius of a particle, the transition to a larger “hydrodynamic radius” suggested a

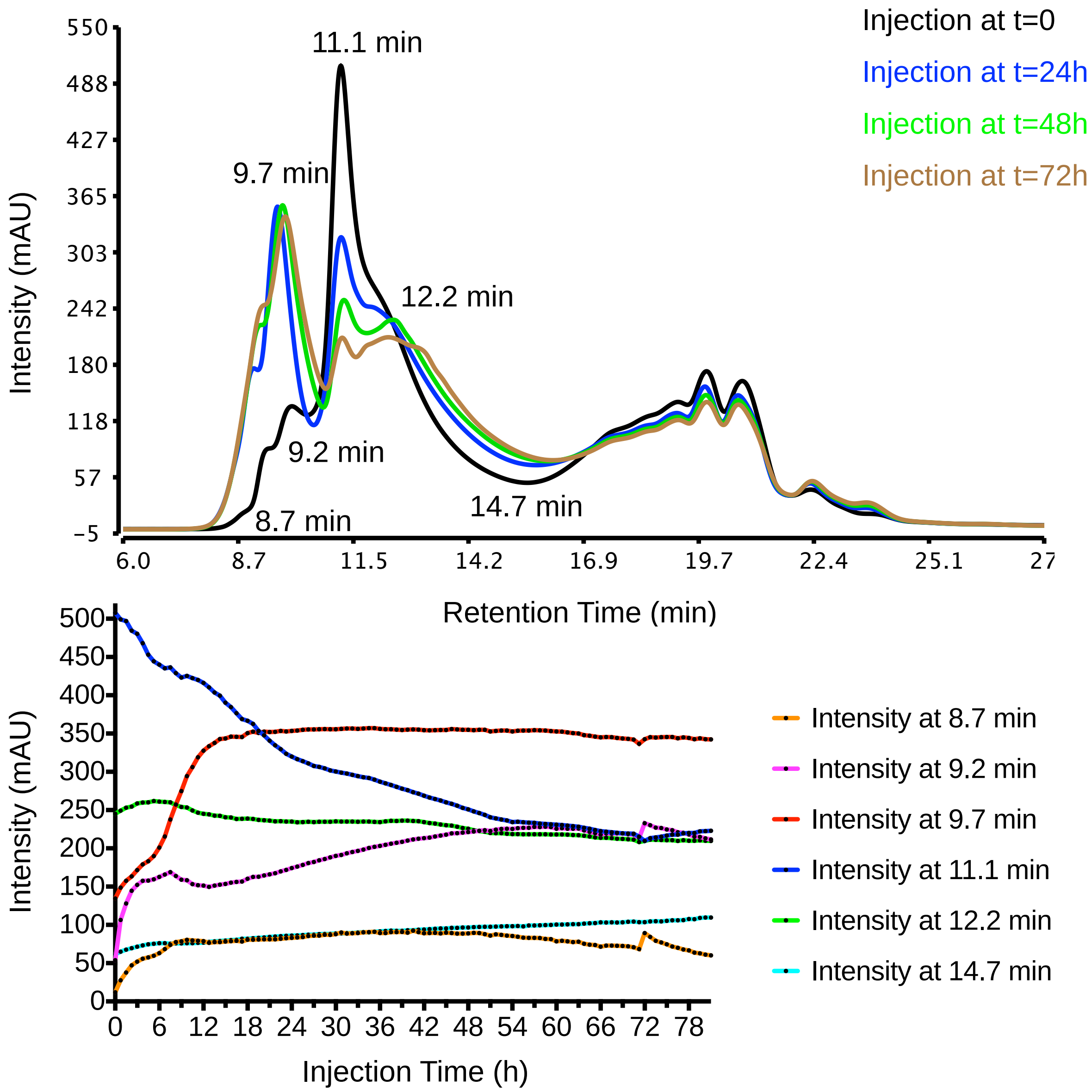

Figure 2.19: (Top) SEC/GPC chromatograms at 24h intervals showing the stability of polymer Boc-**P3** in MeOH over time. (Bottom) Analysis showing the changes in intensity at particular retention times with each 45 min injection interval.

transition to a polymer conformation with a longer length. This could be explained by a change in conformation from *cis*-transoid to *trans*-transoid, which is expected to have the longest helical length (**Fig. 2.20**).

UV-Vis analysis of a sample of polymer Boc-**P3** over 72 hours was overall inconclusive. There seemed to be a small decrease in absorbance over time, mostly

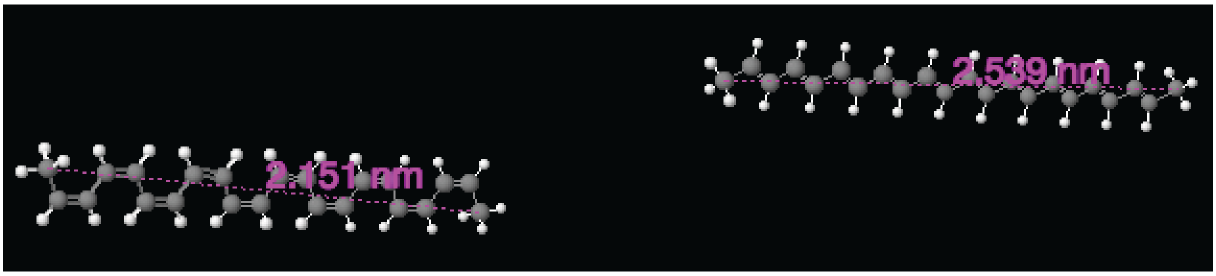

Figure 2.20: Model representations of a 22 carbon cis-transoid chain (left) and trans-transoid chain (right).

evident around 420 nm, but the changes are below 0.05 AU (Fig. **2.21**). Analysis by fluorescence spectroscopy showed interesting trends. The sample was analysed over 9 days by measuring the emission profile at two excitation wavelengths λex_{440} and λex_{484} with emission maxima at λem_{526} and λem_{554} respectively. Over 9 days, the intensity of the emission profiles at λex_{440} and λex_{484} increased 200-fold and 3-fold respectively, and a small blueshift in the emission maxima was observed. However, when the excitation profile at λem_{526} and λem_{554} over the same period was analysed, a 4-fold increase in the intensity was observed, but with a substantial blueshift in the maximum excitation wavelength. λex maxima changed from ~484 nm to ~440 nm, which is consistent with the 200 fold increase in the emission profile when λex_{440} was used. This reinforced the hypothesis that a different polymer conformation was present which had different photophysical properties. This would not be surprising, as the conjugation through the backbone in the *cis*-transoidal model versus the *trans*-transoidal model is different.

Stability studies were also carried out for polymer TFA-**P3** conjugated with isovaleraldehyde. The sample was analysed by SEC/GPC in a similar fashion to polymer Boc-**P3**. The spectra at t0 showed a broad peak at ~9.5 min retention time, and a smaller peak at ~16 min (**Fig. 2.22**). The peak at ~9.5 min, increased 3-fold in intensity and showed further broadening towards lower retention times during the first

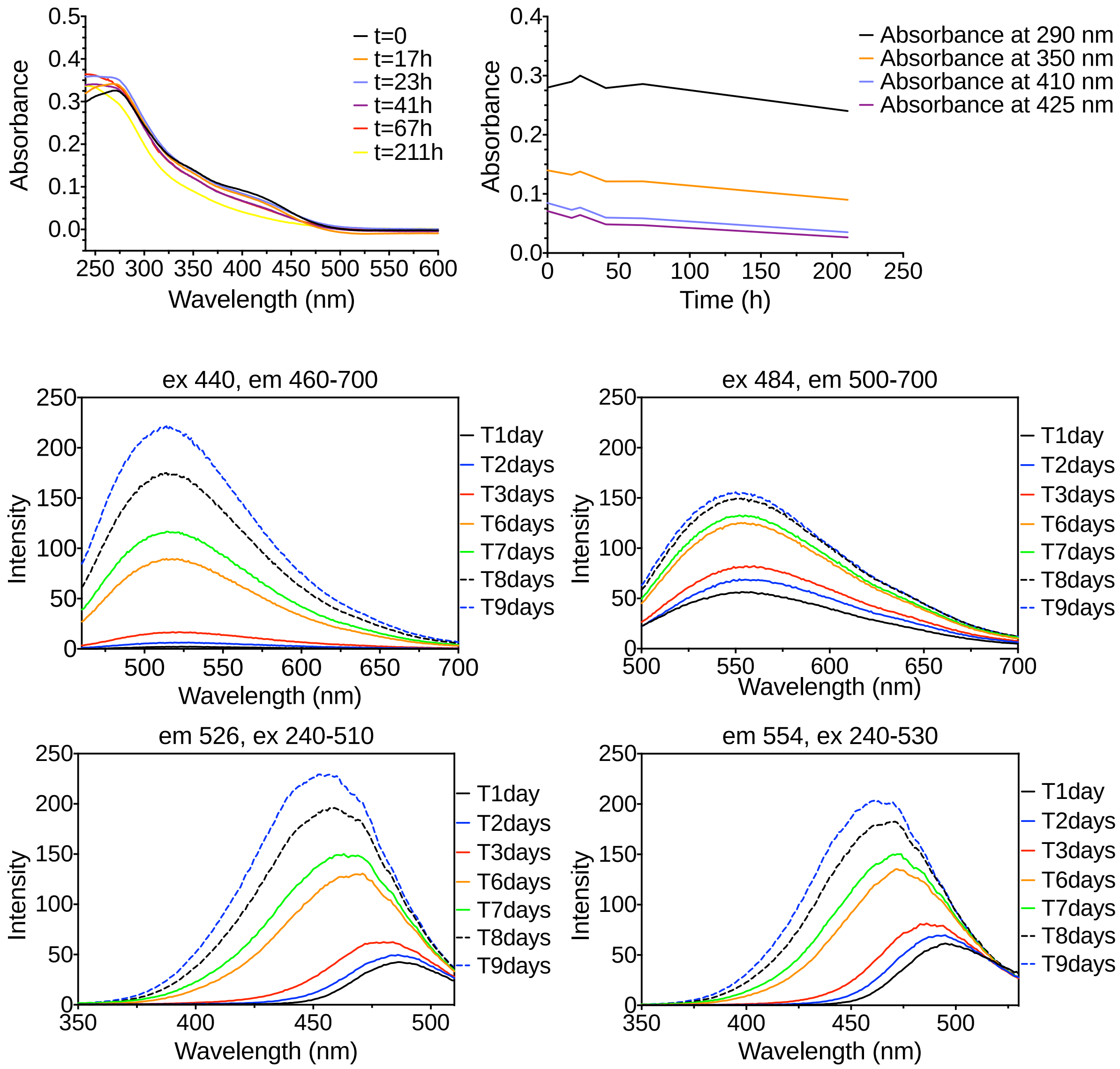

Figure 2.21: (Top) (left) UV-Vis spectra of a 0.01 mg/ml sample of polymer Boc-**P3** at various time intervals in MeOH. (right) Graph showing the changes at various wavelengths in the UV-Vis over time. (Bottom) Spectra showing the changes in the emission and excitation profiles of a sample of polymer Boc-**P3** over time. As can be seen in the bottom two panels, a blue-shift in the excitation profile was observed suggesting conformational changes in the polymer's structure.

24 hours. Past this time point however, a reverse trend is observed with a loss of intensity, broadness and shift of the local maxima towards the initial retention time. The peak ~16 min increased slowly in intensity, but showed no reversal in trends. In fact, it showed a continuous shift towards lower retention time, with a final peak value at ~14.5 min. The trends in the stability of this system are much harder to explain in

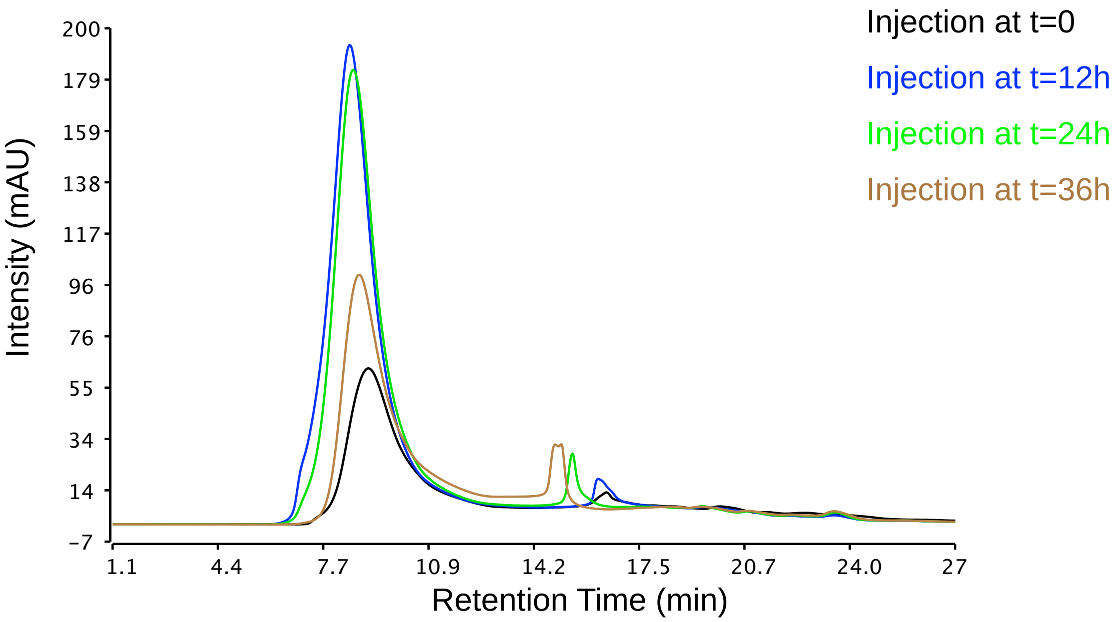

Figure 2.22: SEC/GPC chromatograms at 12h intervals showing the stability in MeOH over time of polymer TFA-**P3** conjugated with isovaleraldehyde (**A17**).

comparison to polymer Boc-**P3**, and there was not sufficient evidence to say whether conformational changes were occurring or if the changes observed were due to the equilibration of the polymer – isovaleraldehyde conjugate.

Overall, considering the stability issues associated with the Boc-**P3** scaffold, the poor solubility of polymer TFA-**P3** in aqueous conditions, and the unpredictable conjugation behaviour, this polymeric scaffold was not taken forward as a scaffold for functional polymers with biological applications at that time.

A third alkyne-based polymer scaffold was synthesised in the group by Andy Wilkinson and Arka Chakraborty under the supervision of the author of this thesis. The aim was to synthesise a helical polymer (**Scheme 2.12**) scaffold akin to the initial poly(acetylene hydrazide) **P2**, which wouldn't suffer from the solubility issues of the **P3** scaffold. A propargyl type monomer **2.9** was chosen, as there was sufficient literature evidence that a hydrazide derivative would be polymerised.[3,4,6,27]

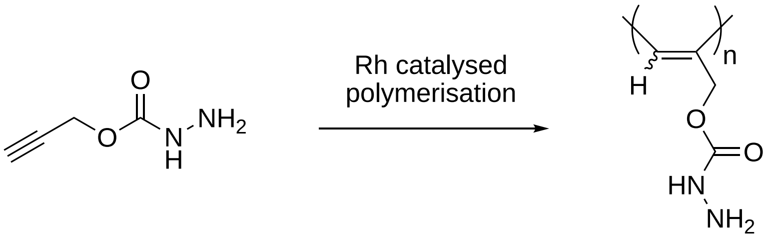

2.9 **P4**

Scheme 2.12: Reaction scheme showing the target scaffold **P4** from propargyl hydrazide monomer **2.9**.

The monomer was synthesised in two steps (**Scheme 2.13**) by first reacting propargyl choloroformate with *tert*-butyl carbazate to obtain the protected monomer **2.10**, followed by deprotection using 2M HCl/Et_2O, which yielded the chloride salt of monomer **2.9**. Polymerisation of both the protected and deprotected monomers was

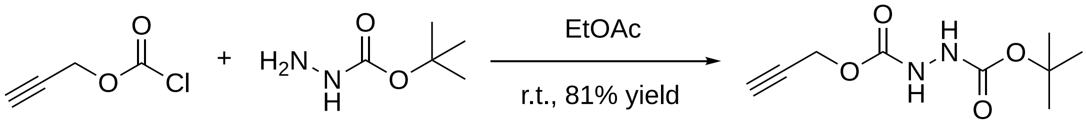

2.10

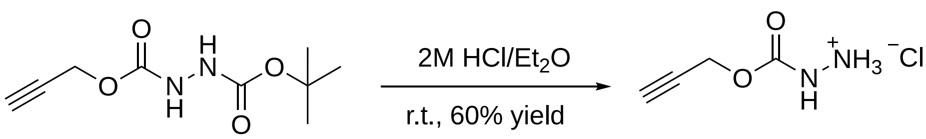

2.10 **2.11**

Scheme 2.13: Reaction scheme showing the synthesis of monomer **2.11**, the chloride salt of monomer **2.9** via the synthesis of the Boc-protected intermediate **2.10** and its subsequent deprotection.

evaluated. Initially, $[Rh(nbd)Cl]_2$ was used as the catalyst with monomer **2.10** but large polydispersities and a large ratio of oligomers were observed. $Rh(nbd)BPh_4$ has been reported to successfully polymerise propargyl-type monomers and it was decided to use it to attempt the polymerisation of monomers **2.10** and **2.11**. Polymerisation of the protected monomer **2.10** (**Scheme 2.14**) was successful and samples with different molecular weights were synthesised (**Table 2.2)** by adjusting

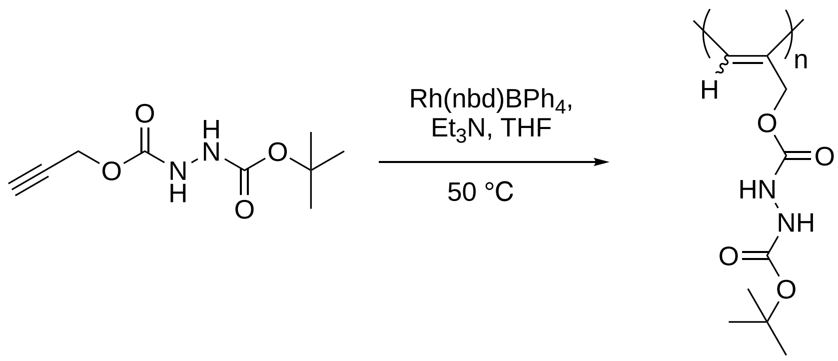

2.10 Boc-**P4**

Scheme 2.14: Reaction scheme showing the synthesis of the Boc-protected poly(propargyl hydrazide) Boc-**P4** from monomer **2.10**.

Entry	Polymer	[M]/[cat.]	Mn[a]	Mw[a]	Đ
1	Boc-**P4**$_{50}$	50	6404	10350	1.62
2	Boc-**P4**$_{100}$	100	9244	18372	1.99
3	Boc-**P4**$_{200}$	200	17467	109535	6.27

Table 2.2: Characterisation data of samples of polymer Boc-**P4** synthesised. [a]Data obtained from SEC/GPC against PMMA calibration standards.

the catalyst to monomer ratio. The experiments showed that below a [M[/[cat.] ratio below 100:1 (**Entry 1,2**) the increase in molecular weight is proportional to the ratio , while the dispersity is sufficiently low. Above this ratio, (**Entry 3**) the number average molar mass continues to be proportional to the ratio, but the weight average deviates significantly and large molecular weight polymers are produced, suggesting that a loss in controlled polymerisation is occurring.

It is that the polymerisation of the chloride salt **2.11** was successful, however the isolated polymer **P4** showed similar solubility issues as those reported for during the synthesis of **P3** by polymerisation of the phenylacetylene hydrazide TFA salt **2.8**. The reaction appeared very fast due to the increased viscosity observed but the product was insoluble and characterisation was not achieved. It is believed that Et_3N added to the reaction as a co-catalyst deprotonated the hydrazonium ion and lead to

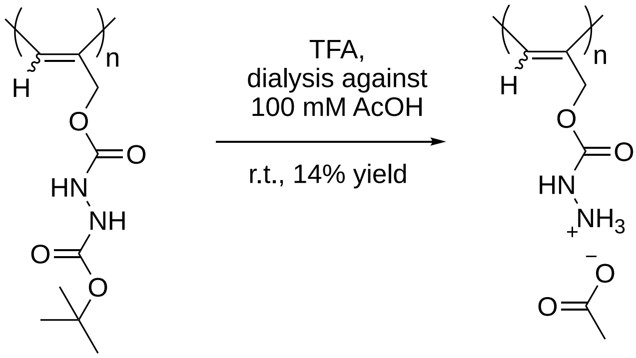

Boc-**P4** AcO-**P4**

Scheme 2.15: Reaction scheme showing the deprotection of the Boc-protected poly(propargyl hydrazide) Boc-**P4** to form the acetate salt (AcO-**P4**) of the target polymer scaffold **P4**.

the formation of polymeric networks bound intermolecularly by strong, extensive H−bonding networks. Deprotection of polymer Boc-**P4** was achieved by reacting in neat TFA followed by purification by dialysis against 100 mM AcOH to exchange the TFA counterions for acetate counterions (**Scheme 2.15**). Dialysis against water resulted to the loss of TFA counterions and deprotonation of the hydrazonium ion and formation of the extensive H-bonded network of the insoluble **P4**.

Coupling experiments with a selection of aldehydes showed mixed results in a solvent dependent manner (**Table 2.3**). Isovaleraldhyde, 5-formylsalicylic acid and imidazole-4-carboxaldehyde (**Entry 1**,**6 and 8**) showed excellent conjugation to the scaffold in DMSO, but other aldehydes, both aromatic (**Entry 2**, **3**, **4**, **5**, **7**) and aliphatic (**Entry 9**, **10**), showed poor coupling. Longer chain aliphatic aldehydes like octanal (**Entry 10**) showed excellent coupling in a mixture of 1:1 DMSO-*d*6, $CDCl_3$, but in this solvent system, no improvement in the coupling of aromatic aldehydes and longer branched aliphatic aldehydes like 2-ethylhexanal was observed. Overall, it appeared that the coupling conditions had to be fine-tuned for each aldehyde, which defeats the purpose of a polymer scaffold useful for fast screening. However, it could be potentially useful to compare a functionalised poly(acryloyl hydrazide) to an equivalent poly(propargyl hydrazide) in order to evaluate differences arising due to random coil versus helical geometry.

AX

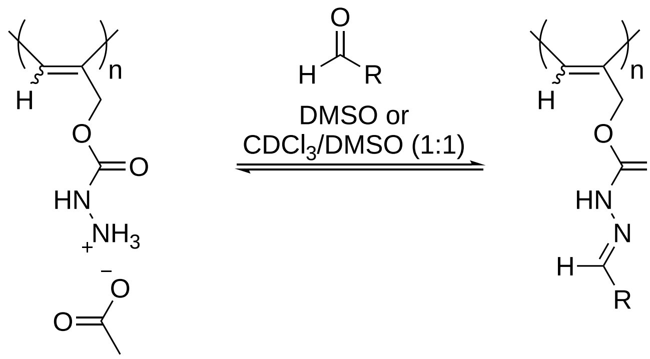

AcO-**P4**$_{50}$ **P4**$_{50}$**AX**

A1

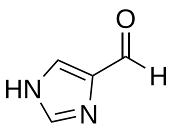

A7

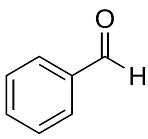

A8

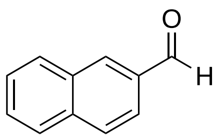

A9

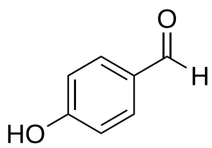

A10

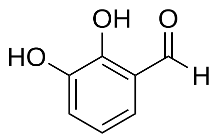

A12

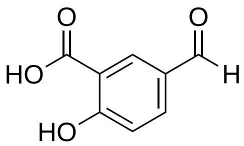

A13

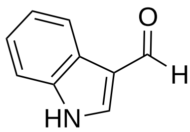

A17

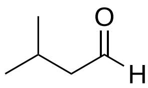

A18

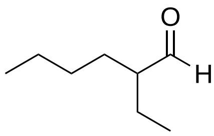

A19

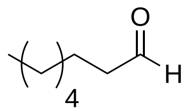

Entry	Polymer	%conjugation[a]	Entry	Polymer	%conjugation[a]
1	**P4**$_{50}$**A1**	88	**6**	**P4**$_{50}$**A12**	99
2	**P4**$_{50}$**A7**	12 (9)[b]	**7**	**P4**$_{50}$**A13**	23
3	**P4**$_{50}$**A8**	— (24)[b]	**8**	**P4**$_{50}$**A17**	79
4	**P4**$_{50}$**A9**	14	**9**	**P4**$_{50}$**A18**	— (—)[b]
5	**P4**$_{50}$**A10**	11	**10**	**P4**$_{50}$**A19**	— (83)[b]

Table 2.3: Coupling experiments between poly(propargyl hydrazide) AcO–**P4**$_{50}$ and different aldehydes. [a]conjugation in DMSO-*d6*; [b]conjugation in $CDCl_3$/DMSO-*d6* (1:1).

Stability studies of the protected polymer were carried out by SEC/GPC in a similar experiment as before. The data showed small changes in the main peak at ~13 min (**Fig. 2.23**), but there was a shift towards shorter retention times in the shouldering peak at ~16.4 min that could be indicative of changes in conformation.

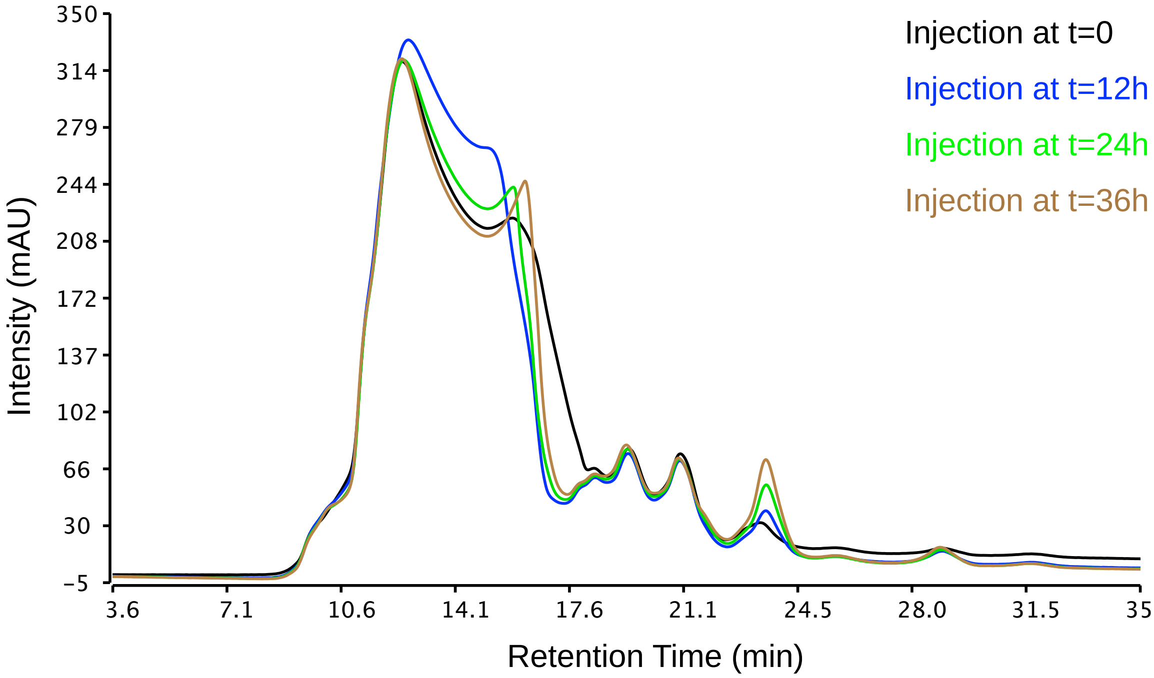

Figure 2.23: SEC/GPC chromatograms at 12h intervals showing the stability of polymer Boc-**P4** in MeOH over time.

2.4 Summary

Synthesis of the propiolohydrazide monomer **2.2** was not accomplished due to difficulties in the deprotecting stage. The target polymer **P2** was not obtained via the polymerisation the Boc−protected substrate **2.1** as it seems that short oligomers and Michael addition by-products were being produced instead of Boc-**P2**. Research was focused towards the phenylacetylene hydrazide monomer **2.4**, which was successfully synthesised. Polymerisation of the deprotected hydrazide led to the formation of an insoluble product **P3** that according to characterisation data showed features a of cis-transoid polymer. Polymers from Boc-protected phenylacetylene hydrazide monomers **2.3** were synthesised and characterised. The stability of these polymers in solution was analysed to show that probable isomerisation of Boc-**P3** from *cis*-transoid to *trans*-transoid conformations are observed. The polymers were successfully deprotected and the **P3** scaffold was isolated as a TFA salt. Deprotonation of the scaffold to form the original target polymer **P3** resulted in an insoluble product. The TFA-**P3** scaffold was slightly soluble in DMSO after heating and its functionalisation with aldehydes was investigated. The coupling reaction was found occur generally very fast, but the polymer undergoes a slow equilibration process over several days. A third scaffold based on poly(propargyl hydrazide) **P4** was successfully synthesised as an alternative to poly(4-ethynylbenzohydrazide). Direct polymerisation of the unprotected hydrazide **2.9** resulted again in an insoluble product. Polymerisation of the Boc-protected monomer **2.10** was successful and samples with different molecular weights were synthesised. Stability studies indicated that this polymer may be more stable than Boc-**P3**. The polymer was deprotected in

TFA and isolated as an acetate salt AcO-**P4** after dialysis. This scaffold showed better solubility compared to scaffold TFA**-P3**, and functionalisation with aldehydes was investigated in a mixture of solvent systems. The conjugations observed were either very efficient or very poor and each aldehyde had to be investigated independently to optimise the coupling conditions. Overall, it is believed that the major limitation of helical hydrazide polymers stems from their extensive H−bonded networks, which rendered them insoluble if the hydrazide is not protonated.

2.5 Future work

There is some scope to use scaffolds TFA**-P3** and AcO**-P4** in order to compare the biological activity of functionalised polymers starting from hits isolated by fast-screening of poly(acryloyl hydrazide) **P1**. This could be potentially useful to study how helical polymers, which have a rigid structure differ in activity compared to a flexible random coil polymer. It may also be worth investigating similar polymers bearing hydrazine or *O*-hydroxylamine instead of hydrazide functionalities to investigate if the solubility of the scaffolds improves. These should form fewer H−bonds between the polymer chains, and could lead to a helical scaffold useful for fast screening of functional polymers in aqueous media. Aside from the functionalisation with aldehydes, there is further scope to use the hydrazide chains as chemoselective handles for reactions with a variety of electrophiles (e.g. epoxides, activated esters, isothiocyantes, etc.), which may be more efficient than the functionalisations of TFA**-P3** or AcO**-P4** with aldehydes.

2.6 Experimental

All chemicals were purchased from Sigma-Aldrich®, Fisher Scientific®, VWR® or Acros® and used without further purification. All solvents were Reagent grade or above, purchased from Sigma-Aldrich®, Fisher Scientific® or VWR® and used without further purification.

Nuclear Magnetic Resonance (NMR) spectra were recorded on either a Bruker Avance III 300 MHz or a Bruker Avance III 400 MHz spectrometer. Chemical shifts are reported in ppm (δ units) referenced[28] to the following solvent signals: residual DMSO in DMSO-*d6* at δH 2.50, H_2O in D_2O at δH 4.79, $CHCl_3$ in $CDCl_3$ at δH 7.26. Infrared (IR) spectra were recorded on a Perkin Elmer Spectrum Two FT−IR spectrometer. Peaks are reported as strong (s), medium (m) or weak (w), sharp (sh) or broad (br). Ultraviolet-visible (UV-Vis) spectra were recorded on a Cary 50 Spectrophotometer. Fluorescence spectra were recorded on a Shimadzu RF-5301PC Spectrofluorophotometer. Mass spectra were recorded on a Waters Xevo G2-XS ToF using electrospray ionisation (ESI) and time-of-flight (ToF) in positive or negative ion mode. Melting points were measured on a Stuart SMP10 digital melting point apparatus. Thin-layer chromatography was carried out on sheets coated with silica gel. Size Exclusion Chromatography/Gel Permeation Chromatography (SEC/GPC) were recorded on a Shimadzu Prominence LC-20A fitted with a Thermo Fisher Refractomax 521 Detector and a Shimadzu SPD20A UV-Vis Detector or fitted with a Shimadzu SPD-M20-A Photodiode Array Detector and a Shimadzu RF-10A Fluorescence Detector. All samples were analysed at 40 ℃ in MeOH as the eluent and a flow rate of 0.6 $mL \cdot min^{-1}$. The instrument was fitted with a Shodex Asaphipak

GF-310 HQ column (300 × 7.5 mm, 5 µm). Molecular weights were calculated based on a standard calibration method using polymethylmethacrylate. All dialyses were carried out using Spectrum Labs SpectraPor® Dialysis Tubing MWCO 1000 in water unless specified otherwise for a minimum of 24 hours and at least 3 changes of solvent.

***tert*-Butyl 2-propioloylhydrazinecarboxylate (2.1)**

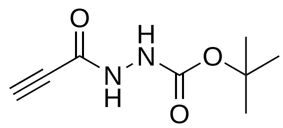

Propiolic acid (0.88 mL, 13.99 mmol) and *tert*-butyl carbazate (1.69 g, 12.59 mmol) were dissolved in H_2O (45 mL) at r.t. *N*-(3-dimethylaminopropyl)-*N'*-ethylcarbodiimide hydrochloride (2.95 g, 15.39 mmol) was added in portions to the solution over 1 min. and stirred for 15 min. The aqueous phase was extracted with EtOAc (3 x 50 mL). The organic layer was washed with sat. $NaHCO_3$ sol^n (3 x 50 mL), H_2O (50 mL), and brine (50 mL). The organic phase was dried with Na_2SO_4 and the solvent removed under reduced pressure to afford a colourless oil. Et_2O (5 x 2 mL) was added to the oil and removed under high vacuum to afford, after drying, **2.1** as a white solid (1.88 g, 81% yield): R_f = 0.85 (100% EtOAc); ν_{max}(neat)/cm^{-1} 3253m sh (N-H), 2948w (C-H), 2116w sh (C≡C), 1725s sh (C=O), 1665s sh (C=O); δ_H(300 MHz, DMSO-*d6*) [calibrated using (C*H*D_2)(CD_3)SO resonance at 2.50 ppm] 1.39 (s, 9H, C(CH_3)$_3$), 4.33 (s, 1H, CC*H*), 8.95 (s, 1H, OC(O)N*H*), 10.31 (s, 1H, CC(O)N*H*); δ_C(100 MHz, DMSO-*d6*) [calibrated using (*C*H_3)$_2$SO resonance at 39.52 ppm] 19.0 (C(*C*H_3)$_3$), 67.1 (*C*(CH_3)$_3$), 68.6 (C*C*H), 72.6 (*C*CH), 145.0 (O*C*(O)NH), 147.7

(C*C*(O)NH); MS (TOF ES-) *m/z* 183 ($[M-H]^-$, 100%). The characterisation data is in accordance to literature.[29]

tert-Butyl 2-(4-iodobenzoyl)hydrazine-1-carboxylate (2.6)

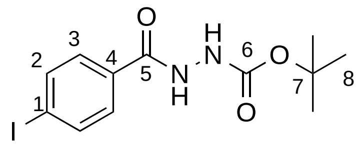

A solution of *tert*-butyl carbazate (2.45 g, 18.18 mmol) in H_2O (80 mL) was added slowly over 1 min. to a stirring solution of 4-iodobenzoic acid (4.00 g, 15.81 mmol) dissolved in THF (40 mL) at room temperature. *N*-(3-dimethylaminopropyl)-*N'*-ethylcarbodiimide hydrochloride (3.49 g, 18.18 mmol) was added to the emulsion in portions over 1 min. and allowed to react for 2 hrs. The aqueous phase was extracted with EtOAc (3 x 100 mL). The organic layer was washed with 0.1 M $HCl_{(aq)}$ (3 x 100 mL), H_2O (100 mL), and brine (100 mL). The organic phase was dried with Na_2SO_4 and the solvent removed under reduced pressure to afford **2.6** as a white solid (4.7 g, 82% yield): R_f = 0.15 (20% EtOAc/Hexane); ν_{max}(neat)/cm^{-1} 3332s sh (N-H), 3225s sh N-H), 2968m sh (C-H), 1720s sh (C=O), 1654s sh (C=O), 1568s sh (C=C); δ_H(300 MHz, DMSO-*d6*) [calibrated using (C*H*D_2)(CD_3)SO resonance at 2.50 ppm] 1.42 (s, 9H, C(CH_3)$_3$), 7.63 (d, *J* 8.4, 2H, C^3H), 7.88 (d, *J* 8.7, 2H, C^2H), 8.95 (s, 1H, C^5(O)N*H*), 10.28 (s, 1H, C^6(O)N*H*); δ_C(100 MHz, DMSO-*d6*) [calibrated using (*C*H_3)$_2$SO resonance at 39.52 ppm] 28.2 (C^8), 79.4 (C^7), 99.5 (C^1), 129.4 (C^3), 132.0 (C^4), 137.4 (C^2), 155.5 (C^6), 165.5 (C^5); MS (TOF ES+) 385.0 ($[M-Na]^+$ 100%; Melting point range 163-166 ℃.

tert-Butyl 2-(4-((trimethylsilyl)ethynyl)benzoyl)hydrazine-1-carboxylate (2.7)

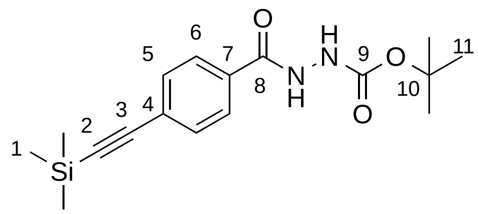

$PdCl_2(PPh_3)_2$ (293 mg, 0.41 mmol) and Copper(I) iodide (132 mg, 0.69 mmol) were added sequentially to a stirring solution of aryl iodide **2.6** (1.00 g, 2.76 mmol) in piperidine (26.5 mL). The solution was degassed by bubbling argon gas for ~10 min after which ethynyltrimethylsilane (1.2 mL, 8.28 mmol) was added dropwise over 2 min. and stirred for 5 hours. The solution was diluted in toluene (100 mL) and washed with sat. NH_4Cl soln. (2 x 100 mL) and brine (3 x 100 mL), dried with Na_2SO_4 and concentrated under reduced pressure to afford a dark brown oil. The product was purified by flash chromatography (20% EtOAc/hexane, dry loading) to afford **2.7** as a cream product (710mg, 77% yield): R_f = 0.45 (25% EtOAc/Hexane); ν_{max}(neat)/cm^{-1} 3250w br N-H), 2965m sh (C-H), 2150w sh (C≡C),1673m sh (C=O), 1647s sh (C=O), 1587m sh (C=C); δ_H(300 MHz, DMSO-*d6*) [calibrated using (C*H*D_2)(CD_3)SO resonance at 2.50 ppm] 0.24 (s, 9H, $(CH_3)_3Si$), 1.42 (s, 9H, $(CH_3)_3C$), 7.57 (d, J = 8.4Hz, 2H, C^6H), 7.84 (d, J = 8.4Hz , 2H, C^5H), 8.96 (s, 1H, C^8(O)NH), 10.29 (s, 1H, C^9(O)NH); δ_C(100 MHz, DMSO-*d6*) [calibrated using $(CH_3)_2SO$ resonance at 39.52 ppm] -0.19 (C^1), 28.1 (C^{11}), 79.3 (C^{10}), 96.8 (C^2), 104.3 (C^3), 125.3 (C^7), 127.7 (C^6), 131.7 (C^5), 132.5 (C^4), 155.4 (C^9), 165.2 (C^8); MS (TOF ES+) 355.1 ($[M\text{-}Na]^+$ 100%).

tert-Butyl 2-(4-ethynylbenzoyl)hydrazine-1-carboxylate (2.3)

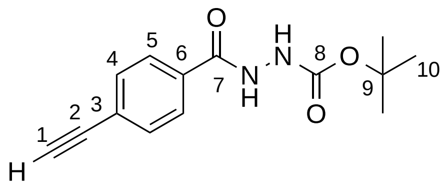

K_2CO_3 (1.17 g, 8.41 mmol) was added to a solution of phenylacetylene **2.7** (0.7 g, 2.10 mmol) in 1:1 MeOH/THF (42 mL). The suspension was left to react for 4 hours and then it was extracted with a 1:2 Et_2O/H_2O (48 mL). The organic phase was washed with water (2 x 30 mL) and brine (3 x 30 mL) and then it was dried with Na_2SO_4. The solvent was removed under reduced pressure to afford crude phenylacetylene, which was purified by trituration with ice-cold Et_2O to afford **2.3** as a light brown powder (347 mg, 64%): δ_H(300 MHz, DMSO-d6) [calibrated using (C*H*D_2)(CD_3)SO resonance at 2.50 ppm] 1.43 (s, 9H, C(CH_3)$_3$), 4.41 (s, 1H, CC*H*), 7.60 (d, 2H, C^5H), 7.86 (s, 2H, C^4H), 8.96 (s, 1H, C^7(O)N*H*), 10.29 (s, 1H, C^8(O)N*H*); δ_C(100 MHz, DMSO-*d6*) [calibrated using (*C*H_3)$_2$SO resonance at 39.52 ppm] 28.1 (C^{10}), 79.4 (C^9), 82.8 (C^2), 83.2 (C^1), 125.0 (C^6), 127.7 (C^5), 131.8 (C^4), 132.6 (C^3), 155.5 (C^8), 165.3 (C^7); MS (TOF ES-) *m/z* 259.29 ([M-H]$^-$, 100%); Melting point range 165-173 ℃ (sample decomposition).

4-Ethynylbenzohydrazide 2,2,2-trifluoroacetate salt (2.8)

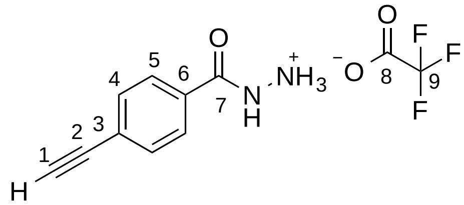

Trifluoroacetic acid (2.0 mL, 26.0 mmol) was added to phenylacetylene **2.7** (600 mg, 1.80) and left to react for 2 hours. The solution was concentrated under a stream of argon gas and then precipitated in Et_2O. The suspension was centrifuged in Et_2O (3 x 10 mL) and the pellet was purified by trituration with ice-cold EtOAc to afford a brown powder (311 mg, 62%) δ_H(300 MHz, DMSO-*d6*) [calibrated using (CHD_2)(CD_3)SO resonance at 2.50 ppm] 4.46 (s, 1H, CC*H*), 7.64 (d, 2H, C^5H), 7.87 (d, 2H, C^4H), 11.23 (s, 1H, C^7(O)N*H*); δ_C(100 MHz, DMSO-d6) [calibrated using (CH_3)$_2$SO resonance at 39.52 ppm] 82.8 (C^1), 82.9 (C^2), 124.3 (C^6), 127.3 (C^5), 131.7 (C^4), 133.3 (C^3), 165.0 (C^7); MS (TOF ES+) 161.1 ($[M-H]^+$ 100%); Melting point range 130-135 ℃ (sample decomposition).

Poly(*tert*-butyl 2-(4-ethynylbenzoyl)hydrazine-1-carboxylate) (Boc-P3)

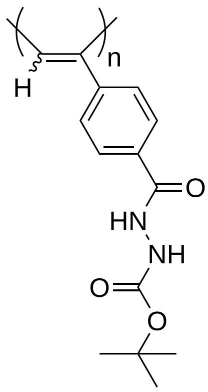

A solution of $[Rh(nbd)Cl]_2$ (8.85 mg, 0.019 mmol) in 1:1 DMSO/Et_3N (0.160 mL) was added under an atmosphere of argon to a solution of phenylacetylene **2.3** (250 mg, 0.960 mmol) in DMSO (0.480 mL) and left to react for 4 hours at 60 ℃. The product was precipitated by addition of H_2O to the reaction vial and the polymer was purified by centrifugation against H_2O (3 x 10 mL). The pellet was re-suspended in H_2O and dried via lyophilisation to afford polymer Boc-**P3** as a brown powder (230 mg, 92% yield): ν_{max}(neat)/cm^{-1} 3269w br N-H), 2968w sh (C-H), 1703m sh (C=O), 1648m sh (C=O), 1462m br (C=C), 1245s sh, 1155s sh; δ_H(300 MHz, DMSO-*d6*) [calibrated using $(CHD_2)(CD_3)SO$ resonance at 2.50 ppm] 1.40 (s, 9H, $C(CH_3)_3$), 5.82 (br, 1H, CC*H*), 6.5-8.25 (br, 4H, C_6H_4), 8.88 (br, 1H, N*H*), 10.09 (br, 1H, N*H*); δ_C(100 MHz, DMSO–*d6*) [calibrated using $(CH_3)_2SO$ resonance at 39.52 ppm] 28.1, 79.2, 127.3, 155.5, 165.4.

Poly(4-ethynylbenzohydrazide) trifluoroacetate (TFA-P3)

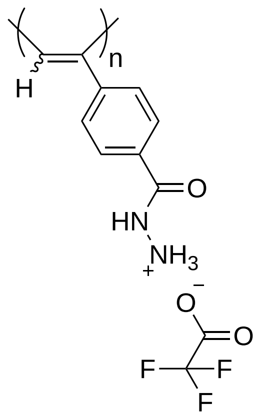

Trifluoroacetic (9 mL) was added to a solution of polymer Boc-**P3** (100 mg) in THF (9 mL) and stirred for 1 hour. The solvent was removed by blowing argon. The resulting oil was diluted with Et_2O and the solvent was removed by blowing Argon until a precipitate was formed. The process was repeated to isolate polymer TFA-**P3** as a brown-red precipitate and dried under high vacuum. (60 mg, 100% yield): δ_H(300 MHz, DMSO-*d6*) [calibrated using $(CHD_2)(CD_3)SO$ resonance at 2.50 ppm] 5.75 (br, 1H, CC*H*), 6.30-8.25 (br, 4H, C_6H_4).

1-(*tert*-Butyl) 2-(prop-2-yn-1-yl) hydrazine-1,2-dicarboxylate (2.10)

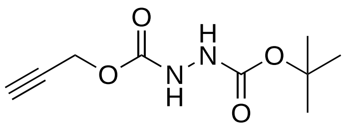

A solution of *tert*-butyl carbazate (1638.5 mg, 12.15 mmol) was stirred until complete dissolution in ethyl acetate (40 mL). The solution was cooled in an ice/ acetone bath for 5 minutes. To this a solution of propargyl chloroformate (0.410 mL, 4.05 mmol) in ethyl acetate (10 mL) was added dropwise over 10 minutes. The resulting mixture was left to stir for 1.5 hours at room temperature and monitored by TLC (ethylacetate, permanganate dip, R_f = 0.9). Once the time had elapsed the solution was neutralised with K_2CO_3 (565.4 mg, 4.05 mmol) and subsequently was washed with 0.1 M HCl (3 x 30 mL), sat. Na_2CO_3 (3x 3 0 mL), water (3 x 30 mL), Brine (3 x 30 mL). The organic phase was dried with excess Na_2SO_4 and filtered. Finally the solution was dried under reduced pressure to remove all solvent. The resulting **2.10** was collected as a white solid (2.336 g, 11.06 mmol, 81%); ν_{max}(neat)/ cm^{-1} 3277m sh (N-H), 2860w, sh (C-H), 2137m sh (C≡C), 1730s sh (C=O),1690s sh (C=O); δ_H(300 MHz, DMSO-*d6*) [calibrated using (C*H*D_2)(CD_3)SO resonance at 2.50 ppm] 9.14 (s, 1H, N*H*), 8.82 (s, 1H, N*H*), 4.66 (d, *J* = 2.5Hz, 2H, C*H*$_2$), 3.50 (br, t, *J* = 2.4Hz, 1H, C≡C-*H*), 1.39 (s, 9H, C(C*H*$_3$)$_3$); δ_C(100 MHz, DMSO-*d6*) [calibrated using (*C*H_3)$_2$SO resonance at 39.52 ppm] 156.2 (CH_2O*C*(O)NH), 155.9 (O*C*(O)NH), 79.7 (*C*(CH_3)$_3$), 79.3 (HC≡*C*), 78.0 (H-*C*≡C), 52.5 (O*C*H_2), 28.5 (C(*C*H_3)$_3$); MS (TOF ES+) *m/z* 237.1 ($[M+Na]^+$, 100%).

Poly(1-(*tert*-butyl) 2-(prop-2-yn-1-yl) hydrazine-1,2-dicarboxylate) (Boc-P4)

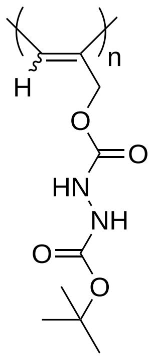

A solution of **2.10** (100 mg, 0.47 mmol) in THF (0.351 mL) was made, argon gas was bubbled over this for 5 minutes. To this a solution of Rh(nbd)BPh_4 (4.49 mg, 0.0093 mmol), in Et_3N (0.058 mL) and THF (0.058 mL) was added. This was left stirring in an oil bath at 50 ℃ for 24 hours. The resulting mixture was pipetted over hexane and polymer Boc-**P4** was collected as a cream precipitate (61 mg, 0.28 mmol, 61%); ν_{max} (neat)/cm^{-1} 3310m br, N-H), 2980w br (C-H), 1708s br (C=O), 1156s br (C-O); δ_H(300MHz, DMSO-*d6*) [calibrated using (C*H*D_2)(CD_3)SO resonance at 2.50 ppm] 9.5-9.0 (br, 2H, (N*H*)$_2$), 5.15 (br, 1H, *H*-C=C), 4.57 (br, 2H, C*H*$_2$), 1.40 (br, s, 9H, C(C*H*$_3$)$_3$).

Prop-2-yn-1-yl hydrazine carboxylate hydrochloride (2.11)

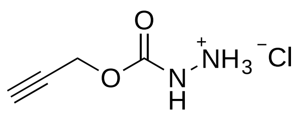

A sample of **2.10** (200 mg, 0.93 mmol) was taken and dissolved in HCl/ether solution 2.0 M (9.35 mL, 18.7 mmol). This solution was left to react for 6 hours, once the time had elapsed the mixture was dried under reduced pressure and **2.11** was collected as a brown solid (120.8 mg, 0.8 mmol, 60%); ν_{max} (neat)/cm^{-1} 3300-2600 (br s, C-H / N-H), 2122 (s, C≡C), 1747 (s, C=O), 1175 (d, C-O); δ_H(300 MHz, DMSO-*d6*) [calibrated using (C*H*D_2)(CD_3)SO resonance at 2.50 ppm] 10.56 (s, 1H, N*H*), 4.79 (d, *J* = 2.4 Hz, 2H, CH_2), 4.5-2.5 (br, s, 3H, $^+NH_3$), 3.64 (t, *J* = 2.4 Hz, 1H, *H*-C≡C); δ_C(100 MHz, DMSO-*d6*) [calibrated using (CH_3)$_2$SO resonance at 39.52 ppm] 53.4 (CH_2), 78.3 (*C*≡CH), 78.4 (H*C*≡C), 155.1 (*C*=O); MS (TOF ES+) *m/z* 115.0 ([M+H]$^+$, 100%).

Poly(prop-2-yn-1-yl hydrazine carboxylate) acetate (AcO-P4)

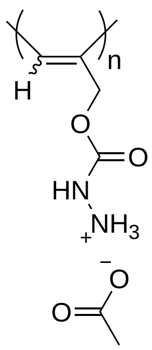

A sample of Boc-**P4** (900 mg, 7 mmol) was dissolved in pure TFA (42 mmol, 3.24 ml). This solution was left to stir for 4 hrs and monitored by NMR spectroscopy. Once complete, the reaction was placed in a dialysis membrane (cellulose, 1 kDa pore size) and diluted with water (5 mL). The sample was dialysed twice against 100 mM AcOH and three times against water. After dialysis, the solution was collected from the membrane and the product was obtained via lyophilisation to afford AcO-**P4** as a cream powder (225 mg, 0.99 mmol, 14%); ν_{max} (neat)/cm^{-1} 3251s br (N-H), 1707s br (C=O), 1500s sh (C=C), 1270s (C-O); δ_H (300 MHz, D_2O) [calibrated using *H*DO resonance at 4.79 ppm] 7.28 (br, 1H, *H*-C=C), 6.5-5.75 (br, 2H, CH_2).

2.7 References

1. F. Sanda, M. Shiotsuki and T. Masuda, *Polymer Science: A Comprehensive Reference Volume 3, 3.27 Alkyne Polymerization*, *Elsevier B.V.*, 2012, 875–954.
2. J. Liu, J. W. Y. Lam and B. Z. Tang, *Chem. Rev.*, 2009, **109**, 5799–5867.
3. F. Sanda, Y. Yukawa and T. Masuda, *Polymer*, 2004, **45**, 849–854.
4. R. Nomura, S. Nishiura, J. Tabei, F. Sanda and T. Masuda, *Macromolecules*, 2003, **36**, 5076–5080.
5. Z. Ke, S. Abe, T. Ueno and K. Morokuma, *J. Am. Chem. Soc.*, 2011, **133**, 7926–7941.
6. Y. Shirakawa, Y. Suzuki, K. Terada, M. Shiotsuki, T. Masuda and F. Sanda, *Macromolecules*, 2010, **43**, 5575–5581.
7. I. Louzao, J. M. Seco, E. Quiñoá and R. Riguera, *Angew. Chem. Int. Ed.*, 2010, **49**, 1430–1433.
8. C. I. Simionescu, V. Percec and S. Dumitrescu, *Journal of Polymer Science: Polymer Chemistry Edition*, 1977, **15**, 2497–2509.
9. C. I. Simionescu and V. Percec, *Journal of Polymer Science: Polymer Chemistry Edition*, 1980, **18**, 147–155.
10. V. Percec, J. G. Rudick, P. Nombel and W. Buchowicz, *J. Polym. Sci. A Polym. Chem.*, 2002, **40**, 3212–3220.
11. R. Nomura, H. Nakako and T. Masuda, *Polym. J.*, 2000, **32**, 303–305.
12. H. Nakako, R. Nomura and T. Masuda, *Polym. Bull.*, 2001, **46**, 147–152.
13. Y. Kishimoto, P. Eckerle, T. Miyatake, M. Kainosho, A. Ono, T. Ikariya and R. Noyori, *J. Am. Chem. Soc.*, 1999, **121**, 12035–12044.
14. T. Fukushima, K. Takachi and K. Tsuchihara, *Macromolecules*, 2006, **39**, 3103–3105.
15. X. A. Zhang, M. R. Chen, H. Zhao, Y. Gao, Q. Wei, S. Zhang, A. Qin, J. Z. Sun and B. Z. Tang, *Macromolecules*, 2011, **44**, 6724–6737.
16. T. Asari, K. Maeda and E. Yashima, *J. Polym. Sci. A Polym. Chem.*, 2004, **42**, 4711–4722
17. S. Leiras, F. Freire, J. M. Seco, E. Quiñoá and R. Riguera, *Chem. Sci.*, 2013, **4**, 2735–2743.
18. M. Lindgren, H. S. Lee, W. Yang, M. Tabata and K. Yokota, *Polymer*, 1991, **32**, 1531–1534.
19. K. Hirao, Y. Ishii, T. Terao, Y. Kishimoto, T. Miyatake, T. Ikariya and R. Noyori, *Macromolecules*, 1998, **31**, 3405–3408.
20. H. Zhang, J. Song and J. Deng, *Macromol. Rapid Commun.*, 2014, **35**, 1216–1223.
21. Ben Zhong Tang, W. H. Poon, S. M. Leung, W. H. Leung and H. Peng, *Macromolecules*, 1997, **30**, 2209–2212.

22. A. M. Saxman, R. Liepins and M. Aldissi, *Prog. Polym. Sci.*, 1985, **11**, 57–89.
23. J. W. Y. Lam, J. Luo, Y. Dong, K. K. L. Cheuk and B. Z. Tang, *Macromolecules*, 2002, **35**, 8288–8299.
24. B. D. Mather, K. Viswanathan, K. M. Miller and T. E. Long, *Prog. Polym. Sci.*, 2006, **31**, 487–531.
25. C. I. Simionescu and V. Percec, *J. Polym. Sci.: Polym. Lett. Ed.*, 1979, **17**, 421–429.
26. A. Furlani, C. Napoletano, M. V. Russo and W. J. Feast, *Polym. Bull.*, 1986, **16**, 311–317.
27. F. Sanda, H. Araki and T. Masuda, *Macromolecules*, 2005, **38**, 10605–10608.
28. H. E. Gottlieb, V. Kotlyar and A. Nudelman, *J. Org. Chem.*, 1997, **62**, 7512–7515.
29. G. M. Coppola and R. E. Damon, Synthetic Communications, 1993, **23**, 2003–2010.

<u>Chapter 3</u>

In Situ Functionalized Polymers for siRNA Delivery

This chapter is based upon the following article:

J. M. Priegue, D. N. Crisan, J. Martínez-Costas, J. R. Granja, F. Fernández-Trillo and J. Montenegro, *Angew. Chem. Int. Ed.*, 2016, **55**, 7492–7495

Foreword

This chapter is concerned with the exploitation of poly(acryloyl hydrazide) **P1** (see **Chapter 1**) towards the discovery of functionalised polymers for siRNA delivery as documented in the collaborative article "*In Situ* Functionalized Polymers for siRNA Delivery" - *Angew. Chem. Int. Ed.* **2016**, 55, 7492-7495 with Dr Javier Montenegro and his laboratory at the University of Santiago de Compostela. In this communication (in which the author of the thesis was 2nd author) it was showed that **P1** could be functionalised with combinations of a cationic aldehyde and a variety hydrophobic aldehydes in a 50:50 mixture of DMSO and H_2O. In the first instance, the percentages of cationic and hydrophobic aldehydes were adjusted to quickly rule out those functional polymers which were insoluble in this mixture and not useful for further evaluation. Those formulations which passed the solubility test (i.e. >50% cationic aldehyde) were evaluated for their membrane activity against a model system. This served to distinguish the polymers which expressed detergent-like properties (i.e. potentially cytotoxic with real cell lines) and the polymers which showed no membrane activity until complexed with dsDNA (as a model siRNA strand). The candidates that showed good dsDNA transport activity with the model egg yolk phosphatidylcholine (EYPC) membrane were tested in the final stage to determine their ability to transport siRNA in modified HeLa cells that expressed GFP (green fluorescent protein) and the knockdown of the gene responsible for GFP was evaluated. The experiments were designed in such a way that no purification steps were required between functionalisation of poly(acryloyl hydrazide) **P1**, complexing to siRNA and testing against the cells, hence the "*in situ*" aspect of the study.

The author of the thesis' contribution to this research, is represented by the synthesis of **P1** and subsequent functionalisation studies (see **Chapter I**). Furthermore, he evaluated the range of percentage cationic and percentage hydrophobic side-chains in which the functionalised polymers were soluble in aqueous conditions. This was carried out by visual inspection to observe the polymers that precipitated out of solution, both during the functionalisation of **P1** in a 50:50 mixture of DMSO and H_2O, and the subsequent dilution in aqueous media. I also carried out the initial evaluation of membrane activity of functionalised polymers with the EYPC model membrane to determine detergent-like activity and the complexation of dsDNA**.** Further activity studies with the EYPC model membrane were carried out by the Montenegro Laboratory to confirm the methodology and the results obtained in our Lab. All the knockdown studies with siRNA in HeLa-GFP cells were carried out in Spain by Juan Priegue under the supervision of Dr Montenegro.

Below, an attempt has been made to contextualise this research by exemplifying the current techniques explored for therapeutic siRNA delivery, the structural and chemical features of nanovectors, and by arguing about the usefulness of polymeric scaffolds to quickly determine formulations which can be applied to different siRNA strands and different cell lines on a case by case basis. As summarised in the article's abstract, the reported method constitutes a blueprint for the high-throughput screening and future discovery of new polymeric functional materials with important biological applications.

3.1 Background

RNA interference (RNAi)[1-3] is a gene expression inhibition process in which RNA molecules cause the destruction of specific messenger RNA (mRNA) molecules[4]. Naturally, this post-transcriptional gene silencing process[5] occurs as a defensive mechanism against invasion by mobile genetic elements such as viruses. RNAi can however be exogenously induced in order to trigger gene suppression in cell cultures and living organisms, and as such is considered a valuable research tool and a practical tool in therapeutics[6,7] and biotechnology.

Mechanistically,[8,9] RNAi is initiated when an endoribonuclease enzyme[10] (i.e. Dicer) cleaves long double-stranded RNA (dsRNA) into short (~21-25 nucleotides) double-stranded fragments known as small interfering RNA (siRNA). One of the siRNA strands is incorporated into a multiprotein RNA-induced silencing complex (RISC). The siRNA strand acts as a recognition template for complementary mRNA, which leads to the activation of proteins which cleave the mRNA. The net result of this cascade process is gene silencing (**Fig. 3.1**).

Although naturally RNAi functions in the presence of dsRNA, the cleaving of the latter by Dicer usually results in a random array of siRNA molecules that have different efficiencies in gene silencing. More efficient gene silencing can be obtained by presenting RISC with the most efficient siRNA strand for a particular mRNA sequence. This can be achieved for research and practical applications through gene delivery.[11,12]

For efficient therapeutic siRNA delivery, multiple obstacles have to be taken into consideration and appropriate measures should be integrated into a delivery

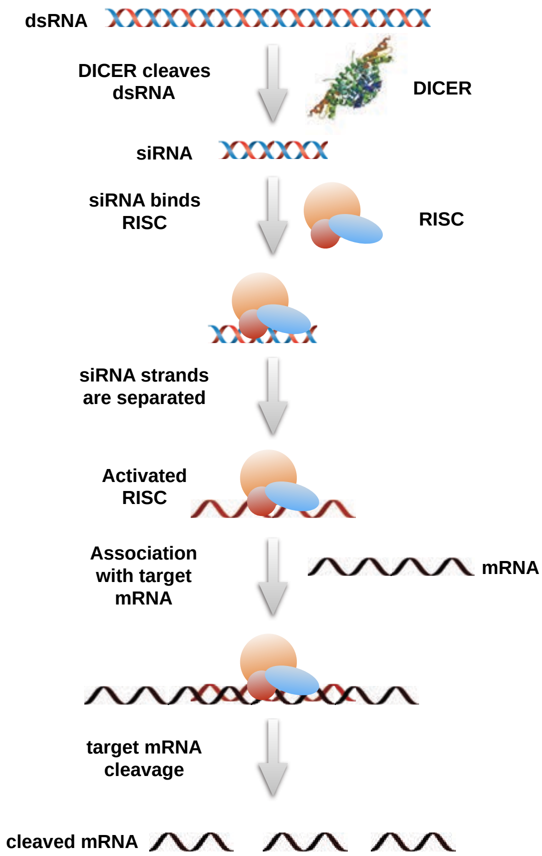

Figure 3.1: Schematic representation of the mechanism of RNA interference.

system. Firstly, 'naked' siRNA fragments are highly susceptible to degradation in bodily fluids due to the presence of nucleases that cleave the phosphodiester bonds[13]. Furthermore, due to its small size (< 5 nm), siRNA has a short circulation time in the body and it is rapidly cleared by the renal system. As a consequence, there is often a higher concentration (up to 40 times) of siRNA in the kidneys compared to other tissues.[14] Thirdly, due to the negatively charged phosphate backbone, siRNA folds into overall negatively charged particles. Since the applications of siRNA therapeutics involves the delivery of siRNA across slightly negatively charged cell membranes, the siRNA particles' negative charge must be shielded to prevent ionic repulsions with the cell membrane.[15] Lastly, the delivery across the cell membranes occurs via the endocytic pathway, through an endosome, before the siRNA encounters the RISC complex in the cytoplasm.[16] As such, the siRNA must be able to efficiently disrupt the endosome and escape in the cytoplasm in order to elicit a therapeutic response.

To improve the overall uptake of siRNA, different strategies[11,12,15,17-20] particularly the chemical modification of the siRNA, or using diverse gene carriers, have been designed to deal with one or more of the obstacles above.

Chemically modified ‘naked’ siRNA has been directly delivered with moderate success through end-group modification, which enhanced the resistance to nucleases.[21,22] RNA is distinguished from DNA by the 2’-OH position, which is also the catalytic target of RNases. Modification at this site, such as substituting non-bridging oxygen atoms with sulfur atoms increases the stability of the siRNA in serum. Despite increased stability, cellular uptake remains comparatively low due to the siRNA - cell membrane anionic repulsions. Further modifications, such as conjugating cholesterol directly to the siRNA, resulted in enhanced cellular uptake and increased biocompatibility.[23] This system was successfully used to target herpes simplex virus[24] after intravaginal administration without triggering an immune response, but the high dose of cholesterol-siRNA required limited its further therapeutic use. Other chemical modifications of siRNA also include conjugation of glycoprotein receptor ligands, which is being investigated in the treatment of amyloidosis.[25] Despite encouraging progress with modified ‘naked’ siRNA, including phase III clinical trials, no approved drug exists at this stage. Complementary to the chemical modification of siRNA is the use of gene delivery vectors, which aim to increase the total circulation time and the overall uptake by forming vector-siRNA nanoparticles that release the nucleic acid inside the cells.

Common nanovectors explored for the delivery of siRNA for therapeutical purposes include lipid-based, non-lipid organic-based and inorganic particle nanovectors. Regardless of its type, every nanovector should aim for the following three properties: i) protect the siRNA from degradation by ribonucleases. ii) enrich siRNA content at the target site. and iii) facilitate the cellular uptake of siRNA.[11]
Although there have been considerable amounts of research and early stage clinical trials for treatment of age-related macular degeneration,[26] metastasised cancers[27] and even post-exposure prophylaxis against lethal dose of Zaire Ebolavirus,[28] there are still features of the delivery nanovectors that require optimisation before mainstream therapeutic use can be achieved. Several nanovectors and their features with their respective advantages and disadvantages are summarised below.

Lipid-based nanovectors such as cationic lipidic liposomes[19] are able to ionically bind the negatively charged siRNA molecules. As such, they can entrap and carry a higher percentage load compared to neutral lipidic liposomes.[29] The slightly cationic surface also supports enhanced interaction between the delivery vector and negatively charged cell membranes, which facilitates the cellular uptake. Furthermore, the siRNA is shielded from RNases by being localised at the core of the nanoparticles and the circulation time is also increased due to the larger size of the liposome nanoparticle compared to the ‘naked’ siRNA particle. Among these, some of the most widely used transfection agents used are Lipofectamine™,[30] Oligofectamine™, DOTAP and DOTMA (**Fig. 3.2**). These reagents have been successfully tested for siRNA delivery against influenza in animal models, as well as several in vitro uses. However, it has been shown that therapeutically, cationic lipidic systems can lead to an inflammatory immune response,[20] which limits their use in

Lipofectamine (DOSPA:DOPE 3:1)

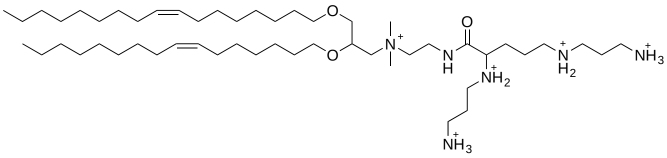

DOSPA

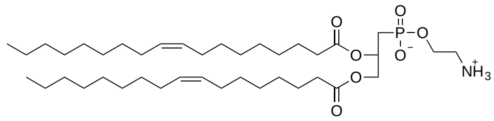

DOPE

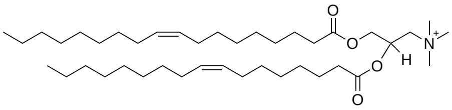

DOTAP

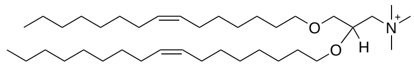

DOTMA

Figure 3.2: Structure of several representative cationic lipidic systems.

vivo. Neutral lipidic liposomes are generally more biocompatible, but they suffer from low entrapment efficiencies due to the absence of the ionic interactions that lead to the formation of vector-siRNA polyionic complexes.[11] Furthermore, there are also fewer favourable interactions between the vector and the negatively charged membranes, which diminishes the cellular uptake. As a consequence, when using neutral lipidic liposomes, larger doses are required to achieve the same therapeutic effect compared to cationic lipid liposomes.

Similarly to binding cholesterol to ‘naked’ siRNA for increased biocompatibility, the effectiveness of cationic lipids has been combined with the biocompatibility of cholesterol in the form of directly conjugated cholesterol-based polyamine lipids[31,32] (**Fig. 3.3**). These nanocarriers were found adept at siRNA-mediated gene silencing in cell culture experiments, but at this stage, it remains to be seen if these nanovectors satisfy the requirements for therapeutic applications.

To harness the advantages of liposomes derived from both cationic and neutral lipids, a series of pH-sensitive ionisable aminolipids[33] have been synthesised. with a view to form nanoparticles with high loading and increased biocompatibility. In

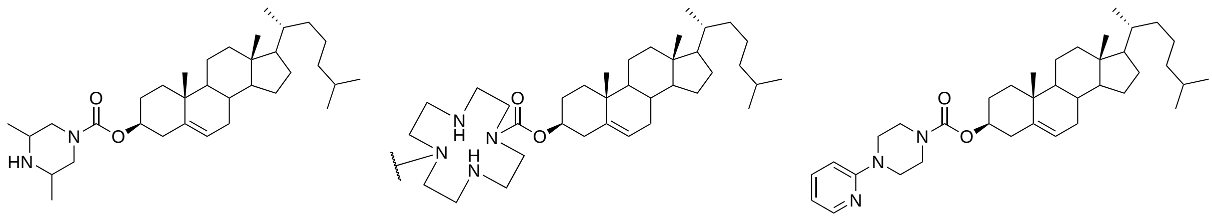

Figure 3.3: Structure of several cholesterol-based polyamine lipids as synthesised by Islam *et al*.[32]

acidic pH, the lipids are cationic and form liposomes with high siRNA percentage load due to favourable ionic interactions. When the liposomes are delivered at neutral pH, the aminolipids are deprotonated resulting in a neutral, biocompatible liposome, with a siRNA percentage load comparable to that of cationic lipids but the biocompatibility of neutral liposomes.

Extended circulation lifetimes, stability and pharmacokinetic properties has also been achieved by synthesising nanovectors that contain poly(ethylene glycol) (PEG).[34] PEG is a non-toxic, FDA approved polymer already in use as a laxative but also as an excipient in pharmaceutical products.[35] PEG-ylation[36] is used to mask active agents from the host immune system, increase solubility in aqueous conditions and increase the size of the nanoparticles, which reduces renal clearance[18]. This process can also be applied in siRNA delivery by providing additional protection against RNases and increase circulation time.[34,37,38] Cationic liposomes with a PEG-ylated surface,[39] have been evaluated in an *in vivo* mouse model against hepatitis B virus and displayed increased pharmacological efficiency. The PEG shell provided the liposomes with a neutral, hydrophilic exterior, that shielded the cationic content and decreased the rate of systemic clearance.

A distinct class of lipid-like nanovectors that have been explored for siRNA delivery are termed lipidoids for which extensive combinatorial libraries of these molecules have been synthesised and tested.[40,41] These branched, almost dendrimer

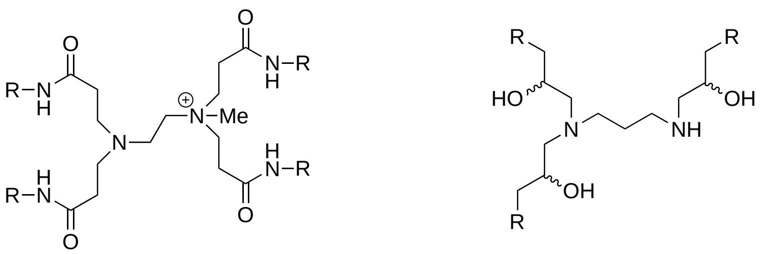

Figure 3.4: Structure of libraries of lipidoids as synthesised by Akinc *et al.*[40] (left) and Love *et al.*[41] (right).

like, molecules combine several features including amide linkages, multiple long and short alkyl tails and multiple amine groups (**Fig. 3.4**) to bind siRNA, protect it from nucleases and enhance its availability at the delivery site. The best performing molecules achieved gene silencing effects similar to Lipofectamine 2000. Formulations of lipidoids with cholesterol and PEG-ylated lipids have been made in order to tune the chemical and physical properties of the siRNA delivery vehicle to achieve promising results *in vivo*.[42] Dynamic amphiphilic lipidoid libraries (**Fig. 3.5**) have been synthesised using a combination of hydrazone or oxime bonds to afford around 900 distinct structures, which were evaluated for siRNA in vitro delivery in HeLa cells.[43,44] This screening assay was used to rapidly compare the influence of the cationic species (ammonium or guanidinium groups) and the different hydrophobic groups on the performance of the delivery vector, with the best targets

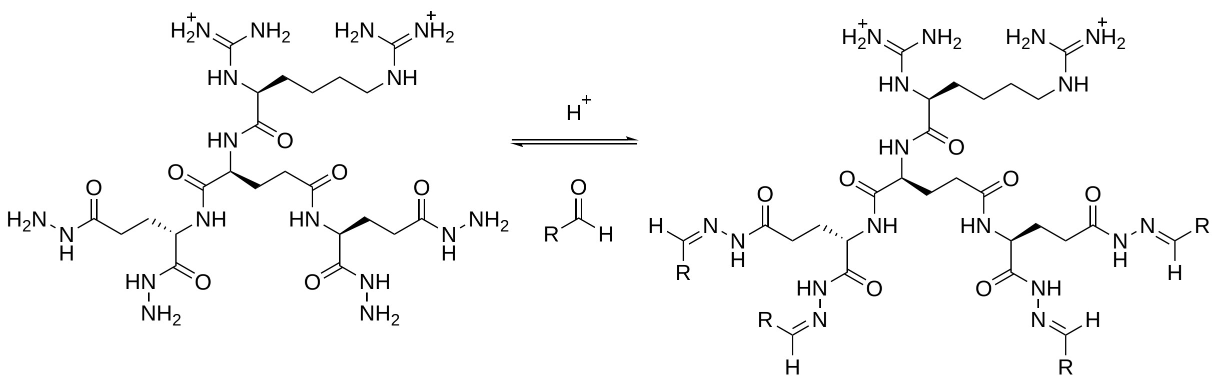

Figure 3.5: Structure of libraries of amphiphilic dynamic lipidoids as synthesised by Gehin *et al.*[43]

showing siRNA related enzyme knockdown two-fold higher compared to Lipofectamine RNAiMax.[43]

Non-lipid organic nanovectors are generally composed of linear or branched polymeric networks and usually with a high content of polycations or amphiphilic character[15,19] (**Fig. 3.6**). Macromolecular structures such as dendrimers and cyclodextrins[11] have been successfully combined with siRNA, targeting factors and PEG for stability in biological fluids to form targeted nanoparticle-delivery systems. Such a system was the focus of a phase I clinical trial but it was also used to probe the RNAi mechanism in humans.[27] Cationic polymers such as polyethylenimines (PEI) have been successfully used, alone or conjugated with other blocks[19] (i.e. PEG), to form nanoparticles with siRNA and they have been shown to reprogram dendritic cells from an immunosuppression state to an anti-tumour state.[45] Their high cationic charge density allows the condensation of the nucleic acid into polyionic complexed particles. Furthermore, polycationic polymers such as PEI also show a good buffering capacity in particular cellular compartments (i.e. endosome).[19] These properties allow these type of polymers to efficiently protect the nucleic acid against nucleases. Amphiphilic polymers[46] are generally composed of segments of polycations and neutral, often hydrophobic components.[47] Like lipidoids, the cationic

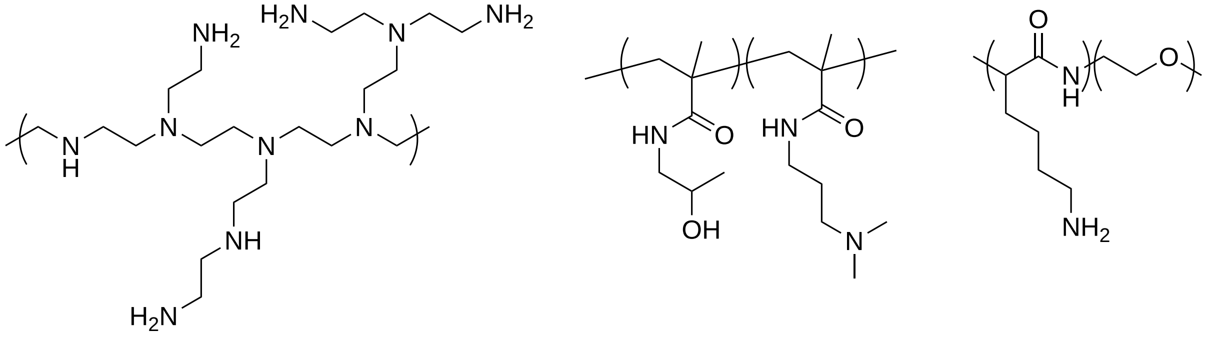

Figure 3.6: Structures of several cationic and amphiphilic polymers explored as gene delivery vectors.

components allow efficient siRNA loading but also good buffering capacity, while the hydrophobic component influences the interactions with the cellular membrane.

Gold nanoparticles have also been employed successfully in gene silencing as an example of an inorganic nanovector. Controlled siRNA delivery was achieved using siRNA-Au nanoparticles of discrete sizes, with a tat-lipid coating for enhanced cellular uptake.[48] The controlled release was obtained by pulsed near-infrared laser exposure in a power and time dependent manner. Such techniques are viewed as a means to achieve therapeutic effects especially with non-targetted delivery vectors, by activating only the nanoparticles accumulated in the tumour sites.

Although this is only a brief overview of different siRNA delivery strategies, several repeated structural motifs can be observed. It is favourable to include a source of cations to increase the percentage load of siRNA[11,17,19] such as including a source of polyamines, guanidinium groups or the gold shell of the Au nanoparticles. The positive charge also aids in cellular uptake due to favourable ionic interactions with the negatively charged membrane. Hydrophobic/lipid residues also aid in cellular uptake due to their interaction with the phospholipid membrane of the cells.[43] PEG-ylation of nanovectors has been shown to enhance the delivery of siRNA by increasing the circulation time, protecting the cargo from nucleases, decreasing cytotoxicity by masking the cationic shell from the host immune system and aiding in aqueous solubility.[34,39]

Despite the encouraging progress and the relatively large number of clinical trials, there are many technical hurdles yet to overcome. In siRNA therapeutics of cancers or targets prone to mutations, sudden changes in the composition of the target tumour tissue or cell-lines[11] for example could decrease the efficacy of a nanovector system, which took precious time and resources to design.

Direct treatment by overloading the system with unmodified siRNA oligos has been shown to trigger an innate immune response.[49,50] While chemically modifying the strand may solve some of these problems,[51] it is improbable that this is a viable solution to wide-spread siRNA therapeutics unless direct injection at the target site is carried out.

Another important technical hurdle is the difficulty in tissue-specific delivery of the nanovectors. There are multiple biological barriers preventing efficient circulation of siRNA-nanovectors to the target site. Firstly, nanoparticle sizes smaller than 300-400 nm can passively cross the endothelial cells of the blood vessels in tumours, which permit therapeutic accumulation at that site.[52] However, before they reach the target site, the nanovector must prolong the circulation time of the siRNA carried by protecting against nucleases.[15] Furthermore, apart from siRNA degradation, there are also lipases that can degrade the carrier exposing the cargo to the aforementioned nucleases. Most examples in successful clinical trials as summarised above, are based to some degree on PEG-ylation of the nanovector to protect the cargo.[17,34] Many currently designed nanovectors generally "target" the liver,[11,20] but not necessarily out of choice, but rather as a limitation to the system. The liver acts a natural filter and is responsible for the uptake and sequestrating of foreign objects such as pathogens and macromolecules, where inevitably the siRNA would be degraded. Again, PEG-ylation increases the biocompatibility and reduces reticulo-endothelial uptake but only with moderate success.[11] As mentioned previously, siRNA oligos can trigger an immune response, as such, the nanovector must be designed to evade cells of the immune system. Finally, targets of siRNA therapy are generally characterised by poor heterogeneity.[53] That is to say, even at the same target site, complete access by one nanovector alone may be impossible, and multiple carriers may be required for efficient delivery.

Using polymer scaffolds such as poly(acryloyl hydrazide) **P1** may offer an attractive screening solution to the technical hurdles summarised above, similar to the work on dynamic amphiphilic lipidoids above[43] (**Fig. 3.5**). Firstly, functionalisation with different sources and ratios of cations can influence the siRNA percentage load and overall charge of the resulting nanoparticle. Furthermore, hydrophobic residues can be used to tune the membrane permeability with respect to different cell-lines and facilitate uptake preferentially to therapeutic target sites (**Fig. 3.7**, **1-3**).

Secondly, polymer scaffolds can be synthesised with different molecular weights and functionalised such that, to produce nanovectors with similar chemical properties but different physical properties and nanoparticle sizes. This could lead to populations of delivery vectors that could selectively access targets in heterogenous sites in a size dependent manner (**Fig. 3.7**, **4**).

Rapidly expanding libraries of functionalised polymers can thus be synthesised based on three parameters: nature and percentage content of cationic component, nature and percentage content of hydrophobic component and size of the starting scaffold. Such libraries can be synthesised and screened rapidly and cheaply, as evidenced in our article.

Structurally, further protection of the cargo, enhanced biocompatibility and better pharmacokinetic properties could be incorporated on the carrier by conjugating additional components (i.e. PEG, cholesterol, targeting vectors) (**Fig. 3.7**, **5**) either

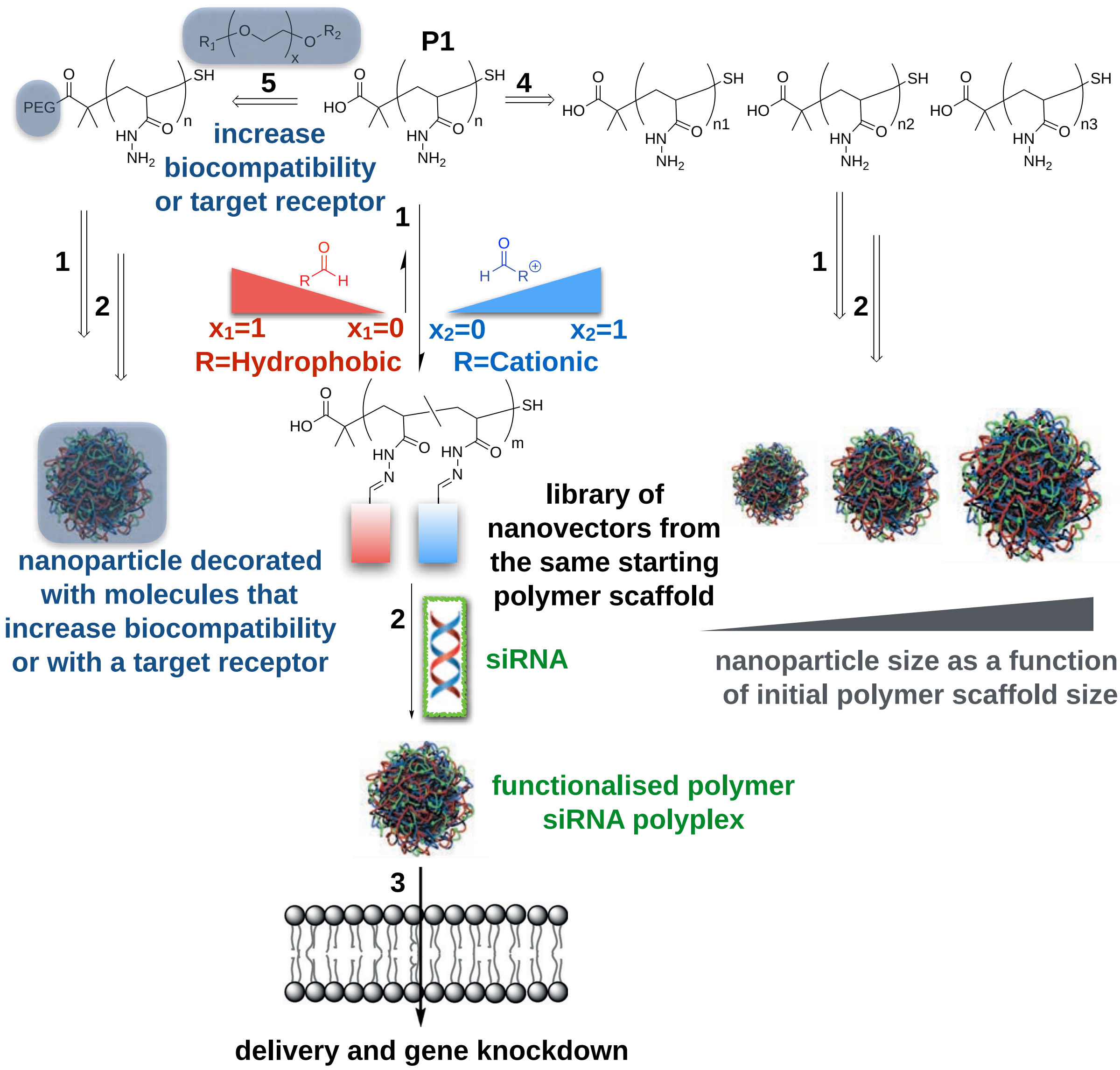

Figure 3.7: Applications of poly(acryloyl hydrazide) **P1** as a scaffold for the synthesis of nanovectors for siRNA delivery. **1** synthesis of functionalised polymers by varying the percentage cationic and hydrophobic aldehyde content. **2** conjugation of siRNA to libraries of nanovectors by ionic interactions. **3** polyplex delivery and gene knockdown. **4** synthesis of polyplexes of varied dimensions by starting from **P1** with varying molecular weights. **5** functionalisation of **P1** with molecules that increase biocompatibility i.e. PEG, cholesterol, or with targeting vectors towards biocompatible nanovectors and polyplexes.

via the side-chains or at the end-groups. These components could be introduced prior to the post-polymerisation functionalisation to afford complex scaffolds that can be used to synthesise more libraries of potential delivery vectors.

As explained in the chapter’s foreword, the progress in collaboration with Javier Montenegro’s Laboratory has explored the first few levels of complexity of this system (**Fig. 3.7**, **1-3**), namely the synthesis of a library of nanovectors by functionalisation of **P1** with a guanidinium aldehyde as the cationic source and a variety of commercially available hydrophobic aldehydes (manuscript and supporting information below). The results have been encouraging, with the best candidate showing similar levels of gene silencing potential as Lipofectamine™ RNAiMAX (currently the standard in the field for in vitro studies) but with 30 times less nanovector required. Furthermore, studies are already underway to better understand the structure/topography/activity relationships of these systems, but this is only the beginning, as it is hoped that the demonstrated blueprint can promote further interest into the next levels of complexity.

3.2 References

1. A. Fire, S. Xu, M. K. Montgomery, S. A. Kostas, S. E. Driver and C. C. Mello, *Nature*, 1998, **391**, 806–811.
2. E. Bernstein, A. A. Caudy, S. M. Hammond and G. J. Hannon, *Nature*, 2001, **409**, 363–366.
3. C. Redi, *Eur. J. Histochem.*, 2010, **54**, 207.
4. S. M. Elbashir, J. Harborth, W. Lendeckel, A. Yalcin, K. Weber and T. Tuschl, *Nature*, 2001, **411**, 494–498.
5. A. J. Hamilton and D. C. Baulcombe, *Science*, 1999, **286**, 950–952.
6. R. C. Mulligan, *Science*, 1993, **260**, 926–932.
7. J. C. Burnett and J. J. Rossi, *Chem. Biol.*, 2012, **19**, 60–71.
8. N. Agrawal, P. V. N. Dasaradhi, A. Mohmmed, P. Malhotra, R. K. Bhatnagar and S. K. Mukherjee, *Microbiol. Mol. Biol. Rev.*, 2003, **67**, 657–685.
9. T. C. Karagiannis and A. El-Osta, *Cancer Biol. and Ther*, 2004, **3**, 1069–1074.
10. Z. Du, J. K. Lee, R. Tjhen, R. M. Stroud and T. L. James, *Proc. Natl. Acad. Sci. U.S.A.*, 2008, **105**, 2391–2396.
11. H. Shen, T. Sun and M. Ferrari, *Cancer Gene Ther.*, 2012, **19**, 367–373.
12. C. Lorenzer, M. Dirin, A.-M. Winkler, V. Baumann and J. Winkler, *J. Control. Release*, 2015, **203**, 1–15.
13. T. S. Zatsepin, Y. V. Kotelevtsev and V. Koteliansky, *Int. J. Nanomedicine*, 2016, **11**, 3077–3086.
14. F. M. van de Water, O. C. Boerman, A. C. Wouterse, J. G. P. Peters, F. G. M. Russel and R. Masereeuw, *Drug Metab. Dispos.*, 2006, **34**, 1393–1397.
15. N. Reynolds, M. Dearnley and T. M. Hinton, *Top. Curr. Chem.*, 2017, **38**, 1–42.
16. S. A. Shorter, A. S. Gollings, M. A. M. Gorringe-Pattrick, J. E. Coakley, P. D. R. Dyer and S. C. W. Richardson, *Expert Opin. Drug Deliv.*, 2017, **14**, 685–696.
17. P. Zhang and E. Wagner, *Top. Curr. Chem.*, 2017, **26**, 1–39.
18. W. Li and F. C. Szoka Jr., *Pharm. Res.*, 2007, **24**, 438–449.
19. S. Zhang, B. Zhao, H. Jiang, B. Wang and B. Ma, *J. Control. Release*, 2007, **123**, 1–10.
20. L. Y. T. Chou, K. Ming and W. C. W. Chan, *Chem. Soc. Rev.*, 2011, **40**, 233–245.
21. B. A. Kraynack and B. F. Baker, *RNA*, 2006, **12**, 163–176.
22. M. Manoharan, A. Akinc, R. K. Pandey, J. Qin, P. Hadwiger, M. John, K. Mills, K. Charisse, M. A. Maier, L. Nechev, E. M. Greene, P. S. Pallan, E. Rozners, K. G. Rajeev and M. Egli, *Angew. Chem. Int. Ed.*, 2011, **50**, 2284–2288.
23. J. Soutschek, A. Akinc, B. Bramlage, K. Charisse, R. Constien, M. Donoghue, S. Elbashir, A. Geick, P. Hadwiger, J. Harborth, M. John, V. Kesavan, G. Lavine, R. K. Pandey, T. Racie, K. G. Rajeev, I. Röhl, I. Toudjarska, G. Wang, S.

Wuschko, D. Bumcrot, V. Koteliansky, S. Limmer, M. Manoharan and H.-P. Vornlocher, *Nature*, 2004, **432**, 173–178.
24. Y. Wu, F. Navarro, A. Lal, E. Basar, R. K. Pandey, M. Manoharan, Y. Feng, S. J. Lee, J. Lieberman and D. Palliser, *Cell Host Microbe*, 2009, **5**, 84–94.
25. D. B. Rozema, D. L. Lewis, D. H. Wakefield, S. C. Wong, J. J. Klein, P. L. Roesch, S. L. Bertin, T. W. Reppen, Q. Chu, A. V. Blokhin, J. E. Hagstrom and J. A. Wolff, *Proc. Natl. Acad. Sci. U.S.A.*, 2007, **104**, 12982–12987.
26. T. R. Friberg, M. Tolentino, LEVEL Study Group, P. Weber, S. Patel, S. Campbell and M. Goldbaum, *Br. J. Ophthalmol.*, 2010, **94**, 1611–1617.
27. M. E. Davis, J. E. Zuckerman, C. H. J. Choi, D. Seligson, A. Tolcher, C. A. Alabi, Y. Yen, J. D. Heidel and A. Ribas, *Nature*, 2010, **464**, 1067–1070.
28. T. W. Geisbert, A. C. Lee, M. Robbins, J. B. Geisbert, A. N. Honko, V. Sood, J. C. Johnson, S. de Jong, I. Tavakoli, A. Judge, L. E. Hensley and I. MacLachlan, *Lancet*, 2010, **375**, 1896–1905.
29. S. Y. Wu and N. A. J. McMillan, *AAPS J*, 2009, **11**, 639–652.
30. Y. Ramgopal, D. Mondal, S. S. Venkatraman, W. T. Godbey and G. Y. Yuen, *J. Biomed. Mater. Res. Part B Appl. Biomater.*, 2009, **89**, 439–447.
31. S. Spagnou, A. D. Miller and M. Keller, *Biochemistry*, 2004, **43**, 13348–13356.
32. R. U. Islam, J. Hean, W. A. L. van Otterlo, C. B. de Koning and P. Arbuthnot, *Bioorg. Med. Chem. Lett.*, 2009, **19**, 100–103.
33. S. C. Semple, S. K. Klimuk, T. O. Harasym, N. Dos Santos, S. M. Ansell, K. F. Wong, N. Maurer, H. Stark, P. R. Cullis, M. J. Hope and P. Scherrer, *Biochim. Biophys. Acta*, 2001, **1510**, 152–166.
34. T. A. Werfel, M. A. Jackson, T. E. Kavanaugh, K. C. Kirkbride, M. Miteva, T. D. Giorgio and C. Duvall, *J. Control. Release*, 2017, **255**, 12–26.
35. R. Zangaglia, E. Martignoni, M. Glorioso, M. Ossola, G. Riboldazzi, D. Calandrella, G. Brunetti and C. Pacchetti, *Mov. Disord.*, 2007, **22**, 1239–1244.
36. F. M. Veronese and J. M. Harris, *Adv. Drug Deliv. Rev.*, 2002, **54**, 453–456.
37. E. Ambegia, S. Ansell, P. Cullis, J. Heyes, L. Palmer and I. MacLachlan, *Biochim. Biophys. Acta*, 2005, **1669**, 155–163.
38. C. Y. Zhang, S. Peng, Bin Zhao, W. Luo and L. Zhang, *Mater. Sci. Eng. C.*, 2017, **78**, 546–552.
39. D. V. Morrissey, J. A. Lockridge, L. Shaw, K. Blanchard, K. Jensen, W. Breen, K. Hartsough, L. Machemer, S. Radka, V. Jadhav, N. Vaish, S. Zinnen, C. Vargeese, K. Bowman, C. S. Shaffer, L. B. Jeffs, A. Judge, I. MacLachlan and B. Polisky, *Nat. Biotechnol.*, 2005, **23**, 1002–1007.
40. A. Akinc, A. Zumbuehl, M. Goldberg, E. S. Leshchiner, V. Busini, N. Hossain, S. A. Bacallado, D. N. Nguyen, J. Fuller, R. Alvarez, A. Borodovsky, T. Borland, R. Constien, A. de Fougerolles, J. R. Dorkin, K. Narayanannair Jayaprakash, M. Jayaraman, M. John, V. Koteliansky, M. Manoharan, L. Nechev, J. Qin, T. Racie,

D. Raitcheva, K. G. Rajeev, D. W. Y. Sah, J. Soutschek, I. Toudjarska, H.-P. Vornlocher, T. S. Zimmermann, R. Langer and D. G. Anderson, *Nat. Biotechnol.*, 2008, **26**, 561–569.

41. K. T. Love, K. P. Mahon, C. G. Levins, K. A. Whitehead, W. Querbes, J. R. Dorkin, J. Qin, W. Cantley, L. L. Qin, T. Racie, M. Frank-Kamenetsky, K. N. Yip, R. Alvarez, D. W. Y. Sah, A. de Fougerolles, K. Fitzgerald, V. Koteliansky, A. Akinc, R. Langer and D. G. Anderson, *Proc. Natl. Acad. Sci. U.S.A.*, 2010, **107**, 1864–1869.
42. A. Akinc, M. Goldberg, J. Qin, J. R. Dorkin, C. Gamba-Vitalo, M. Maier, K. N. Jayaprakash, M. Jayaraman, K. G. Rajeev, M. Manoharan, V. Koteliansky, I. Röhl, E. S. Leshchiner, R. Langer and D. G. Anderson, *Mol. Ther.*, 2009, **17**, 872–879.
43. C. Gehin, J. Montenegro, E.-K. Bang, A. Cajaraville, S. Takayama, H. Hirose, S. Futaki, S. Matile and H. Riezman, *J. Am. Chem. Soc.*, 2013, **135**, 9295–9298.
44. J. Montenegro, E.-K. Bang, N. Sakai and S. Matile, *Chem. Eur. J.*, 2012, **18**, 10436–10443.
45. J. R. Cubillos-Ruiz, X. Engle, U. K. Scarlett, D. Martinez, A. Barber, R. Elgueta, L. Wang, Y. Nesbeth, Y. Durant, A. T. Gewirtz, C. L. Sentman, R. Kedl and J. R. Conejo-Garcia, *J. Clin. Invest.*, 2009, **119**, 2231–2244.
46. K. Romøren, B. J. Thu, N. C. Bols and Ø. Evensen, *Biochim. Biophys. Acta*, 2004, **1663**, 127–134.
47. D. Oupický, Č. Koňák, K. Ulbrich, M. A. Wolfert and L. W. Seymour, *J. Control. Release*, 2000, **65**, 149–171.
48. G. B. Braun, A. Pallaoro, G. Wu, D. Missirlis, J. A. Zasadzinski, M. Tirrell and N. O. Reich, *ACS Nano*, 2009, **3**, 2007–2015.
49. V. Hornung, M. Guenthner-Biller, C. Bourquin, A. Ablasser, M. Schlee, S. Uematsu, A. Noronha, M. Manoharan, S. Akira, A. de Fougerolles, S. Endres and G. Hartmann, *Nat. Med.*, 2005, **11**, 263–270.
50. A. D. Judge, V. Sood, J. R. Shaw, D. Fang, K. McClintock and I. MacLachlan, *Nat. Biotechnol*., 2005, **23**, 457–462.
51. C. R. Allerson, N. Sioufi, R. Jarres, T. P. Prakash, N. Naik, A. Berdeja, L. Wanders, R. H. Griffey, E. E. Swayze and B. Bhat, *J. Med. Chem.*, 2005, **48**, 901–904.
52. F. Yuan, M. Leunig, S. K. Huang, D. A. Berk, D. Papahadjopoulos and R. K. Jain, *Cancer Res.*, 1994, **54**, 3352–3356.
53. M. Stohrer, Y. Boucher, M. Stangassinger and R. K. Jain, *Cancer Res.*, 2000, **60**, 4251–4255.

J. M. Priegue, D. N. Crisan, J. Martínez-Costas, J. R. Granja, F. Fernández-Trillo and J. Montenegro, *Angew. Chem. Int. Ed.*, 2016, **55**, 7492–7495

In Situ Functionalized Polymers for siRNA Delivery

Manuscript and Supporting Information

siRNA delivery

International Edition: DOI: 10.1002/anie.201601441
German Edition: DOI: 10.1002/ange.201601441

In Situ Functionalized Polymers for siRNA Delivery

Juan M. Priegue, Daniel N. Crisan, José Martínez-Costas, Juan R. Granja, Francisco Fernandez-Trillo, and Javier Montenegro**

Abstract: *A new method is reported herein for screening the biological activity of functional polymers across a consistent degree of polymerization and in situ, that is, under aqueous conditions and without purification/isolation of candidate polymers. In brief, the chemical functionality of a poly(acryloyl hydrazide) scaffold was activated under aqueous conditions using readily available aldehydes to obtain amphiphilic polymers. The transport activity of the resulting polymers can be evaluated in situ using model membranes and living cells without the need for tedious isolation and purification steps. This technology allowed the rapid identification of a supramolecular polymeric vector with excellent efficiency and reproducibility for the delivery of siRNA into human cells (HeLa-EGFP). The reported method constitutes a blueprint for the high-throughput screening and future discovery of new polymeric functional materials with important biological applications.*

Polymers are emerging as one of the most promising scaffolds for the multivalent presentation of relevant biological information.[1,2] Polymeric displays of chemical motifs trigger new opportunities for cargo conjugation and delivery of the resulting covalent and/or supramolecular nanocomposites.[3] Polymers have been suggested as one of the best nanomaterials for drug delivery.[3,4] Along these lines, the delivery of exogenous small interfering RNA (siRNA)[5,6] is one potential therapy where polymers have attracted great attention.[7] RNA interference (RNAi) can regulate gene expression in a catalytic manner, and as such, offers several advantages over other gene therapies.[8] However, the potential biosafety problems associated with viral vectors and the intrinsic limitations of siRNA (for example, nuclease digestion) strongly hinder the development of suitable therapies.[6] It is therefore crucial to innovate and to identify new synthetic vectors for the delivery of functional polynucleotides.

Current progress in polymer synthesis allows the preparation of materials with multiple functionalities capable of mimicking some of the desired characteristics of viral vectors for gene delivery.[7,9] To speed up this discovery process, screening strategies have been developed.[10–14] However, in most of these cases the monomer composition strongly affects the outcome of the polymerization results.[15] Furthermore, these platforms are often compromised by the lack of strategies that allow evaluation of a range of chemical compositions across a consistent molecular weight and/or polymer length. Moreover, there are even fewer procedures that allow the in situ evaluation of the generated polynucleotide vectors.[12] Therefore, purification/isolation steps have to be implemented, even for inactive candidates, increasing the time required and the cost of the discovery process. Unfortunately, as the sophistication in polymer design increases, so does the synthetic effort required to prepare polymer vectors.

In this Communication we report the synthesis of poly(acryloyl hydrazide)s for their straightforward functionalization with aldehydes to afford amphiphilic polymers that can be screened in situ (that is, under aqueous conditions and without further purification) for the activated transport of nucleotides across lipid membranes (Scheme 1). Optimization of these hydrazone-activated polymers can be performed under aqueous conditions and without purification, minimizing the synthetic effort and the time required to identify novel candidates for polynucleotide delivery. This versatile technology allowed the rapid identification of a single component formulation for the delivery of siRNA with better performance than one of the best commercial reagents (lipofectamine RNAiMAX).

Post-polymerization functionalization is an ideal strategy to develop and to evaluate polymer compositions across a consistent degree of polymerization.[16] Post-polymerization often relies on highly efficient reactions (such as cycloadditions, reversible carbonyl chemistry, thiol-ene) to modify polymer properties.[16] Of these, we anticipated that using a poly(acryloyl hydrazide) scaffold (**P1**, Scheme 1) would give the required solubility in water to be able to screen for siRNA delivery without the need to purify the candidate amphiphiles. Poly(hydrazides) are weakly protonated at neutral pH[10] and can readily react with aldehydes to form acyl hydrazones that are sufficiently stable under physiological conditions.[17] Accordingly, hydrazone formation has been widely used in biological settings including drug delivery,[18] sensing,[19,20] or even in the synthesis of polynucleotide delivery vectors.[21,22] However, the use of poly(hydrazide) as a "clickable" and versatile scaffold has been limited and only a few examples report its use to synthesize glycopolymers or for pH-

[*] J. M. Priegue, Prof. Dr. J. R. Granja, Dr. J. Montenegro
Departamento de Química Orgánica
Centro Singular de Investigación en Química Biolóxica e Materiais Moleculares (CIQUS)
Universidade de Santiago de Compostela E-15782 (Spain)
E-mail: javier.montenegro@usc.es

Dr. J. Martínez-Costas
Departamento de Bioquimica y Biología Molecular
Centro Singular de Investigación en Química Biolóxica e Materiais Moleculares (CIQUS)
Universidade de Santiago de Compostela E-15782 (Spain)

D. N. Crisan, Dr. F. Fernandez-Trillo
School of Chemistry, University of Birmingham
B15 2TT (UK)
E-mail: f.fernandez-trillo@bham.ac.uk

Supporting information and the ORCID identification number(s) for the author(s) of this article can be found under http://dx.doi.org/10.1002/anie.201601441.

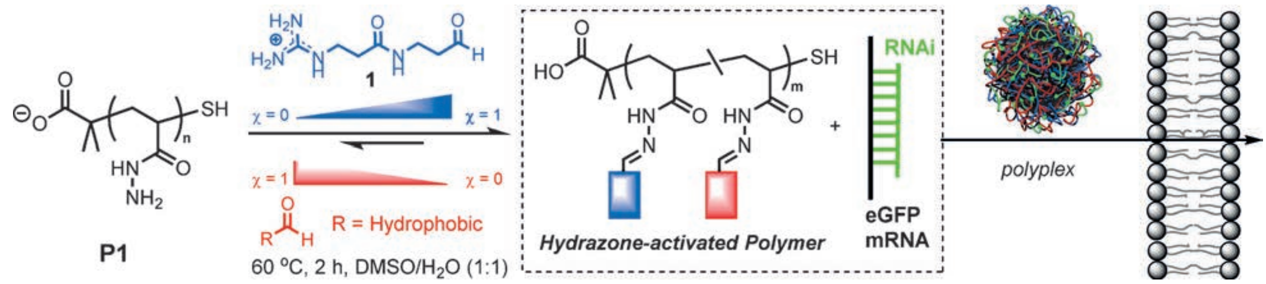

Scheme 1. Post-polymerization functionalization with cationic and hydrophobic aldehydes is followed by supramolecular conjugation of activated polymers with cargo (siRNA) and polyplex delivery. χ = molar fraction.

responsive drug delivery.[16,23,24] Alternative elegant strategies for multi-hydrazone formation have also been developed in the context of DNA or protein-templated dynamic combinatorial libraries.[25–28]

The proposed poly(acryloyl hydrazide) scaffold (**P1**) was prepared using controlled free radical polymerization (see the Supporting Information). **P1** was highly water soluble and aqueous hydrazone formation was readily confirmed by employing the UV-active 4-imidazolecarboxaldehyde. ^{1}H NMR spectroscopic analysis of **P1** incubated (for less than 1 h) with 4-imidazolecarboxaldehyde (0.3–0.9 equiv in 100 mM AcOH in D_2O) showed a broadening of the aromatic proton resonance signals of the aldehyde (see Figure S3 in the Supporting Information). Comparison of the residual aldehyde signal against the overall amount of protons revealed that the loading of 4-imidazolecarboxaldehyde on **P1** was about 70% (Figure S3).[23] No increase in loading was detected with a higher number of equivalents of aldehyde, longer times (up to 4 h), different solvents, or even with heating. Further characterization was obtained from gel permeation chromatography (GPC; Figure 1). A clear peak for the polymer **P1**(**Imidazole**) (retention time $R_t = 18$ min)

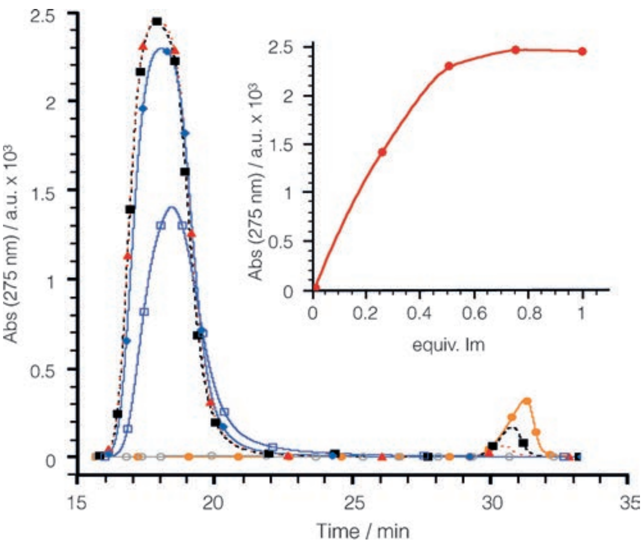

Figure 1. GPC ($\lambda_{Abs} = 275$ nm) analysis of **P1** incubated with 1 (black ■), 0.75 (red ▲), 0.5 (blue ◆), 0.25 (purple □), or 0 (gray ○) equiv of 4-imidazolecarboxaldehyde. The spectrum for pure 4-imidazolecarboxaldehyde (orange ●) is also shown. Conditions: 100 mM acetic acid, pH 2.9, 2 h. Inset: Increase in absorbance of the high molecular weight peak ($R_t = 18$ min) with increasing amounts of 4-imidazolecarboxaldehyde.

was already detected with only 0.25 equiv of 4-imidazolecarboxaldehyde added to **P1**, confirming attachment of the chromophore to **P1** (Figure 1). Increasing amounts of 4-imidazolecarboxaldehyde resulted in an increase in the intensity of the peak at 18 min, with the signal reaching a maximum at around 0.75 equiv. Further equivalents simply increased the amount of free 4-imidazolecarboxaldehyde ($R_t = 31$ min), validating the NMR estimation of a maximum polymer loading of about 70% (Figure S3).

Having established the feasibility of modifying **P1** with a model aldehyde, we explored the use of **P1** for the in situ screening of membrane-active polymers. A close inspection of some of the structural motifs commonly found in membrane-active polymers (for example antimicrobial or cell-penetrating polymers) highlights a high prevalence of amphiphilic structures with the presence of both cationic (such as guanidinium) and hydrophobic moieties (such as isopropyl or benzyl).[19,29,30] The potential of establishing bidentate hydrogen bonding and stable protonation under physiological conditions makes the guanidinium group ($pK_a \approx 12.5$) the optimal cationic moiety for membrane penetration. Thus, we decided to investigate a small library of aldehydes where the cationic aldehyde (**1**, Scheme 1) was kept constant and independently combined with different hydrophobic aldehydes (Figure 2; see also the Supporting Information).

Activated polymers for membrane transport were thus prepared by combining an aqueous stock solution of **P1** with a DMSO solution containing the cationic and the corresponding hydrophobic aldehydes in different molar ratios (see the Supporting Information for details). Hydrazone formation of **P1** with long hydrophobic aldehydes (≥ 8 carbon atoms) lead to the rapid precipitation of the resulting polymers, making these combinations inappropriate for further evaluation. However, the combination of a series of short hydrophobic aldehydes (for example isovaleraldehyde (**2**)) with **1** afforded water-soluble and stable polyhydrazone nanoparticles (Figure S4). Dynamic light scattering (DLS) analysis revealed suitable sizes for membrane transport (about 200 nm) at a molar ratio of cationic/hydrophobic aldehydes = 0.85:0.15 (Figures S4 and S17).[21] Neighboring effects (i.e. cation repulsion) could impact the final composition of the final hydrazone-modified polymer. Therefore, to further characterize the post-polymerization reaction, we measured the DLS properties and the zeta potential of **P1** combined with different ratios of guanidinium aldehyde (**1**) and isovaleraldehyde (**2**). These measurements showed that increasing the molar fraction of hydrophobic aldehyde increased the size

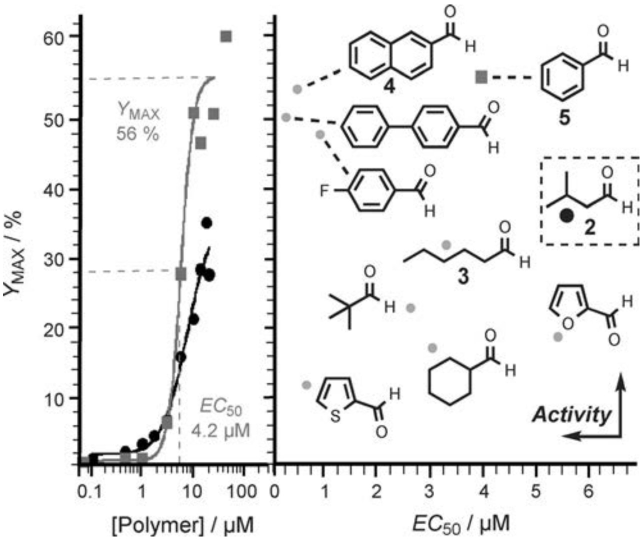

Figure 2. Y_{MAX} values versus polymer concentration (left) or versus EC_{50} (half maximal effective concentrations; right) for the DNA transport experiments in EYPC-LUVs⊃HPTS/DPX for hydrazone-activated polymers at χ(Hydrophobic) = 0.15 and χ**1** = 0.85. In the left plot, **5** (squares) and **2** (circles) are employed as the hydrophobic aldehydes.

and thus the cationic character of the resulting polymeric nanoparticles (Figure S4 b). The maximum increase was detected at a molar fraction of **2** of χ**2** = 0.3–0.4, with further increases causing an important decrease in both the size and the zeta potential (Figure S4 B). These results confirmed that changes in the aldehyde molar ratios are directly translated into the composition of the hydrazone-modified polymer.

Lead hydrazone-activated polymers from DLS analysis were then evaluated in supramolecular DNA transport experiments using large unilamellar vesicles (egg yolk L-α-phosphatidylcholine (EYPC LUVs)) loaded with 8-hydroxypyrene-1,3,6-trisulfonic acid trisodium salt and *p*-xylene-bis-pyridinium bromide (EYPC LUVs⊃HPTS/DPX).[19,20] This routine assay reports the release of internal dye molecules as an increase in the fluorescence of HPTS (Figure S5). This model allows the quick identification of inactive formulations as well as compositions that lead to significant membrane damage. In these experiments, a heterogeneous mixture of short double-stranded DNA molecules (dsDNAs; herring DNA) was selected to model siRNA. Transport experiments in these fluorogenic vesicles revealed isovaleraldehyde (**2**) and hexanal (**3**), and 2-naphthaldehyde (**4**) and benzaldehyde (**5**), as the leading hits for the aliphatic and the aromatic series, respectively (Figure 2; Figure S8, Table S2). Increasing the molar fraction of hydrophobic aldehydes over 0.15 (χ(Hydrophobic) > 0.15) afforded amphiphilic polymers with membrane-disrupting behaviors (Figure S6). Control experiments confirmed a lack of activity for the parent hydrazide **P1** either pure or independently combined with hydrophilic (**1**) or hydrophobic aldehydes (Figure S7).

Following the synthesis and in situ screening of polyhydrazones for membrane activity and DNA transport, the aldehyde lead candidates from fluorogenic assays, **2**, **3**, **4**, and **5**, were taken forward for their evaluation in siRNA delivery (EGFP (enhanced green fluorescent protein) gene knockdown) in HeLa-EGFP cells (Figure 3; see the Supporting Information for details).[31] Again, isolation and purification of the synthesized activated polymers was not required and transfection experiments were performed by simply diluting freshly prepared polyhydrazones (buffer/DMSO; see the Supporting Information for details) in culture media. In these experiments, activated polymers with aldehydes **3**, **4**, and **5** showed no activity for siRNA delivery in cells (Figure S11). Aliphatic isovaleraldehyde (**2**), however, showed efficient EGFP knockdown with an accurate reproducibility in all the transfection replicates measured (Figures S9–S14).

The biocompatible experimental conditions for the preparation of hydrazone-activated polymers allowed the straightforward optimization of this polymeric vector. We evaluated **P1** with different molar ratios of isovaleraldehyde (χ**2** = 0–0.4) and different polymer concentrations to maximize transfection efficiency and cell viability (Figure 3; Figure S15). Interestingly, the optimum molar ratio of the hydrophobic aldehyde (χ**2** = 0.15; Figure 3 A) correlated well with the molar ratio identified in vesicle transport experiments (Figure 2; Figures S6, S8). Maximum transfection efficiency for **P1**(**1**)$_{85}$(**2**)$_{15}$ (where the subindices indicate the percentage of the corresponding aldehyde) could be achieved at a concentration of 4 µM (Figure S12). Under these conditions, we could confirm the formation of supramolecular polyplexes (150 nm) with a positive ζ-potential of +7 mV (Figure S17). Additionally, gel electrophoresis showed complete complexation of RNA into the polymeric polyplexes with as little as 0.12 µM of **P1**(**1**)$_{85}$(**2**)$_{15}$ (Figure S18).

Cell viability was optimal for the parent polymer **P1** and for the entire range of molar fractions and concentrations of the active **P1**(**1**)$_{85}$(**2**)$_{15}$ (Figure 3 A; Figures S15, S16). However, increasing the molar ratio of the hydrophobic aldehyde (χ**2** = 0.4) caused a slight decrease in cell viability together

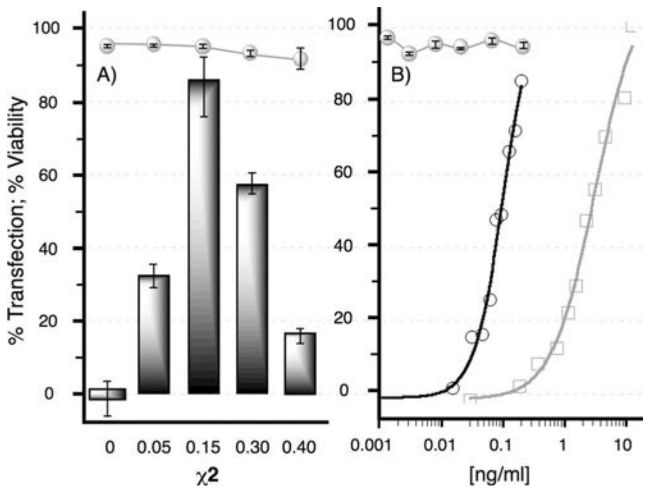

Figure 3. A) Transfection efficiency (bars) and cell viability (circles) in HeLa-EGFP cells at constant siRNA (14 nM) and **P1**(**1**)$_{85}$(**2**)$_{15}$ (4 µM) concentrations and prepared with different molar fractions of **2**.
B) Dose–response curves of lead candidate **P1**(**1**)$_{85}$(**2**)$_{15}$ (empty circles; EC_{50} = 0.09 ng mL^{-1}) and Lipofectamine RNAiMAX (empty squares; EC_{50} = 2.5 ng mL^{-1}), as well as the percentage cell viability for **P1**(**1**)$_{85}$-(**2**)$_{15}$ (gray filled circles, top).

with an increase in the standard deviation of the assay (Figure 3 A, circles). This observation could be related with the membrane detergent behavior detected for highly hydrophobic polyhydrazones in vesicle experiments (Figure 3 A; Figure S15, Figure S6). Remarkably, a comparison of the dose–response curves of transfection efficiency revealed that the polymeric vector performed with almost equal efficiency using a concentration more than ten times less than that of the commercial reagent lipofectamine RNAiMAX (Figure 3 B). Furthermore, the stability of all the components involved in the preparation of this polymeric cytofectin allowed the storage of the stock solutions for months while keeping intact their transfection efficiency.

In conclusion, we have developed a novel strategy for the in situ evaluation (that is, under aqueous conditions and without purification) of polymers with biological activity. Poly(hydrazide) functionality has been "activated", under aqueous conditions, to yield amphiphilic functional polymers that did not require any further purification for their evaluation in relevant biological assays. This procedure allowed the rapid identification of a single-component supramolecular polymeric formulation for siRNA transfection with better performance than the current gold standard for siRNA delivery. We believe that the reported method is not limited to the screening of polynucleotide delivery and that it can be easily adapted (through an informed choice of aldehydes) for the high-throughput screening of polymers with complex chemical functionalities and different biological relevance. The control over the distribution and sequential arrangement of the aldehyde groups onto the polymer scaffold will be a great future challenge that will allow the investigation of intriguing topology/activity relationships. Our efforts in these directions will be reported in due course.

Acknowledgements

This work was supported by the Royal Society, U.K (IE130688) and the Spanish Ministry of Economy and Competitiveness (CTQ2014-59646-R, CTQ2013-43264-R, and BFU2013-43513-R). We thank Rebeca Menaya-Vargas for assistance with cell protocols. F.F.-T. thanks the Birmingham Science City and the European Regional Development Fund, the Royal Society (RG140273), and the University of Birmingham for a John Evans Fellowship. J.M.P. received an F.P.I. contract from MEC. J.M. received a Ramon y Cajal from MINECO and a Starting Grant from the ERC (DYNAP-677786).

Keywords: lipid bilayer membranes · polymers · siRNA delivery · supramolecular chemistry · vesicles

How to cite: *Angew. Chem. Int. Ed.* **2016**, *55*, 7492–7495
Angew. Chem. **2016**, *128*, 7618–7621

[1] S. F. M. van Dongen, H.-P. M. de Hoog, R. J. R. W. Peters, M. Nallani, R. J. M. Nolte, J. C. M. van Hest, *Chem. Rev.* **2009**, *109*, 6212–6274.
[2] C. S. Mahon, D. A. Fulton, *Nat. Chem.* **2014**, *6*, 665–672.
[3] J. Nicolas, S. Mura, D. Brambilla, N. Mackiewicz, P. Couvreur, *Chem. Soc. Rev.* **2013**, *42*, 1147–1235.
[4] M. W. Tibbitt, J. E. Dahlman, R. Langer, *J. Am. Chem. Soc.* **2016**, *138*, 704–717.
[5] M. E. Davis, J. E. Zuckerman, C. H. J. Choi, D. Seligson, A. Tolcher, C. A. Alabi, Y. Yen, J. D. Heidel, A. Ribas, *Nature* **2010**, *464*, 1067–1070.
[6] J.-P. Behr, *Acc. Chem. Res.* **2012**, *45*, 980–984.
[7] K. Miyata, N. Nishiyama, K. Kataoka, *Chem. Soc. Rev.* **2012**, *41*, 2562–2574.
[8] R. C. Mulligan, *Science* **1993**, *260*, 926–932.
[9] T. Wang, J. R. Upponi, V. P. Torchilin, *Int. J. Pharm.* **2012**, *427*, 3–20.
[10] M. P. Xiong, Y. Bae, S. Fukushima, M. L. Forrest, N. Nishiyama, K. Kataoka, G. S. Kwon, *ChemMedChem* **2007**, *2*, 1321–1327.
[11] J. J. Green, R. Langer, D. G. Anderson, *Acc. Chem. Res.* **2008**, *41*, 749–759.
[12] S. Barua, A. Joshi, A. Banerjee, D. Matthews, S. T. Sharfstein, S. M. Cramer, R. S. Kane, K. Rege, *Mol. Pharm.* **2009**, *6*, 86–97.
[13] A. C. Rinkenauer, L. Tauhardt, F. Wendler, K. Kempe, M. Gottschaldt, A. Traeger, U. S. Schubert, *Macromol. Biosci.* **2015**, *15*, 414–425.
[14] J. Hao, P. Kos, K. Zhou, J. B. Miller, L. Xue, Y. Yan, H. Xiong, S. Elkassih, D. J. Siegwart, *J. Am. Chem. Soc.* **2015**, *137*, 9206–9209.
[15] D. M. Lynn, D. G. Anderson, D. Putnam, R. Langer, *J. Am. Chem. Soc.* **2001**, *123*, 8155–8156.
[16] M. A. Gauthier, M. I. Gibson, H.-A. Klok, *Angew. Chem. Int. Ed.* **2008**, *48*, 48–58; *Angew. Chem.* **2008**, *121*, 50–60.
[17] J. Kalia, R. T. Raines, *Angew. Chem. Int. Ed.* **2008**, *47*, 7523–7526; *Angew. Chem.* **2008**, *120*, 7633–7636.
[18] C. C. Lee, E. R. Gillies, M. E. Fox, S. J. Guillaudeu, J. M. J. Fréchet, E. E. Dy, F. C. Szoka, *Proc. Natl. Acad. Sci. USA* **2006**, *103*, 16649–16654.
[19] T. Takeuchi, V. Bagnacani, F. Sansone, S. Matile, *ChemBioChem* **2009**, *10*, 2793–2799.
[20] J. M. Priegue, J. Montenegro, J. R. Granja, *Small* **2014**, *10*, 3613–3618.
[21] C. Gehin, J. Montenegro, E.-K. Bang, A. Cajaraville, S. Takayama, H. Hirose, S. Futaki, S. Matile, H. Riezman, *J. Am. Chem. Soc.* **2013**, *135*, 9295–9298.
[22] C. Bouillon, D. Paolantoni, J. C. Rote, Y. Bessin, L. W. Peterson, P. Dumy, S. Ulrich, *Chem. Eur. J.* **2014**, *20*, 14705–14714.
[23] K. Godula, C. R. Bertozzi, *J. Am. Chem. Soc.* **2010**, *132*, 9963–9965.
[24] A. Kumar, R. R. Ujjwal, A. Mittal, A. Bansal, U. Ojha, *ACS Appl. Mater. Interfaces* **2014**, *6*, 1855–1865.
[25] C. S. Mahon, D. A. Fulton, *Chem. Sci.* **2013**, *4*, 3661–3666.
[26] C. S. Mahon, M. A. Fascione, C. Sakonsinsiri, T. E. McAllister, W. Bruce Turnbull, D. A. Fulton, *Org. Biomol. Chem.* **2015**, *13*, 2756–2761.
[27] E. Bartolami, Y. Bessin, V. Gervais, P. Dumy, S. Ulrich, *Angew. Chem. Int. Ed.* **2015**, *54*, 10183–10187; *Angew. Chem.* **2015**, *127*, 10321–10325.
[28] C. S. Mahon, A. W. Jackson, B. S. Murray, D. A. Fulton, *Chem. Commun.* **2011**, *47*, 7209–7211.
[29] K. Lienkamp, G. N. Tew, *Chem. Eur. J.* **2009**, *15*, 11784–11800.
[30] F. Sgolastra, B. M. deRonde, J. M. Sarapas, A. Som, G. N. Tew, *Acc. Chem. Res.* **2013**, *46*, 2977–2987.
[31] C. Piñero-Lambea, G. Bodelón, R. Fernández-Periáñez, A. M. Cuesta, L. Álvarez-Vallina, L. Á. Fernández, *ACS Synth. Biol.* **2015**, *4*, 463–473.

Received: February 9, 2016
Published online: April 21, 2016

Angewandte Chemie
Eine Zeitschrift der Gesellschaft Deutscher Chemiker

Supporting Information

In Situ Functionalized Polymers for siRNA Delivery

Juan M. Priegue, Daniel N. Crisan, José Martínez-Costas, Juan R. Granja, Francisco Fernandez-Trillo, and Javier Montenegro**

anie_201601441_sm_miscellaneous_information.pdf

Supporting Information

Table of Contents

Materials and Methods

2-(((ethylthio)carbonothioyl)thio)-2-methylpropanoic acid (**CTA**)[S1] was synthesised according to protocols described in the literature. 8-Hydroxypyrene-1,3,6-trisulfonic acid trisodium salt (HPTS) was purchased from Sigma-Aldrich® and *p*-xylene-bis-pyridinium bromide (DPX) was purchased from Invitrogen™. Egg yolk L-αphosphatidylcholine (EYPC) was purchased from Avanti Polar Lipids, Inc. All other chemicals were purchased from Sigma-Aldrich®, Scharlau, Panreac Química SLU, Fisher Scientific® or Acros® and used without further purification. All solvents were HPLC grade, purchased from Sigma-Aldrich® or Fisher Scientific®, and used without further purification.

Nuclear Magnetic Resonance (NMR) spectra were recorded on either a Bruker Avance III 300 MHz, a Bruker Avance III 400 MHz spectrometer, a Varian Mercury 300 MHz or a Varian Inova 500 MHz spectrometer. Chemical shifts are reported in ppm (δ units) referenced to the following solvent signals: DMSO-*d6* δH 2.50, D_2O δH 4.79 and $CDCl_3$, δH 7.26. Electrospray ionization mass spectrometry (ESI-MS) for the characterization of new compounds was performed on a Finnigan MAT SSQ 7000 instrument or an ESI API 150EX and are reported as mass-per-charge ratio *m/z* (intensity in %, [assignment]). Accurate mass determinations (HR-MS) using ESI-MS were performed on a Sciex QSTAR Pulsar mass spectrometer. Infrared (IR) spectra were recorded on a Perkin Elmer Spectrum Two FT-IR spectrometer. Ultraviolet-visible (UV-vis) spectra were recorded on a Campsec M550 Double Beam Scanning UV-vis Spectrophotometer. Fluorescence measurements were performed with a FluoroMax-2 spectrofluorometer (Jobin-Yvon Spex) equipped with a stirrer and a temperature controller. Size Exclusion Chromatography (SEC) spectra were recorded on a Shimadzu Prominence LC-20A fitted with a Thermo Fisher Refractomax 521 Detector (**Boc-P1**) or a SPD20A UV-vis Detector (**P1**). **Boc-P1** was analyzed using 0.05 M LiBr in DMF at 60 °C as the eluent and a flow rate of 1 $mL{\cdot}min^{-1}$. The instrument was fitted with a Polymer Labs PolarGel guard column (50 × 7.5 mm, 5 µm) followed by two PLGel PL1110-6540 columns (300 × 7.5 mm, 5 µm). Molecular weights were calculated based on a standard calibration method using polymethylmethacrylate. Activation of **P1** was analyzed using 100 mM acetic acid at pH 2.9 as the eluent and a flow rate of 1 $mL{\cdot}min^{-1}$. The instrument was fitted with a Shodex Asaphipak GF-510 HQ column and a Shodex Asaphipak GF-310 HQ column (300 × 7.5 mm, 5 µm). Vesicles were homogenized using a Mini-Extruder from Avanti Polar Lipids Inc. Activated polymer and Polyplex hydrodynamic diameter and ζ-potential were determined using a Malvern Zetasizer Nano ZS90. For cell experiments, the absorbance at 560 nm (cytotoxicity assays) and fluorescence (λ_{ex} 489nm; λ_{em} 509nm, transfection experiments) were measured using a microplate reader (Infinite F2000pro Tecan). Gels were resolved on an electrophoresis cell (Fisher Scientific UK), while an UV image station (Chem-genius, Syngene) was used to record and analyze gel images.

Synthesis of Guanidinium Aldehyde (1)

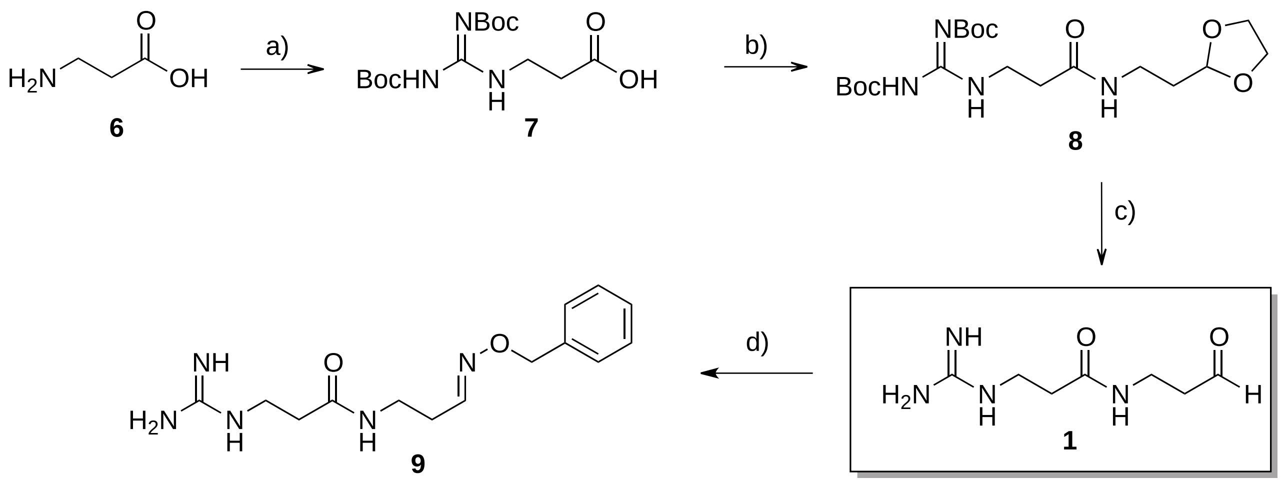

Scheme S1: Synthesis of aldehyde 1. a) *N,N'*-di-Boc-1*H*-pyrazole-1-carboxamidine, DIPEA, CH_3CN/H_2O, 55 ºC, 73%. b) 2-(1,3-dioxolan-2-yl)ethanamine, DCM, HBTU, DIPEA, rt, 80%. c) HCl 3M, 60 ºC, 70%.

Compound 7. β-alanine (**6**) (750 mg, 8.42 mmoles) was dissolved in CH_3CN/H_2O (6:1, 35 mL) and treated with *N,N'*-di-Boc-1*H*-pyrazole-1-carboxamidine (627.3 mg, 2.03 mmoles) and *N,N*-diisopropylethylamine (DIPEA) (868 µl, 5.07 mmoles). The resulting solution was stirred for 2 h at 55 ºC. The product was extracted with DCM (3x 10 mL) and the solution was washed with aqueous HCl (5%, 3 x 20 mL). The organic layers were combined, dried over Na_2SO_4 and concentrated under vacuum. The residue was purified by flash chromatography (gradient DCM/MeOH 98:2→90:10, R_f (90:10) = 0.70) to give 675 mg of compound **7** (73%). Spectroscopic data matched those reported in the literature.[S2]

Compound 8. A solution of **7** (520 mg, 1.57 mmoles) in DCM (30 mL) was treated with TBTU (519.67 mg, 1.57 mmoles), 2-(1,3-dioxolan-2-yl)ethanamine (316 µl, 2.83 mmoles) and DIPEA (1 mL, 6.28 mmoles, added dropwise). The reaction mixture was stirred at rt under Argon atmosphere for 1 hour. The reaction crude was washed with aqueous HCl (5%, 3 x 20 mL) and aqueous saturated $NaHCO_3$ (2 x 20 mL). The organic layer was dried with anhydrous Na_2SO_4, filtered and concentrated under vacuum. The residue was purified by flash chromatography (gradient DCM/MeOH 99:1→90:10, R_f (90:10) = 0.76) to give 542.6 mg of compound **8** (80%) (**Figure S19**). ^{1}H-NMR (300 MHz, $CDCl_3$) δ (ppm) 11.4 (s, 1H), 8.7 (t, $^3J_{H,H}$ = 4.9 Hz, 1H), 6.66-6.57 (m, 1H), 4.8 (td, $^3J_{H,H}$ = 4.3, 0.7 Hz, 1H), 3.95-3.91 (2H, m), 3.85-3.81 (2H, m), 3.70-3.59 (2H, m), 3.4-3.3 (2H, m), 2.41 (t, $^3J_{H,H}$ = 6.2 Hz, 2H, m), 1.86-1.84 (2H, m), 1.49 (9H, s), 1.48 (9H, s). ^{13}C-NMR (500 MHz, $CDCl_3$) δ (ppm) 170.79 (s), 163.40 (s), 156.25 (s), 152.84 (s), 103.89 (d), 83.09 (s), 79.28 (s), 64.89 (t), 36.05 (t), 35.40 (t), 34.71 (t), 32.80 (t), 28.30 (q), 28.05 (q). ESI-MS (H_2O/CH_3CN) m/z 431 (100, $[M+H]^+$), 453 (20, $[M+Na]^+$). IR (neat) ν_{max} 3314 (m sh, N-H), 3124 (w, N-H), 2975 (m sh, C-O), 1721 (m sh, C=O), 1611 (s, N-H), 1409 (s, C-H), 1364 (s, C-H), 105 (s, C-O) cm^{-1}.

Compound 1. A solution of compound **8** (0.69 mmoles, 300 mg) in water was treated with an aqueous solution of HCl (3M, 10 ml mL). The reaction mixture was stirred at 60 ºC for 1 hour. Then the solvent was evaporated under vacuum. The reaction crude was dissolved in H_2O and purified by RP-HPLC. The collected fractions (R_t = 4.0 min,) were lyophilized and stored at -20 °C to give 90 mg of compound **1** (70%) (**Figure S20** and **S21**). RP-HPLC [Nucleosil 100-7 C18 H_2O (0.1% TFA)/CH_3CN (0.1% TFA) 100:0 (0→10 min), 100:0→75:35 (10→35 min), 0:100 (>35 min)]. Purity and characterization were confirmed by analytical RP-HPLC, ^{1}H-NMR and ESI-MS. ^{1}H-NMR (300 MHz, D_2O) δ (ppm) 9.53 (s, 1H), 5.00-4.77 (m, 1H), 3.40-3.25 (m, 2H), 3.24-3.04 (m, 2H), 2.65-2.60 (m, 2H), 2.52-2.29 (m, 2H), 1.94-1.73 (m, 1H), 1.70-1.60 (m, 2H). ESI-MS (H_2O/CH_3CN) m/z 187 (100, $[M+H]^+$, 205 (30, $[M+H_2O]^+$). HR-MS (MS): Calcd for $C_7H_{15}N_4O_2$: 187.1185; found: 187.1190. IR (neat) ν_{max} 3312 (m b, N-H), 3121 (m b, N-H), 2976 (w sh, C-O), 1722 (m, C=O), 1614 (s, N-H), 1363 (s, C-H) 1057 (s, C-O) cm^{-1}. NMR analysis of **1** revealed a discrete mixture of isomers due to potential intramolecular cyclization and/or aldehyde oligomerization.[S3] Treatment of **1** with benzylhydroxylamine afforded the corresponding oxime **9** as a pure single product.

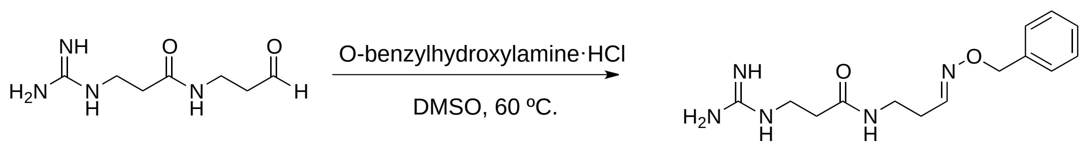

Scheme S2. To determine the purity of the isomer mixture present in **1**, this mixture was reacted with benzyl hydroxylamine to afford oxime **9** as a pure single product. This result suggested that all isomers of compound **4** reacted, under the coupling conditions, to afford the desired oxime **5**.

Compound 9. A solution of compound **1** (100 mM) in aqueous acetic acid ($AcOH_{aq}$) (100 mM, pH = 4.5) was mixed with 1.2 equivalents of O-benzylhydroxylamine (100 mM) in DMSO. The mixture was stirred at 60 ºC for 2 h. The crude was purified by RP-HPLC (The collected fractions (R_t = 18.8 min) were lyophilized and stored at -20 °C to give 9.0 mg of compound **9** (80%) (**Figures S22**, **S23** and **S24**). RP-HPLC [Nucleosil 100-7 C18 H_2O (0.1% TFA)/CH_3CN (0.1% TFA) 100:0 (0→5 min), 100:0→35:75 (5→35 min), 0:100 (>35 min)]. The presence and purity of the O-akyloxime **9** was checked by analytical RP-HPLC, NMR and ESI-MS. ^{1}H-NMR (500 MHz, D_2O) δ (ppm) 7.5 (t, $^3J_{H,H}$ = 6.4 Hz, 1H, Isomer *E*), 7.43-7.35 (5H, m), 6.85 (t, $^3J_{H,H}$ = 5.7 Hz; 1H, Isomer *Z*), 5.10 (s, 2H, Isomer *Z*), 5.05 (s, 2H, Isomer *E*), 3.40-3.30 (m, 4H), 2.59 (dd, $^3J_{H,H}$ = 12.3, 6.4 Hz, 1H), 2.40-2.30 (m, 3H). ^{13}C-NMR (500 MHz, D_2O) δ (ppm) 173.5 (s), 152.2 (d) Isomer *E*, 152.0 (d) Isomer *Z*, 137.2 (s), 137.0 (s), 128.6 (d), 128.3 (d), 128.2 (d), 128.1 (d), 128.0 (d), 75.39 (t) Isomer *Z*, 75.0 (t) Isomer *E*, 37.4 (t), 36.0 (t) Isomer *Z*, 35.9 (t) Isomer *E*, 34.7 (t) Isomer *E*, 34.6 (t) Isomer *Z*, 29.2 (t), 25.7 (t). ESI-MS (H_2O/CH_3CN) m/z 292 (100, $[M+H]^+$). HR-MS (ESI): Calcd for $C_{14}H_{22}N_5O_2$: 292.1771; found: 283.1768. IR (neat) ν_{max} 3369 (m b, N-H), 3246 (m b, N-H), 3010 (w, C-H), 1671 (s, C=O), 1491 (m, C=C), 1382 (m, N-O), 1347 (s, C-H), 1120 (s) cm^{-1}.

Synthesis of Activated Polymers

- **Synthesis of Poly(acryloyl hydrazide) P1**

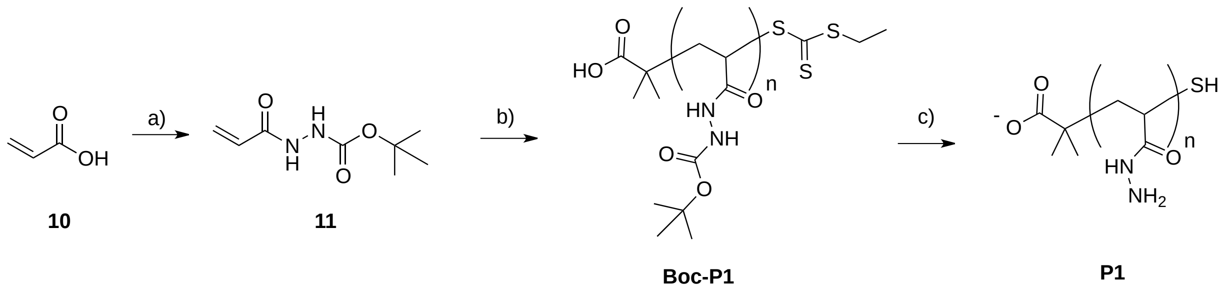

Scheme S3: a) *tert*-butyl carbazate, EDC, H_2O/THF (2:1), 25 ^oC, 50%. b) CTA, ACVA, DMSO, 70 ^oC, 73%. c) *i*. TFA, 25 ^oC; *ii*. H_2O, $NaHCO_3$, 25 ^oC, 92%.

Compound 11. Acrylic acid (**10**) (3.81 mL, 54.95 mmol) and *tert*-butyl carbazate (8.89 g, 65.95 mmol) were dissolved in a H_2O/THF mixture (2:1, 180 mL) at rt. *N*-(3-dimethylaminopropyl)-*N'*-ethylcarbodiimide hydrochloride (EDC) (11.75 g, 61.29 mmol) was added in portions to the solution over 15 minutes and left stirring for 3 h. The crude reaction was extracted with EtOAc (3 x 75 mL) and the organic layer was washed with 0.1 M HCl (3 x 75 mL), H_2O (50 mL) and brine (2 x 50 mL). The organic phase was dried with anhydrous Na_2SO_4 and the solvent was removed under reduced pressure to afford the crude product as a white solid. The crude product was purified by recrystallization from EtOAc (70 ^oC to rt) to afford a 5.05 g of a white crystalline powder identified as **11** (50%) (**Figure S25**). R_f = 0.87 (100% EtOAc). ^{1}H-NMR (300 MHz, DMSO-*d6*) δ (ppm) 9.79 (s, 1H), 8.84 (s, 1H), 6.17-6.20 (m, 2H), 5.69 (dd, $^3J_{H,H}$ = 7.8, 4.5 Hz, 1H), 1.40 (s, 9H). ^{13}C-NMR (100 MHz, DMSO-*d6*) δ (ppm) 164.3 (s), 155.3 (s), 129.4 (d), 126.2 (t), 79.2 (s), 28.1 (q). IR (neat) ν_{max} 3311 (m sh, N-H), 3221 (m sh, N-H), 2981 (w sh, C-H), 1715 (s sh, C=O), 1668 (s sh, C=O) cm^{-1}.

Boc-P1. A solution of 4,4'-azobis(4-cyanovaleric acid) (ACVA) (18.4 mg, 0.064 mmol) in DMSO (1.5 mL) and a solution of CTA (72.3 mg, 0.322 mmol) in DMSO (1.5 mL) were added sequentially to a solution of *tert*-butyl-2-acryloylhydrazine-1-carboxylate (**11**) (3.00 g, 16.095 mmol) in DMSO (14.88 mL). A 50 µL aliquot of this solution was taken at this stage to aid in the calculation of conversion. The reaction mixture was then sealed and degassed with Argon for 30 min. The degassed solution was left to react at 70 ^oC for 7 h. The reaction was stopped by allowing it to cool down to room temperature and by exposing it to air. A 50 µL aliquot of this solution was taken at this stage to aid in the calculation of conversion. The polymer was purified by dialysis against water. The water was removed by lyophilisation and by drying in a desiccator with P_2O_5 to afford 2.2 g of **Boc-P1** (**Figure S26**) as an off-white powder (73% yield). UV (DMSO) λ_{max} 300 nm. ^{1}H-NMR (300 MHz, DMSO-*d6*) δ (ppm) 9.22 (1H, br), 8.60 (1H, br), 2.03 (1H, br), 1.41 (11H, br). Conversion 80%. Mn (DMF GPC) 10270, $Đ_M$ (DMF GPC) 1.39. DP (UV-Vis) 45.

- <u>Calculation of Conversion</u>

50 µL aliquots of the reaction mixture were taken before and after the polymerization. These aliquots were mixed with 50 µL of a 0.8 M stock solution of syringic acid (used as internal standard) and 650 µL of DMSO-*d6*.

Monomer conversion was calculated by ^{1}H-NMR spectra by comparing the integration of the vinyl proton signals from the monomers (5.69 and 6.19 ppm) to the integration from the aromatic groups in syringic acid (7.20 ppm).

– Calculation of Degree of Polymerization (DP) Using UV

DP in **Boc-P1** was calculated by measuring the absorbance at 300 nm (λ_{max} for **Boc-P1**), 305 nm and 310 nm (λ_{max} for **CTA**) and comparing against calibration curves using **CTA** (**Figure S1** and **Table S1**). This way, the amount (mg·mL^{-1}) of trithiocarbamate in **Boc-P1** was estimated,[†] and the ratio between monomer units and end-groups calculated.

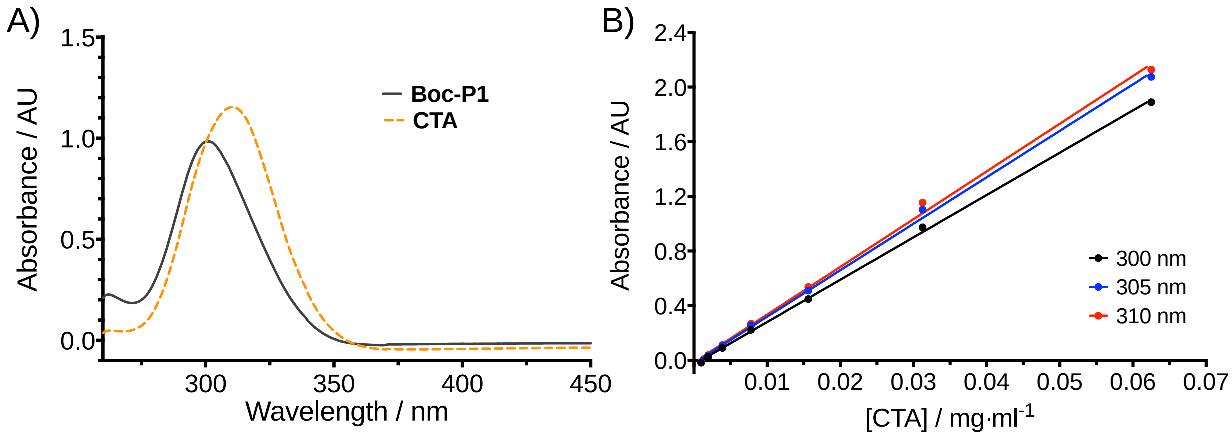

Figure S1: A) UV-vis of **Boc-P1** (1.3 mg·mL^{-1}) and **CTA** (0.03 mg·mL^{-1}) solutions in DMSO. B) Calibration curves showing the linear relationship between absorbance and [CTA].

Poly(acryloyl hydrazide) P1. Trifluoroacetic acid (TFA) (15 mL) was added dropwise to poly(*tert*-butyl-2-acryloylhydrazine-1-carboxylate) (**Boc-P1**) (1.5 g) and the yellow solution was stirred at rt for 2 h. Excess of TFA was removed by blowing a steady stream of Argon and the resulting oil was diluted in water (15 mL). The **P1**·TFA salt formed was neutralised by adding $NaHCO_3$ until no foaming was observed. The colourless solution was allowed to stir overnight. The crude polymer was purified by dialysis against water. The water was removed by lyophilisation and by drying in a desiccator with P_2O_5 to afford 650 mg of **P1** (**Figure S27**) as a white powder (92%). ^{1}H-NMR (300 MHz, D_2O) δ (ppm) 1.59-2.08 (br m, (3·DP)H), 1.01 (s, 3H), 0.95 (s, 3H). ^{13}C-NMR (100 MHz, D_2O) δ (ppm) 174.9 (s), 40.2-40.5 (d), 34.4-35.7 (d). DP (^{1}H-NMR) 40. IR (neat) ν_{max} 3254 (w br, N-H), 1609 (m br, C=O), 1428 (s sh) cm^{-1}.

– Calculation of DP using ^{1}H-NMR

DP in **P1** was calculated from the ^{1}H-NMR spectra by comparing the integration of the methyl substituents in the end-group (0.95 and 1.01 ppm, 6 H) to the integration from the aliphatic region in the polymer backbone (1.59-2.08 ppm) (**Figure S2** and **Table S1**).

[†] DP of polymerization calculated this way is approximate. Absorption (*i.e.* molar extinction coefficient, λ_{max}) properties for **CTA** and **P1** are not necessarily the same. Similarly, not all polymer chains will incorporate a trithiocarbamate as an end-group. However, the calculated value is within error of those calculated by ^{1}H-NMR (**Table S1**).

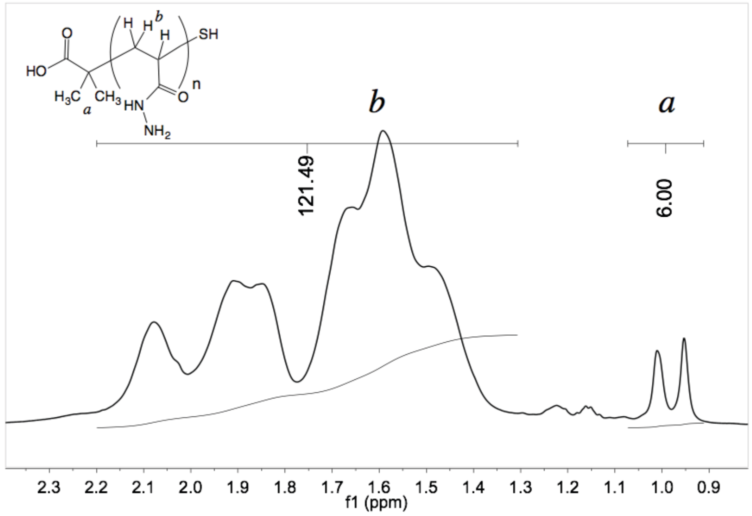

Figure S2: ^{1}H-NMR spectra of **P1** showing the relevant region where the methyl substituents (a) and the aliphatic hydrogens (b) can be identified.

Table S1

	[M] / [CTA][a]	DP (conversion)[b]	DP (UV-vis)[c]	DP (^{1}H-NMR)[d]
Boc-P1	50:1	40	45	-
P1	-	-	-	40

[a] Calculated from the initial monomer and **CTA** concentrations used for the polymerization.
[b] Calculated from the initial monomer and **CTA** ratio and the conversion of monomer from ^{1}H-NMR.
[c] Calculated by UV-vis against a **CTA** standard as the ratio of monomer to trithiocarbamate in **Boc-P1** (**Figure S1**).
[d] Calculated by ^{1}H-NMR, using the methyl groups as an internal standard, as the ratio between monomer and end-group (**Figure S2**).

- **Conjugation of Poly(acryloyl hydrazide) with Aldehydes**

Poly(acryloyl hydrazide) (**P1**) in aqueous acetic acid ($AcOH_{aq}$, 100 mM, pH 3.0) was reacted with 6 equivalents of a solution of different molar fractions of **1** and hydrophobic aldehyde in DMSO. For instance, in a model experiment with pure guanidinium aldehyde (χ**1** = 1), **P1** (25 µl, 35 mM in $AcOH_{aq}$) was reacted with **1** (25 µl, 200 mM in DMSO) to afford a final concentration of activated polymer of 50 mM. In a typical experiment with a mixture of aldehydes (χ**1** = 0.85, χ**2** = 0.15), 25 µl of a solution of **P1** (35 mM in $AcOH_{aq}$ pH 3.0) was mixed with a solution of 25 µl composed by 3.8 µl of a solution of hydrophobic aldehyde (200 mM in DMSO) and 21.2 µl of a solution of **1** (200 mM in DMSO) to give a final concentration of polymer of 50 mM (**Table S2**). This mixture was shaken at 60 ºC for 2 h. Activated polymers were used without further purification in the transport vesicle experiments.

– Calculation of loading using ^{1}H-NMR

Loading in **P1**-4-imidazolecarboxaldehyde was calculated from the ^{1}H-NMR spectra by comparing the integration of the residual aldehyde (9.7 ppm, XH) against the overall number of protons in that region (3H, 1H from aldehyde or hydrazone, 2H from 4-imidazolecarboxaldehyde ring). Signal at 6.0 ppm corresponds to the cyclic acetal and has been included in the overall integration.

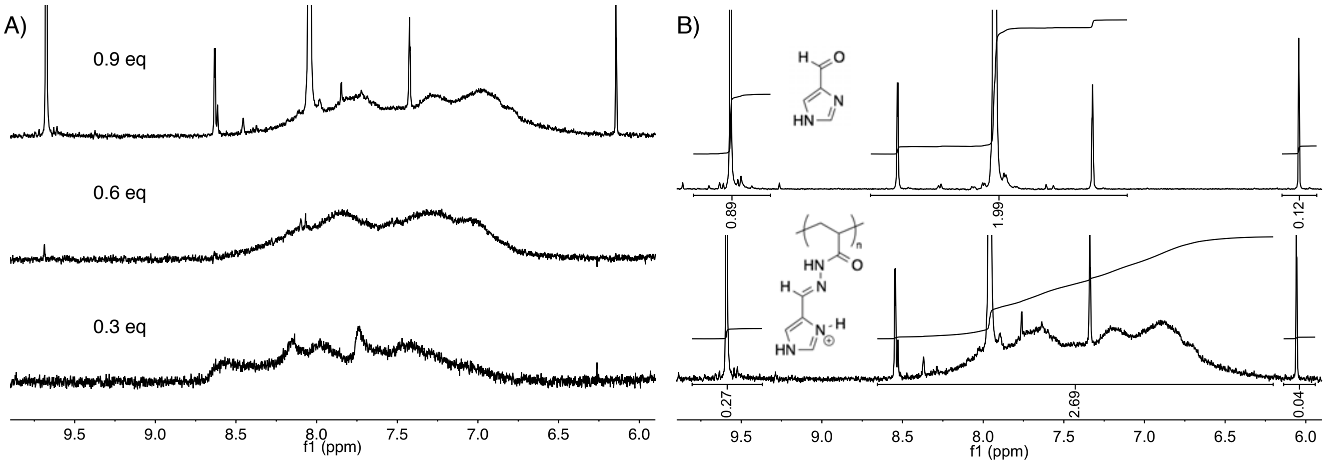

Figure S3: A) ^{1}H NMR spectra of **P1** (1.3 mg/mL) incubated (< 1h) with increasing amounts of 4-imidazolecarboxaldehyde. From bottom: 0.3, 0.6 and 0.9 eq. of 4-imidazolecarboxaldehyde. B) Integration of residual aldehyde (9.7 ppm) against the overall number of protons (3H) in this region.

– <u>Dynamic light scattering of **P1(1)$_{85}$(2)$_{15}$**</u>

P$_1$(1)$_{85}$(2)$_{15}$ was prepared accordingly to the general procedure for the conjugation of poly(acryloyl hydrazide) with aldehyde aldehydes. The final concentration in the reaction vessel was 17 mM. From this stock solution 20 µl were diluted with 1980 µl of MilliQ water to afford a final concentration of 17 µM of activated polymer. For DNA conjugates, 20 µl of 17 mM activated polymer stock solution was diluted with 1960 µl of MilliQ water and 20 µl of 2 µM DNA from Herring sperm were added and the mixture was gently mixed by pipetting and immediately transferred to the cuvette for DLS experiment.

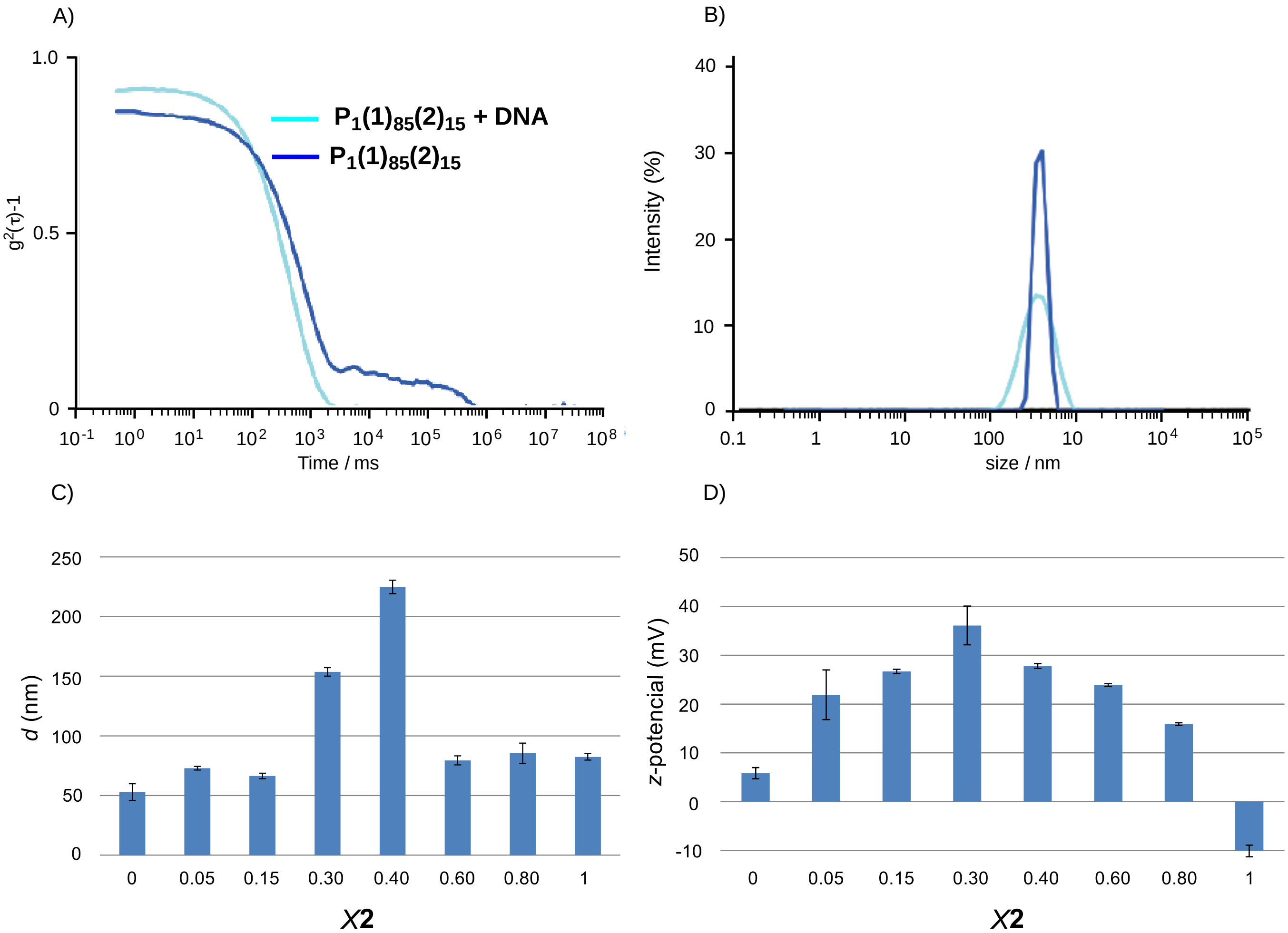

Figure S4: Representative dynamic light scattering data for **P1(1)$_{85}$(2)$_{15}$** in the absence and presence of dsDNA (Herring DNA). A) Autocorrelation function (ACF) curves and B) intensity distributions measured in milliQ water. [activated polymer] = 17 µM. C) Diameter and D) ζ-potential for representative activated polymer **P1(1)$_{85}$(2)$_{15}$** = 3 µM at increasing molar fractions of isovaleraldehyde (χ**2** = 0-1).

Evaluation of Transport Across Model Membranes: Vesicle Experiments

- **Preparation of Large Unilamellar Vesicles (LUV)**

A thin lipid film was prepared by evaporating a solution of EYPC (25 mg) in MeOH/$CHCl_3$ (1:1, 1 mL) on a rotary evaporator (at rt) and then in vacuo overnight. The resulting film was hydrated with 1.0 mL buffer (5 mM HPTS, 16.5 mM DPX, 10 mM Tris, 72 mM NaCl, pH 7.4) for more than 30 min, subjected to freeze-thaw cycles (5 x) and extrusions (15 x) through a polycarbonate membrane (pore size 100 nm). Extravesicular components were removed by gel filtration (Sephadex G-50) with 10 mM Tris, 107 mM NaCl, pH 7.4. Final conditions: ~5 mM EYPC; inside: 5 mM HPTS, 16.5 mM DPX, 10 mM Tris, 72 mM NaCl, pH 7.4; outside: 10 mM Tris, 107 mM NaCl, pH 7.4.

- **Evaluation of Transport of Nucleic Acids across EYPC-LUV**

EYPC-LUV stock solutions (5 μl) were diluted with buffer (10 mM Tris, 107 mM NaCl, pH 7.4), placed in a thermostated fluorescence cuvette (25 °C) and gently stirred (total volume ~2000 μl; final lipid concentration ~13 μM). HPTS efflux was monitored at λ 511 nm (λ_{ex} 413 nm) as a function of time after addition of activated polymer (20 μl in DMSO/AcOH buffer, t = 25 s), nucleic acid (NA, 20 μl of 2 μM stock solution in buffer, t = 50 s) and aqueous triton X-100 (1.2%, 40 μl, 370 μM final concentration, t = 225 s). Total experiment time = 250 s. Fluorescence intensities were normalized to fractional emission intensity *I*(t) using Equation S1.

$$\text{Equation S1: } I(t) = (I_t - I_0)/(I_\infty - I_0)$$

where $I_0 = I_t$ at NA addition, $I_\infty = I_t$ at saturation after lysis. Effective concentration for activated polymer or NA - EC_{50} - and Hill coefficient - n - were determined by plotting the fractional activity Y (= *I*(t) at saturation just before lysis, t = 200 s) as a function of activated polymer or NA concentration *[Analyte]* and fitting them to the Hill equation (Equation S2).

$$\text{Equation S2: } Y = Y_0 + (Y_{max} - Y_0)/\left\{1 + \left(\frac{EC_{50}}{[Analyte]}\right)^n\right\}$$

where Y_0 is Y without NA (or activated polymer), Y_{max} is Y with an excess of activated polymer (or NA) at saturation, EC_{50} is the concentration of NA (or activated polymer) required to reach 50% activity and n is the Hill coefficient (**Figure S5** and **Table S2**).

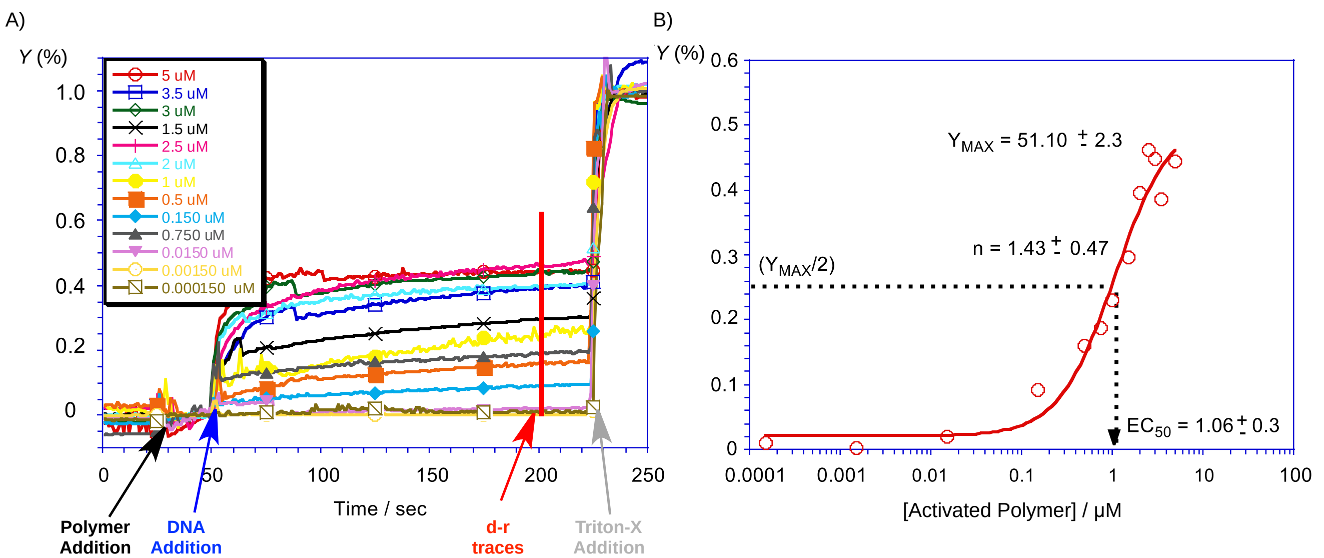

Figure S5: A) Changes to fractional emission intensity *I*(t) for EYPC-LUVs⊃HPTS/DPX after the addition of activated polymer (17 μM, **χ1**: 0.85 and **χ5**: 0.15) at t = 25 sec, Herring DNA (5 μM-0.15 nM final concentrations) at t = 50 sec and Triton-X (370 μM final concentration) at t = 225 sec. B) Dose response curve obtained from the plot of fractional activity *vs* activated polymer concentration and fitting to the *Hill* equation (Equation S2) Y_{MAX} = 51.10 ± 2.3%, EC_{50} = 0.33 ± 0.3 μM, n = 1.43 ± 0.47.

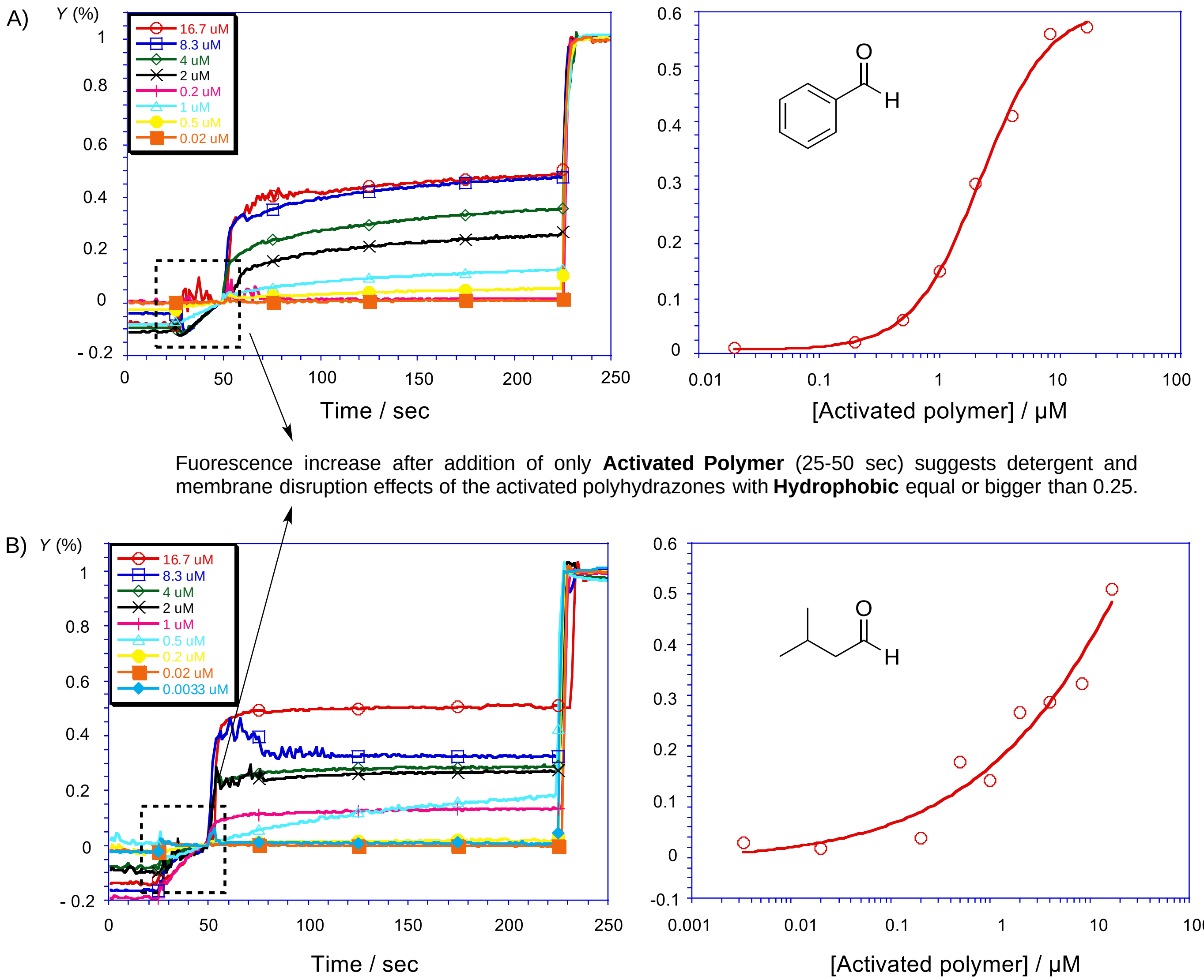

Figure S6: Changes to fractional emission intensity *I*(t) and dose-response curve for the transport of Herring DNA (2 μM) in EYPC-LUVs⊃HPTS/DPX in the presence of activated polymer (17 μM, **χ1**: 0.75 and **χHydrophobic**: 0.25). A) **χHydrophobic** = Benzaldehyde and in B) **χHydrophobic** = isovaleraldehyde (2). The increase in fluorescence observed immediately after the addition of activated polymer depicts membrane disruption profiles when using molar fractions of 0.25 of the hydrophobic aldehydes.

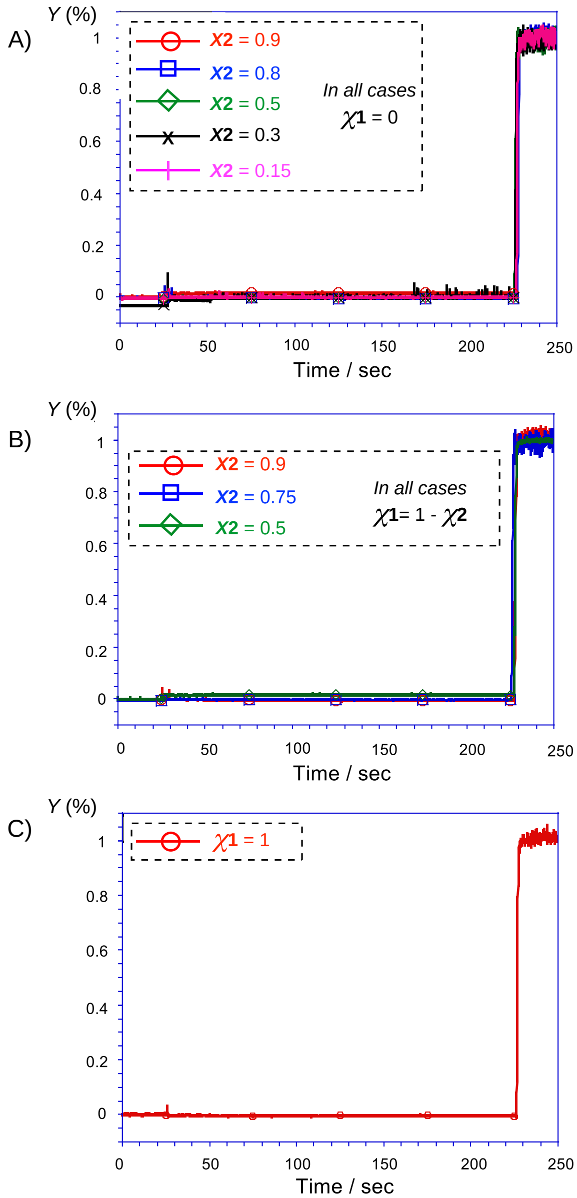

Figure S7: A) Changes to fractional emission intensity *I*(t) for the transport of Herring DNA (2 μM) in EYPC-LUVs⊃HPTS/DPX in the presence of activated polymer (17 μM) prepared from χ**2** (0.9-0.1) in the absence of cationic aldehyde (χ**1** = 0). B) Same plot for activated polymers (17 μM) prepared with higher molar fractions of **2** (χ**2** = 0.5, 0.75 or 0.9) and χ**1** = 1 - χ**1**. C) Same control showing no activity in vesicles for the purely cationic activated polymer (χ**1** = 1).

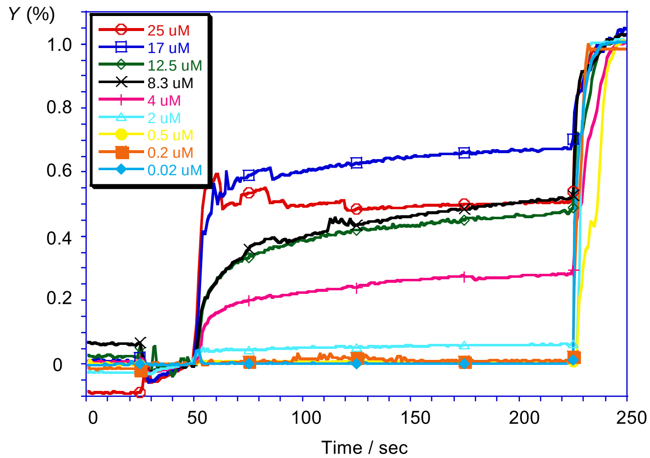

Y (%)
25 uM
17 uM
12.5 uM
8.3 uM
4 uM
2 uM
0.5 uM
0.2 uM
0.02 uM
Time / sec

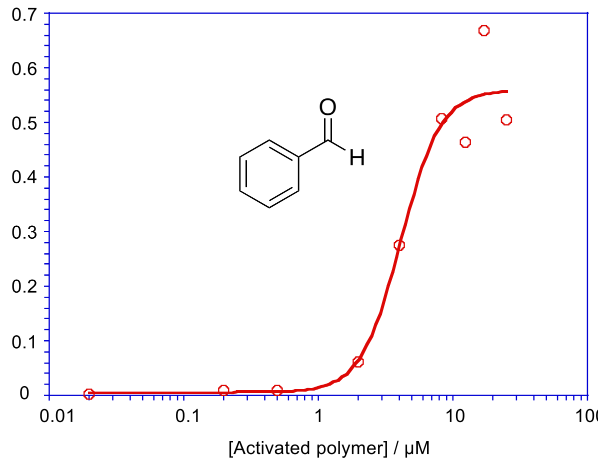

O
H
[Activated polymer] / μM

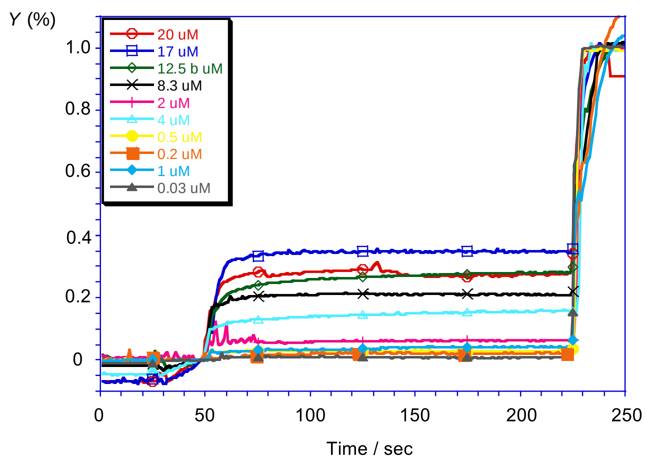

Y (%)
20 uM
17 uM
12.5 b uM
8.3 uM
2 uM
4 uM
0.5 uM
0.2 uM
1 uM
0.03 uM
Time / sec

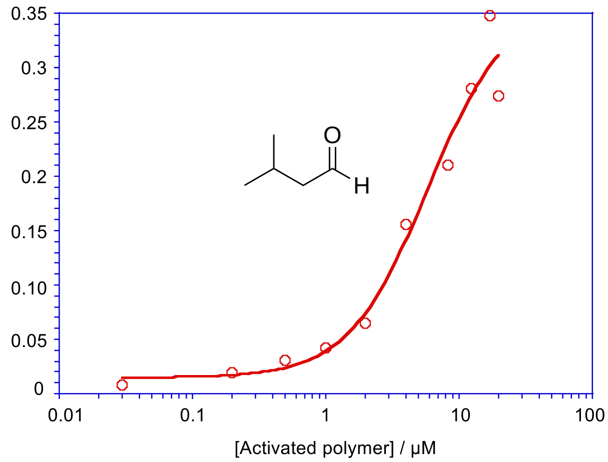

O
H
[Activated polymer] / μM

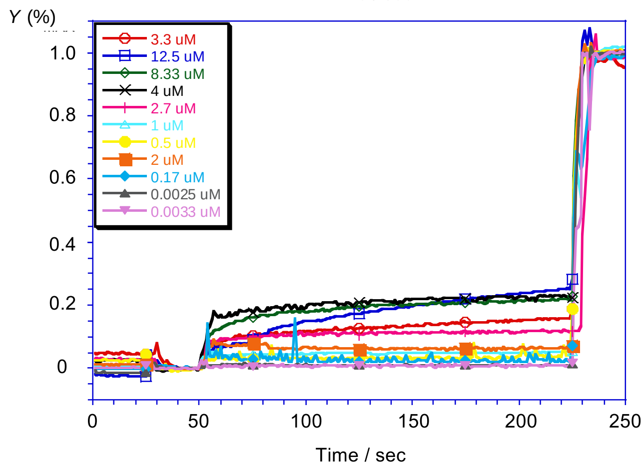

Y (%)
3.3 uM
12.5 uM
8.33 uM
4 uM
2.7 uM
1 uM
0.5 uM
2 uM
0.17 uM
0.0025 uM
0.0033 uM
Time / sec

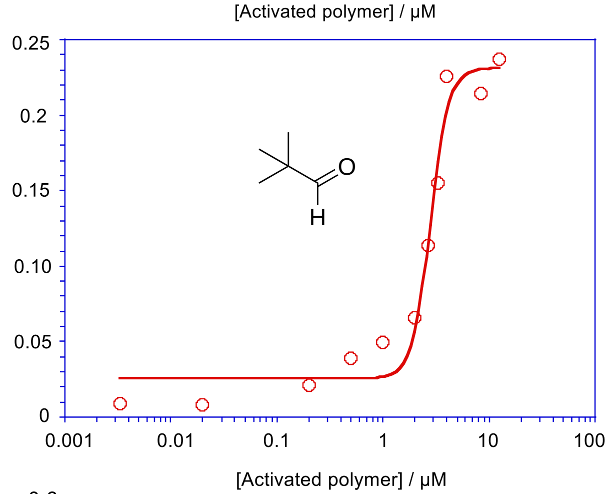

O
H
[Activated polymer] / μM

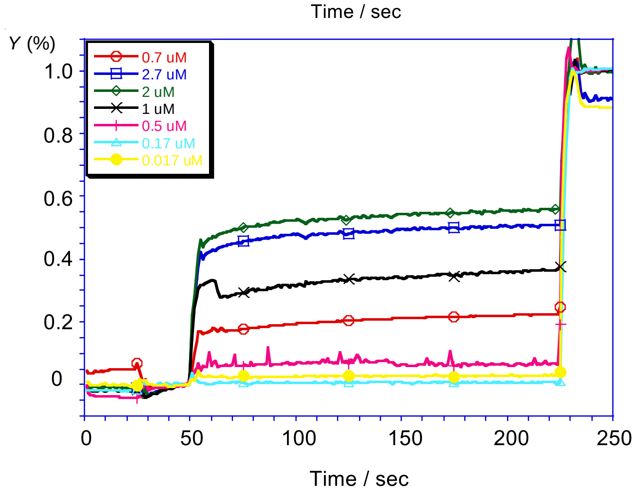

Y (%)
0.7 uM
2.7 uM
2 uM
1 uM
0.5 uM
0.17 uM
0.017 uM
Time / sec

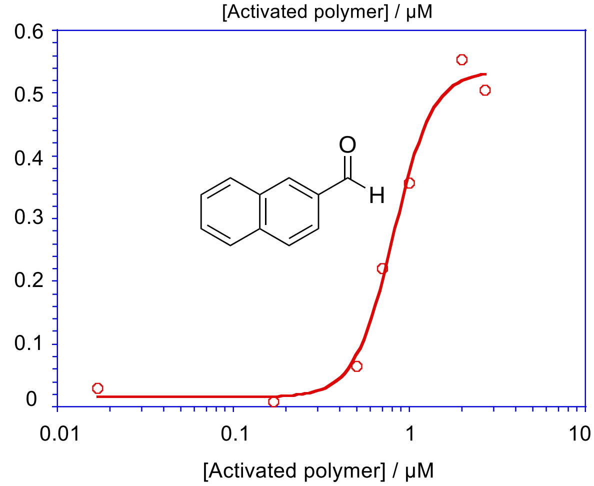

O
H
[Activated polymer] / μM

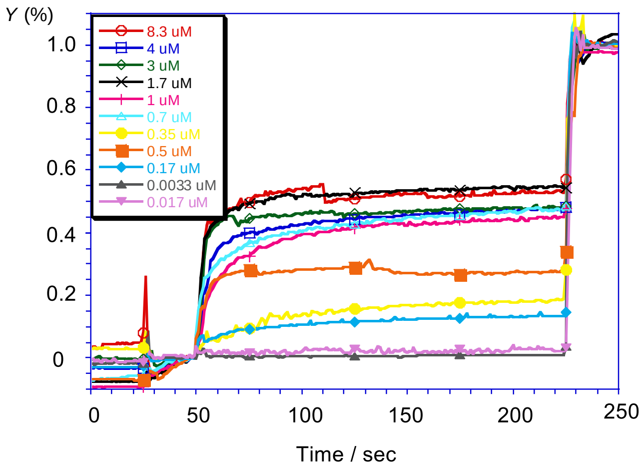
Y (%)
8.3 uM
4 uM
3 uM
1.7 uM
1 uM
0.7 uM
0.35 uM
0.5 uM
0.17 uM
0.0033 uM
0.017 uM
Time / sec

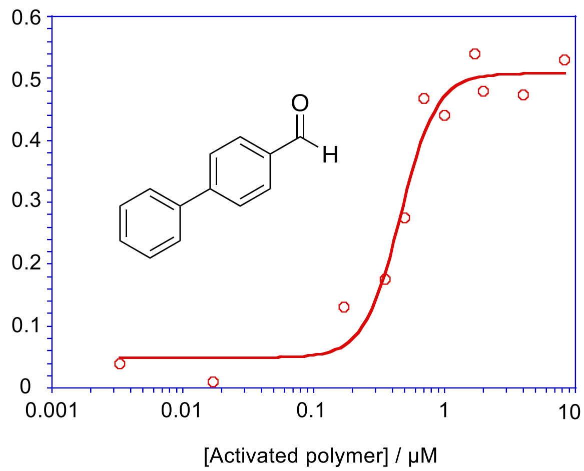
O
H
[Activated polymer] / μM

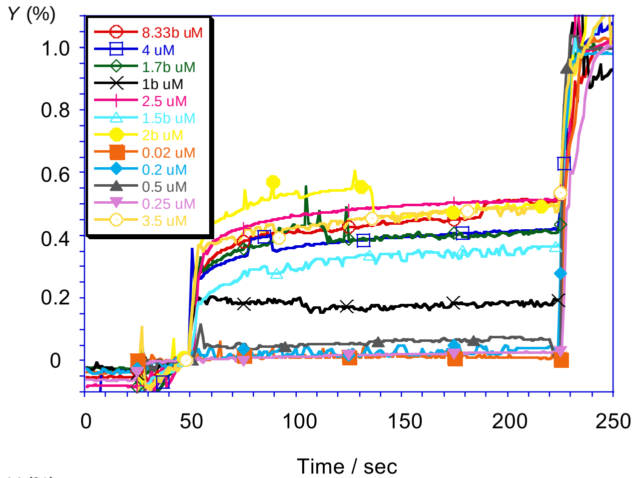
Y (%)
8.33b uM
4 uM
1.7b uM
1b uM
2.5 uM
1.5b uM
2b uM
0.02 uM
0.2 uM
0.5 uM
0.25 uM
3.5 uM
Time / sec

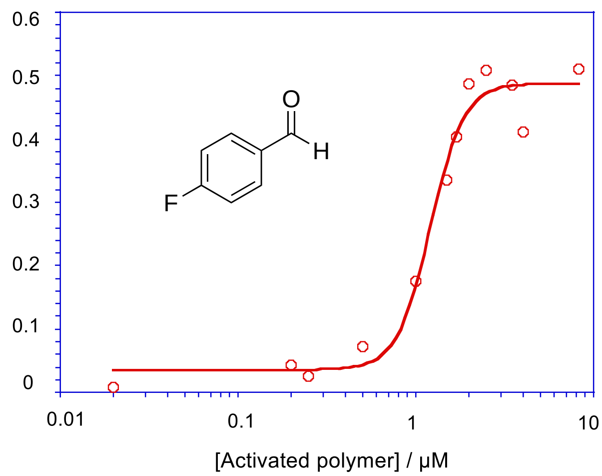
O
H
F
[Activated polymer] / μM

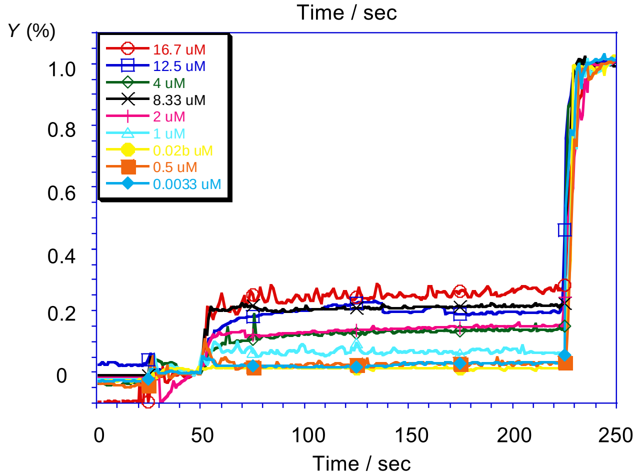
Y (%)
16.7 uM
12.5 uM
4 uM
8.33 uM
2 uM
1 uM
0.02b uM
0.5 uM
0.0033 uM
Time / sec

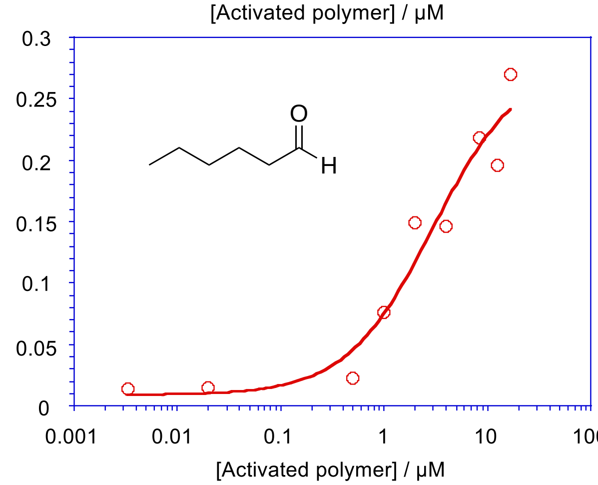
O
H
[Activated polymer] / μM

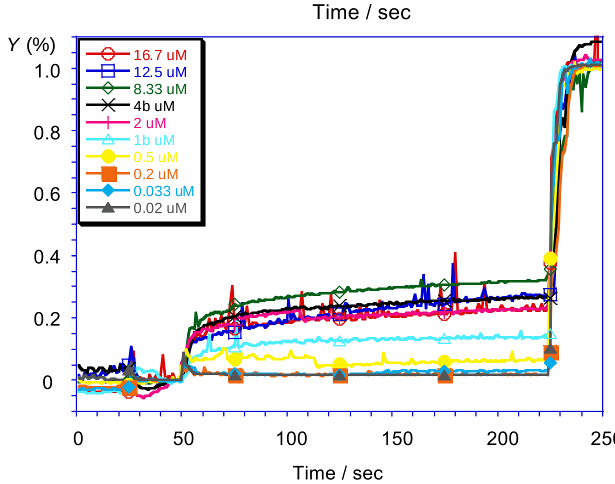
Y (%)
16.7 uM
12.5 uM
8.33 uM
4b uM
2 uM
1b uM
0.5 uM
0.2 uM
0.033 uM
0.02 uM
Time / sec

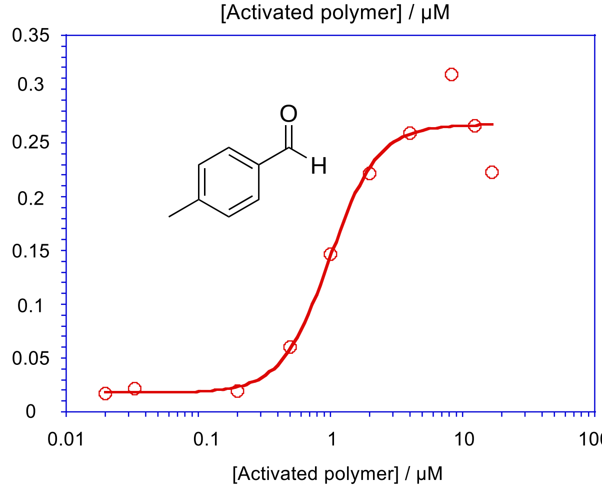
O
H
[Activated polymer] / μM

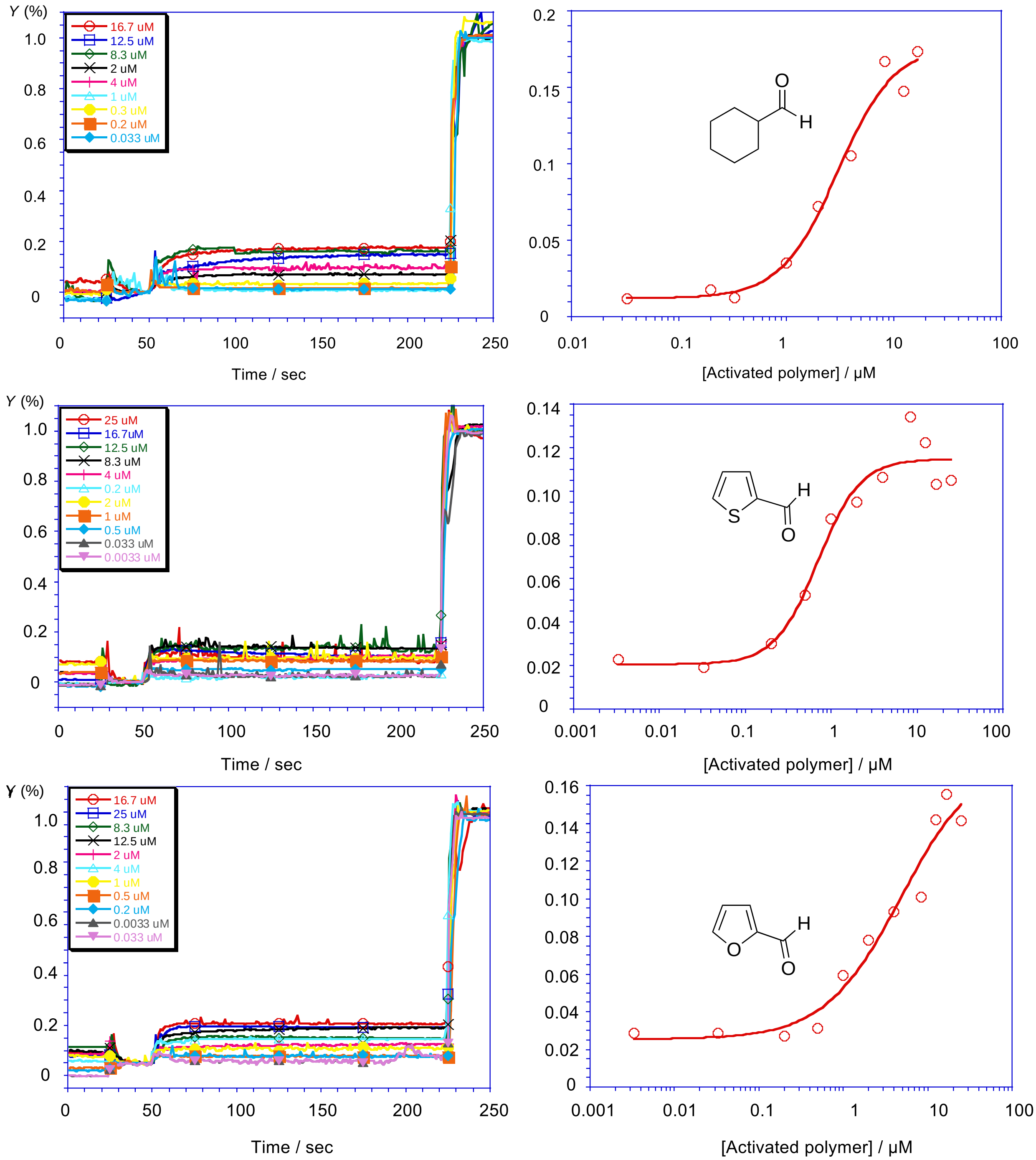

Figure S8: Changes to fractional emission intensity *I*(t) (A) and dose-response curve (B) for the transport of Herring DNA (2 μM) in EYPC-LUVs ⊃ HPTS/DPX with increasing concentrations of activated polymer (χ**1**: 0.85 and χ**Hydrophobic**: 0.15) (**Table S2**).

Table S2: EC_{50} (μM), Y_{MAX} (%) and n for the transport of Herring DNA (125 μM) in EYPC-LUVs⊃HPTS/DPX with increasing concentrations of activated polymer **P1(1)$_{85}$(n)$_{15}$** prepared from 15% of hydrophobic aldehyde (**2-18**) and 85% of **1**. All experiments were done in triplicate. **P1(1)$_{85}$(n)$_{15}$** stands for **P1:** Polymer 1; (**1**)$_{85}$: guanidinium aldehyde at a χ**1** = 0.85; (**n**)$_{15}$: hydrophobic aldehyde at a χ**n** = 0.15.

Polymer	Aldehyde Number	Aldehyde	EC_{50} (μM)	Y_{max} (%)	n
P1(1)$_{85}$**(2)**$_{15}$	**2**	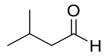	5.73 ± 2.36	35.94 ± 7.80	1.47 ± 0.61
P1(1)$_{85}$**(3)**$_{15}$	**3**	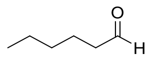	2.95 ± 2.25	28.00 ± 8.4	1.04 ± 0.57
P1(1)$_{85}$**(4)**$_{15}$	**4**	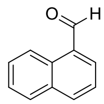	0.81 ± 0.05	53.50 ± 2.70	3.91 ± 0.94
P1(1)$_{85}$**(5)**$_{15}$	**5**	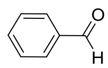	4.10 ± 0.74	56.00 ± 5.00	2.92 ± 1.48
P1(1)$_{85}$**(12)**$_{15}$	**12**	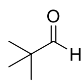	5.10 ± 1.40	23.10 ± 2.30	2.80 ± 0.17
P1(1)$_{85}$**(13)**$_{15}$	**13**	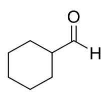	3.01 ± 0.61	17.74 ± 1.68	1.64 ± 0.50
P1(1)$_{85}$**(14)**$_{15}$	**14**	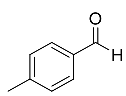	0.98 ± 0.17	26.71 ± 1.51	2.37 ± 0.89
P1(1)$_{85}$**(15)**$_{15}$	**15**	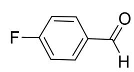	1.21 ± 0.08	48.80 ± 1.90	4.60 ± 1.19
P1(1)$_{85}$**(16)**$_{15}$	**16**	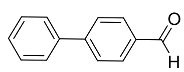	0.46 ± 0.05	50.9 ± 2.60	3.13 ± 1.02
P1(1)$_{85}$**(17)**$_{15}$	**17**	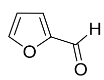	4.83 ± 3.30	17.58 ± 4.10	0.96 ± 0.39
P1(1)$_{85}$**(18)**$_{15}$	**18**	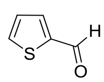	0.70 ± 0.16	11.50 ± 0.56	1.75 ± 0.66

Cells Lines and Culture

HeLa cells stably expressing enhanced green fluorescent protein (HeLa-EGFP) were maintained in Dulbecco´s Modified Eagle´s Medium from Life Technologies™ (DMEM, high glucose, GlutaMAX™, pyruvate) supplemented with 10% (v/v) of fetal bovine serum (FBS) from Hyclone™ (Thermo Fisher Scientific Inc) and 500 $\mu g \cdot mL^{-1}$ of Geneticin® (Life Technologies™). Transfection of HeLa-EGFP was performed in the same medium, free of serum and antibiotics. Cells incubations were performed in a water-jacketed 37 ºC/5% CO_2 incubator.

- ***In Vitro* Screening for siRNA Delivery**

Activated polymer stock solutions were prepared in DMSO/$AcOH_{aq}$ (v/v) as described above and diluted with DMSO to afford a range of stock solutions concentrations of (3-0.1 mM). These stock solutions were then sequentially diluted with DMEM medium free of serum and antibiotics to afford the final concentration in cells (17-0.3 µM). The solutions of siRNA/ activated polymer polyplexes were freshly prepared prior to the transfection experiments. 10 µl of the siRNA solution (1 µM in DMEM) and 8 µl of activated polymer solution at variable concentrations in DMEM, high Glucose, GlutaMAX™, 10% (v/v) DMSO, were added to 190 µl DMEM, high glucose, GlutaMAX™, and the mixture was homogenized by pipetting. Then, cell medium was aspirated from 96-well plate and 50 µl of the mixture was added in each well. The final concentration of DMSO in each well was 0.125% (v/v). After 4 hours of transfection the medium was aspirated and replaced by 100 µl of fresh DMEM, high glucose, GlutaMAX™, pyruvate, supplemented with 10% (v/v) FBS. The total fluorescence knockdown was quantified after 72 hours in a microwell plate reader (Infinite F2000pro Tecan). For the best performing activated polymers, at the most efficient and less toxic concentration, siRNA solutions were prepared at different concentrations (Table S3). For control and normalization experiments forward transfection with Lipofectamine® RNAiMAX was performed according to the supplier instructions. All experiments were done in triplicate.

Table S3: Conditions employed in the optimization of the transfection experiments. All experiments were done at a final concentration of activated polymer **P1(1)**$_{\chi 1}$**(2)**$_{\chi 2}$ of 4 μM.

χ**2** [a]	[siRNA] (nM)[b]	siRNA (pmol)
0.05	14	1.5
0.15	0	0
	1.75	0.2
	3.5	0.4
	7	0.8
	14	1.5
	28	3
0.3	14	1.5
0.4	14	1.5

[a] Molar fraction of χ**1** = 1 - χ**2**. [b][siRNA] refers to the final concentration of siRNA.

- **Transfection in HeLa-EGFP**

HeLa-EGFP were transfected either with Ambion® Silencer® GFP (EGFP) siRNA (siEGFP) from Life Technologies™ or scramble RNA (siMock, All Star Negative Control) from Qiagen. 72 h post siRNA transfection, cell supernatant was removed and EGFP expression was measured by fluorimetry (λ_{ex} 489nm; λ_{em} 509nm). The percentage of EGFP knockdown was calculated as the percentage of fluorescence decrease observed in cells transfected with siEGFP compared to transfection with siMock with the same reagents at the same conditions. Percentage of cell viability was calculated as the percentage of remaining fluorescence in samples transfected with siMock compared to non-transfected cells in DMEM, high glucose, GlutaMAX™ and pyruvate, supplemented with 0.125% (v/v) DMSO.

Lipofectamine® RNAiMAX was used as a positive control of siRNA transfection in the *in vitro* screening of activated polymers in HeLa-EGFP. The quality of the transfection experiments was assessed calculating the *Z-factor* using Equation S3,

$$\text{Equation S3: } Z\text{–}factor = 1 - \frac{3(\sigma_p+\sigma_n)}{|\mu_p-\mu_n|}$$

In where μ stands for the mean value and σ for the corresponding standard deviation of relative fluorescence units (RFU) of both the positive (*p* = cells transfected with mixture of siEGFP and activated polymers or Lipofectamine® RNAiMAX) and negative (*n* = non-transfected cells in medium supplemented with 0.125% (v/v) DMSO) controls (μ_p, σ_p, and μ_n, σ_n). A *Z-factor* between 0.5 and 1.0 indicates an excellent assay, 0.5 is equivalent to a separation of 12 standard deviations between μ_p and μ_n (**Figure S9**).

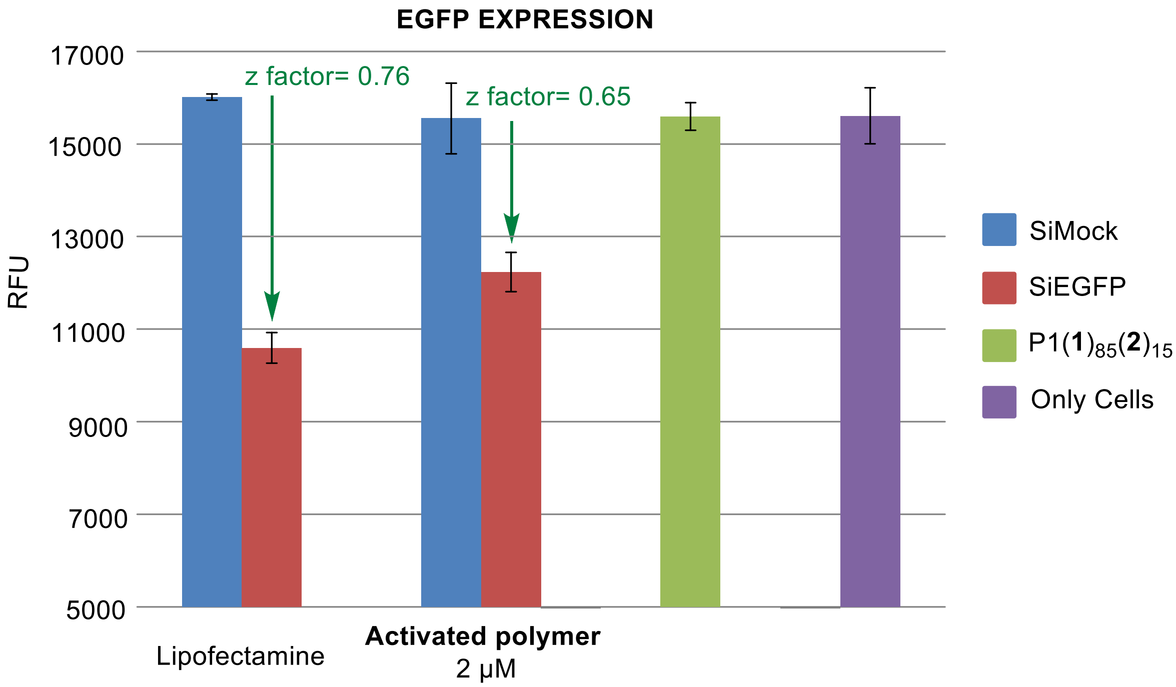

Figure S9: RFUs and *Z-factor* for the knock-down of EGFP in HeLa-EGFP with activated polymer (χ**1**: 0.85 and χ**Hydrophobic**: 0.15) or Lipofectamine® RNAiMAX.

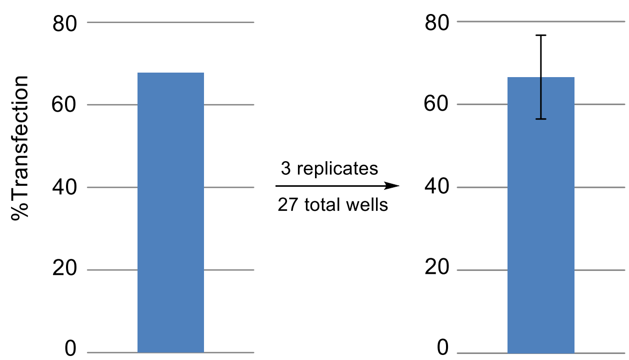

Figure S10: Transfection efficiency (percent of EGFP Knockdown) in HeLa-EGFP by 2 μM activated polymer (χ**1**: 0.85 and χ**Hydrophobic**: 0.15).

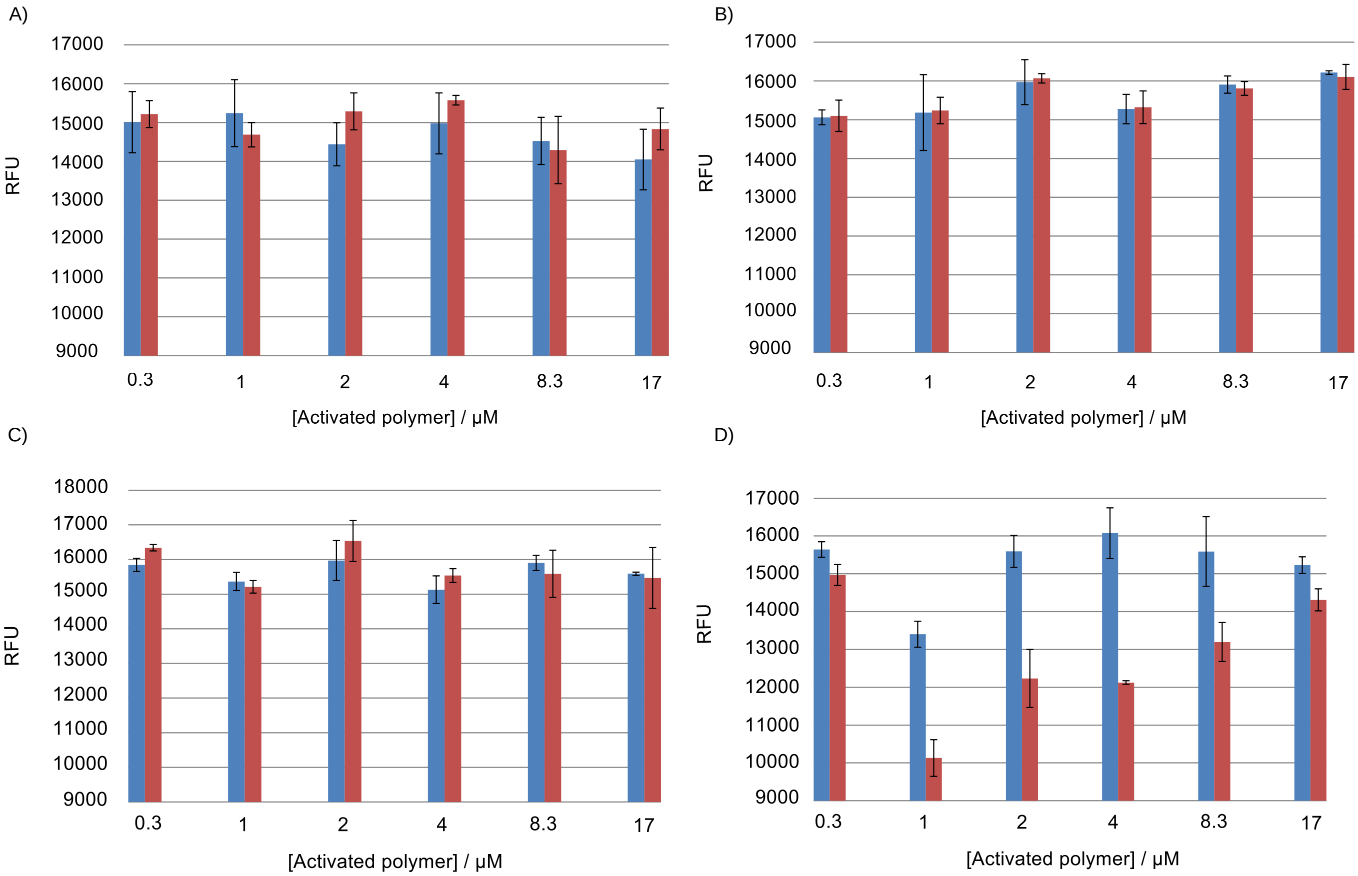

Figure S11: Relative fluorescent units (RFUs) for the siRNA transfection experiments. In all cases and in all concentrations, transfection experiments were performed with siRNA (red) and *siMock* (negative control experiment in blue). In all cases the molar fractions were χ**1** = 0.85 and χ**Hydrophobic** = 0.15. a) Hexanal (**3**), **P1(1)$_{85}$(3)$_{15}$**, b) Naphthaldehyde (**4**), **P1(1)$_{85}$(4)$_{15}$**, c) Benzaldehyde (**5**), **P1(1)$_{85}$(5)$_{15}$**, d) Knock-down of EGFP in HeLa-EGFP is only observed for isovaleraldehyde (**2**), **P1(1)$_{85}$(2)$_{15}$**. A satisfactory *Z* factor was obtained for the different concentrations: 0.3 µM: 0.91, 1 µM: 0.89, 2 µM: 0.65, 4 µM: 0.46; 8 µM: 0.79, 17 µM: 0.88.

To optimize the concentration of activated polymer, HeLa-EGFP were treated with siEGFP/ activated polymer polyplexes with different final concentrations of activated polymer or different molar fractions of **2** (**Figure S12**).

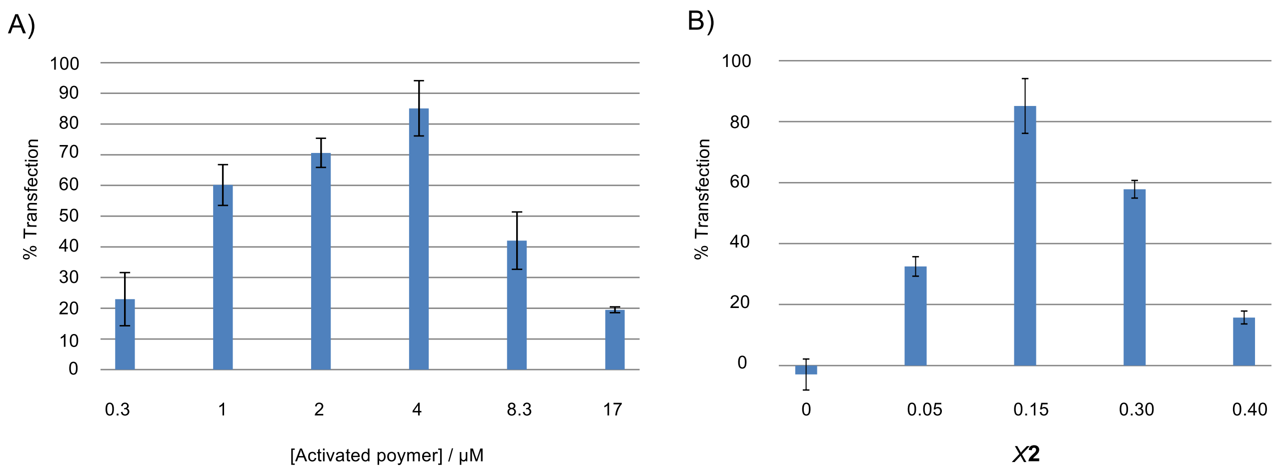

Figure S12: A) Transfection efficiency in HeLa-EGFP at a constant siRNA concentration (14 nM) and increasing concentrations of activated polymer (χ**1** = 0.85 and χ**Hydrophobic** = 0.15). B) Transfection efficiency in HeLa-EGFP at a constant siRNA concentration (14 nM) and constant concentration of activated polymer (4 µM) prepared from different molar fractions of **2** (χ**1** = 1- χ**2**).

To optimize the concentration of siRNA, HeLa-EGFP were treated with siEGFP/ activated polymer polyplexes, at a constant activated polymer concentration (12.25 µM) and with variable siEGFP concentrations (**Figure S13**).

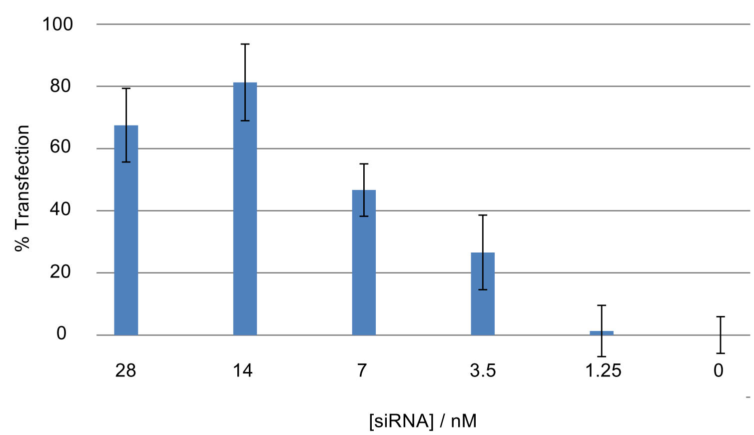

Figure S13: Transfection efficiency in HeLa-EGFP at a constant concentration of activated polymer (4 µM, χ**1** = 0.85 and χ**Hydrophobic** = 0.15) and decreasing concentrations of siEGFP.

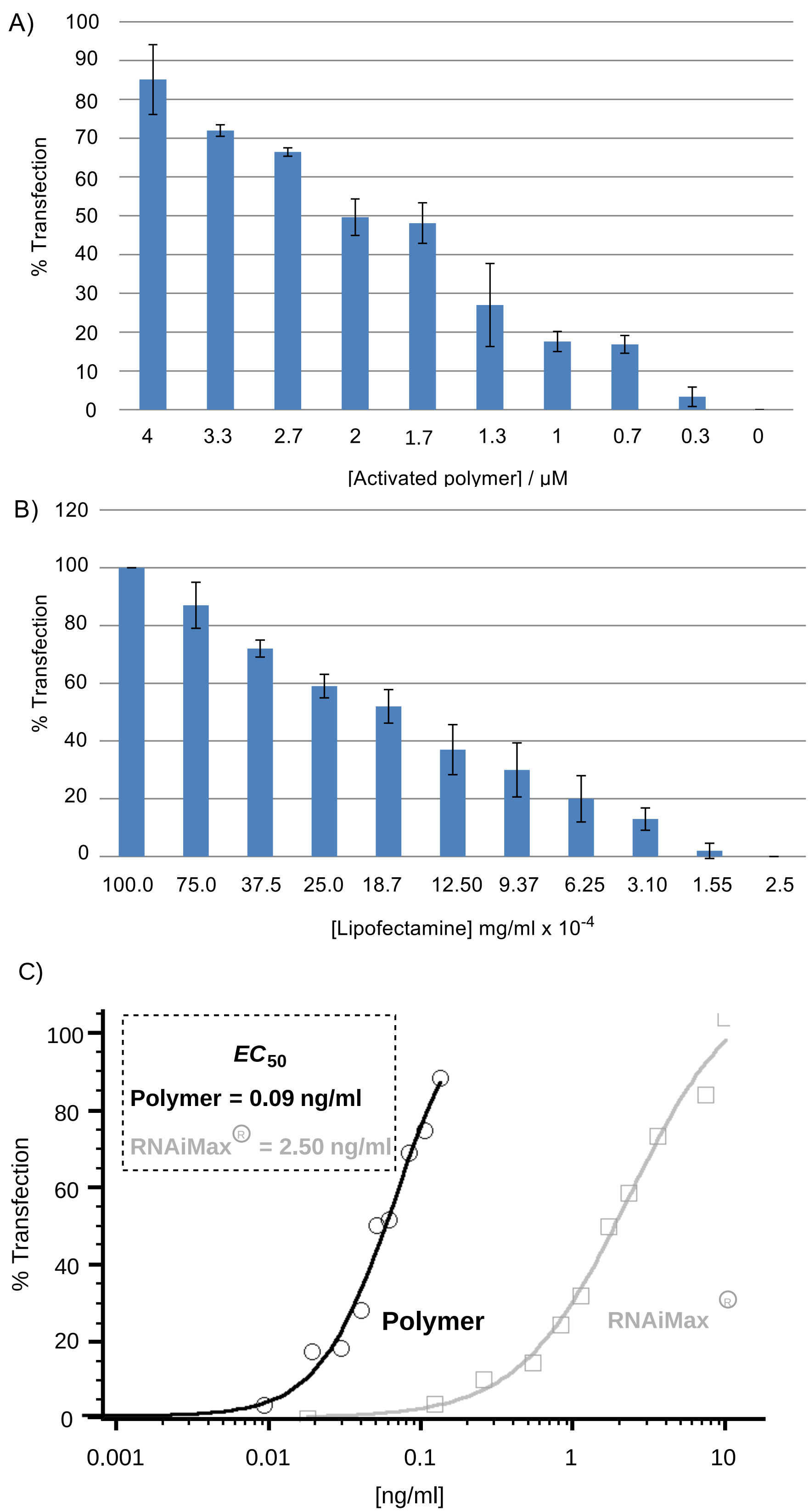

Figure S14: Transfection efficiency in HeLa-EGFP at a constant concentration of activated polymer (4 µM, χ**1** = 0.85 and χ**Hydrophobic** = 0.15) and increasing concentrations of siEGFP.

- **Cell viability: MTT Assay**[S4]

Cell viability was established by a standard MTT assay (Fig. S15).[S4] One day before the assay, a suspension of HeLa-EGFP cells was plated in 96-well tissue culture plates (Costar 96 Flat Bottom Transparent Polystyrol) by adding 100 µl (~30.000 cells) per well. The next day, the medium was aspirated and cells were incubated in DMEM containing 10% Fetal Bovine Serum (FBS) in the presence of activated polymer (50 µl/well). After 4 h of incubation at 37ºC, the medium was aspirated and replaced by fresh medium (DMEM) containing 10% FBS (100 µl). Control cells were incubated with cell culture medium (100 µl final medium). The viability was measured by quantifying the cellular ability to reduce the water-soluble tetrazolium dye 3-4,5-dimethylthiazole-2,5-diphenyl tetrazolium bromide (MTT) to its insoluble formazan salt as follows. At 72 h, MTT (5 mg/ml in PBS, 10 µl/well) was added to the wells and the cells were further incubated for 4 h. The supernatant was carefully removed and the water-insoluble formazan salt was dissolved in DMSO (100 µl/well). The absorbance at 560 nm was measured. Data points were collected in triplicate and expressed as normalized values for untreated control cells (100%).

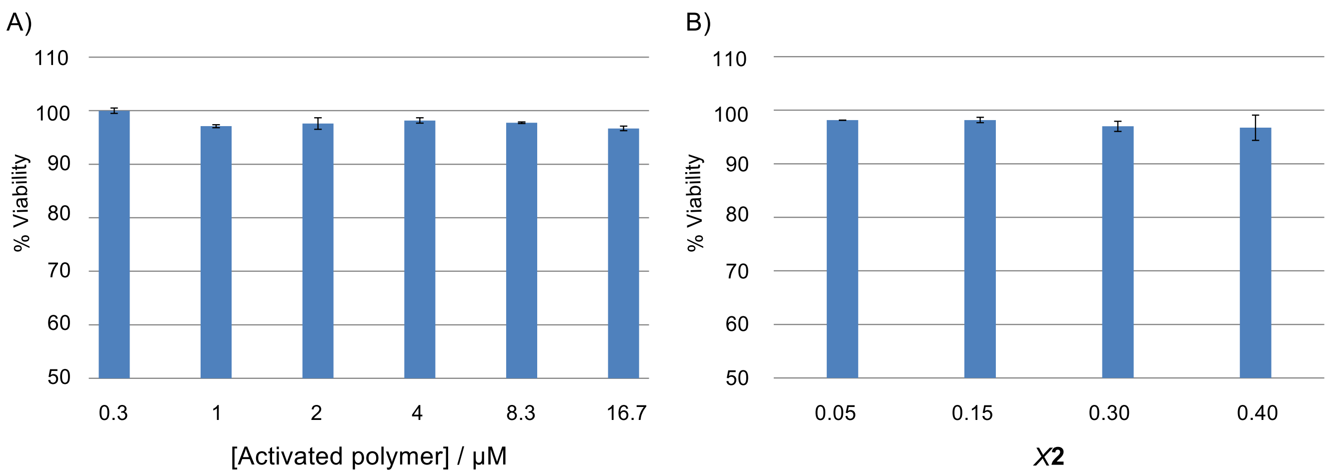

Figure S15: Cell viability from MTT assay in HeLa-EGFP cells at a constant siRNA concentration (14 nM). A) Increasing concentrations of activated polymer (χ**1** = 0.85 and χ**Hydrophobic** = 0.15). B) Constant concentration of activated polymer (4 µM) and with different molar fractions of **2** (χ**1** = 1- χ**2**).

To further investigate cell viability in the presence of the parent polymer **P1**, the activated polymer **$P_1(1)_{85}(2)_{15}$** and the Lipofectamine® RNAiMAX we performed additional viability experiments (in HeLa cells) at the working concentrations of the transfection experiments. Following the same protocol described above, but without medium replacement after the initial 4 hours, cells were incubated in the presence of either Lipofectamine® RNAiMAX **P1**, the activated polymer **$P_1(1)_{85}(2)_{15}$** (**Figure S16**).

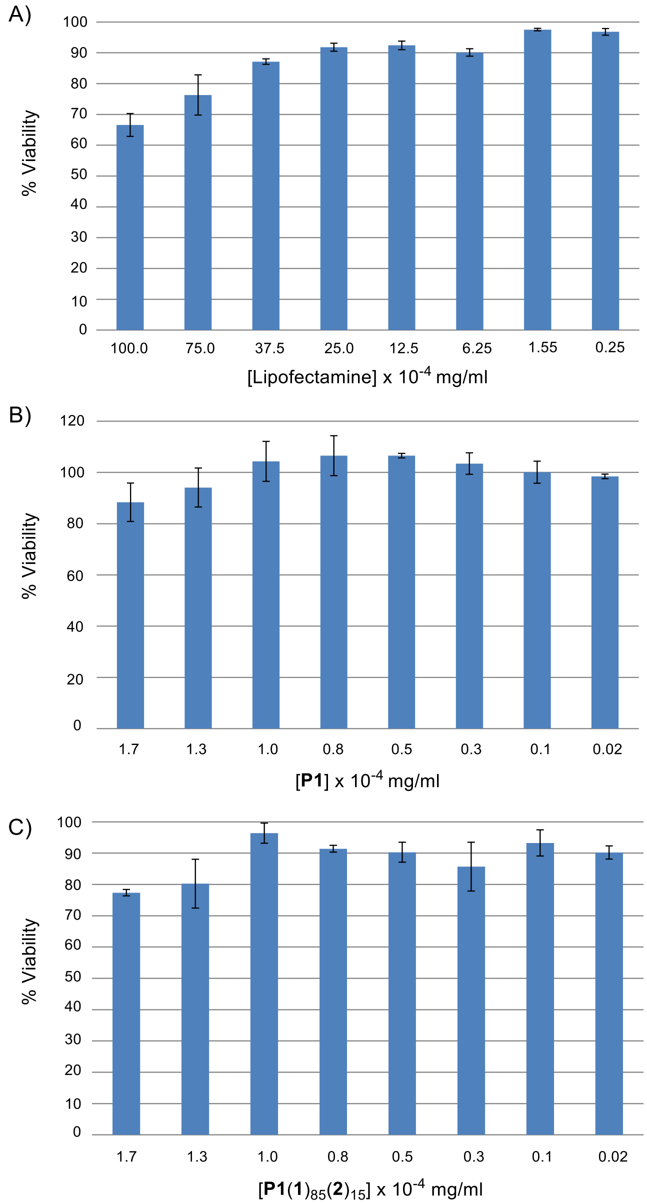

Figure S16: Comparison of cell viability (MTT assay in HeLa cells) at the working concentrations of the transfection experiments for the polymer and for the Lipofectamine® RNAiMAX (A), **P1** (B) and Activated polymer **= $P_1(1)_{85}(2)_{15}$** (C). In all cases [siRNA] = 14 nM.

Characterization of Polyplexes

- **Hydrodynamic Radius and ζ-potential**

10 μl of activated polymer's stock solutions were diluted in MilliQ water to afford the desired final concentrations (67-4 μM) and were mixed with a solution of siRNA (10 nM, 995 μl in MilliQ water) before measuring. To measure activated polymer alone, the 995 μl of siRNA solution was replaced by the same amount of bi-distilled water. Bi-distilled water was filtered through a nylon syringe filter (0.45 μm) before use. All experiments were performed at 25 ºC and the mean values and standard deviations obtained from triplicates.

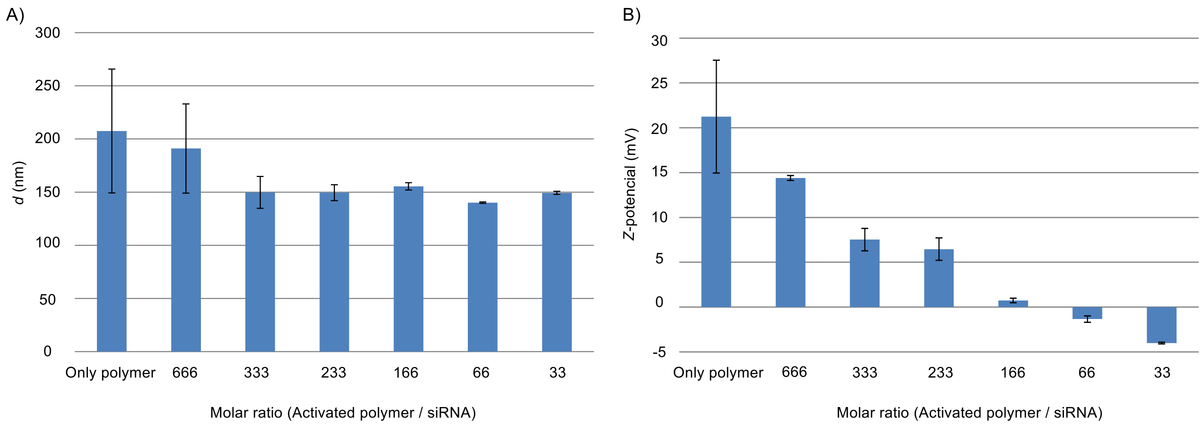

Figure S17: Diameter (A) and ζ-potential (B) for representative siMock/Activated polymer polyplexes. [siMock] = 14 nM. Activated polymer (χ**1** = 0.85 and χ**2** = 0.15).

- **Gel Retardation Assay**

Pre-mixed siRNA/Activated polymer polyplexes (3 pmol) were loaded onto a 2% agarose gel. The gels were run at 100 V for 60 min in TAE buffer (40 mM Tris, 20 mM acetic acid, and 1 mM EDTA) (**Figure S18**).

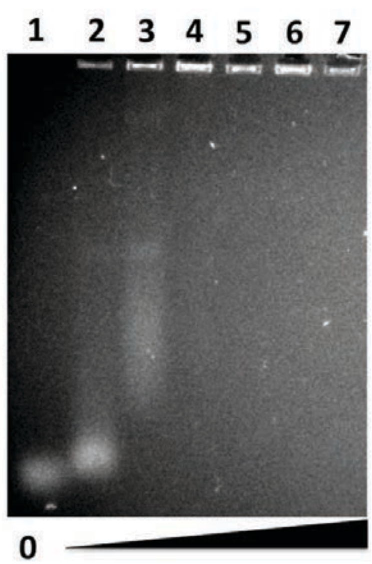

Figure S18: Gel retardation assay. siMock (lane 1) and siMock/Activated polymer polyplexes with molar ratios of of 2 (lane 2), 4.3 (lane 3), 8.3 (lane 4), 16.7 (lane 5), 33.3 (lane 6) and 66.7 (lane 7) were loaded. [siRNA] = 14 nM in all cases. [Activated polymer] = [$\mathbf{P_1(1)_{85}(2)_{15}}$] = 28 nM (lane 2), 60 nM (lane 3), 0.12 μM (lane 4), 0.23 μM (lane 5), 0.46 μM (lane 6), 0.93 μM (lane 7).

Additional Figures

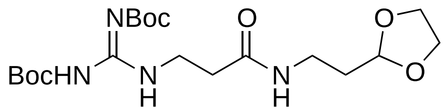

8

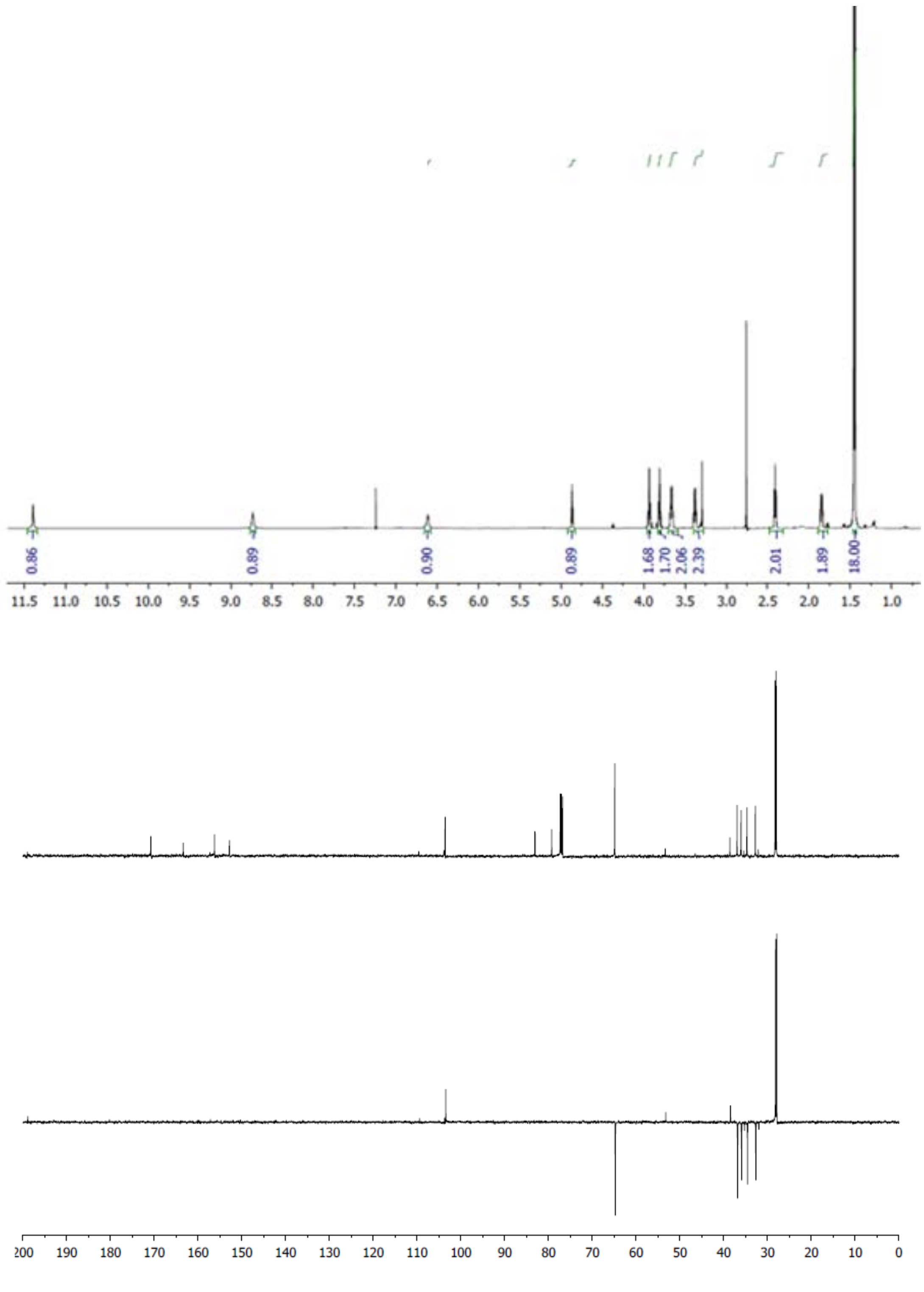

Figure S19: ^{1}H-NMR and ^{13}C-NMR in $CDCl_3$ spectra of compound **8**.

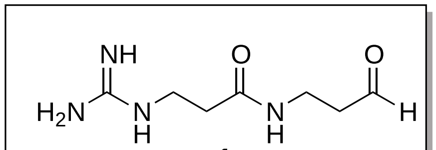

1

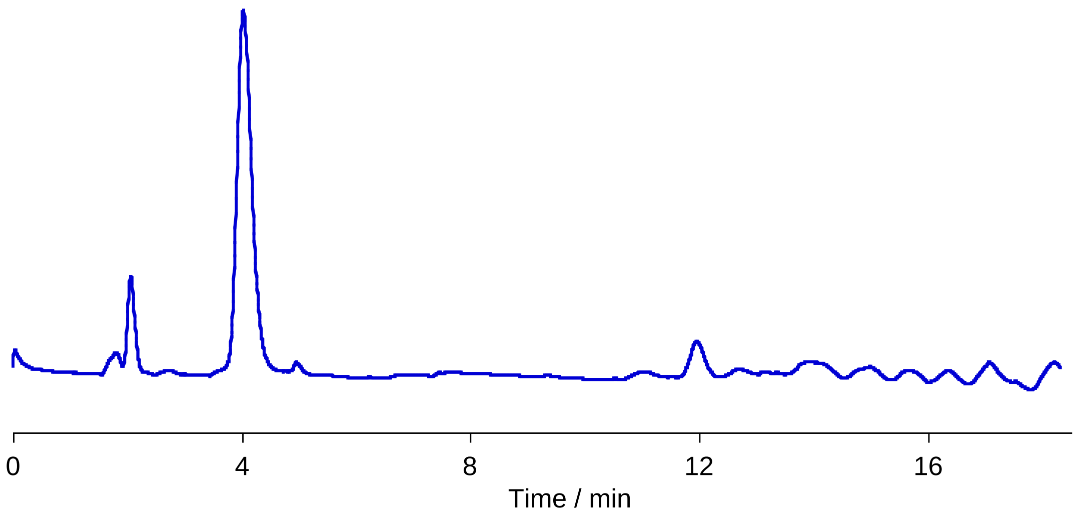

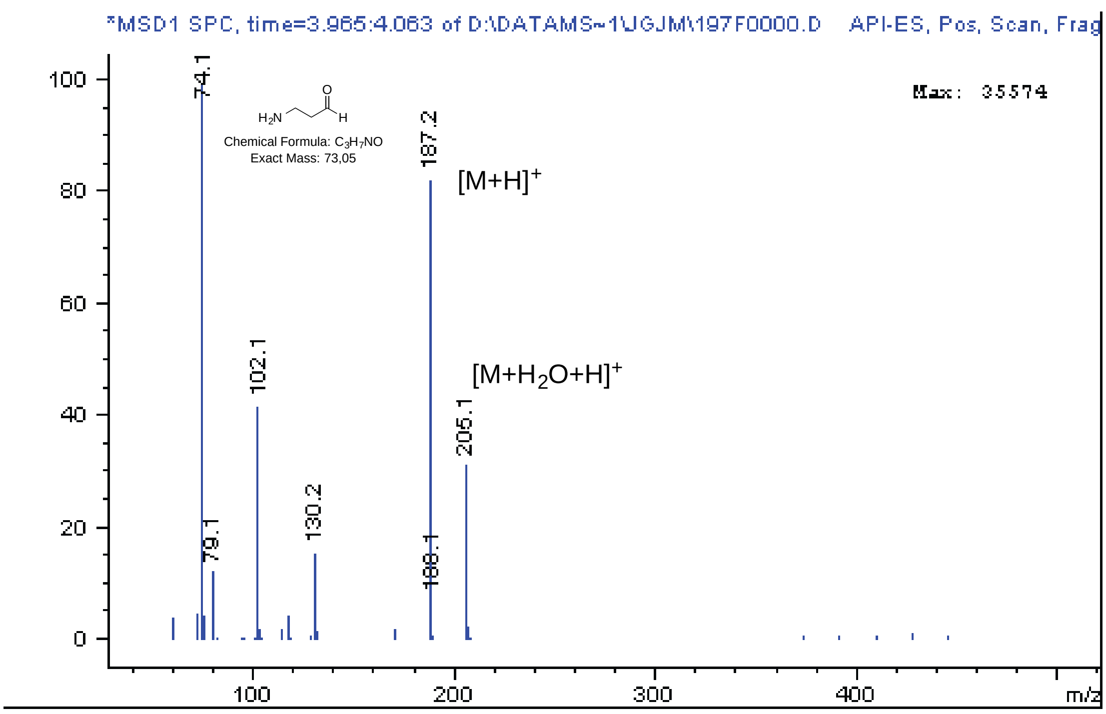

Figure S20: RP-HPLC [Nucleosil 100-7 C18, H_2O (0.1% TFA)/CH_3CN (0.1% TFA) 100:0 (0→10 min), 100:0→75:35 (5→35 min), 0:100 (>35 min)] (R_t 4.0 min) and ESI-MS for compound **1**.

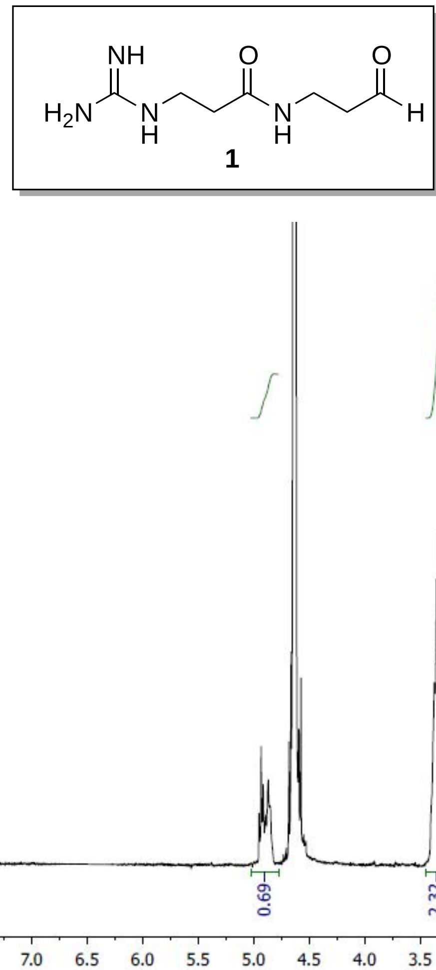

Figure S21: ^{1}H-NMR spectra in D_2O of compound **1**.

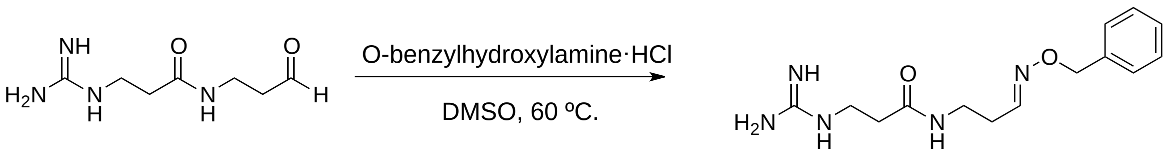

1 **9**

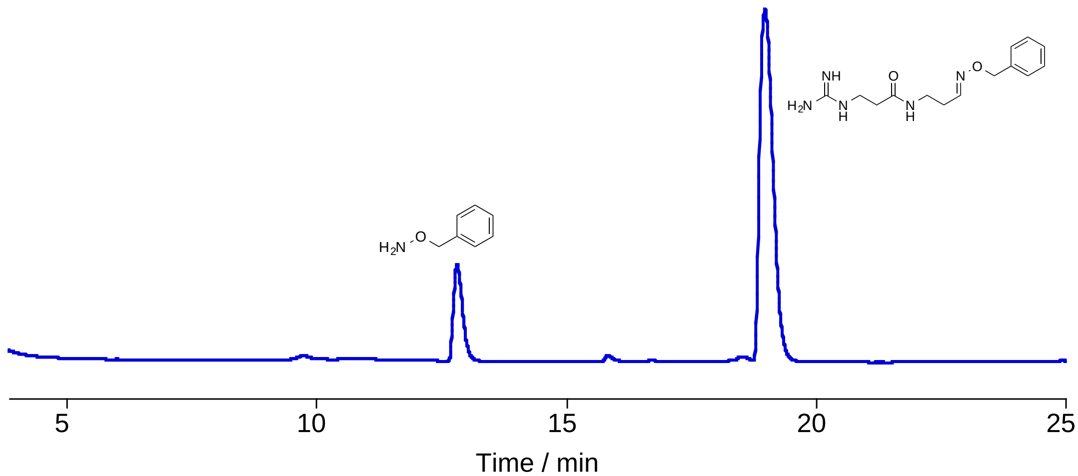

Figure S22: RP-HPLC [Nucleosil 100-7 C18, H_2O (0.1% TFA)/CH_3CN (0.1% TFA) 100:0→80:20 (5→35 min), 0:100 (>35 min)] for the reaction of **1** with benzyl hydroxylamine. The chromatogram after oxime formation shows the presence of the final compound **9** and the excess of hydroxylamine.

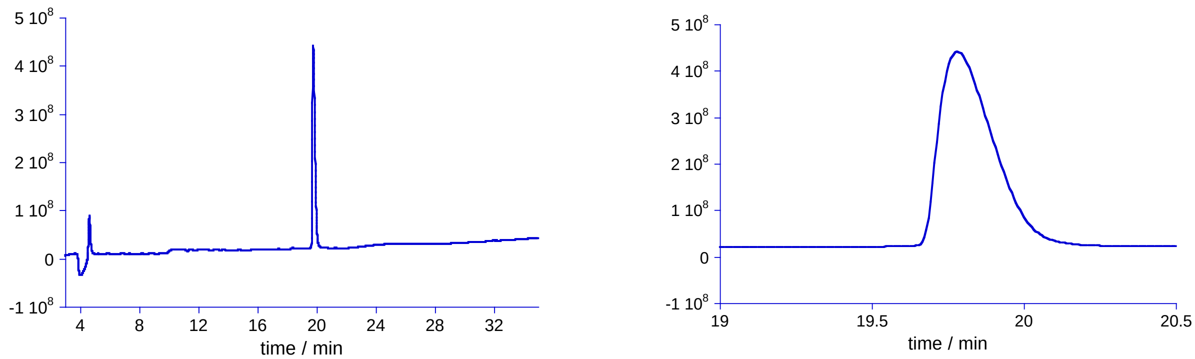

Figure S23: RP-HPLC [Nucleosil 100-7 C18, H_2O (0.1% TFA)/CH_3CN (0.1% TFA) 100:0 (0→5 min), 100:0→35:75 (5→35 min), 0:100 (>35 min)] of compound **9**.

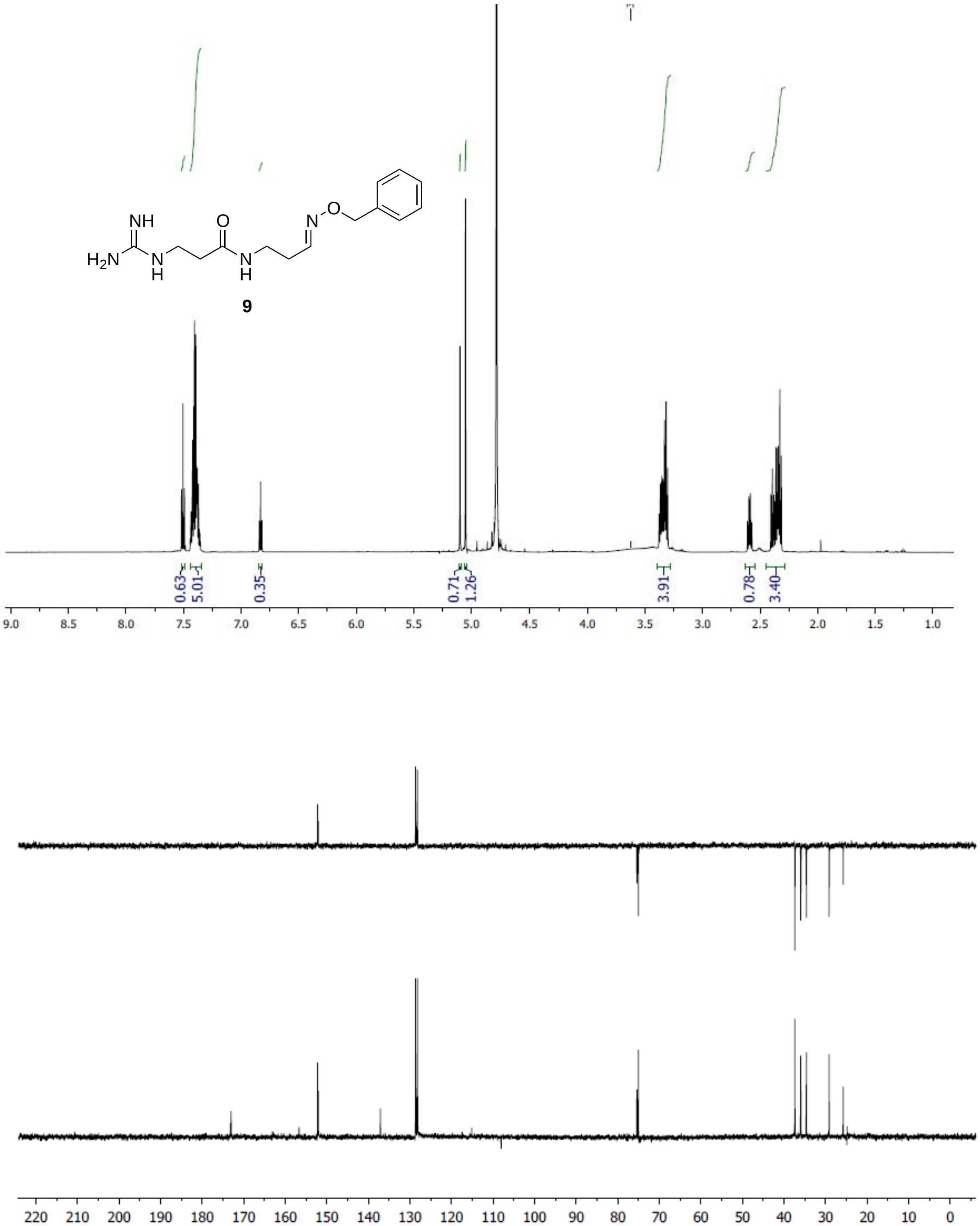

Figure S24: ^{1}H-NMR and ^{13}C-NMR spectra in D_2O of compound **9**.

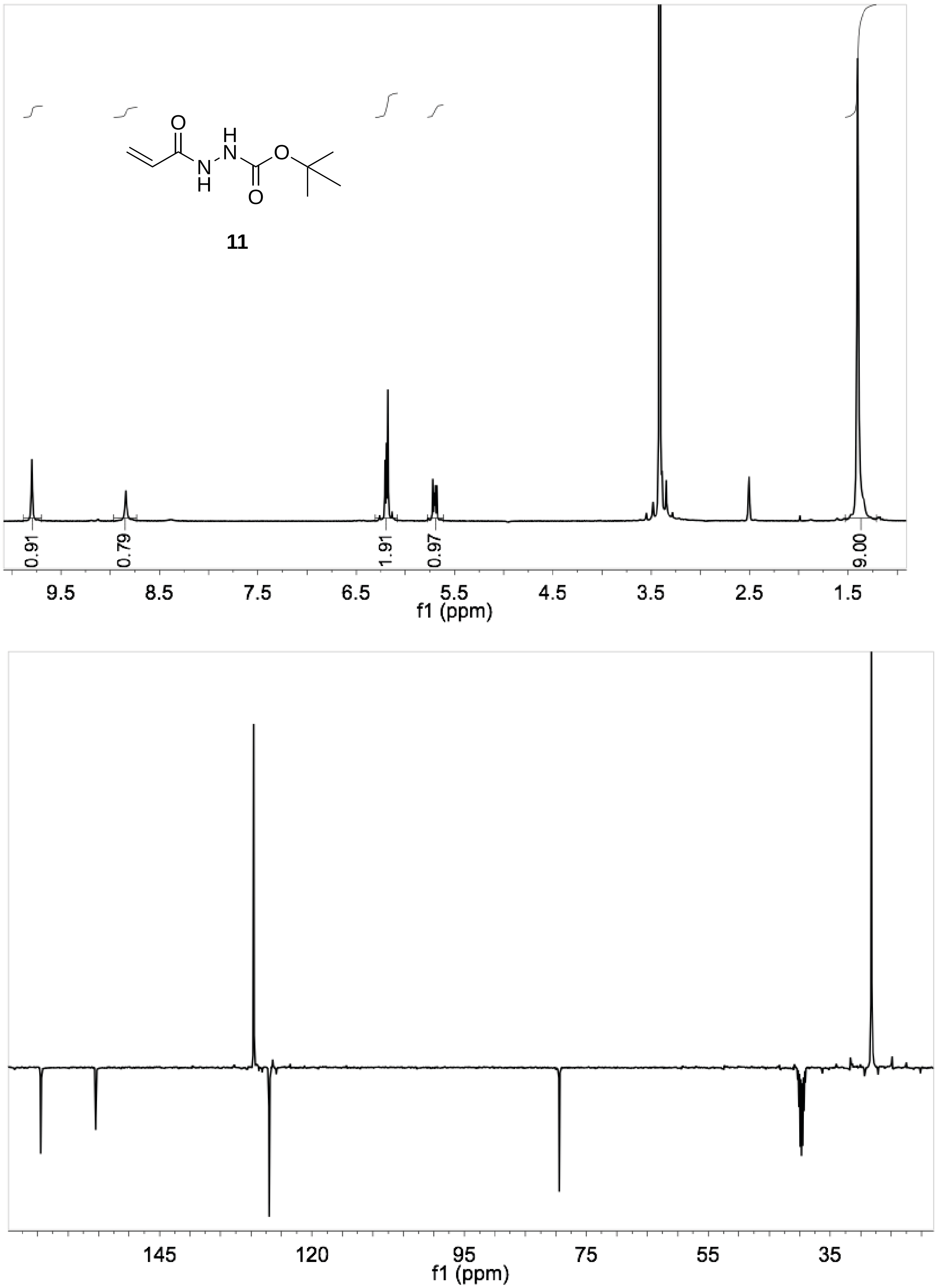

Figure S25: ^{1}H-NMR and ^{13}C-NMR spectra in DMSO-*d6* for compound **11**.

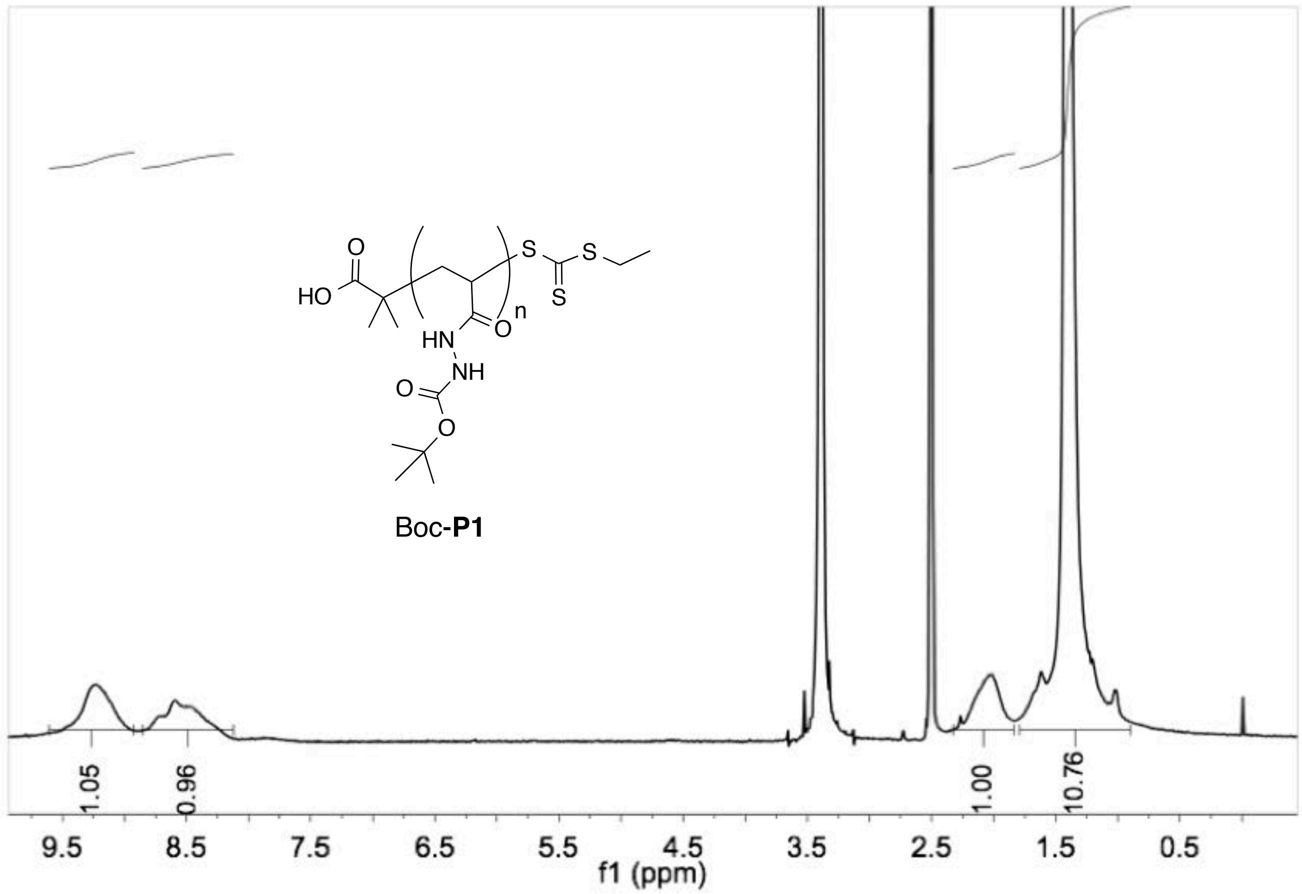

Figure S26: ^{1}H-NMR spectra in DMSO-*d6* of **Boc-P1**.

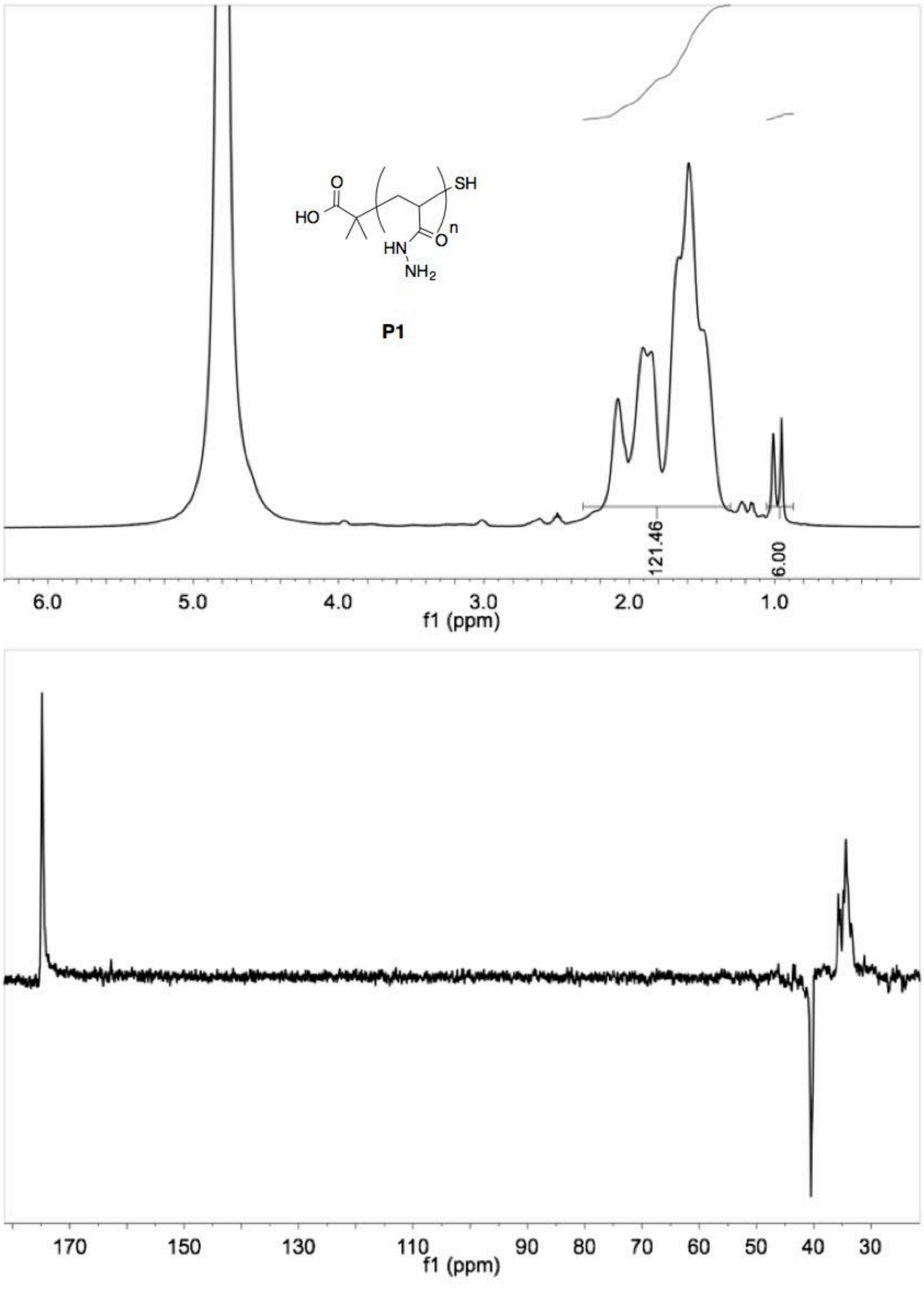

Figure S27: ^{1}H-NMR and ^{13}C-NMR spectra in DMSO-*d6* of **P1**.

Supporting References

S1. J. Skey, R. K. O'Reily, *Chem. Commun.* **2008**, *35*, 4183–4185.

S2. N. S. Freeman, Y. Tal-Gan, S. Klein, A. Levitzki, C. Gilon, *J. Org. Chem.* **2011**, *76*, 3078–3085.

S3. S. Y. Tamura, J. E. Semple, R. J. Ardecky, P. Leon, S. H. Carpenter, G. Yu, B. M. Shamblin, M. I. Weinhouse, W. C. Ripka, R. F. Nutt, *Tetrahedron Lett.*, **1996**, *37*, 4109–4112.

S4. X. Li, J. Guo, J. Asong, M. A. Wolfert, G.-J. Boons, *J. Am. Chem. Soc.* **2011**, *133*, 11147–11153.

Conclusions

In this thesis, a case has been made regarding the usefulness of polymer scaffolds as tools for the synthesis of functional polymers. The argument was that functional polymers, derived from a polymer scaffold, require the synthesis of one monomer and only one subsequent polymerisation. As such, all functional polymers derived would have the same degree of polymerisation, reducing the number of characterisation steps required. Furthermore, complex functional groups could be introduced onto polymers in situations where the corresponding functionalised monomer would be difficult to polymerise using existing techniques. It has been argued that polyhydrazides could be useful scaffolds towards the synthesis of functional polymers for biological applications. Hydrazides react readily with aldehydes, which are commercially available with a diversity of functional groups. The reaction between hydrazides and aldehydes can be carried out in a variety of solvents including aqueous conditions and DMSO, with water as the byproduct of the reaction. This was argued to be advantageous for testing polymers for biomedical applications, as scaffolds could be functionalised and tested "*in-situ*" without the necessity of first isolating and purifying the product. This should eventually lead to a faster identification of suitable functional polymer targets with useful biological properties.

Towards this goal, several polyhydrazide scaffolds were synthesised, characterised and their functionalisation with aldehydes explored. Poly(acryloyl hydrazide) was successfully synthesised via the RAFT polymerisation of *tert*-butyl 2−acryloylhydrazine-1-carboxylate and subsequent deprotection. Different molecular weight samples were synthesised and characterised by ^{1}H and ^{13}C NMR, UV-Vis spectroscopies and SEC/GPC, and the functionalisation with aldehydes was investigated by ^{1}H NMR spectroscopy in biologically compatible solvents (i.e. aqueous conditions or mixtures of aqueous solvent and DMSO). Solvent mixtures with 95% DMSO and 5% aqueous solution (5% AcOH in H_2O) were found to provide a suitable percentage functionalisation (i.e. ~70% when 1 equivalent aldehyde was used per hydrazide side-chain) and accommodate for most of the aldehydes' and the resulting polymers' poor solubility in water. It was also found that the percentage functionalisation could be increased by using an excess of aldehyde, while using a polymer scaffold with a larger degree of polymerisation generally resulted to a small decrease. This was attributed to increased steric hinderance and unavailability of the side-chains to react. Hydrazone reduction was explored as a tool to permanently immobilise aldehydes to the scaffold, and a combination of borane-pyridine was found to be a suitable mild reducing agent. The carboxylic acid terminus of the poly(acryloyl hydrazide) scaffold was modified with a diamine to serve as an anchor for labelling with fluorescent tags (i.e. fluorescein-5-isothiocyanate) with a view to synthesise a fluorescent polymer scaffold towards libraries of fluorescent functional polymers.

Poly(4-ethynylbenzohydrazide) was synthesised via the rhodium catalysed polymerisation of *tert*-butyl 2-(4-ethynylbenzoyl)hydrazine-1-carboxylate and isolated as the polymer·TFA salt after deprotection. This scaffold was synthesised due to the helical nature of the backbone of poly(phenyl acetylenes), which could be used for the synthesis of functional polymers that mimic naturally occurring helical moieties. Stability studies via SEC/GPC and fluorescence spectroscopy showed that isomerisation from *cis*-transoid to *trans*-transoid likely occurs in solution at room temperature. Synthesis of poly(4-ethynylbenzohydrazide) via the deprotected monomer, as well as the neutralisation of the polymer·TFA salt resulted in a insoluble polymer, believed to be due to extensive hydrogen bonded networks between the hydrazide side-chains. Functionalisation studies with the polymer·TFA salt and aldehydes revealed that fast, almost complete coupling was occurring followed by a slow equilibration over several days, in which aldehyde was regenerated. Solubility of the scaffold was problematic however, as in aqueous conditions the scaffold was insoluble and moderately successful dissolution in DMSO was achieved only after heating. As a consequence, poly(prop-2-yn-1-yl hydrazine carboxylate) was synthesised via the metal catalysed polymerisation of 1-(*tert*-butyl) 2-(prop-2-yn-1-yl) hydrazine-1,2-dicarboxylate and subsequent deprotection. Due to solubility problems with the neutral scaffold associated with extensive hydrogen bonded networks between the hydrazide side-chains, the polymer was isolated as the acetate salt. Functionalisation of the polymer with aldehydes revealed that high percentage loading could be achieved, but in a solvent dependent manner, which defeated the purpose of a polymer scaffold useful for fast screening.

To demonstrate the potential of the "*in-situ*" aspect of polyhydrazide scaffolds, poly(acryloyl hydrazide) was functionalised with a cationic guanidinium aldehyde and with diverse hydrophobic aldehydes to form functional amphiphilic polymers. The biological activity of these polymers was tested, by complexing siRNA without the necessity for purification and isolation of the target compounds. The biological activity of these complexes was tested on GFP-HeLA cells, which allowed the identification of a target functional polymer with potent activity.

Future plans

The methodology developed for the functionalisation and testing of polymers derived from poly(acryloyl hydrazide) is being used to further explore the delivery of useful biological cargo such as siRNA and plasmids. Because of the significant size difference of a siRNA strand compared to a plasmid, poly(acryloyl hydrazide)s of different molecular weights are being tested to identify suitable combinations of aldehydes and relationships between polymer size and biological activity. Other applications currently being explored using poly(acryloyl hydrazide) scaffolds involve the clustering of bacteria using functional polymers, but further opportunities exist in the development of novel mimics of antimicrobial peptides, formation of antifouling surfaces and chelators for metal ions.

The development of fluorescent poly(acryloyl hydrazide) is being continued towards the synthesis of a tool towards libraries of fluorescent functional polymers, which could be exploited in identifying a variety of biological mechanisms (e.g. membrane transport pathway), as well as potentially monitoring the biological distribution of functional polymers in a system (e.g. targeted drug delivery).

Despite the solubility issues of poly(4-ethynylbenzohydrazide), there is scope to improve this polymer by copolymerising with phenyl acetylenes bearing functional groups that do not participate in hydrogen bonding and that could potentially improve the water solubility of the polymer. This could lead to a helical polyhydrazide scaffold that would have interesting applications in the development of functional polymers, which mimic the function of naturally occurring helical biological molecules.